

PDF hosted at the Radboud Repository of the Radboud University Nijmegen

The following full text is a publisher's version.

For additional information about this publication click this link.

<http://hdl.handle.net/2066/105819>

Please be advised that this information was generated on 2017-12-06 and may be subject to change.

Bioactive Electrospun Fibrous Scaffolds for Bone Tissue Engineering

Biomolecules release, bioactivity preservation
and biological performance



Colofon

Thesis Radboud University Nijmegen Medical Center, with summary in English, Dutch and Chinese.

Bioactive Electrospun Fibrous Scaffolds for Bone Tissue Engineering: biomolecules release, bioactivity preservation and biological performance.

Wei Ji, Nijmegen, 2013.

All rights reserved.

ISBN: 978-90-8891-570-3

Layout: Wei Ji

Cover design: Wei Ji; Proefschriftmaken.nl | | Uitgeverij BOXPress

Printing : Proefschriftmaken.nl | | Uitgeverij BOXPress

Publisher : Uitgeverij BOXPress, Oisterwijk

Bioactive Electrospun Fibrous Scaffolds for Bone Tissue Engineering

Biomolecules release, bioactivity preservation
and biological performance

Proefschrift

Ter verkrijging van de grad van doctor

Aan de Radboud Universiteit Nijmegen

Op gezag van de rector magnificus prof. mr. S.C.J.J. Kortmann,

volgens besluit van het college van decanen

in het openbaar te verdedigen op maandag 25 feburari 2013

om 15.30 uur precies

door

Wei Ji

geboren op 2 mei 1983

te Wuhan, China

Promotor

Prof. dr. J.A. Jansen

Copromotoren

Dr. F. Yang

Dr. ing. J.J.J.P.van den Beucken

Manuscriptcommissie

Prof. dr. W. B. van den Berg

Prof. dr. P.J. Slootweg

Prof. dr. M.J.T.H. Goumans (Leids Universitair Medisch Centrum)

Paranimfen

Wanxun Yang

Alexey Klymov

**Bioactive Electrospun Fibrous Scaffolds
for Bone Tissue Engineering**

Biomolecules release, bioactivity preservation
and biological performance

Doctoral thesis

to obtain the degree of doctor

from Radboud University Nijmegen

on the authority of the rector Magnificus prof. dr. S.C.J.J. Kortmann,

according to the decision of the Council of Deans

to be defended in public on Monday, February 25, 2013

at 15.30

By

Wei Ji

Born in Wuhan, China

on 2 May, 1983

Supervisor

Prof. dr. J.A. Jansen

Co-supervisors

Dr. F. Yang

Dr. ing. J.J.J.P.van den Beucken

Doctoral Thesis Committee

Prof. dr. W. B. van den Berg

Prof. dr. P.J. Slootweg

Prof. dr. M.J.T.H. Goumans (Leiden University Medical Center)

Ushers

Wanxun Yang

Alexey Klymov

“Our greatest glory is not in never failing,
but in rising up every time we fail.”

Ralph Waldo Emerson

1803-1882

To my beloved parents and families

谨以此书献给我的父母和家人

Contents

Chapter 1	General introduction	11
Chapter 2	Local delivery of small and large biomolecules in cranio-maxillofacial bone	19
Chapter 3	Bioactive electrospun scaffolds delivering growth factors and genes for tissue engineering applications	51
Chapter 4	Incorporation of stromal cell-derived factor-1 α in PCL/gelatin electrospun membranes for guided bone regeneration	73
Chapter 5	Fibrous scaffolds loaded with protein prepared by blend and coaxial Electrospinning	97
Chapter 6	Coaxially electrospun scaffolds based on hydroxyl-Functionalized poly(ϵ -caprolactone) and loaded with VEGF for tissue engineering applications	117
Chapter 7	Biocompatibility and degradation characteristics of poly (lactide-co-glycolide)-based electrospun nanofibrous scaffolds with nanoapatite incorporation	141
Chapter 8	Summary, closing remarks and future perspectives Samenvatting, slotwoord en toekomstperspectieven 结语及展望	163
	Acknowledgements	185
	List of Publications & Awards	191
	Curriculum Vitae	193



1

General introduction

1. Background

Bones are rigid organs that constitute part of the endoskeleton of vertebrates. The adult human skeleton contains 213 bones that are vitally important to support and protect the various organs of the body. Clinically, the occurrence of bone defects is common and can be caused by a variety of factors, including congenital deformity, trauma/injuries, infection, osteoporosis, and tumorectomy. In daily life, bone defects have a significant impact on an individual's life quality, as well as on overall health care cost. For example, the estimated cost of treating all musculoskeletal injuries in 2004 was \$127.4 billion in the United States¹. In addition, treatment of fractures and other musculoskeletal injuries will continue to increase as a result of population aging and growth, which might be a major cost to the medical community and society.

A conventional strategy to reconstruct bone defects (particularly large bone gaps and composite defects) involves transplantation of bone grafts, which can be harvested from the iliac crest, fibula, scapula or radius (either autogenous or allogeneous)². This approach has established itself as the "gold standard" in bone reconstructive surgery because of its high success rates owing to the osteogenic, osteoinductive and osteoconductive properties of autologous bone³. However, the inherent drawbacks of this approach, including insufficient autogenous resources, contour irregularities and donor-site morbidity², strongly urge clinicians and researchers to explore alternative treatment options.

2. Bone tissue engineering

In view of the drawbacks of conventional bone graft strategies, bone tissue engineering recently has emerged as a promising approach for bone reconstruction. The fundamental concept behind bone tissue engineering is to utilize the body's own biological capacity for bone healing in conjunction with engineering principles. There are three important elements for bone tissue engineering, namely scaffolds, cells and biomolecules (Figure 1). A conventional tissue engineering strategy starts with pre-culturing progenitor cells on synthetic scaffolds, followed by transplantation of cell/scaffold complexes into the defect site. In this approach, the progenitor/stem cells isolated from bone marrow, which have been recognized as the most efficient cell type for osteogenic differentiation⁴, provide the main resource to form new bone tissue; while the scaffolds mainly provide physical accommodation to cells to enable them secrete extracellular bone matrix and form new bone tissues.

In principle, an optimal tissue engineering scaffold should mimic the structural and functional characteristics of bone extracellular matrix (ECM). Natural bone ECM is composed of nanoscale collagen fibers, in which biomolecules (e.g. cytokines and growth factors) are incorporated. The nanoscale architecture of the ECM influences the adhesion and orientation of cells⁵, while the release of biomolecules from the ECM regulates cellular

proliferation and differentiation⁶. In view of this, an optimal tissue engineering scaffold should provide more than only physical support for cells; it should also direct the local biological processes (e.g. via the release of biomolecules) in order to modulate optimal cell and tissue responses.

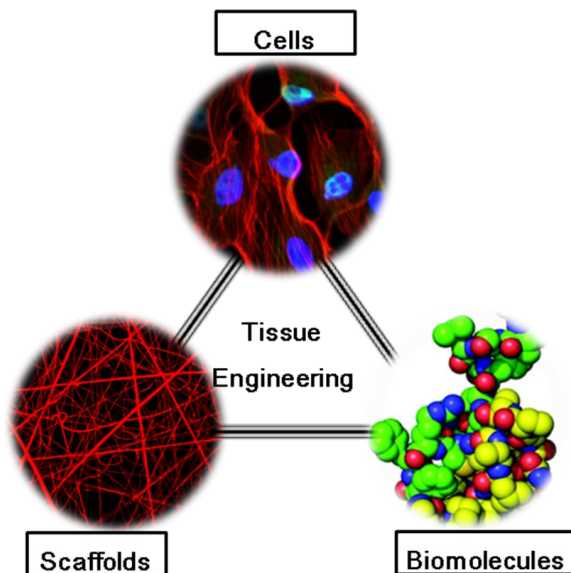


Figure 1. Three key elements for tissue engineering, namely cells, scaffolds and biomolecules

3. Electrospun scaffolds for bone tissue engineering

Tissue engineering scaffolds have been prepared using a multitude of different techniques, such as gas foaming, emulsion freeze drying and rapid prototyping⁷. Recently, electrospinning has emerged as a popular technique to prepare tissue engineering scaffolds due to its relative simplicity regarding the generation of fibrous scaffolds with nanoscale dimensions. In addition, due to the nanoscale properties, electrospun scaffolds have been considered as an effective delivery system owing to the stereological porous structure and high specific surface area⁸.

Electrospinning utilizes electrostatic forces to spin polymer solutions or melts into whipped jets, resulting in continuous fibers with diameters from a few nanometers to micrometers after solvent evaporation in the spinning process⁹. A typical electrospinning set up contains four parts: (1) a syringe pump, which controls the feeding rate of polymer solution to be electrospun; (2) a needle, through which the solution goes into a high electric field; (3) a high voltage source, which stretches the polymer solution into ultrathin fibers; and (4) a grounded fiber collector, where electrospun fibers can be collected in a static or dynamic way.-

There is a wide range of material choices to prepare electrospun scaffolds for tissue engi-

neering applications, which mainly includes two categories: natural polymers and synthetic polymers. In principle, the material choice for scaffold preparation depends on the purpose of application and feasibility of electrospinning. Compared to the natural polymers, synthetic polymers (especially the polyesters) are much easier to be optimized for electrospinning, and hence are more commonly applied. Among multiple choices of synthetic polymers, poly(ϵ -caprolactone) (PCL), poly(lactic acid) (PLA), poly(glycolic acid) (PGA) and their copolymers poly(lactic-co-glycolic acid) (PLGA) are most extensively used for biomedical applications, as they are constituents of many products approved by the US Food and Drug Association (FDA) and have demonstrated suitable biocompatibility as well as biodegradability.

4. Bioactive electrospun scaffolds with biomolecules incorporation

As aforementioned, a successful tissue engineering approach requires scaffolds to provide biological functionality in addition to simple physical support. Consequently, it is important to enhance the biological functionality of electrospun scaffolds by incorporating biomolecules that can stimulate bone regeneration process.

Multiple kinds of biomolecules play important roles in regulating recruitment, proliferation, and differentiation of osteogenic progenitor cells. **Chapter 2** comprehensively describes various biomolecules with potential for application in bone regeneration. Based on their molecular weight, therapeutic biomolecules can be divided as macromolecules and small molecules. Macromolecules include growth factors, cytokines as well as their corresponding encoding nucleic acids, which mainly regulate the morphogenesis and regeneration of bone tissue. Comparatively, small molecules, predominantly drugs, peptides, and oligonucleotides, are emerging in recent years as an effective adjuvant therapy to improve the conditions for bone regeneration¹⁰.

Currently, the mainstream of research interest in tissue engineering still focuses on growth factor/cytokines incorporation, as these biomolecules are the most straightforward candidates to modulate bone regeneration. For example, stromal cell derived factor-1 alpha (SDF-1 α) has shown to be a powerful chemokine involved in cell recruitment in a variety of tissues¹⁰; bone morphogenetic protein-2 (BMP-2) is critically involved in mediating mesenchymal condensation that appears prior to the formation of mature bony structures¹¹; while vascular-endothelial growth factor (VEGF) plays important roles in the regulation of angiogenesis during bone healing¹¹. In view of this, the focus of this thesis is to functionalize electrospun scaffolds with aforementioned growth factors/cytokines.

In order to incorporate electrospun scaffolds with biomolecules, there currently are four fabrication techniques, i.e. physical adsorption, blend electrospinning, coaxial electrospinning, and covalent immobilization. The principles, their application as well as pros

and cons of these techniques are extensively described in Chapter 3. Among these four techniques, physical adsorption is the easiest way to load biomolecules, albeit that it generates a large burst release and a relatively short release period. Blend and coaxial electrospinning are the most commonly used methods to generate electrospun scaffolds with slow and sustained release profiles, since the biomolecules are embedded within polymeric scaffolds during electrospinning. In contrast, covalent immobilization is not a routine way to deliver biomolecules from electrospun scaffolds due to its technical complexity. In addition, some researchers also doubt the uniformity loss of the scaffolds during surface modification processes¹², which might affect topographical and mechanical properties of the scaffolds. In consequence, this thesis particularly focuses on biomolecule incorporation within electrospun scaffolds through physical adsorption, blend electrospinning, and coaxial electrospinning.

5. Objectives of this thesis

This thesis aimed to cover research on the development of bioactive electrospun scaffolds with biomolecule incorporation via different techniques. In addition, the evaluation of the efficacy of obtained bioactive electrospun scaffolds for guided bone regeneration was an objective. Finally, this thesis also aimed to explore strategies to improve host tissue responses upon implantation of nanofibrous electrospun scaffolds.

The following research questions were covered:

1. What is the current state of the art in local delivery of biomolecules for bone regeneration?
2. What are current available methods to functionalize electrospun scaffolds with biomolecules, and what are pros and cons for different methods?
3. Can electrospun scaffolds be functionalized with SDF-1 α by physical adsorption to achieve cell recruitment?
4. What is the superior method to generate bioactive electrospun scaffolds with sustained release of biomolecules, in respect of spinnability, release profiles, and bioactivity preservation?
5. What is the application potential for coaxial electrospun nanofibrous scaffolds with growth factor release?
6. What are biocompatibility and degradation characteristics of PLGA-based nanofibrous electrospun scaffolds?

6. References

1. Jacobs JJ; Andersson GBJ; JE, B.; SL, W.; JP, D.; SM, G.; N, L.; JE, P.; EW, S. C.; EH, Y. The burden of skeletal muscular diseases in the United States: prevalence, societal and economical Cost; United States Bone and Joint Decade: Rosemont, 2008.
2. Buck, D. W., 2nd; Dumanian, G. A. *Plast Reconstr Surg* 2012, 129, 950-956.
3. Hallman, M.; Thor, A. *Periodontol 2000* 2008, 47, 172-92.
4. Gamie, Z.; Tran, G. T.; Vyzas, G.; Korres, N.; Heliotis, M.; Mantalaris, A.; Tsiridis, E. *Expert Opin Biol Ther* 2012, 12, 713-729.
5. Rosenberg, M. D. *Science* 1963, 139, 411-412.
6. Ma, Z.; Kotaki, M.; Inai, R.; Ramakrishna, S.,. *Tissue Eng* 2005, 11, 101-109.
7. Weigel, T.; Schinkel, G.; Lendlein, A. *Expert Rev Med Devices* 2006, 3, 835-851.
8. Ji, W.; Yang, F.; van den Beucken, J. J.; Bian, Z.; Fan, M.; Chen, Z.; Jansen, J. A. *Acta Biomater* 2010, 6, 4199-4207.
9. Pham, Q. P.; Sharma, U.; Mikos, A. G. *Tissue Eng* 2006, 12, 1197-1211.
10. Ji, W.; Wang, H.; van den Beucken, J. J.; Yang, F.; Walboomers, X. F.; Leeuwenburgh, S.; Jansen, J. A. *Adv Drug Deliv Rev* 2012, 64, (12), 1152-1164.
11. Gerstenfeld, L. C.; Cullinane, D. M.; Barnes, G. L.; Graves, D. T.; Einhorn, T. A. *J Cell Biochem* 2003, 88, 873-884.
12. Ma, Z. W.; Kotaki, M.; Ramakrishna, S. *Journal of Membrane Science* 2006, 272, 179-187.



Local delivery of small and large biomolecules in craniomaxillofacial bone

Wei Ji, Huanan Wang, Jeroen J.J.P. van den Beucken,
Fang Yang, X. Frank Walboomers, Sander Leeuwenburgh,
John A. Jansen

Advanced Drug Delivery Reviews. **2012**, 64, 1152-1164.

1. Introduction

The bones of the craniomaxillofacial (CMF) skeleton include the neurocranium and facial bones. These bony structures provide the foundation for oral-facial soft tissues and protections for organs (i.e. brain, nerve, and vasculature) located inside, and are thus functionally and aesthetically important. The occurrence of CMF bone defects are common and can be caused by a variety of factors, including congenital deformity, trauma, infection, and tumorectomy. For example, in 2007 over 400.000 people in the United States required maxillofacial surgery for injuries to the face and jaw¹. Affected patients suffer from functional disorder, social incapacitation, and biomedical and economical burden. This patient population ultimately demands an effective restoration strategy to fulfil aesthetic and functional requirements.

Current state of the art reconstruction of bony defects in the CMF area involves transplantation of bone grafts harvested from the iliac crest, fibula, scapula or radius (either autogenous or allogenuous), which inherently contain microvascular structures^{2, 3}. This approach has established itself as the “gold standard” in bone reconstructive surgery because of high success rates due to the osteogenic, osteoinductive and osteoconductive properties of autologous bone⁴. However, the inherent drawbacks of this approach, including insufficient autogenous resources, contour irregularities, and donor-site morbidity⁵, strongly urge clinicians and researchers to explore alternative treatment options.

With an improved understanding of CMF biology as well as progress in biomedical therapeutic techniques, an alternative strategy in CMF reconstruction termed *regenerative* craniofacial surgery emerged, which aims to repair CMF defects by inducing the regeneration of autogenous bone instead of using exogenous transplants with their inherent shortcomings⁶. An important approach for regenerative craniofacial surgery is based on the concept of tissue engineering, which aims to utilize the body’s natural biological response to tissue damage in conjunction with engineering principles⁷.

There are three key factors involved in tissue engineering, namely cells, scaffolds, and biomolecules⁸. In recent years, an increasing trend toward the combination of scaffolds and biomolecules became obvious⁹⁻¹², in which scaffolds with controlled release of biomolecules induce ((pre)seeded) cells to proliferate and differentiate during an *ex vivo* pre-culture period, thereby encouraging tissue formation after implantation *in vivo*. Upon implantation, those scaffolds continue to release signal molecules to enhance the desired biological response, and hence enhance tissue regeneration in the defect area¹³. Bone regeneration involves a complex cascade of processes during which resident or bone marrow-derived precursor cells migrate to the site of damage and undergo differentiation into the osteogenic lineage¹⁴. As such, a large number of small and large biomolecules (including hormones, cytokines, and growth factors) are involved in bone regeneration that modulate the cellular behavior of progenitor and inflammatory cells

in terms of migration, proliferation, and differentiation¹⁵. Considering the importance of these biomolecules during bone regeneration, it is not surprising that exogenous delivery of a single or multiple biomolecules at the defect site has been heavily explored as a promising therapeutic strategy in CMF bone regeneration.

Based on the molecular weight, a threshold can be set at 5 kDa to divide therapeutic biomolecules in CMF bone into either macromolecules or small molecules. Macromolecules include growth factors, cytokines as well as their corresponding encoding nucleic acids, which mainly regulate the morphogenesis and regeneration of CMF skeleton and have been investigated extensively in the past to promote bone regeneration. Comparatively, small molecules, predominantly including drugs, peptides, and oligonucleotides, are emerging in recent years as an effective adjuvant therapy to interfere with infection, osteoporosis and tumor metastasis in CMF bone, thereby improving the conditions for CMF bone regeneration.

In general, biomolecules can be administered either systemically or locally. Due to the low oral and transdermal bioavailability, short biological half-life, tissue specificity, and potential dose-dependent carcinogenicity^{16,17}, systemic administration of biomolecules is often not effective. Consequently, localized controlled delivery via a carrier material is advantageous for therapeutic applications in order to optimize efficacy of biomolecules and increase the comfort, convenience, and compliance of involved patients¹⁷.

This review will focus on the effects of locally delivered small and large biomolecules for the clinical treatment of CMF bone defects. We will describe biomolecules that are involved in the process of CMF bone healing with specific emphasis on small molecule drugs, followed by a description of currently explored carrier materials and their requirements to achieve optimal biomolecule delivery. Finally, we will provide a perspective on the applicability of biomolecule delivery in CMF repair by reviewing the pre-clinical studies carried out so far in various animal models.

2. Lessons from biology: biomolecules involved in CMF bone healing

2.1. Biomedical fundamentals for CMF bone

From a biological point of view, it should be realized that several differences can be discerned between CMF bone formation and axial skeleton formation. First of all, the CMF bone and axial bone arise from different embryonic lineages, in which the CMF bone is formed by cranial neural crest cells, whereas the axial skeleton is derived from paraxial mesoderm (somites)¹⁸. Secondly, the CMF bone and axial bone undergo different bone formation pathways. Two different pathways are involved in skeletogenesis, i.e. intramembranous ossification and endochondral ossification¹⁹. During embryonic development, the CMF bones, including the cranial vault, maxilla, mandible, and frontal region of the facial skeleton, undergo intramembraneous formation, which involves a

direct differentiation of mesenchymal precursors into osteoblasts as well as direct deposition of bone matrix by osteoblasts²⁰.

In contrast, long bone structures are formed by endochondral ossification²¹, which starts with the condensation of mesenchymal precursors into the chondrogenic lineage, which then go into hypertrophy before finally entering terminal chondrogenic differentiation resulting in a mineralized cartilage matrix²². Many morphogenetic factors play important roles in CMF bone development¹⁸, which will be explained in detail in section 2.2.2.

From a clinical therapeutic point of view, the unique location of the CMF skeleton raises another consideration in treatment compared to axial bone. The CMF skeleton is interconnected with the oral cavity, which hosts over 700 species of bacteria²³. This unique location makes that the infection risk is high in bone tissue close to the oral cavity (e.g. alveolar bone, mandible, and maxilla). For example, in clinics, osteomyelitis of the jaws is a common infectious disease, leading to surgical debridement of the infected bone and long-term antibiotic therapy²⁴. The main causes for osteomyelitis are odontogenic microorganisms²⁵. In addition to the high risk of infection, the numerous lymph nodes, nerves and vasculature structures in the CMF area increase the risk of tumor metastases to CMF bone from surrounding tissues. It has been reported that 1% of oral cancers metastases to the mandible, while the occurrence of other mandible metastases is mainly caused by malignant tumors from breast, lung, kidney, and colon²⁶. Therefore, when treating the CMF bony lesions caused by tumorectomy, an indispensable therapy to the routine bone regeneration is the administration of anti-tumor drugs to prevent further metastasis.

2.2. Candidate biomolecules for CMF bone defect therapy

As aforementioned, a highly promising therapy for reconstruction of CMF bone is to induce bone regeneration in the defect site, rather than simply fill the defect with grafting materials. The regeneration processes in CMF bone are initiated in response to injury followed by normal bone development coordinated by cells derived from periosteum, bone, and external soft tissues surrounding the defect site²⁷. As aforementioned, candidate biomolecules for therapeutic applications in CMF bone regeneration can be categorized into two groups according to their molecular weight (threshold: 5 kDa): (i) large molecules, including growth factors, cytokines as well as their corresponding encoding nucleic acids, and (ii) small molecules, including drugs, peptides, and oligonucleotides. The large molecules can be further subcategorized by their functions in the process of craniomaxillofacial bone regeneration: (i) inflammatory cytokines and chemokines, which orchestrate inflammatory responses and chemotaxis of regenerative cells; (ii) morphogenetic factors which regulate skeleton formation and morphogenesis; (iii)

angiogenic factors, which direct vascularisation to allow transport of nutrients, oxygen and waste during bone formation; The small molecules also include different subgroups based on their functions such as (i) short peptides derived from therapeutic proteins, which play similar roles as proteins in physiological process of CMF bone regeneration, (ii) anti-infection molecules, (iii) anti-tumor molecules, as well as the (iv) antiosteoporotic molecules. The latter three groups of small molecules have intrinsic capacity to alleviate compromised conditions that may hinder CMF bone regeneration (Figure 1).

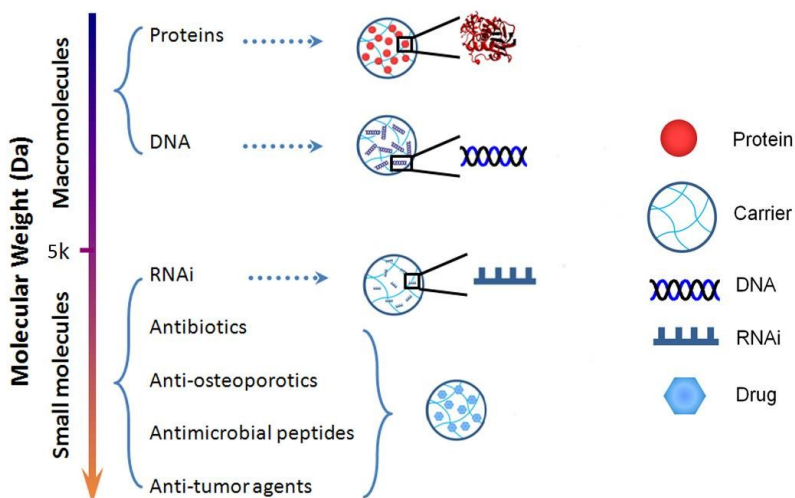


Figure 1. Classification and controlled release of biomolecules involved in therapeutic applications in CMF bone regeneration. Macromolecules, primarily including proteins and DNA, can be loaded by carrier devices and released extracellularly or intracellularly to guide cell behaviors and regulate bone healing process; while small molecules, hereby defined as biomolecules with molecular weight lower than 5kDa, mainly target bone regeneration under compromised conditions such as infection, skeletal malignancies and metastases in CMF bone and osteoporosis.

2.2.1. Large molecules

2.2.1.1. Inflammatory cytokines and chemokines. Bone healing is initiated with hematoma formation and activation of the immune system¹⁵. During this initial stage, a number of cytokines are secreted by macrophages and inflammatory cells, which regulate the healing process. The detailed categories of cytokines and their function during immune response have already been clearly reviewed²⁸. Among different kinds of cytokines, interleukin 1 (IL-1) and tumor necrosis factor- α (TNF- α) are known to be the most important pro-inflammatory cytokines, as they play an important role in initiating the inflammatory cascade²⁸, whereas interleukin-4 (IL-4), and interleukin-13 (IL-13) are considered as pro-wound healing cytokines, as they suppress the production of pro-inflammatory cytokines hence promoting wound healing^{29,30}.

In recent years, the chemotactic capacity of cytokines has gained interest rapidly, as researchers realized that recruitment of precursor cells plays a critical role during bone repair. Stromal cell derived factor-1 alpha (SDF-1 α) has shown to be a powerful chemokine involved in cell recruitment in a variety of tissues³¹. It has been demonstrated that SDF-1 α is critical to migration of hematopoietic stem cells (HSCs) and can be used to target stem cells to a desired site within the body³². Furthermore, recent studies revealed that SDF-1 α improves the efficiency of BMPs *in vivo* by increasing the number of osteoprogenitor cells that are mobilized from the bone marrow³³. In addition to SDF-1 α , TNF- α has also been reported to promote recruitment of mesenchymal stem cells (MSCs), induce apoptosis of hypertrophic chondrocytes, and stimulate osteoclastic function³⁴.

2.2.1.2. Morphogenetic factors. During the morphogenetic process, several soluble factors, including TGF- β superfamily members, fibroblast growth factors (FGFs), sonic hedgehog (SHH), and Wingless- and Int-related proteins (Wnts), participate in a complex series of events that guide mesenchymal precursor cells in the skull through patterning, proliferation, and differentiation to form the craniofacial skeleton. Previous studies have already comprehensively reviewed the detailed molecular mechanisms of TGF- β superfamily³⁵, FGFs³⁶, SHH³⁷, and Wnts³⁸ in CMF skeleton development, for which only key functions of these biomolecules are highlighted below.

TGF- β superfamily members are the most extensively studied growth factors in recent years. This family includes five TGF- β isoforms (TGF- β 1-5), bone morphogenetic proteins (BMPs), the inhibins/activins, and a number of distantly-related molecules³⁹. BMPs (BMP -2, 4, 7), have been demonstrated to play important roles in determination, migration, condensation, proliferation, and apoptosis of skeletal cells. More particularly, BMP-4 and BMP-7 have been reported to be responsible for neural crest cell induction³⁵, whereas BMP-2 is critically involved in mediating mesenchymal condensation that appears prior to the formation of mature bony structures in both intramembranous and endochondral ossification⁶. The other members of the TGF- β superfamily (TGF- β 1-3) also participate in bone formation induction⁴⁰, but the osteoinductive activity of TGF- β proteins is specifically found in heterotopic sites in primates⁴¹.

Fibroblast growth factors (FGFs) are humoral factors originally identified by their ability to stimulate cell proliferation⁴². The family of FGFs consists of twenty-two members that are involved in diverse biological roles in the regulation of cell proliferation, differentiation, and function⁴². During craniofacial bone development, FGFs are required for the regulation of intramembranous ossification, and absence of FGF-2 was reported to inhibit osteogenesis in cranial vault development⁴³. During bone healing, FGFs can be secreted by monocytes, macrophages, mesenchymal cells, osteoblasts, and chondrocytes, in the early stages of fracture healing²⁷.

Compared to the morphogenetic molecules mentioned above, Wnts and SHH are less

known to clinicians, but gained increasing interest in recent years because of their important function during the process of craniofacial development. Wnts are associated with the maintenance and proliferation of mesenchymal stem cells during craniofacial development⁴⁴. SHH is involved in regulating the transdifferentiation of epithelial cells to a mesenchymal cell fate, as well as the proliferation of mesenchymal cells during craniofacial patterning, and this process is indispensable for fusions between the palatal shelves⁴⁵.

Furthermore, insulin-like growth (IGFs), platelet-derived growth factor (PDGF), growth hormone, parathyroid hormone, and vitamin D have also been demonstrated to mediate osteoblast activity during the process of bone remodeling⁴⁶.

2.2.1.3. Angiogenic factors. Optimal bone healing requires adequate blood supply to transport nutrients and oxygen. Two separate pathways are involved in the regulation of angiogenesis during bone healing: a vascular-endothelial growth factor (VEGF)-dependent pathway, and an angiopoietin (Ang)-dependent pathway⁴⁷. VEGF isoforms are involved in the regulation of the interaction between angiogenesis and osteogenesis⁴⁸. It has been demonstrated that VEGF promotes endochondral bone formation via synergistically acting with BMP-4 for the recruitment of mesenchymal stem cells⁴⁹. A previous study showed that the expression of Ang-2 and its receptor Tie-1 significantly increased during the chondrogenic phase of fracture repair⁵⁰, which might indicate the participation of Ang-2 in endochondral ossification. On the other hand, the role of the angiopoietin pathway and its contribution in bone healing process are still not fully understood⁴⁷.

2.2.2. Small molecules

2.2.2.1. Peptides derived from therapeutic proteins. Short peptides derived from therapeutic proteins can exert similar biological functions without involving complicated structures of the entire proteins and are delicate in the biological environment. A vivid example for this category are synthetic peptides corresponding to the knuckle epitope of BMPs. It has been reported previously that a synthetic peptide derived from BMP-2 knuckle epitope, NSVNSKIPKACCVPELSAI (residues 68–87), recruited osteocalcin positive osteoblasts, and induced ectopic calcification when a peptide-conjugated alginate gel was implanted into a rat's muscle⁵¹. Another synthetic peptide, KIP-KASSVPELSAISTLYL (residues 73–92, C78,79S and M89T) has been demonstrated to induce differentiation of osteoblast precursor cells and activate osteoblasts to promote repair of bone defects⁵². Beside peptides derived from BMP-2, synthetic peptides from BMP-7, including SNVILKKYRN, (residues 121-130), KPSSAPTQLN (residues 101-110), and KAISVLYFDDS (residues 110- 120) have been reported to promote proliferation and calcium deposition of osteoblasts⁵³. Recently, Bergeron et al⁵⁴ incorporated a 23-residue syn-

thetic peptide Ac-CGGKVGKACCVPTKLSPIVLYK-NH₂ derived from human BMP-9 (residues 68–87) into collagen and chitosan gels and investigated effects on ectopic bone formation. Their results indicated that chitosan gels containing 100 µg of BMP-9 peptides induced lamellar bone formation in mouse quadriceps after 24 days, although bone formation was not as strong compared to the same gel containing full length of BMP-9. Together, these studies suggest a promising future for the application of short peptides instead of entire proteins in the field of regenerative medicine.

2.2.2.2. Anti-infection molecules. It is generally accepted that resistant microbial infection, due to periodontitis²³ or osteomyelitis⁵⁵, is the main cause for alveolar bone loss. Therefore, an effective anti-microbial infection treatment is indispensable to achieve bone regeneration. Antibiotic therapy is the mainstay of treating microbial infection in CMF skeleton. Several types of antibiotics have become commercially available in the past decades, and the most commonly used antibiotics in clinics include tetracyclines, penicillins (amoxicilin), metronidazole and cephalosporins^{55,56}. However, the increasing microbial resistance following the use of antibiotics remains a critical concern for therapeutic application of antibiotics in clinics⁵⁷. Beside commercially available antibiotics, antimicrobial peptides (AMPs) from saliva and gingival crevicular fluid are recently emerging as effective therapeutic molecules. These AMPs constitute a diverse class of host-defense molecules ranging from small cationic peptides to enzymes that play a role in balancing oral pathogens and commensals²³.

2.2.2.3. Anti-tumor molecules. In clinics, anti-tumor therapy is often required for reconstruction of the skeletal malignancies and surgical removal of metastases to slow down tumor growth and metastasis outgrowth. Classical drugs include cyclophosphamide, methotrexate, and 5-fluorouracil, while new generation agents include anthracyclines and texanes, such as epirubicin, doxorubicin and paclitaxel⁵⁸. It needs to be emphasized that the combined usage of these drugs may also weaken the bone further, hence the dosage and administration route should be well controlled. Nowadays, RNA interference (RNAi) provide a new perspectives in disease treatment by targeted degradation of mRNA with the introduction of small interfering RNAs (siRNAs) or small hairpin RNAs (shRNAs)⁵⁹. To date, RNAi for therapeutic purposes has been explored in different applications including anti-cancer and antiviral treatment in different organs⁶⁰. For instance, it is well established that the VEGF-receptor pathway is important in the pathogenesis and angiogenesis of human cancers⁶¹, for which the introduction of a VEGF-targeted shRNA was hypothesized to inhibit angiogenesis in the progression of cancers. This therapeutic approach has recently been shown to result in a significant delay of tumor growth⁶².

2.2.2.4. Anti-osteoporotic molecules. Anti-osteoporotic treatment is another increasing issue in view of regenerative treatments of CMF bone defects, as osteoporosis systemi-

cally influences general bone formation and remodelling. It is generally accepted that systemic osteoporosis and its milder form osteopenia, can cause substantial bone loss in alveolar and jaw bone⁶³. Currently, an effective pharmaceutical treatment for osteoporosis is the application of use anti-resorptive drugs, including bisphosphonates, calcitonin, estrogen, and estrogen agonist/antagonist. All of these biomolecules inhibit (directly or indirectly) osteoclast activity to diminish bone loss and hence mainly act to stabilize the balance of bone turnover. Recently, N-methylpyrrolidone (NMP) was found to inhibit osteoclast differentiation and attenuate bone resorption⁶⁴. In addition, the combination of genistein, zinc, and vitamin D has also been shown to improve bone mineral density⁶⁵. On the other hand, the anabolic agents that enhance bone mass and improve bone architecture are clinically very important in treating established osteoporosis. The most frequently used anabolic agent is parathyroid hormone (PTH), for which it has been reported previously that it promotes osteoblast function to increase new bone formation⁶⁵. Currently, several PTH analogs are being investigated, and finally human (h) PTH (1-34) has been approved for use in osteoporosis treatments in the United States⁶⁶. Recently, 3-hydroxy-3-methylglutaryl coenzyme A reductase inhibitors (statins), which have been principally used as the most effective class of drugs to reduce serum cholesterol concentrations, were found to have anabolic effects on bone metabolism. It was discovered that treatment with statins can stimulate cellular osteogenic differentiation by enhancing BMP-2 mRNA expression and increasing trabecular bone volume when orally administered to ovariectomized rats⁶⁷⁻⁶⁹. Although statins are considered as potential therapeutic agents for anti-osteoporotic treatment, due to different kinds of statins available on the market and different dosages and administration methods, controversial results still exist regarding their biological effect on bone metabolism (see also review by Horiuchi et al⁶⁶).

3. Carrier material requirements for the delivery of biomolecules in CMF bone regeneration

After discovery of the important biological function of above-described small and large biomolecules during CMF bone healing, extensive research efforts have been dedicated to enable delivery of these biomolecules into the defect site to enhance bone healing. Regardless of the delivery form, the fragile nature of biomolecules demands for controlled delivery carriers to achieve an optimal therapeutic application. Generally, carrier systems for biomolecule delivery should be biocompatible and biodegradable. In addition to these general requirements, an optimal carrier device should also ensure the biological activity of biomolecules as well as allow for controlled release profiles in line with the time window of tissue regeneration⁷⁰. Compared to the small molecule drugs, delivery of proteins and genes is more challenging due to their complicated structure and fragile

structure. Therefore, we will specifically list some important considerations for those biomolecules delivery.

3.1. Preservation of biological activity

Carrier devices for delivery of proteinaceous biomolecules should preserve the conformational stability of these proteins. The conformational stability of proteins can be compromised at different stages: (i) during carrier/protein construct fabrication, (ii) during carrier/protein storage, and (iii) after implantation⁷¹. Two main pathways towards loss of conformational stability of proteins can be discerned: (i) physical or noncovalent degradation, which leads to changes in secondary or tertiary structures; and (ii) chemical inactivation, which results from changes in primary structure.

Noncovalent degradation mainly refers to the destruction of noncovalent interactions (i.e., hydrogen bonds, van der Waals interactions, salt bridges, and hydrophobic interaction) in the native protein structure caused by elevated temperature, extremes of pH, denaturants, and adsorption to hydrophobic surfaces⁷². Due to noncovalent degradation, a protein may unfold locally and globally from its native structure to yield an inactivation or aggregation state¹⁷. Chemical inactivation includes hydrolysis of the peptide bonds, deamidation, oxidation, β -elimination, isomerization, and disulfide bond breakage and formation, which are mainly influenced by the temperature and pH value of the solution⁷². In view of this, the overall strategy for preserving protein stability is to prevent protein inactivation or aggregation from above-mentioned environmental conditions.

Different from proteinaceous molecules, which act extracellularly by binding to corresponding cell surface receptors, gene-based biomolecules will only work intracellularly. Based on this principle, the prerequisite for successful gene delivery is that the target gene can be released from the carrier, after which it needs to be taken up by the host cell and remain functional to be transcribed and translated to generate proteins. As naked genes are vulnerable to ubiquitously available extracellular DNA-degrading enzymes and intracellular lysozymes⁷³, the target gene is commonly protected by chaperone vectors, which can be categorized into either viral or non-viral vectors^{74, 75}.

3.2. Controlled release kinetics

Another important issue for biomolecule delivery is to control the spatiotemporal availability at the defect site. Logically, mimicking release kinetics of multiple biomolecules in different time windows during bone regeneration will provide attractive options. As, the release kinetics related to the *in vivo* efficacy is difficult to investigate, mainly extensive studies have been performed to evaluate the effect of dual and multiple biomolecules release on cellular behavior in order to optimize the delivery systems^{76, 77}.

Optimally, the release of biomolecules from a carrier should initially release a substantial part of loaded amount, termed as “burst release”⁷⁸, to rapidly obtain the effective thera-

peutic concentration, followed by a well-defined release to prolong the time window of a supra-threshold dosage⁷⁹. However, it needs to be emphasized that this burst release should be controlled to achieve an optimal therapeutic efficacy, thereby avoiding supraphysiological concentrations of biomolecules (e.g., BMPs, etc) at the defect site that may cause adverse effects^{80, 81}.

Similar to protein delivery, gene delivery relies on efficient concentrations for sufficient duration. In view of this, too low concentrations of plasmid^{82, 83}, or too fast release of plasmid⁸³ have been demonstrated to result in low gene transfection efficiency, mainly because the surrounding cells cannot capture sufficient gene-vector complexes or super-abundant gene complexes may lose activity when transfection is not achieved in due time.

3.3. Targeted delivery

Besides the biological activity preservation and controlled release kinetics, tissue-target releasing becomes nowadays another important issue for the local delivery of biomolecules to improve the efficacy and safety of biomolecules delivery, especially for the anti-cancer drug delivery. In a clinical oncological situation, it is difficult to exactly localize the drug delivery vehicles solely within the tumor tissue because tumor tissue is usually adjacent to healthy tissue. In order to make the anticancer drugs only target tumor cells, it is necessary to make the delivery vehicles specific or targeted for the diseased cells. Two strategies can be discerned to obtain targeted local delivery of biomolecules: (i) ligand-free strategy, and (ii) ligand-functionalization strategy. Ligand-free strategy is to increase the affinity of incorporated biomolecules to the target tissues by mixing with other additives. For example, some groups reported that growth factors can be mixed with bisphosphonates, tetracyclines, glutamic and aspartic oligopeptides, and peptides derived from non-collagenous proteins, which have high affinity to bone⁷⁰ to achieve bone-targeting function. Ligand-functionalization strategy is to modify the surface structure of the carrier device by conjugating a cell-specific ligand to direct the biomolecules to be released more or less exclusively in close association with the target cells. For example, PEG-tethered ligands are reported as a potential platform technology to delivery bone cell-specific biomolecules for bone repair purpose⁷⁰. Various molecules that specifically bind to an antigen or receptor that is either uniquely expressed or overexpressed on the tumor cell surface can be conjugated to the carrier device to selectively deliver anti-cancer biomolecules to tumor cells⁸⁴.

4. Mechanisms for biomolecule release from carrier devices

To optimize the pharmacokinetics of biomolecule delivery, it is of paramount importance to understand the mechanisms of biomolecule loading and release in various delivery systems, which may directly influence the resulting efficacy of delivery.

In general, the release of biomolecules in various delivery systems can be regulated by (i) desorption, (ii) diffusion, (iii) carrier degradation, and (iv) environmental stimuli, or controlled by the combination of the abovementioned factors⁸⁵⁻⁸⁸ (Figure 2).

4.1. Desorption-controlled release

Typical desorption-controlled delivery vehicles are carriers consisting of dense or non-swollen biomaterials, in which biomolecules cannot penetrate through or be entrapped inside the carrier network. Since adsorption/desorption happens at the interface between a biomaterial surface and its physiological environment, surface properties and design/geometry of delivery systems are main factors that affect the resulting release profiles⁸⁹. Most delivery systems using particulate carriers are based on desorption-controlled release owing to more active surface properties allowing high loading capacity and ease of surface functionalization⁹⁰. However, limitations of this strategy are obvious, including the tendency of biomolecules to deactivate during adsorption, poor capacity of delivering hydrophilic molecules, and poor control over delivery, retention, orientation, or desorption rate of biomolecules⁹¹.

4.2. Diffusion-controlled release

Diffusion occurs in numerous delivery systems, in which small biomolecules are self-propelled by thermal energy and spread into/out of carrying vehicles when dispersed into media. This process is a physical entrapment strategy, which can be affected by the characteristics of either biomolecules to be released (e.g. size, solubility and diffusion efficiency) or delivery vehicles (e.g. geometry, mesh size of network and affinity to small molecules). Typical carriers of this kind include hydrogels and polymeric fibrous membranes that allow diffusional loading of biomolecules into polymer networks, thus providing a protective environment for biomolecules and prolonging their retention at treatment sites. The release profile for diffusion-controlled delivery systems is normally characterized by an initial burst release, followed by a phase of sustained release that can be further regulated by fine-tuning the physicochemical properties of carrier materials⁹².

4.3. Degradation-controlled release

Degradation-controlled release systems are defined as erodible systems, where biomolecules can be either: (i) physically entrapped in the carrier and released by carrier's degradation, or (ii) chemically immobilized to a polymer backbone and released upon hydrolytic or enzymatic cleavage of the bond^{85, 87, 88}. By physical or chemical immobilization, fragile biomolecules can be preserved from harsh environmental factors, and released with high degree of controllability by tailoring molecular weight, crosslinking and morphology of the carrier materials. Generally, these degradation-controlled release systems are favored over other release mechanisms since biomolecules are presented at the

treatment site in a so-called matrix-bound manner, similar to the way in which biomolecules are presented in the physiological environment⁹³⁻⁹⁶.

4.4. Stimuli-triggered release

Recently, intelligent delivery systems have gained considerable attention owing to their capacity to release biomolecules governed by environmental factors (e.g. pH, protein, glucose) or by external stimuli (e.g. temperature, ultrasound and irradiation)^{88, 94}. These devices are referred to as “programmed” or “triggered” release systems, which show great potential for use in sequentially or spatiotemporally controlled delivery of multiple biomolecules^{88, 94}. For example, self-exploding microcapsules based on a biodegradable microgel core surrounded by a bio-polyelectrolyte membrane have been developed, which can release their content in a pulsatile manner after a certain incubation time at physiological conditions^{97, 98}.

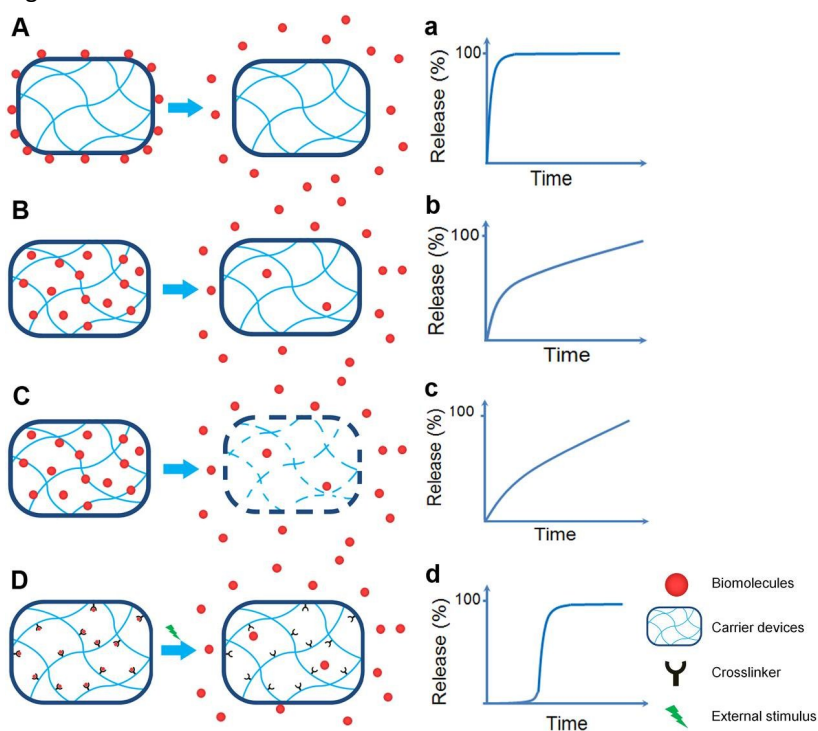


Figure 2. Schematic diagram of various mechanisms for biomolecules release from carrier devices. (A-D) and typical corresponding pharmacokinetics (a-d). (A) and (a), desorption-controlled release; (B) and (b), diffusion-controlled release; (C) and (c), degradation-controlled model; (D) and (d), stimuli-triggered release.

5. Carrier devices for delivery of biomolecules

From a materials perspective, the design of delivery systems plays a critical role for controlled delivery of biomolecules with respect of chemical composition (including polymer, ceramics and composites) and geometry (such as micro/nanoparticles, membrane and bulk materials). Therefore, in this section, we particularly focus on the classification of delivery carriers by reviewing the delivery systems that have been extensively used in CMF bone regeneration.

Microparticles (MP) and, more recently, nanoparticles (NP), are the most extensively used platforms for controlled delivery of biomolecules, owing to their inherently small size and corresponding large specific surface area, a high drug loading efficiency, a high reactivity towards surrounding tissues *in vivo* as well as a high diffusibility and mobility of drug-loaded particles^{94, 99-103}.

The basic strategy of using particles for biomolecules delivery is to simply adsorb them onto the particle surface or encapsulate them inside the particle, and release their payload by desorption, diffusion, or degradation depending on the chemical composition and geometry of the delivery vehicle. Recently, microcapsules have been developed to physically encapsulate labile biomolecules and prevent them from the harsh environment. Release profiles of encapsulated biomolecules normally display sustained release kinetics favorable for long-term delivery in comparison to molecules adsorbed onto biomaterial surfaces^{104, 105}. Another strategy is to incorporate biomolecule-loaded (via adsorption or encapsulation) particles into a continuous matrix of monolithic biomaterials, and hence gain prolonged retention of biomolecules, and simultaneously provide bulk materials with enhanced features for sustained release of biomolecules^{94, 99, 100, 106-108}. Moreover, the use of particles facilitates programmable delivery of multiple biomolecules with precise spatiotemporal control over the distribution through carrier materials and release profiles of various molecules^{109, 110}.

Membranes have been extensively used in CMF tissue regeneration by acting as scaffolding matrix supporting cell adhesion and proliferation, as well as effective biomolecules delivery carriers likely due to the large tissue-biomaterial interface. Especially, guided bone regeneration (GBR) technique has recently emerged as a promising approach by employing membrane materials, which mechanically exclude non-osteogenic cell populations from the surrounding soft tissues, thus securing the population of osteogenic cells and osteoconduction events^{111, 112}. More importantly, therapeutic components can be loaded to GBR membranes via different strategies, aiming to improve bone healing. Direct incorporation of biomolecules normally leads to a desorption-controlled release profile with complete release of loaded agents within days, while the introduction of additional carriers (such as MP/NPs) as molecules delivery vectors gives rise to a more sustained release, which is typically tailored by a combination of biomolecules diffusion

and membrane degradation¹¹³.

Hydrogels are one of the most important groups of biomaterials for tissue regeneration and controlled delivery. Hydrogels are widely used in the biomedical field because of their favorable biological performance, hydrophilic nature, mild preparation conditions, versatility for biomolecule encapsulation, tunable release characteristics, and injectability/moldability¹¹⁴. The three-dimensional hydrophilic network of hydrogels facilitates absorption of large volumes of aqueous solutions, allowing either physical or chemical immobilization of molecules into the polymer network, thereby protecting biomolecules from detrimental conditions¹¹⁵. Hydrogels have been increasingly advocated as promising devices for delivery of biomolecules and stem cells, which can be obtained via minimally invasive methods to fill shape-specific defects¹¹⁶. Injectable hydrogel precursors can be easily delivered and subsequently solidified *in situ* via either physical or chemical cross-linking^{116, 117}. Especially, physical gels undergoing gelation based on physical interactions (e.g. electrostatic or hydrophobic interactions) are highly suitable for carrying biomolecules⁹². Colloidal gels comprising electrostatically crosslinked PLGA nanocapsules have recently been developed as injectable carrier material for release of dexamethasone according to a zero-order manner *in vitro*¹¹⁸. However, it needs to be emphasized that due to their poor mechanical properties, hydrogels are barely used for load-bearing applications.

Ceramic materials such as calcium phosphate (CaP) ceramics also showed potential for use in localized delivery of biomolecules as granules, bulk scaffolds or injectable cements¹¹⁹. Due to the high affinity of ceramics for biomolecules, ceramic carriers can easily adsorb biomolecules, thus resulting into strong retention of biomolecules. Alternatively, CaP nanoparticles display an extremely high surface-to-volume ratio which -in addition to their tunable phase composition and capacity to permeate cell membranes- offers specific advantages for controlled delivery of biomolecules¹²⁰⁻¹²³. On the other hand, injectable calcium phosphate cements (CPC) have been investigated as injectable reservoirs of biomolecules. Biomolecules can be added to the cement by simply adding biomolecules to the liquid hardener, thereby obtaining homogeneous distribution throughout the cement matrix. Further, additional carriers (e.g. PLGA microspheres) can be mixed with cement to encapsulate biomolecules¹²⁴⁻¹²⁶ in order to protect the biological activity and obtain a more controlled release profile of loaded biomolecules.

6. Preclinical evaluation of different carriers with biomolecules delivery

Although different categories of carrier devices have been developed in the past decades to achieve local delivery of different biomolecules, the functional evaluation of these carrier devices is mostly based on *in vitro* model systems (i.e. model protein release, bio activity assay). However, *in vitro* cell-based systems cannot fully reflect the *in vivo* re-

lease kinetics of biomolecules as well as the tissue performance evoked by the biomolecule gradients. Therefore, it is necessary to set up animal models and use these preclinical models¹²⁷ to fully understand the biological performance of these devices in an entire organism and as such make a translational step from bench-side to organism¹²⁸. Although different animal models for biomolecule delivery have been recently reviewed regarding long bone defects¹²⁹, it has to be emphasized that the biological performance of biomolecules has to be evaluated under similar conditions as present in the intended application due to e.g. differences in the bone formation process in different anatomical locations, effect of local conditions on biomolecule release and efficacy, and effect of local conditions on the response to the carrier material. Therefore, the next section of this review will summarize the biological performance of the biomolecules delivered by the afore-mentioned carriers in representative animal models specifically for CMF bone reconstruction.

6.1. Animal models used in CMF bone reconstruction

For studies investigating CMF bone reconstruction, it is important to understand the species-specific bone characteristics, including bone microstructure and composition, as well as bone modelling and remodelling properties when generalizing the obtained results to the clinical situation¹³⁰. Since no single animal model will be appropriate to meet all requirements, as a consequence, different animal models, including small and large size animals have both been involved in the evaluation of CMF bone reconstruction. Small animals mainly include rodents such as mouse, rat, and guinea pig as well as non-rodents, such as rabbits. Due to their easy maintenance and relatively low cost, small animal models are frequently used in CMF bone regeneration research to obtain fundamental and applied knowledge about the performance of biomaterials. However, the limited CMF area obtained from those animals raises difficulties in surgery. Compared to the small animal models, large animals (e.g. sheep, minipig, dog, and non-human primate) provide larger defect sizes for more control in the surgical area⁵, and more close physiology to humans, but the expensive housing cost, as well as the related ethical issues hinder their usage in biomedical research.

6.1.1. Calvarial defects

Calvarial defects represent the most commonly used defect model in CMF bone reconstruction because calvarial defects provide good first phase (non-load bearing) bone healing models with relative biological inertness due to poor blood supply and limited bone marrow, which is thought to resemble the atrophic mandibular bone in humans¹³⁰. The standard rodent calvarial bone defect is typically created by using a trephine drill that makes a circular defect in the cranial skeleton on the midline⁵ (Figure 3). Researchers recognized that the defects are critical sized depending on their size (5 mm diameter

in mouse, and 8 mm in rat)¹³¹, which means that these are “above the threshold size intraosseous defect dimensions that will not heal spontaneously during the lifetime of the animal”¹³². However, in recent years, some researchers suggested that the use of the term of “critical sized defect” had to be discontinued¹³¹, because the definition of a critical sized defect is based on the *size* of the defect that will not heal within the *life time* of the animal, whereas most studies in reality are of limited duration. Consequently, many calvarial defects below the threshold of critical sized have been investigated in previous studies. Instead of creating one defect in the center of the skull, a bilateral calvarial defect model was also developed by creating one defect (5 mm diameter in rat¹³³, 8 mm diameter in rabbit¹³⁴) in each parietal (cranial) bone next to the middle line, which reduces the risk of significant trauma to the sagittal suture.

In addition to studying the healing pattern in the CMF skeleton, calvarial defect models also enable monitoring the *in vivo* release kinetics of loaded biomolecules by using fluorescent or gamma radioactive signals^{135, 136} owing to its superficial location. On the other hand, this model also involves additional requirements for the surgical techniques as well as the mechanical properties of filling materials. It is suggested the sagittal suture and the dura mater underlying the defect have to be carefully protected during the surgery, which is important for the cranial skeleton healing¹³¹. Furthermore, the filling material should be strong and resistant enough to avoid the dilation of brain tissue beneath the defect.

6.1.2. Periodontal and mandibular bony defects

Besides the calvarial defect, the periodontal and mandibular bony defect models are also very useful in the evaluation of periodontal bone regeneration as well as mandibular reconstruction. Periodontal and mandibular bone defect models include the suprainfrabony defect, periodontal fenestration defect, artificial furcation defects, guided bone regeneration (GBR) defect, as well as the segmental defect in the mandible. Due to the small size of the surgical area, periodontal and mandibular bone defects are usually created in relatively large-size animals (e.g. rat, rabbit, dog, etc.) in order to gain sufficient surgical field view and practical surgical access. Further, the unique location of this defect model also requires the carrier device to be adaptable to provide space maintenance as graft materials, and to support the mucoperiosteal flap or to restrict the epithelial down growth as barrier membrane¹³⁷.

The surrainfrabony defect was developed by Nemcovsky et al¹³⁸ to investigate periodontal tissue regeneration. In this model, bone defects of reasonable dimensions were created at the mesial aspect of the mesial root of the first maxillary molar in rats. Periodontal fenestration defects were usually created bilaterally at the first and second molars in the mandible using an ultrasonic device to remove the alveolar bone (Figure 3), together with the periodontal ligament and cementum, and followed by preparation of a

square shape bone window (e.g. 4×4 mm in rabbit)¹³⁹. Artificial furcation defects were performed by removing 5 mm of coronal bone and 2 mm of horizontal bone within the furcation site of the third molar to mimic the class II furcation defect, which is a common symptom for periodontitis¹⁴⁰. Additionally, Salata et al¹⁴¹ produced 3-mm diameter bilateral transcortical defects in the mandibular ramus as an effective model to evaluate the biological performance of a GBR membrane. Beside the aforementioned models that mainly focus on the periodontal bone regeneration, the mandibular segmental defect is an important model, which aims specifically at mandibular reconstruction. Mandibular segmental defects are often created in ruminating animals, like sheep and goats are, because these animals have mandibles that come close to the human anatomy as far as the gonial region is concerned¹⁴². Fennis et al¹⁴² created a 3 mm wide segmental defect in goat mandible after careful ligation of neurovascular bundle that enters the mandible. It needs to be mentioned that mandibular segmental defect was performed unilaterally in order to avoid malocclusion and subsequent jaw function disturbance of animals. Further, the bone stumps at each side of the defect were stabilized with specially designed fixation plates.

6.1.3. Sinus elevation

Sinus elevation is a frequently used model to study bone augmentation by using bone grafting materials, because it is commonly used in dental clinics to improve the height of sinus floor to support dental implant placement. Preclinical models for sinus elevation are usually set in large animals, including rabbits¹⁴³, goat¹⁴⁴, sheep¹⁴⁵ and pigs¹⁴⁶. The basic approach to the sinus (Caldwell-Luc operation) involves an osteotomy performed on the lateral maxillary wall, elevation of the Schneiderian membrane, and placement of bone graft material, which can be derived from autogenous bone, allografts (harvested from human cadavers), alloplasts (synthetic materials), and xenografts (grafts from a nonhuman species)¹⁴⁷ (Figure 3).

6.2. Biological performance of locally delivered biomolecules

Given the multiple types of candidate biomolecules involved in CMF bone healing, current preclinical studies still mainly focus on the morphogenetic molecule and angiogenic molecule delivery, and only limited research involves local application of small molecule drugs.

Among different types of morphogenetic molecules, recombinant human BMPs (rhBMPs) are the most commonly used for the animal study because of its dominant osteoinduction. It is reported that rhBMP-2 coated onto titanium porous oxide implant surfaces induced clinically relevant local bone formation including vertical augmentation of the alveolar ridge and osseointegration¹⁴⁸. Successful *in vivo* rhBMP-2 delivery has been

achieved using particles¹⁴⁹, hydrogels^{150, 151}, electrospun membranes¹⁵², as well as CaP cement¹⁵³. The local delivery of rhBMP2 using different carriers has been evaluated in calvarial defect^{149, 152, 153}, mandibular-alveolar defect^{150, 154} as well as sinus elevation models^{144, 151}, which all concluded that bone formation was enhanced in the defect site after local delivery of rhBMP-2. Instead of directly BMPs delivery, Jiang et al recently reported the use of adenovirus encoding BMP-2 (AdBMP-2) transfected bone marrow cells seeded onto a β -TCP carrier¹⁵⁵ and ceramic scaffolds¹⁴³, and the BMP-2 gene transfected cells significantly improved sinus floor bone augmentation in New Zealand White rabbits after 8 weeks compared to the bare materials. Instead of using BMP-2, Zhang et al¹⁵⁶ recently reported that adenovirus encoding BMP-7 (AdBMP-7) could be delivered via silk fibroin scaffolds prepared by solid-liquid phase separation and improved new bone formation in mouse calvarial defect compared to the silk scaffold containing virus alone. Besides the BMPs, TGF- β 1 has also been evaluated *in vivo* to improve the CMF bone formation. Blom et al.¹³⁵ mixed rhTGF- β 1 in CaP-cement during setting and implanted the mixture in a rat calvarial defect. Their results indicated that TGF- β 1 loaded CaP stimulated bone growth in the defect site after 8 weeks of implantation compared to non-loaded scaffolds, although the effect was minimal. In addition to the commercial recombinant growth factors, enamel matrix derivatives (EMDs), which are commercially available as Emdogain[®], have already been clinically applied and are considered to enhance bone regeneration. It has also been hypothesized that EMDs show osteopromotive capability because of the presence of bone growth stimulating factors¹⁵⁷. On the other hand, Nemcovsky et al¹³⁸ achieved local delivery of Emdogain[®] via propylene glycol alginate in suprainfrabony defect in rat, and showed that Emdogain[®] induced new cementum formation, but limited new bone formation compared to plain alginate.

Delivery of angiogenic molecules is also explored in preclinical studies of CMF bone regeneration in recent research, because it was found that exogenous VEGF enhanced BMP2-induced bone formation and bone healing by improving angiogenesis, which in turn led to accelerated cartilage resorption and enhanced mineralized bone formation¹⁵⁸. The single VEGF delivery or dual delivery of VEGF combined with BMP2 in calvarial defect has been achieved using calcium phosphate ceramics¹⁵⁹, and gelatin particles^{160, 161}. It has been reported that VEGF release at low concentration from ceramic scaffolds is beneficial for bone regeneration¹⁵⁹. However, the addition of VEGF did not affect the amount of bone formation achieved by BMP-2^{160, 161}, which confirmed the dominant osteoinductive function of BMPs. Previous research also revealed that the local application of platelet-rich plasma (PRP), which is considered to be a rich source of autologous growth factors, also improved bone formation in rabbit cranial defects¹⁶².

As mentioned above, published reports on the *in vivo* efficacy of small molecules delivery in CMF bone regenerative therapy are rather limited. Most of such studies have been

conducted to explore the local delivery of antibiotics¹⁶³⁻¹⁶⁶ to reduce bone loss in alveolar and jaw bone caused by infectious disease. Local antibiotic therapy via antibiotic-impregnated cement was used for osteomyelitis⁵⁵. As an alternative to introducing large deposits of antibiotic-impregnated cement at sites of chronic osteomyelitis, gentamicin-impregnated cement beads can temporarily fill the dead space created by the debridement of infected bone⁵⁵. Besides the osteomyelitis, the local delivery of doxycycline in an alveolar bone defect was reported by using membrane¹⁶⁷ and nanoparticles¹⁶⁶, and it was shown that the topical application of doxycycline resulted in a more pronounced new bone formation in the defects compared to the group without antibiotics, which indicated that the local delivery of antibiotics is beneficial for the treatment of periodontitis related bone loss. Furthermore, a recent study revealed that the combined delivery of antibiotics and BMP-2 resulted in more new bone formation and a modest infection compared to BMP-2 delivery alone in rat calvarial defects¹⁶⁸. Most importantly, the incorporated antibiotics did not interfere with the biological activity of BMP-2¹⁶⁹, demonstrating that anti-infection therapy is important to improve the clinical outcome of contaminated open fractures.

In addition to antibiotics, anti-osteoporotics such as bisphosphonates¹⁷⁰⁻¹⁷⁶ have been delivered into alveolar bone defects to reduce bone resorption. Yaffe et al¹⁷¹ reported that the topical application of 20 mg/ml of alendronate, as applied at the surgical mucoperiosteal site, produced a striking reduction of alveolar bone loss in the rat model. They also found that the alendronate gave an adequate distribution of bisphosphonate to the bone, because of the high affinity to bone mineral¹⁷⁶. In addition, the effect of alendronate can be synergistically enhanced when combined with local delivery of tetracycline¹⁷⁰. However, concern is emerging related to the potential risks of alendronate application. Bodde et al¹⁷⁷ discovered that a high dose of alendronate (8.8 mg per implant) resulted in cell death of fibroblasts surrounding the alendronate specimen after 72h incubation. Recently, osteonecrosis of the jaw (ONJ) has been linked to the use of bisphosphonates, which raises another critical concern for bisphosphonates delivery. Bisphosphonate-related ONJ is defined as the presence of “exposed, necrotic bone” of the jaw or face that has been present for at least 8 weeks in a patient who has received bisphosphonate treatment but has not been exposed to radiation therapy¹⁷⁸. A total of 481 patients with ONJ were reported in previous studies in the 44 case reports¹⁷⁹. Although the reported cases were mostly associated with intravenous or oral administration of bisphosphonates, it stresses the fact that the efficacy and safety of topical application of bisphosphonates should be studied in more details.

Considering the potential risks of bisphosphonates, the topical delivery of NMP and statins appears to be a promising approach to enhance bone generation. Miguel et al¹⁸⁰ investigated the *in vivo* performance of PLGA-based guided bone regeneration membrane with or without NMP treatment in rabbit calvarial defects (6 mm in diameter), and

their results showed that the membrane with NMP resulted in significantly enhanced bone regeneration after 4 weeks via increased BMP-2 activity. These results highlighted NMP as a novel, locally applicable drug for accelerated bone regeneration. Besides NMP, the osteopromotive effect of local delivery of statins has been investigated using different carriers in various animal models. Previous research revealed that gelatin sponges with incorporated statins resulted in 2-fold increased new bone formation compared to plain materials in 3 mm diameter defects in the angulus mandibular region of rats¹⁸¹. Nyan et al^{182, 183} implanted calcium phosphate loaded with statins in rat calvarial defects, and their results showed that the combination of statins and calcium phosphate remarkably stimulated bone regeneration after 8 weeks of implantation.

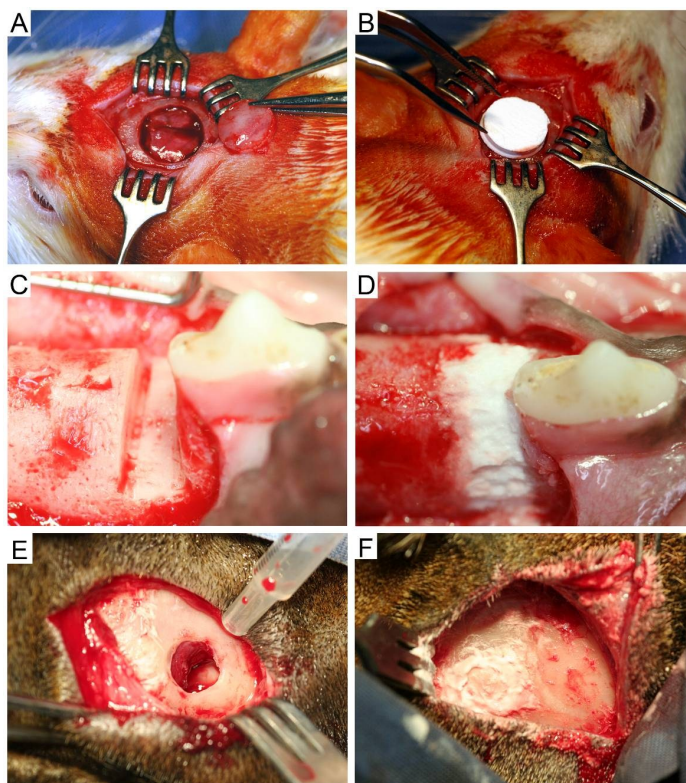


Figure 3. Animal models used in CMF bone reconstruction. (A) Critical-sized calvarial bone defect (diameter 8 mm) was created using rat, and (B) filled with pre-set calcium phosphate cement (CPC) containing PLGA microspheres. (C) Mandibular bone defect (4 mm depth, 5 mm height) was created in Beagle dog, and (D) treated using CPC containing growth factor loaded PLGA microspheres. (E) Sinus elevation in sheep. A bony window (diameter 10mm) was created to access to the maxillary sinus, and (F) filled with CPC.

7. Future perspective

Surgical interventions based on the concepts of tissue engineering and regenerative medicine are evolving as promising strategies for the reconstruction of bony defects in

the CMF area. Controlled local delivery of therapeutic biomolecules is a particularly powerful tool to this end by combining local pharmacotherapy with tissue-engineered carrier devices. In this way, the clinical success of regenerative craniofacial surgery can be considerably improved, especially in patients with compromised healing conditions. Among the various choices for certain bioactive molecules, small molecules (< 5kDa) are particularly promising for future biomedical applications due to their therapeutic efficacy, relatively simple synthesis and long-term stability, thus allowing for cost-effective industrial upscaling of production and commercialization.

However, despite a substantial number of *in vivo* studies, the vast majority of studies that report on local delivery of biomolecules in CMF bone are still the pre-clinical testing phase, whereas data from clinical trials is limited. This infantile status can be attributed to two main reasons. First of all, although systemic delivery of biomolecules has been extensively investigated, local delivery of such biomolecules from carrier devices still needs to be optimized. For instance, optimal *in vivo* dosing of biomolecules for local delivery is still largely unknown. Furthermore, translation of data on dosing from preclinical to clinical studies is hardly possible. Secondly, the aforementioned drug delivery vehicles generally are categorized as medical devices incorporating, as an integral part, an ancillary medicinal substance. As a result, these medical delivery devices belong to the 'Class III' devices, *which are usually those that support or sustain human life, are of substantial importance in preventing impairment of human health, or which present a potential, unreasonable risk of illness or injury* (General and Special Controls. Medical Devices. FDA. Retrieved 2010-10-15). It is obligatory to obtain a premarket approval (PMA) for a 'Class III' device to fully prove its safety and efficacy prior to final clinical application. The regulatory pathway for these devices is rather complicated which has hampered translation of basic knowledge towards clinical applications.

Compared to cell therapy and tissue engineering strategies that employ encapsulated cells, clinical application of local delivery of biomolecules is still far more feasible from a regulatory and ethical point of view. Therefore, extensive research needs to be carried out to optimize local delivery of biomolecules, particularly small molecules, in terms of loading, dosing, and controlled release from suitable carrier biomaterials.

8. Conclusions

Currently, a wide interest exists in local delivery of small and large biomolecules for CMF bone regeneration. In addition to inflammatory cyto- and chemokines, morphogenetic and angiogenic factors, small molecules are rapidly emerging in recent years as an interesting adjunct for upgrading the clinical treatment of CMF bone regeneration under compromised healing conditions. Small molecules (including antibiotics, AMPs, antitumor drug, siRNA and shRNA, as well as anti-osteoporotics) can effectively interfere with infec-

tion, tumor-metastasis and osteoporosis, thereby considerably improving conditions for bone regeneration.

Regardless of the biomolecules, the carrier device should be able to preserve the biological activity of biomolecules and offer controlled release kinetics to yield an optimal tissue response. Different materials have been investigated as carrier device, including particles, membranes, hydrogels, and ceramic scaffolds. The release of biomolecules from these carrier devices can be controlled via desorption, diffusion, degradation, and stimuli-triggered mechanisms.

So far, different kinds of preclinical models have been developed to evaluate the efficiency and efficacy of biomolecules-loaded carrier devices in CMF bone regeneration, in which calvarial defects, mandibular and alveolar bony defects and sinus elevation are included. Most of the preclinical studies have so far been focused on the morphogenetic molecules and angiogenic molecules delivery, and quite limited research involved delivery of small molecules.

9. References

1. Allareddy, V.; Allareddy, V.; Nalliah, R. P. *J Oral Maxillofac Surg* **2011**, 69, 2613-2618.
2. Disa, J. J.; Cordeiro, P. G. *Semin Surg Oncol* **2000**, 19, 226-234.
3. Emerick, K. S.; Teknos, T. N. *Expert Rev Anticancer Ther* **2007**, 7, 1781-1788.
4. Hallman, M.; Thor, A. *Periodontol 2000* **2008**, 47, 172-192.
5. Szpalski, C.; Barr, J.; Wetterau, M.; Saadeh, P. B.; Warren, S. M. *Neurosurg Focus* **2010**, 29, E8.
6. Smith, D. M.; Cooper, G. M.; Mooney, M. P.; Marra, K. G.; Losee, J. E. *J Craniofac Surg* **2008**, 19, 1244-1259.
7. Porter, J. R.; Ruckh, T. T.; Popat, K. C. *Biotechnology Progress* **2009**, 25, 1539-1560.
8. Langer, R.; Vacanti, J. P. *Science* **1993**, 260, 920-926.
9. Martins, A.; Duarte, A. R. C.; Faria, S.; Marques, A. P.; Reis, R. L.; Neves, N. M. *Biomaterials* **2010**, 31, 5875-5885.
10. Wang, F.; Li, Z. Q.; Khan, M.; Tamama, K.; Kuppusamy, P.; Wagner, W. R.; Sen, C. K.; Guan, J. *J. Acta Biomaterialia* **2010**, 6, 1978-1991.
11. Murphy, W. L.; Peters, M. C.; Kohn, D. H.; Mooney, D. J. *Biomaterials* **2000**, 21, 2521-2527.
12. Moioli, E. K.; Clark, P. A.; Xin, X.; Lal, S.; Mao, J. J. *Adv Drug Deliv Rev* **2007**, 59, 308-324.
13. Ji, W.; Sun, Y.; Yang, F.; van den Beucken, J.; Fan, M. W.; Chen, Z.; Jansen, J. A. *Pharm Res* **2011**, 28, 1259-1272.
14. Kitaori, T.; Ito, H.; Schwarz, E. M.; Tsutsumi, R.; Yoshitomi, H.; Oishi, S.; Nakano, M.; Fujii, N.; Nagasawa, T.; Nakamura, T. *Arthritis Rheum* **2009**, 60, 813-823.
15. Giannoudis, P.; Psarakis, S.; Kontakis, G. *Injury* **2007**, 38, S81-S89.
16. Lee, S. H.; Shin, H. *Adv Drug Deliv Rev* **2007**, 59, 339-359.
17. Putney, S. D.; Burke, P. A. *Nat Biotechnol* **1998**, 16, 153-157.
18. Olsen, B. R.; Reginato, A. M.; Wang, W. *Annu Rev Cell Dev Biol* **2000**, 16, 191-220.
19. Yang, Y. *Crit Rev Eukaryot Gene Expr* **2009**, 19, 197-218.
20. Opperman, L. A. *Dev Dyn* **2000**, 219, 472-485.
21. Mackie, E. J.; Ahmed, Y. A.; Tatarczuch, L.; Chen, K. S.; Mirams, M. *Int J Biochem Cell Biol* **2008**, 40, 46-62.
22. Gawlitta, D.; Farrell, E.; Malda, J.; Creemers, L. B.; Alblas, J.; Dhert, W. J. *Tissue Eng Part B Rev* **2010**, 16, 385-395.
23. Gorr, S. U.; Abdolhosseini, M. *J Clin Periodontol* **2011**, 38, 126-141.
24. Carek, P. J.; Dickerson, L. M.; Sack, J. L. *Am Fam Physician* **2001**, 63, 2413-2420.
25. Wald, E. R. *Am J Med* **1985**, 78, 206-212.
26. Eichhorn, W.; Wehrmann, M.; Blessmann, M.; Pohlenz, P.; Blake, F.; Schmelzle, R.; Heiland, M. *Oral Surg Oral Med Oral Pathol Oral Radiol Endod* **2010**, 109, 582-586.
27. Tsiridis, E.; Upadhyay, N.; Giannoudis, P. *Injury* **2007**, 38, S11-S25.
28. Feghali, C. A.; Wright, T. M. *Front Biosci* **1997**, 2, d12-26.
29. Brodbeck, W. G.; Voskerician, G.; Ziats, N. P.; Nakayama, Y.; Matsuda, T.; Anderson, J. M. *J Biomed Mater Res A* **2003**, 64, 320-329.
30. Dinarello, C. A. *Chest* **2000**, 118, 503-508.

31. Peled, A.; Petit, I.; Kollet, O.; Magid, M.; Ponomaryov, T.; Byk, T.; Nagler, A.; Ben-Hur, H.; Many, A.; Shultz, L.; Lider, O.; Alon, R.; Zipori, D.; Lapidot, T. *Science* **1999**, *283*, 845-848.
32. Sordi, V.; Malosio, M. L.; Marchesi, F.; Mercalli, A.; Melzi, R.; Giordano, T.; Belmonte, N.; Ferrari, G.; Leone, B. E.; Bertuzzi, F.; Zerbini, G.; Allavena, P.; Bonifacio, E.; Piemonti, L. *Blood* **2005**, *106*, 419-427.
33. Higashino, K.; Viggewarapu, M.; Bargouti, M.; Liu, H.; Titus, L.; Boden, S. D. *Tissue Eng Part A* **2010**, *17*, 523-530.
34. Gerstenfeld, L. C.; Cho, T. J.; Kon, T.; Aizawa, T.; Tsay, A.; Fitch, J.; Barnes, G. L.; Graves, D. T.; Einhorn, T. A. *J Bone Miner Res* **2003**, *18*, 1584-1592.
35. Nie, X.; Luukko, K.; Kettunen, P. *Int J Dev Biol* **2006**, *50*, 511-521.
36. Hatch, N. E. *Crit Rev Eukaryot Gene Expr* **2010**, *20*, 295-311.
37. Cohen, M. M., Jr. *Am J Med Genet A* **2010**, *152A*, 1875-1914.
38. Agholme, F.; Aspenberg, P. *Acta Orthop* **2011**, *82*, 125-130.
39. Wozney, J. M. *Prog Growth Factor Res* **1989**, *1*, 267-280.
40. Ripamonti, U.; Herbst, N. N.; Ramoshebi, L. N. *Cytokine Growth Factor Rev* **2005**, *16*, 357-368.
41. Heliotis, M.; Ripamonti, U.; Ferretti, C.; Kerawala, C.; Mantalaris, A.; Tsidis, E. *Br J Oral Maxillofac Surg* **2009**, *47*, 511-514.
42. Itoh, N.; Ornitz, D. M. *Trends Genet* **2004**, *20*, 563-569.
43. Nie, X.; Luukko, K.; Kettunen, P. *Oral Dis* **2006**, *12*, 102-111.
44. Willert, K.; Brown, J. D.; Danenberg, E.; Duncan, A. W.; Weissman, I. L.; Reya, T.; Yates, J. R., 3rd; Nusse, R. *Nature* **2003**, *423*, 448-452.
45. Young, D. L.; Schneider, R. A.; Hu, D.; Helms, J. A. *Crit Rev Oral Biol Med* **2000**, *11*, 304-17.
46. Alsberg, E.; Hill, E. E.; Mooney, D. J. *Crit Rev Oral Biol Med* **2001**, *12*, 64-75.
47. Gerstenfeld, L. C.; Cullinane, D. M.; Barnes, G. L.; Graves, D. T.; Einhorn, T. A. *J Cell Biochem* **2003**, *88*, 873-884.
48. Keramaris, N. C.; Calori, G. M.; Nikolaou, V. S.; Schemitsch, E. H.; Giannoudis, P. V. *Injury* **2008**, *39*, S45-57.
49. Vaibhav, B.; Nilesh, P.; Vikram, S.; Anshul, C. *Injury* **2007**, *38*, 1227-1235.
50. Lehmann, W.; Edgar, C. M.; Wang, K.; Cho, T. J.; Barnes, G. L.; Kakar, S.; Graves, D. T.; Rueger, J. M.; Gerstenfeld, L. C.; Einhorn, T. A. *Bone* **2005**, *36*, 300-310.
51. Suzuki, Y.; Tanihara, M.; Suzuki, K.; Saitou, A.; Sufan, W.; Nishimura, Y. *J Biomed Mater Res* **2000**, *50*, 405-409.
52. Saito, A.; Suzuki, Y.; Ogata, S.; Ohtsuki, C.; Tanihara, M. *J Biomed Mater Res A* **2005**, *72*, 77-82.
53. Chen, Y.; Webster, T. J. *J Biomed Mater Res A* **2009**, *91*, 296-304.
54. Bergeron, E.; Leblanc, E.; Drevelle, O.; Giguere, R.; Beauvais, S.; Grenier, G.; Faucheux, N. *Tissue Eng Part A* **2012**, *18*, 342-352.
55. Rao, N.; Ziran, B. H.; Lipsky, B. A. *Plast Reconstr Surg* **2011**, *127*, 177S-187S.
56. Heitz-Mayfield, L. J. *Aust Dent J* **2009**, *54*, S96-101.
57. Bidault, P.; Chandad, F.; Grenier, D. *J Can Dent Assoc* **2007**, *73*, 721-725.
58. Guarneri, V.; Conte, P. F. *Eur J Nucl Med Mol Imaging* **2004**, *31*, S149-161.

59. Li, Y. L.; Quarles, L. D.; Zhou, H. H.; Xiao, Z. S. *Biochem Biophys Res Commun* **2007**, 361, 817-821.
60. Aigner, A. *Appl Microbiol Biotechnol* **2007**, 76, 9-21.
61. Hicklin, D. J.; Ellis, L. M. *J Clin Oncol* **2005**, 23, 1011-1027.
62. Liu, T.; Ye, L.; Chen, X.; Peng, J.; Zhang, X.; Yi, H.; Peng, F.; He, Y.; Leng, A. *Exp Mol Pathol* **2011**, 91, 745-752.
63. Payne, J. B.; Golub, L. M. *Pharmacol Res* **2011**, 63, 121-129.
64. Ghayor, C.; Corroero, R. M.; Lange, K.; Karfeld-Sulzer, L. S.; Gratz, K. W.; Weber, F. E. *J Biol Chem* **2011**, 286, 24458-24466.
65. Alexander, I. M. *Nurse Pract* **2009**, 34, 30-40; quiz 41.
66. Horiuchi, N.; Maeda, T. *Oral Dis* **2006**, 12, 85-101.
67. Mundy, G.; Garrett, R.; Harris, S.; Chan, J.; Chen, D.; Rossini, G.; Boyce, B.; Zhao, M.; Gutierrez, G. *Science* **1999**, 286, 1946-1949.
68. Mundy, G. R. *Bone* **2001**, 29, 495-497.
69. Sugiyama, M.; Kodama, T.; Konishi, K.; Abe, K.; Asami, S.; Oikawa, S. *Biochem Biophys Res Commun* **2000**, 271, 688-692.
70. Luginbuehl, V.; Meinel, L.; Merkle, H. P.; Gander, B. *Eur J Pharm Biopharm* **2004**, 58, 197-208.
71. Ji, W.; Sun, Y.; Yang, F.; van den Beucken, J.; Fan, M. W.; Chen, Z.; Jansen, J. A. *Pharm Res* **2011**, 28, 1259-1272.
72. Könnings, S.; Göpferich, A., Lipospheres as Delivery Systems for Peptides and Proteins. In *Lipospheres in drug targets and delivery: approaches, methods, and applications*, Nastruzzi, C., Ed. CRC Press LLC: 2005; 67-86.
73. Roy, K.; Wang, D.; Hedley, M. L.; Barman, S. P. *Mol Ther* **2003**, 7, 401-408.
74. Storrie, H.; Mooney, D. J. *Adv Drug Deliv Rev* **2006**, 58, 500-514.
75. Thomas, C. E.; Ehrhardt, A.; Kay, M. A. *Nat Rev Genet* **2003**, 4, 346-358.
76. Dinbergs, I. D.; Brown, L.; Edelman, E. R. *J Biol Chem* **1996**, 271, 29822-29829.
77. Seeherman, H.; Wozney, J. M. *Cytokine Growth Factor Rev* **2005**, 16, 329-345.
78. Huang, X.; Brazel, C. S. *J Control Release* **2001**, 73, 121-136.
79. Grassi, M.; Grassi, G. *Curr Drug Deliv* **2005**, 2, 97-116.
80. Gautschi, O. P.; Frey, S. P.; Zellweger, R. *ANZ J Surg* **2007**, 77, 626-631.
81. Giannoudis, P. V.; Kanakaris, N. K.; Einhorn, T. A. *Osteoporos Int* **2007**, 18, 1565-1581.
82. Nie, H.; Ho, M. L.; Wang, C. K.; Wang, C. H.; Fu, Y. C. *Biomaterials* **2009**, 30, 892-901.
83. Nie, H.; Wang, C. *J Control Release* **2007**, 120, 111-121.
84. Chen, Z. G. *Trends Mol Med* **2010**, 16, 594-602.
85. Haidar, Z.; Hamdy, R.; Tabrizian, M. *Biotechnology Letters* **2009**, 31, 1817-1824.
86. Tayalia, P.; Mooney, D. J. *Adv Mater* **2009**, 21, 3269-3285.
87. Luginbuehl, V.; Meinel, L.; Merkle, H. P.; Gander, B. *Eur J Pharm Biopharm* **2004**, 58, 197-208.
88. Chen, F.-M.; Zhang, M.; Wu, Z.-F. *Biomaterials* **2010**, 31, 6279-6308.
89. Mahmoudi, M.; Lynch, I.; Ejtehadi, M. R.; Monopoli, M. P.; Bombelli, F. B.; Laurent, S. *Chemical Reviews* **2011**, 111, 5610-5637

90. Anglin, E. J.; Cheng, L.; Freeman, W. R.; Sailor, M. J. *Adv Drug Deliv Rev* **2008**, 60, 1266-1277.
91. Sharon, J. L.; Puleo, D. A. *Acta Biomater* **2008**, 4, 1016-1023.
92. Lin, C.-C.; Metters, A. T. *Adv Drug Deliv Rev* **2006**, 58, 1379-1408.
93. Degat, M.-C.; Dahri-Correia, L.; Lavigne, F.; Meunier, A.; Sedel, L.; Correia, J.; Petite, H.; Logeart-Avramoglou, D. *J Biomed Mater Res Part A* **2009**, 91A, 1178-1188.
94. Biondi, M.; Ungaro, F.; Quaglia, F.; Netti, P. A. *Adv Drug Deliv Rev* **2008**, 60, 229-242.
95. Masters, K. S. *Macromol Biosci* **2011**, 11, 1149-63
96. Chiu, L. L. Y.; Radisic, M. *Biomaterials* **2010**, 31, 226-241.
97. De Geest, B. G.; De Koker, S.; Demeester, J.; De Smedt, S. C.; Hennink, W. E. *J Control Release* **2009**, 135, 268-273.
98. De Geest, B. G.; De Koker, S.; Immesoete, K.; Demeester, J.; De Smedt, S. C.; Hennink, W. E. *Adv Mater* **2008**, 20, 3687-3691.
99. Mouriño, V.; Boccaccini, A. R. *J R Soc Interface* **2010**, 7, 209-227.
100. Tabata, Y. *Pharm Sci Technolo Today* **2000**, 3, 80-89.
101. Freiberg, S.; Zhu, X. X. *Int J Pharm* **2004**, 282, 1-18.
102. Yang, L.; Webster, T. J. *Expert Opin Drug Deliv* **2009**, 6, 851-864.
103. Tabata, Y. *Tissue Eng* **2003**, 9, 5-15.
104. Habraken, W. J. E. M.; Wolke, J. G. C.; Mikos, A. G.; Jansen, J. A. *J Biomater Sci Polym Ed* **2008**, 19, 1171-1188.
105. Eley, J. G.; Mathew, P. *J Microencapsul* **2007**, 24, 225-234.
106. Kumari, A.; Yadav, S. K.; Yadav, S. C. *Colloids Surf B Biointerfaces* **2010**, 75, 1-18.
107. Silva, G. A.; Coutinho, O. P.; Ducheyne, P.; Reis, R. L. *J Tissue Eng Regen Med* **2007**, 1, 97-109.
108. Zhu, G.; Mallery, S. R.; Schwendeman, S. P. *Nat Biotechnol* **2000**, 18, 52-57.
109. Ungaro, F.; Biondi, M.; d'Angelo, I.; Indolfi, L.; Quaglia, F.; Netti, P. A.; La Rotonda, M. I. *J Control Release* **2006**, 113, 128-136.
110. Wang, X.; Wenk, E.; Zhang, X.; Meinel, L.; Vunjak-Novakovic, G.; Kaplan, D. L. *J Control Release* **2009**, 134, 81-90.
111. Needleman, I.; Tucker, R.; Giedrys-Leeper, E.; Worthington, H. *J Periodontal Res* **2002**, 37, 380-388.
112. Retzepi, M.; Donos, N. *Clin Oral Implants Res* **2010**, 21, 567-576.
113. Nie, H.; Wang, C.-H. *J Control Release* **2007**, 120, 111-121.
114. Slaughter, B. V.; Khurshid, S. S.; Fisher, O. Z.; Khademhosseini, A.; Peppas, N. A. *Adv Mater* **2009**, 21, 3307-3329.
115. Yamamoto, M.; Ikada, Y.; Tabata, Y. *J Biomater Sci Polym Ed* **2001**, 12, 77-88.
116. Kretlow, J. D.; Young, S.; Klouda, L.; Wong, M.; Mikos, A. G. *Adv Mater* **2009**, 21, 3368-3393.
117. Quick, D. J.; Anseth, K. S. *J Control Release* **2004**, 96, 341-351.
118. Wang, C.; Varshney, R. R.; Wang, D.-A. *Adv Drug Deliv Rev* **2010**, 62, 699-710.
119. Bergeron, E.; Marquis, M.; Chrétien, I.; Fauchoux, N. *J Mater Sci Mater Med* **2007**, 18, 255-263.
120. Uskoković, V.; Uskoković, D. P. *J Biomed Mater Res B Appl Biomater* **2011**, 96B, 152-191.
121. Habraken, W. J. E. M.; Wolke, J. G. C.; Jansen, J. A. *Adv Drug Deliv Rev* **2007**, 59, 234-248.

122. Bisht, S.; Bhakta, G.; Mitra, S.; Maitra, A. *Int J Pharmaceut* **2005**, *288*, 157-168.
123. Epple, M.; Ganesan, K.; Heumann, R.; Klesing, J.; Kovtun, A.; Neumann, S.; Sokolova, V. *J Mater Chem* **2010**, *20*, 18-23.
124. Habraken, W. J. E. M.; Wolke, J. G. C.; Mikos, A. G.; Jansen, J. A. *J Biomater Sci Polym Ed* **2006**, *17*, 1057-1074.
125. Habraken, W. J. E. M.; Jonge, L. T. d.; Wolke, J. G. C.; Yubao, L.; Mikos, A. G.; Jansen, J. A. *J Biomed Mater Res A* **2008**, *87A*, 643-655.
126. Li, M.; Liu, X.; Liu, X.; Ge, B.; Chen, K. *J Mater Sci Mater Med* **2009**, *20*, 925-934.
127. Muschler, G. F.; Raut, V. P.; Patterson, T. E.; Wenke, J. C.; Hollinger, J. O. *Tissue Eng Part B Rev* **2010**, *16*, 123-145.
128. Gomes, P. S.; Fernandes, M. H. *Lab Anim* **2011**, *45*, 14-24.
129. Horner, E. A.; Kirkham, J.; Wood, D.; Curran, S.; Smith, M.; Thomson, B.; Yang, X. B. *Tissue Eng Part B Rev* **2010**, *16*, 263-271.
130. Oortgiesen, D. A. W.; Meijer, G. J.; de Vries, R. B. M.; Walboomers, X. F.; Jansen, J. A., Animal models for the evaluation of tissue engineering constructs. In *Tissue Engineering; from lab to clinic*, Pallua, N.; Suschek, C. V., Eds. Springer-Verlag: Berlin, 2011; pp 131-154.
131. Cooper, G. M.; Mooney, M. P.; Gosain, A. K.; Campbell, P. G.; Losee, J. E.; Huard, J. *Plast Reconstr Surg* **2010**, *125*, 1685-1692.
132. Schmitz, J. P.; Hollinger, J. O. *Clin Orthop Relat Res* **1986**, (205), 299-308.
133. Develioglu, H.; Saraydin, S. U.; Bolayir, G.; Dupoirieux, L. *J Biomed Mater Res A* **2006**, *77*, 627-631.
134. Kim, K. H.; Jeong, L.; Park, H. N.; Shin, S. Y.; Park, W. H.; Lee, S. C.; Kim, T. I.; Park, Y. J.; Seol, Y. J.; Lee, Y. M.; Ku, Y.; Rhyu, I. C.; Han, S. B.; Chung, C. P. *J Biotechnol* **2005**, *120*, 327-339.
135. Blom, E. J.; Klein-Nulend, J.; Yin, L.; van Waas, M. A.; Burger, E. H. *Clin Oral Implants Res* **2001**, *12*, 609-616.
136. Woo, B. H.; Fink, B. F.; Page, R.; Schrier, J. A.; Jo, Y. W.; Jiang, G.; DeLuca, M.; Vasconez, H. C.; DeLuca, P. P. *Pharm Res* **2001**, *18*, 1747-1753.
137. King, G. N. *Curr Pharm Biotechnol* **2001**, *2*, 131-142.
138. Nemcovsky, C. E.; Zahavi, S.; Moses, O.; Kebudi, E.; Artzi, Z.; Beny, L.; Weinreb, M. *J Periodontol* **2006**, *77*, 996-1002.
139. Oortgiesen, D. A.; Meijer, G. J.; Bronckers, A. L.; Walboomers, X. F.; Jansen, J. A. *Tissue Eng Part C Methods* **2010**, *16*, 133-40.
140. Dogan, A.; Ozdemir, A.; Kubar, A.; Oygur, T. *Tissue Eng* **2002**, *8*, 273-282.
141. Salata, L. A.; Craig, G. T.; Brook, I. M. *Int J Oral Maxillofac Implants* **1998**, *13*, 44-51.
142. Fennis, J. P.; Stoeltinga, P. J.; Jansen, J. A. *Int J Oral Maxillofac Surg* **2002**, *31*, 281-286.
143. Sun, X. J.; Xia, L. G.; Chou, L. L.; Zhong, W.; Zhang, X. L.; Wang, S. Y.; Zhao, J.; Jiang, X. Q.; Zhang, Z. Y. *Arch Oral Biol* **2010**, *55*, 195-202.
144. Nevins, M.; Kirker-Head, C.; Nevins, M.; Wozney, J. A.; Palmer, R.; Graham, D. *Int J Periodontics Restorative Dent* **1996**, *16*, 8-19.
145. Lopez-Nino, J.; Caballero, L. G.; Gonzalez-Mosquera, A.; Seoane-Romero, J.; Varela-Centelles, P.; Seoane, J. *J Periodontol* **2011**, *83*, 354-361.
146. Stelzle, F.; Benner, K. U. *Clin Oral Implants Res* **2010**, *21*, 1370-1378.
147. Kaufman, E. *J Esthet Restor Dent* **2003**, *15*, 272-282; discussion 283.

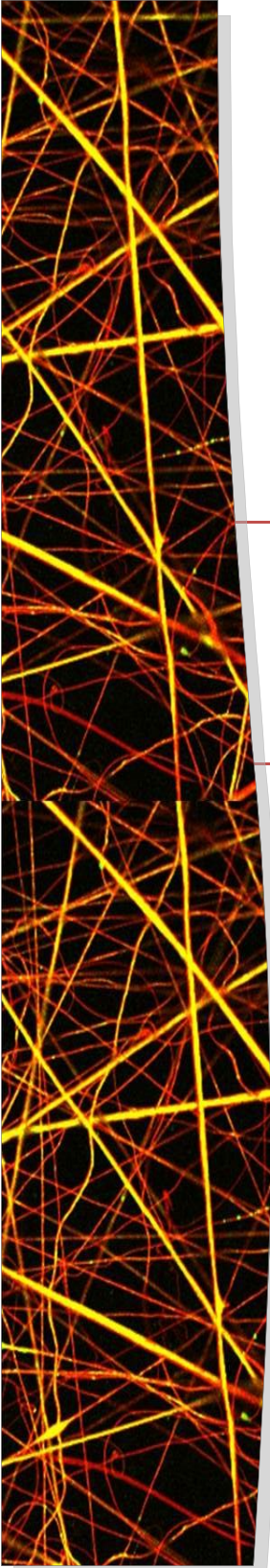
148. Wikesjo, U. M.; Qahash, M.; Polimeni, G.; Susin, C.; Shanaman, R. H.; Rohrer, M. D.; Wozney, J. M.; Hall, J. *J Clin Periodontol* **2008**, *35*, 1001-1010.
149. Bodde, E. W.; Boerman, O. C.; Russel, F. G.; Mikos, A. G.; Spauwen, P. H.; Jansen, J. A. *J Biomed Mater Res A* **2008**, *87*, 780-791.
150. Chen, F. M.; Zhao, Y. M.; Zhang, R.; Jin, T.; Sun, H. H.; Wu, Z. F.; Jin, Y. *J Control Release* **2007**, *121*, 81-90.
151. Gutwald, R.; Haberstroh, J.; Stricker, A.; Ruther, E.; Otto, F.; Xavier, S. P.; Oshima, T.; Marukawa, E.; Seto, I.; Enomoto, S.; Hoogendijk, C. F.; Schmelzeisen, R.; Sauerbier, S. *J Cranio-maxillofac Surg* **2010**, *38*, 571-579.
152. Srouji, S.; Ben-David, D.; Lotan, R.; Livne, E.; Avrahami, R.; Zussman, E. *Tissue Eng Part A* **2011**, *17*, 269-277.
153. Ruhe, P. Q.; Kroese-Deutman, H. C.; Wolke, J. G.; Spauwen, P. H.; Jansen, J. A. *Biomaterials* **2004**, *25*, 2123-2132.
154. Yan, X. Z.; Ge, S. H.; Sun, Q. F.; Guo, H. M.; Yang, P. S. *J Periodontol* **2010**, *81*, 1289-1298.
155. Jiang, X. Q.; Sun, X. J.; Lai, H. C.; Zhao, J.; Wang, S. Y.; Zhang, Z. Y. *Clin Oral Implants Res* **2009**, *20*, 1333-1340.
156. Zhang, Y.; Fan, W.; Nothdurft, L.; Wu, C.; Zhou, Y.; Crawford, R.; Xiao, Y. *Tissue Eng Part C* **2011**, *17*, 789-797.
157. Hammarstrom, L. *J Clin Periodontol* **1997**, *24*, 658-668.
158. Peng, H.; Usas, A.; Olshanski, A.; Ho, A. M.; Gearhart, B.; Cooper, G. M.; Huard, J. *J Bone Miner Res* **2005**, *20*, 2017-2027.
159. Wernike, E.; Montjovent, M. O.; Liu, Y.; Wismeijer, D.; Hunziker, E. B.; Siebenrock, K. A.; Hofstetter, W.; Klenke, F. M. *Eur Cell Mater* **2011**, *19*, 30-40.
160. Young, S.; Patel, Z. S.; Kretlow, J. D.; Murphy, M. B.; Mountziaris, P. M.; Baggett, L. S.; Ueda, H.; Tabata, Y.; Jansen, J. A.; Wong, M.; Mikos, A. G. *Tissue Eng Part A* **2009**, *15*, 2347-2362.
161. Patel, Z. S.; Young, S.; Tabata, Y.; Jansen, J. A.; Wong, M. E.; Mikos, A. G. *Bone* **2008**, *43*, 931-940.
162. Aghaloo, T. L.; Moy, P. K.; Freymiller, E. G. *Int J Oral Maxillofac Implants* **2004**, *19*, 59-65.
163. Tonetti, M. S.; Cortellini, P.; Carnevale, G.; Cattabriga, M.; de Sanctis, M.; Pini Prato, G. P. *J Clin Periodontol* **1998**, *25*, 728-736.
164. Mombelli, A.; Feloutzis, A.; Bragger, U.; Lang, N. P. *Clin Oral Implants Res* **2001**, *12*, 287-294.
165. Rathbone, C. R.; Cross, J. D.; Brown, K. V.; Murray, C. K.; Wenke, J. C. *J Orthop Res* **2001**, *19*, 1070-1074.
166. Botelho, M. A.; Martins, J. G.; Ruela, R. S.; Queiroz, D. B.; Ruela, W. S. *J Appl Oral Sci* **2010**, *18*, 335-342.
167. Chang, C. Y.; Yamada, S. *J Periodontol* **2000**, *71*, 1086-1093.
168. Guelcher, S. A.; Brown, K. V.; Li, B.; Guda, T.; Lee, B. H.; Wenke, J. C. *J Orthop Trauma* **2011**, *25*, 477-482.
169. Suzuki, A.; Terai, H.; Toyoda, H.; Namikawa, T.; Yokota, Y.; Tsunoda, T.; Takaoka, K. *J Orthop Res* **2006**, *24*, 327-332.
170. Yaffe, A.; Herman, A.; Bahar, H.; Binderman, I. *J Periodontol* **2003**, *74*, 1038-1042.
171. Yaffe, A.; Golomb, G.; Breuer, E.; Binderman, I. *J Periodontol* **2000**, *71*, 1607-1612.

172. Yaffe, A.; Iztkevich, M.; Earon, Y.; Alt, I.; Lilov, R.; Binderman, I. *J Periodontol* **1997**, *68*, 884-889.
173. Binderman, I.; Adut, M.; Yaffe, A. *J Periodontol* **2000**, *71*, 1236-1240.
174. Srisubut, S.; Teerakapong, A.; Vattraphodes, T.; Taweechaisupapong, S. *Oral Surg Oral Med Oral Pathol Oral Radiol Endod* **2007**, *104*, e11-6.
175. Wang, C. Z.; Chen, S. M.; Chen, C. H.; Wang, C. K.; Wang, G. J.; Chang, J. K.; Ho, M. L. *Bio-materials* **2010**, *31*, 8674-8683.
176. Yaffe, A.; Binderman, I.; Breuer, E.; Pinto, T.; Golomb, G. *J Periodontol* **1999**, *70*, 893-895.
177. Bodde, E. W.; Kowalski, R. S.; Spauwen, P. H.; Jansen, J. A. *Tissue Eng Part A* **2008**, *14*, 29-39.
178. American Association of Oral and Maxillofacial Surgeons position paper on bisphosphonate-related osteonecrosis of the jaws Advisory Task Force on Bisphosphonate-Related Osteonecrosis of the Jaws. *J Oral Maxillofac Surg* **2007**, *65*, 369-76.
179. King, A. E.; Umland, E. M. *Pharmacotherapy* **2008**, *28*, 667-677.
180. Miguel, B. S.; Ghayor, C.; Ehrbar, M.; Jung, R. E.; Zwahlen, R. A.; Hortschansky, P.; Schmoekel, H. G.; Weber, F. E. *Tissue Eng Part A* **2009**, *15*, 2955-2963.
181. Ozec, I.; Kilic, E.; Gumus, C.; Goze, F. *J Craniofac Surg* **2007**, *18*, 546-550.
182. Nyan, M.; Sato, D.; Oda, M.; Machida, T.; Kobayashi, H.; Nakamura, T.; Kasugai, S. *J Pharmacol Sci* **2007**, *104*, 384-386.
183. Nyan, M.; Sato, D.; Kihara, H.; Machida, T.; Ohya, K.; Kasugai, S. *Clin Oral Implants Res* **2009**, *20*, 280-287.

**Bioactive electrospun scaffolds delivering
growth factors and genes for tissue
engineering applications**

Wei Ji, Yan Sun, Fang Yang, Jeroen J.J.P. van den Beucken,
Mingwen Fan, Zhi Chen, John A. Jansen

Pharmaceutical Research. 2011, 28, 1259-1272.



1. Introduction

Tissue engineering is an interdisciplinary field that applies the principles of engineering and life sciences toward the development of functional substitutes for damaged tissues. The fundamental concept behind tissue engineering is to utilize the body's natural biological response to tissue damage in conjunction with engineering principles¹. To achieve successful tissue regeneration, three key factors are to be considered: cells, scaffolds, and biomolecules (e.g., growth factor, gene, and etc.). Currently, two strategies have emerged as most promising tissue engineering approaches (Figure 1)². One is to implant pre-cultured cells-synthetic scaffolds complexes into the defect place. In this approach, the seeded cells are generally isolated from host target tissues, for which they provide main resource to form newly born tissue. The synthetic scaffolds, on the other hand, provide porous three dimensional structures to accommodate the cells to form extracellular matrix (ECMs) and regulate the cell growth *in vivo*^{3,4}. These synthetic scaffolds are biodegradable and degrade in accordance with the tissue regeneration time frame. The other approach is to place acellular scaffolds immediately after injury. The governing principle of this approach is using scaffolds to deliver appropriate biomolecules to the defect area; the biomolecules are released from the scaffolds in a controlled manner and may recruit progenitor cells toward the defect area and promote their proliferation and differentiation, thereby enhancing tissue regeneration.

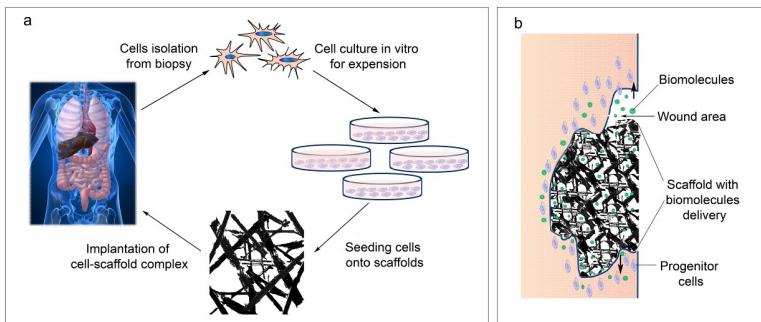


Figure 1. Current tissue engineering approaches. (a) To implant pre-cultured cells-scaffolds complex into the defect place. In this approach, cells are isolated from biopsy and then cultured *in vitro* for expansion. Then the cells are seeded onto synthetic scaffolds, which provide porous three dimensional structure to accommodate seeding cells to form extracellular matrix; (b) To place acellular scaffolds with biomolecules delivery immediately after injury. In this approach, the biomolecules are released from scaffolds in a controlled manner and they may recruit the progenitor cells in wound area and promote their proliferation and differentiation.

In recent years, an increasing trend toward the combination of these two approaches is observed⁵⁻⁸, because the scaffolds with controlled release of biomolecules can induce the seeded cells to proliferate and differentiate during an *ex vivo* pre-culture period, thereby encouraging tissue formation after implantation *in vivo*. Meanwhile, the scaffolds will continue to release signal molecules after implantation to enhance the desired physio-

logical response, and consequently enhance tissue regeneration in the defect area. In view of these strategies, to achieve successful and efficient tissue engineering, an increasing demand for bioactive scaffolds that can provide more than only physical support for cells but also a local release of biomolecules to influence surrounding tissue regeneration is observed. This type of scaffold is termed as “bioactive scaffold”¹.

The importance of bioactive scaffolds in tissue engineering has been comprehensively reviewed⁹. Various biomolecules can be incorporated within tissue engineered scaffolds to enhance their functional properties for biomedical applications. The most frequently used biomolecules are proteins (e.g., growth factors or cytokines) and growth factor coding-genes. Growth factors (GFs) are endogenous proteins capable of binding cell-surface receptors and directing cellular activities involved in the regeneration of new tissue¹⁰. Localized delivery of exogenous GFs is suggested to be therapeutically effective for production of cellular components involved in tissue development and the healing process, thus making them important factors for tissue regeneration¹¹. Nevertheless, it has to be emphasized that the success of direct growth factor delivery from scaffolds depends on the large-scale production of recombinant GFs, which is quite expensive. Additionally, protein bioactivity after incorporation within scaffolds also needs to be considered in view of efficacy issues. Instead of growth factor delivery, gene therapy presents a new paradigm in tissue engineering. This concept gives birth to gene-activated scaffolds (GASs), which are defined as scaffolds incorporating therapeutic protein encoding genes¹². GASs ensure the delivery of genes at the desired site¹³, after which transfection into target cells is required to produce therapeutic proteins¹⁴. Compared to growth factor delivery, gene delivery is advantageous in its long-time effect as well as relatively low cost, which makes it promising for tissue engineering application.

Since the last decade, huge efforts have been made to explore strategies for the preparation of bioactive scaffolds to deliver therapeutic proteins or genes, and a series of comprehensive reviews has provided detailed information for these strategies¹⁴⁻¹⁶. In general, proteins or genes can be delivered by micro/nano-particles¹⁷, hydrogels¹⁸ or electrospun fibrous matrices^{19,20}. For micro/nano-particles, due to their fluidity, it is difficult to keep them localized in the defected area giving new tissues enough support²¹. Therefore, such particles can only be used as carriers for biomolecules rather than scaffolds for tissue engineering. Comparably, hydrogels have been used as drug delivery systems for many years, but the poor mechanical properties of hydrogel-based scaffolds limits their use for load-bearing applications, and this disadvantage can even result in the premature dissolution or displacement of the hydrogel from a targeted local site²². Electrospinning is a popular technique to prepare tissue engineering scaffolds due to its relative simplicity regarding the generation of fibrous scaffolds with nano- or submicron-scale dimensions, which morphologically resemble the natural ECM. Due to the possibil-

ity of ultrathin fiber diameters, electrospun fibrous matrices can have a large specific surface area, which enables effective delivery of biomolecules. Furthermore, the loose bonding between fibers is beneficial for tissue growth and cell migration²³. These characteristics endue electrospinning with superiority in preparation of bioactive scaffolds. In 2003, electrospinning has been first used to prepare bioactive scaffolds with gene release²⁴, and thereafter, this technique has gained an exponentially increasing popularity in this area (Figure 2). The aim of this paper is to review the techniques to incorporate growth factors or genes into electrospun scaffolds. Additionally, the existing challenges of using electrospinning in the area of tissue regeneration will be discussed.

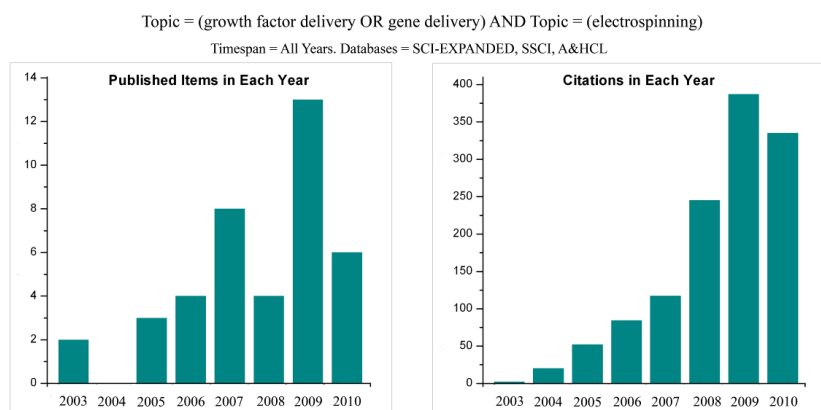


Figure 2. Publications and citations report from ISI web of Science®, as at August 18, 2010.

2. Basics relevant to electrospinning

Electrospinning is a cost-efficient technique to prepare ultra fine polymeric fibers, which can be easily employed in the laboratory and scaled up to an industrial process. It utilizes electrostatic forces to spin polymer solutions or melts into whipped jets, resulting in continuous fibers with diameters from a few nanometers to micrometers after solvent evaporation in the spinning process^{25, 26}. A typical electrospinning apparatus consists of four major components: (1) a syringe pump, which controls the feeding rate of polymer solution to be electrospun; (2) a needle, through which the solution goes into a high electric field; (3) a high voltage source, which stretches the polymer solution into ultrathin fibers; and (4) a grounded fiber collector, where electrospun fibers can be collected in a static or dynamic way (Figure 3).

The technique of electrospinning has been comprehensively reviewed^{25, 27}: when high voltage is applied, the polymer solution droplet from the needle becomes highly electrified and tends to form a conical shape known as the Taylor cone depending on the surface tension of the liquid and the force of electric field; once the electric field surpasses a threshold, the electric force overcomes the surface tension and viscoelastic force of the

polymer droplet, which results in a finely charged jet from the tip of the Taylor cone; then the jet sprays into one continuous ultrathin fiber. The random or aligned fibers can be collected on a grounded metallic collector, in the form of a plate, cylinder or disc type²⁷. Based on this theory, it is clear that the electrospinning process can be manipulated by a number of variables. These variables include solution properties (polymer concentration, polymer molecular weight), system set up (applied voltage, feeding rate and collecting distance), and environmental factors (temperature and humidity)^{20, 25}. Among these variables, solution properties are crucial for a successful electrospinning. Further, literature indicates that low polymer weight, high fluidity or high density of the polymer solution will cause instabilities, including whipping and droplet instead of uniform fiber formation²⁸. In addition, sub-optimal voltage is another key factor that could lead to bead-like defects in the spun fibers or even failure in jet formation^{20, 25}.

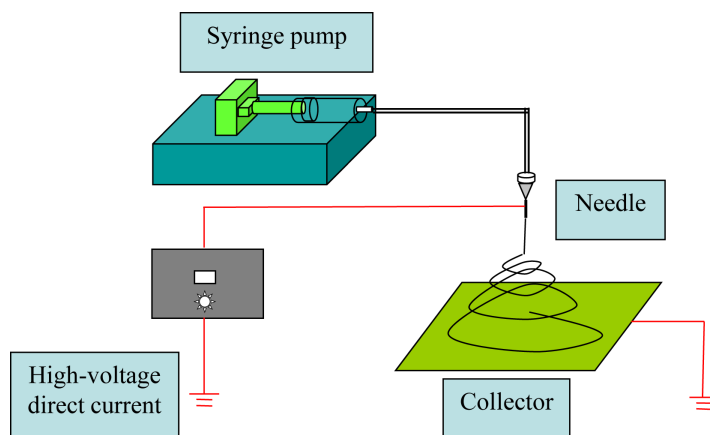


Figure 3. Scheme for electrospinning apparatus.

There is a wide range of material choices to prepare electrospun scaffolds for tissue engineering applications, which mainly includes two categories: natural polymers and synthetic polymers. In principle, the material choice for scaffolds preparation depends on the purpose of application and feasibility of electrospinning. Electrospun fibrous scaffolds prepared from natural polymers, especially collagen, are mostly used because these can mimic the properties of natural ECM for engineered tissues²⁹. However, some natural polymers are not easy to handle during electrospinning, as they tend to display poor processibility, which needs to be modified to achieve better electrospinning³⁰. Furthermore, it is difficult to confirm that native structure and biological characteristics of natural polymers are still preserved after electrospinning³¹. In contrast, synthetic polymers (especially the polyesters) are much easier to be optimized for electrospinning process, and hence are more commonly applied. Dong et al.³² gave a comprehensive review listing different synthetic polymers that can be used to prepare electrospun scaffolds. Among multiple choices of synthetic polymers, poly(ϵ -caprolactone) (PCL), poly(lactic-

acid) (PLA), poly(glycolic acid) (PGA) and their copolymers poly(lactic-co-glycolic acid) (PLGA) are most extensively used for biomedical applications because they are approved by US Food and Drug Association (FDA) for their good biocompatibility as well as biodegradability.

3. Current progress of electrospun scaffolds with biomolecule delivery

3.1. General considerations for growth factor and gene delivery

There are two important aspects to achieve a successful delivery: (1) to ensure the bioactivity of the biomolecules incorporated within the scaffolds; (2) to fit the release profile of biomolecules with time frame of tissue regeneration.

3.1.1 Principles for growth factor delivery

Growth factors easily lose their activity upon chemical or physical processing. Therefore, the preservation of protein activity is a prerequisite for successful growth factor delivery. There are three stages during which the stability of a growth factor incorporated in a scaffold must be preserved: (i) scaffold fabrication, (ii) scaffold storage, and (iii) scaffold degradation. The source of the protein stability in each stage and available strategies to improve the protein stability will be explained in detail in *section 4.1*.

The release profile is another important issue to take into account when designing electrospun scaffolds to deliver growth factors. Considering the half-lives of most growth factors in serum are very short, it is essential for bioactive scaffolds to maintain a desired temperospatial growth factor concentration to direct tissue regeneration. For this purpose, an optimal growth factor delivering scaffold should be able to initially release part of the dosage contained, which is typically termed “burst release”³³, to rapidly get the effective therapeutic concentration. Subsequently, well defined release kinetics follow in order to provide the maintenance dosage enabling the attainment of the desired concentration³⁴.

3.1.2 Principles for gene delivery

Different from growth factors, which act extracellularly and initiate biological response by binding to cell surface receptors, target genes will only have an intracellular effect by integrating into the host genome of endogenous cells and transformed the transfected cells into local bio-activated actors to enhance tissue formation. Consequently, a prerequisite for a successful gene delivery scaffold is that the active gene can be released from the scaffold, after which it needs to be integrated into the host genome. To achieve this goal, the target gene is always packed within vectors before incorporated into the scaffolds, because vectors can protect the target genes from extracellular DNA-degrading enzymes and intracellular lysosomes that contain digestive enzymes in the process of

being taken up by surrounding cells¹³. On the other hand, vectors can transport genes through the lipid bilayer of the cell membrane, and the latter is the biggest obstacle in gene transfection. Currently, two categories of vectors are used: viral and non-viral vectors. The strategies of effective vectors have been clearly reviewed by Storrie et al. and Kootstra et al.^{14, 35}.

Similar to growth factor delivery, an important issue for gene delivery is to modulate both the concentration and duration of the gene particles released from scaffolds, which dictates a well controlled release profile. To achieve successful gene transfection, the effective concentration of target gene-vector complexes should be released into the cell surrounding microenvironment within an optimal time frame. It is found that low concentration of DNA always results in low transfection efficiency^{36, 37} and much too fast gene release leads to a low transfection efficiency, because superabundant gene complexes may lose activity if transfection is not achieved in due time³⁷.

3.2. Fabrication techniques for electrospun scaffolds with biomolecule delivery capacity

In general, biomolecules can be delivered either directly from the electrospun scaffolds or from additional separate release system (i.e., micro/nanospheres) loaded into the scaffolds, where the electrospun scaffolds behave only as a supporting structure. Since using micro/nano-spheres to deliver biomolecules has been comprehensively reviewed³⁸⁻⁴¹, this topic will not be addressed in this review. Different proteins and genes that have been loaded in electrospun scaffolds are listed in Table I & II, respectively.

3.2.1. Physical adsorption

The easiest way to load biomolecules into electrospun scaffolds is to dip the scaffolds into an aqueous phase containing biomolecules (Figure 4a). In this approach, biomolecules can be in the form of pure solution or emulsions and they can attach to the scaffolds via electrostatic forces. Although this approach gives little interference with the activity of loaded biomolecules, it is seldom used to load protein or genes in electrospun scaffolds due to the uncontrolled release profiles. It has been shown that bone morphogenetic protein-2 (BMP2) adsorbed to PLGA scaffolds reached over 75% release within 5 days and nearly complete release within 20 days. This release rate was much faster than that of the same amount of protein loaded in PLGA scaffolds using blend electrospinning²¹. Similar evidence is available for gene delivery using this approach. Although some researchers could obtain transfected cells in an early stage (most likely due to a large amount of target gene bulk release^{36, 37}, the released gene exhausted within a short time and over 95% of incorporated DNA released within 10 days³⁷.

3.2.2. Blend electrospinning

In blend electrospinning, biomolecules are mixed within the polymer solution, after

which the mixed solution is used in the electrospinning process to fabricate a hybrid scaffold (Figure 4b). Some researchers made emphasis on the preparing process of suspending the protein solution in polymer solution by emulsifying using ultra-sonication or homogenizer, therefore named the process as “emulsion electrospinning”⁴². The idea for emulsification arises from the improvement of biomolecule suspension in organic solvents. Considering its same principle, we assume that it still belongs to blend electrospinning approach.

As blend electrospinning localizes biomolecules within the fibers of the scaffolds rather than simply adsorb them superficially to the scaffolds, it is assumed that this approach allows more sustained release profiles compared to physical adsorption. Researchers have used blend electrospinning to incorporate various types of proteins and genes in scaffolds, including bovine serum albumin (BSA)⁴³⁻⁴⁵, lysozyme^{42, 46} and growth factors e.g., BMP2^{21, 47}, epidermal growth factor (EGF)⁴⁸. In general, a sustained release profile can be obtained over several weeks using this technique.

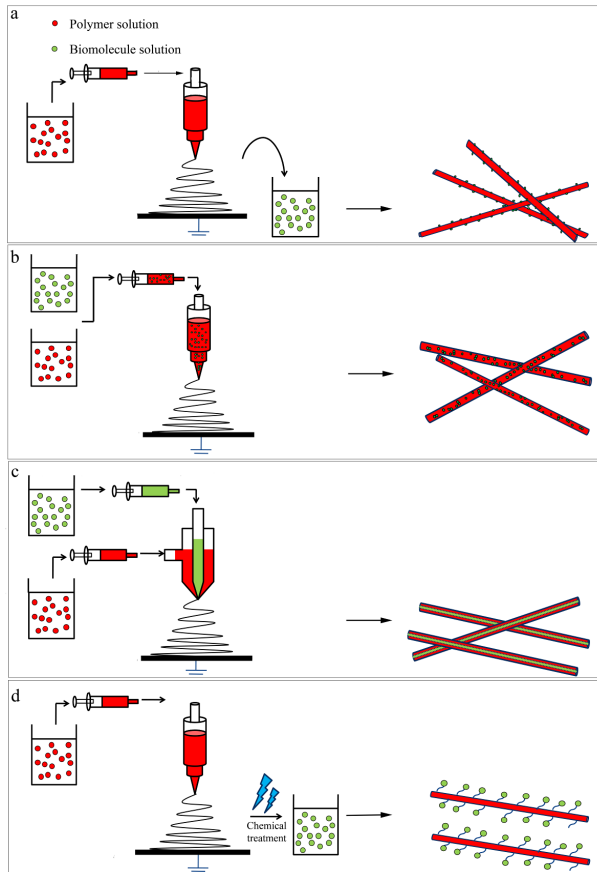


Figure 4. Fabrication techniques of bioactive electrospun scaffolds (a) physical adsorption; (b) blend electrospinning; (c) coaxial electrospinning; (d) covalent immobilization

Although blend electrospinning is assumed to be relatively easy to perform, an inconvenient issue is the activity loss of incorporated biomolecules. This is especially vital for proteins, because they may lose their bioactivity due to conformational changes in the organic solution environment. On the other hand, the process to prepare protein emulsions, which involves mechanical stirring, homogenization or ultrasonication, can also damage protein function⁴⁹. In previous studies, several strategies have been applied to improve protein stability. A strategy is to use salt complexation instead of emulsification to improve protein solubility in organic solvents. Li et al.⁴⁶ incorporated lysozyme-oleate complex into electrospun membranes and their results showed that the released lysozyme retained over 90% of bioactivity. Another strategy is to use hydrophilic additives to minimize the hydrophobic interaction of protein and organic solvents during electrospinning⁵⁰⁻⁵². It has been reported that hydrophilic polymers, such as poly(ethylene glycol) (PEG) and poly(ethylene oxide) (PEO) added in the aqueous protein solution^{46,47,53} are beneficial for improving protein stability. Furthermore, a recent study showed that hydroxyapatite (HAp) particles were able to preserve the activity of BMP2 loaded in electrospun PLGA scaffolds, as proteins can attach to these hydrophilic particles so as to escape the harsh electrospinning process²¹.

A typical protein release profile from blend electrospun scaffolds is an initial burst release followed by a sustained release close to a linear mode^{24,44,46,54,55}. The burst release usually occurs within 24 hours, regardless of polymer type for scaffolds preparation. This initial burst release may be related to the migration of protein during drying and storage steps, which localizes a certain fraction of protein molecules near the fiber surface⁵⁶. The high solubility and partition coefficients of the incorporated protein can lead to a rapid release through short diffusion pathways due to thermodynamic imbalances³³. After burst release, the protein release behavior is mainly driven by protein diffusion or the effect of polymer degradation and protein diffusion. For slowly degradable polymers, such as PCL, the protein release profile behaves as a relatively linear mode⁵⁶; whereas for PLGA, a polymer with relatively short degradation time, the protein release profile shows a sustained mode followed by an obvious increased release rate once the polymer starts to degrade^{21,54}. The protein release profile can be modulated by additives loaded together with protein during blend electrospinning. The addition of hydrophilic additives, such as hydroxyapatite particles^{21,54} and PEG⁴⁶, will improve the hydrophilicity of scaffolds and hence enhance water uptake of the scaffolds as well as accelerate protein release from electrospun scaffolds.

The first gene delivery using blend electrospinning approach was reported by Luu et al.²⁴. In this study, the authors mixed pCMV β plasmid (7164 bp) encoding β -galactosidase with PLA-PEG-PLA tri-block copolymer and high molecular weight (75kDa) PLGA (LA/GA=75/25). Since then, many groups have used this approach to incorporate *bmp2* with

different plasmids into electrospun scaffolds^{37, 47}. In this approach, the plasmid gene is able to withstand the electrospinning process because of the protection from complexation with vectors. Luu et al.²⁴ found that DNA kept its structural integrity after release out of PLGA scaffolds. Nie et al.³⁶ also showed that the incorporated *bmp2* was still capable to induce BMP2 expression *in vivo* after 4 weeks.

Different from protein release, gene release shows two types of profiles from blend electrospun scaffolds, which might be related to different fiber compositions. Luu et al.²⁴ reported a burst release within 2 hours followed by a sustained DNA release until 20 days using PLA-PEG block copolymers blended with different variations of PLGA, whereas others obtained a linear release profile up to 2 months from composite PLGA electrospun scaffolds^{37, 57}.

3.2.3. Coaxial electrospinning

Coaxial electrospinning, also known as co-electrospinning, was first demonstrated by Sun et al.⁵⁸. In coaxial electrospinning, two solutions (i.e. polymer solution and biological solution) are coaxially and simultaneously electrospun through different feeding capillary channels in one needle to generate composite nano-fibers with core-shell structures (Figure 4c). Coaxial electrospinning is a very dynamic process, and many factors such as feeding rate of the inner and outer fluids, interfacial tension and visco-elasticity of the two solutions affect the entrapment of components in the core part^{58, 59}. Although this technique was developed more than ten years ago⁶⁰, the application of coaxial electrospinning to deliver biomolecules has only been explored since five years^{24, 44} due to the complexity of this technique.

Recently, coaxial electrospinning has gained increased popularity in the protein delivery field because the produced core-shell fibers have great potential in preserving proteins during the electrospinning process. In addition, it provides homogeneous protein distribution throughout the fibers and proteins can be delivered in a controlled manner due to the shell barrier (Figure 5). Researchers have achieved encapsulation of different types of proteins in coaxially electrospun scaffolds, including BSA^{56, 61-63}, lysozyme⁶², platelet-derived growth factor-bb (PDGF-bb)^{64, 65}, nerve growth factor (NGF)⁶⁶ and fibroblast growth factor (FGF)⁶⁷. These studies indicated that released growth factors had efficient bioactivity to stimulate corresponding cell growth. Some authors attribute this bioactivity preservation only to the superiority of coaxial electrospinning, as during coaxial electrospinning, the electric charges are located predominantly at the outer fiber surface so that the inner protein solutions are not charged at all²⁵. In contrast, we compared the effect of blend and coaxial electrospinning on protein activity by using alkaline phosphatase (ALP) as a model protein, and our results indicated that both electrospinning techniques depressed the biological activity of the incorporated ALP, suggesting that high

voltage and contact with organic solvents are harmful to the loaded biomolecules; the ALP through coaxial electrospinning without PEG loaded maintained significantly lower enzyme activity, than the one with PEG loaded regardless of electrospinning method⁶⁸.

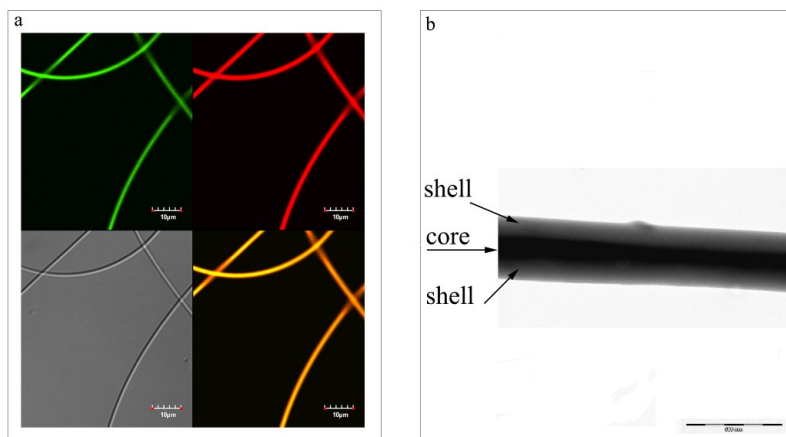


Figure 5. Protein distribution and core-shell structure of coaxial electrospun fibers. (a) Laser scanning confocal microscopy images to visualize protein distribution in coaxial electrospun fibers. The panels in each image are: upper left: fitc labelled protein (green); upper right: rhodamin B labelled polymer (red); bottom left: natural light; bottom right: the merger of fitc and rhodamin B. (b) Transmission electron microscopy image to visualize core-shell structure of the same coaxial electrospun fibers. Arrows indicate the core and shell parts within the fiber.

The protein release profile from coaxial electrospun fibers also includes an initial burst release followed by a sustained release stage^{56, 61, 62, 66, 67}, which is similar to the one from blend electrospun scaffolds. However, compared to blend electrospinning, the burst release from coaxial fibers is significantly lower and the entire release profile is more sustained^{56, 68}, because core-shell-structured fibers provide a protein reservoir system with a barrier membrane that controls the protein diffusion rate⁶⁸.

To date, only a limited number of studies on gene delivery via coaxial electrospinning scaffolds has been published. Saraf et al.⁶⁹ incorporated pDNA into an aqueous poly(ethylene glycol) (PEG) solution to fabricate the core of fibers, and loaded hyaluronic acid (HA) derivative of poly(ethylenimine) (PEI) as gene delivery vector into an organic sheath polymer solution of poly(ϵ -caprolactone) (PCL) to form the shell part. Their results suggested that the plasmid diffusing out of the fiber cores could complex with the positively charged vector PEI-HA released from the fiber shells. In addition, the released gene-vector complex could sustainably transfect cells present on the scaffolds over 60 days with 15% transfection efficiency on average. The authors concluded that transfection efficiency was related to the concentration and molecular weight of the core polymer PEG. However, the pDNA release was not directly measured in their study. Liao et al.⁷⁰ used core-shell fibers to deliver the adenovirus (Ad) encoding gene of green fluorescence

(GFP) *in vitro*. They succeeded to detect cells expressing GFP for more than 30 days and the cell transfection efficiency could reach over 80%. However, the high transfection efficiency only sustained for two weeks, which is related to the initial burst release. Their results showed that different polymer compositions have different pore formation ability on the fiber surface, which contributed to different release profiles and cell transfection efficiencies.

3.2.4. Covalent immobilization

Covalent immobilization immobilizes biomolecules onto the fiber surface via chemical bond, for instance forming peptide bond through amino groups⁷¹ (Figure 4d). Compared to the above mentioned strategies, this approach is predominantly used to improve the surface properties of electrospun fibers⁷², but some researchers are applying this approach to deliver protein aiming to achieve controlled release profiles, because the release rate of the immobilized biomolecules can be controlled by the external enzymes.

Choi et al.⁷³ reported that BSA-immobilized nanofibers showed no obvious burst release, although the authors only observed the release within one week. Using the same strategy, they prepared electrospun scaffolds with epidermal growth factor (EGF) delivery and succeeded in effective application of these bioactive scaffolds *in vivo*⁷⁴.

Kim et al.⁷¹ introduced a matrix metalloproteinases (MMPs)-cleavable linker between gene-vector complex and the electrospun scaffolds, so that gene release can be controlled by external MMPs cleavage. Their results showed that a fast gene release can be achieved in presence of MMP-responsive peptides, for which the maximum released amount was 82% within 12 hours, whereas less than 40% of incorporated gene was released if MMPs were absent.

So far, covalent immobilization is not a routine way to deliver protein or genes from electrospun scaffolds due to its technical complexity. In addition, some researchers also doubt the uniformity loss of the scaffolds during surface modification process⁷⁵, which might affect mechanical properties of the scaffolds. In addition, the manipulation of protein configuration and function by choosing specific binding sites in the protein molecule is still a big challenge. However, surface covalent immobilization represents an option to achieve delivery of multiple biomolecules in combination with the biomolecules directly incorporated within the scaffolds¹¹.

Table I. Proteins that have been loaded into electrospun scaffolds

Fabrication technique	Loaded Protein	Scaffold material	Biological application	Ref
<i>Physical adsorption</i>	BMP2	PLGA	BMP2 release <i>in vitro</i> & human bone marrow stem cell culture	21
	BMP2	PLGA	Implantation of tibia defect in nude mice	54
<i>Blend electro-spinning</i>	BSA	PEO	---	43
	BSA	PVA	BSA release <i>in vitro</i>	44
	BSA	PDLLA	BSA release <i>in vitro</i> & structural integrity analysis	45
	lysozyme	PDLLA	Lysozyme release <i>in vitro</i> , structural integrity & enzymatic analysis	42
	lysozyme	PCL	Lysozyme release <i>in vitro</i> & enzymatic analysis	46
	bFGF	PLGA	bFGF release <i>in vitro</i> & rat bone marrow cell culture to test bioactivity of released bFGF	67
	EGF	Silk fibroin	EGF release <i>in vitro</i> & human dermal fibroblasts culture	48
<i>Coaxial electro-spinning</i>	BMP2	Silk fibroin	Human bone marrow stem cell culture	47
	BMP2	PLGA	BMP2 release <i>in vitro</i> & human bone marrow stem cell culture	21
	BSA	PCL	BSA release <i>in vitro</i>	61, 62, 64, 68
	BSA	PLCL	BSA release <i>in vitro</i>	63
	lysozyme	PCL	Enzymatic analysis of released lysozyme	62
	PDGF-bb	PCL	NIH3T3 cell culture to test bioactivity of released PDGF-bb	64
	PDGF-bb	PLCL	PDGF-bb release <i>in vitro</i> & vascular smooth muscle cells to test bioactivity of released PDGF-bb	65
	NGF	PLCL	Rat pheochromocytoma cell line culture to test bioactivity of released NGF	66
	bFGF	PLGA	bFGF release <i>in vitro</i> & rat bone marrow cell culture to test bioactivity of released bFGF	67
	ALP	--	Enzymatic analysis of the post-electrospun ALP	68
<i>Covalent immobilization</i>	BSA	PEG-b-PDLLA	<i>In vitro</i> culture of human dermal fibroblast	76
	BSA	PCL/PCL-b-PEG mixture	<i>In vitro</i> culture of NIH3T3 cells	73
	EGF	PCL/PCL-b-PEG mixture	<i>In vitro</i> culture of human primary keratinocytes	74
	bovine collagen I	PMMAAA	<i>In vitro</i> culture of cortical neural stem cells	72
	BSA	PSU	---	75

Table II. Genes that have been loaded into electrospun scaffolds

Fabrication technique	Loaded gene particles	Scaffold material	Application	Ref
	pGL3	PLA	Deliver gene into COS-7 cell line <i>in vitro</i>	77
<i>Physical adsorption</i>	pBMP-2	PLGA/HAp	Deliver gene into hMSC <i>in vitro</i> & bone regeneration in nude mice	36, 37
	pBMP-2	PLGA/HAp	Deliver gene into hMSC <i>in vitro</i> & bone regeneration in nude mice	36, 37
<i>Blend electro-spinning</i>	pBMP-2	Silk/PEO/nHAp	Deliver gene into hMSCs <i>in vitro</i> for bone tissue engineering	47
	Adenovirus E1	Chitosan/PEG/FA	Deliver gene into HEK293 cell line for cancer therapy	78
	pCMV β	PLA-PEG/PLGA	<i>In vitro</i> gene delivery into MC3T3-E1 cell line	24, 57
	pCMV-EGFP	PEI-HA/PCL	Non-viral gene delivery into CRL1764 cell line <i>in vitro</i>	69
<i>Coaxial electro-spinning</i>	Adenovirus E1/E3	PCL/PEG	Viral gene delivery into HEK293 cell line <i>in vitro</i> Deliver gene into NIH3T3 cell line <i>in vitro</i> & animal	70
<i>Covalent immobilization</i>	LPEI-pEGFP-N1	PCL-PEG	study <i>in vivo</i> for local gene therapy of diabetic ulcers	71

4. Challenges and outlook

Although electrospinning shows huge potential and promising application possibilities to prepare tissue engineering scaffolds with biomolecule delivery, challenges still exist for further application of such bioactive scaffolds, which includes concerns about (i) protein instability, (ii) low gene transfection efficiency, and (iii) difficulties in release kinetics control.

4.1. Protein instability

Maintaining protein conformation within the scaffolds will be essential for further biomedical application of protein delivery from electrospun scaffolds, because the loss of conformation of a protein might not only be detrimental to the bioactivity and hence therapeutic potential, but also causes immunogenic effects related to exposure of non-native peptide epitopes⁷⁹. Although it has been reported that protein released from freshly prepared electrospun scaffolds was capable to induce various cellular responses^{21, 42, 45, 54, 65}, indicating the preservation of protein activity after the electrospinning process, it is too easy to claim that proteins incorporated within electrospun scaffolds will behave similar to the virgin proteins. As aforementioned, the threat for protein in-

stability regarding electrospun scaffolds might arise from fabrication, storage or degradation period. Also, it needs to be mentioned that the instability of protein during storage and degradation period is a general problem for polymeric protein delivery system. Therefore, the development of methods to optimize protein stability during these three stages is a major challenge for effective protein delivery from electrospun scaffolds.

During the scaffold preparation process, high voltage and contact with organic solvents may be harmful to the growth factor activity^{42, 53, 80}. Although using coaxial electrospinning and adding hydrophilic additives (e.g. PEG, hydroxyapatite) was reported to minimize the interaction between protein and organic phase^{21, 42}, the protein still loses 20% bioactivity due to the loss of α -helix in secondary structure compared with virgin protein solution⁶⁸.

Once the scaffolds are prepared, normally they are lyophilized for storage before application. It has been recognized that protein stresses may also arise from the drying process without appropriate stabilizing excipients⁸¹. As a result, it is wise to include protein stabilizer within the electrospun scaffolds to avoid the protein degradation during lyophilization. The commonly used lyoprotectants include sugars (e.g. sucrose) and polymers with relative high collapse temperature (e.g. dextran)⁸¹. Some authors used PEG⁵⁶ or dextran⁶¹ as protein stabilizer during coaxial electrospinning, but they rarely mentioned the effect of these additives on protein stability during lyophilization. Sucrose is suggested to be effective at inhibiting unfolding during lyophilization⁸¹, but its effect on electrospun scaffolds fabrication and protein stabilization still needs further investigation.

When the synthetic polymeric electrospun scaffolds start to degrade, the acidic microenvironment induced by hydrolysis products of polyesters is also likely to be destructive to growth factor integrity^{82, 83}. This is especially a serious concern for PLGA, which is attractive for biomolecules delivery because of its tailored degradation rate to achieve controlled release. The instability of incorporated proteins comes from deamidation at asparagine residues, peptide bond hydrolysis and acylation of protein primary amines (e.g., N-terminus, Lysine group) in degrading PLGA systems. All these instabilities are related to the acidic microclimate pH produced by the accumulation of acidic monomers and oligomers during PLGA degradation⁸³. In consequence, it is necessary to maintain the pH during scaffold degradation to stabilize the protein incorporated within PLGA delivering systems. Currently, there are two effective approaches to maintain pH within a PLGA protein delivery system. One is using hydrophilic polymer PEG as porogen in PLGA scaffolds to enhance acidic degraded products release⁸⁴, but this approach will decrease the mechanical properties of electrospun scaffolds, which might limit its further application. The other approach is adding poorly water-soluble basic salts such as $Mg(OH)_2$ to neutralize acidic microenvironment during scaffolds degradation⁸⁵. However, it is interesting that the use of this approach is not widespread in spite of its apparent simplicity.

4.2. Low gene transfection efficiency

Although many studies showed that it is feasible to deliver target genes at the desired tissue site via electrospun scaffold implantation^{24, 36, 47, 71}, the low gene transfection efficiency remains a drawback. Basically, the low efficiency is not only an obstacle for electrospun scaffolds with gene release, but a key technical barrier for full exploitation of the potential of gene therapies. In order to improve gene transfection efficiency, viral vectors seem to be a straightforward option, as viral vectors have natural tropism for living cells. However, their immunogenic potential and the threat of disturbing normal gene function from retroviruses and adeno-associated viruses limit their further clinical application^{86, 87}. In recent years, other options for improving transfection efficiency have been experimented, including nano-scaled delivery carriers⁸⁸, gene gun⁸⁹, disulfide linkages in cationic polymers⁹⁰ and bioresponsive polymers⁶⁸. Unfortunately, those methods are difficult to combine with electrospun scaffolds.

The poor interaction between released gene particles and cells is another possible reason for the low gene transfer efficiency via electrospun scaffolds. It is known that the released gene dose has to reach a threshold to induce gene transfection in cells, as recent studies have demonstrated that low concentrations of released gene always yield a low transfection efficiency^{36, 37}.

4.3. Release kinetics control

In order to achieve an effective dose and a target release profile, it is necessary to use mathematical models to predict release kinetics on the basis of good estimates of the required composition, geometry, and dimensions of the biomolecular delivery system. A mechano-realistic mathematical model is based on equations that describe real phenomena, e.g. mass transport by diffusion, dissolution of biomolecules, and/or the transition of a polymer from a glassy to rubbery state⁹¹. The mathematical modelling of biomolecule delivery from polymeric matrices have been clearly reviewed^{34, 91}. Among different models, a simple and useful empirical equation is the so-called power law equation³⁴: $M_t/M_\infty = kt^n$,

where M_∞ is the amount of drug released after an infinite time, k is a constant related to the structure and geometric characteristics of the system, and n is the release exponent indicating the mechanism of protein release⁹¹. However, it needs to be mentioned that, in practice, the release kinetics are likely affected by many factors, including polymer swelling, polymer erosion, biomolecular dissolution/diffusion characteristics, biomolecules distribution inside the matrix, biomolecule/polymer ratio and system³⁴. Apparently, it is impossible for a single mathematic model to consider all variables. Therefore, deviation will always exist between theoretical prediction and practical realization. Furthermore, *in vivo* biomolecule delivery from degradable polymeric scaffolds will be strongly

affected by the surrounding tissue environment (e.g. pH value and cellular tissue reaction). Nevertheless, there is no mathematical model available that estimates biomolecule release from biodegradable vehicles under physiological conditions. Consequently, it is necessary to design advanced mathematical models considering *in vivo* conditions.

5. Summary

Tissue engineering is a promising research area for present and future regenerative medicine, and the fundamental concept behind tissue engineering is to utilize the body's natural biological response to tissue damage in conjunction with engineering principles¹. In order to achieve successful and efficient tissue engineering applications, there is an increasing demand for bioactive scaffolds that can provide more than only physical support for cells but also local release of biomolecules to direct tissue regeneration in the defect area. Growth factors and growth factor coding-genes are the most straightforward biological stimuli to promote tissue regeneration. Consequently, studies related to the controlled delivery of growth factors and genes from bioactive scaffolds show an exponential increase over the last decade. Bioactive scaffolds with growth factor or gene delivery can be prepared in the form of micro/nano-spheres, hydrogel, as well as electrospun fibers. In recent years, electrospun fibrous scaffolds have attracted increasing attention due to the relative simplicity regarding the generation of fibrous scaffolds with nanoscale dimensions.

Electrospinning utilizes electrostatic forces to spin polymer solutions or melts into whipped jets, revealing continuous fibers with diameters from a few nanometers to micrometers after solvent evaporation in the spinning process. Because of the ultrathin fiber diameter, electrospun scaffolds are considered as an effective delivery system for biomolecules due to the stereological porous structure and high specific surface area. Biomolecules can be incorporated within electrospun scaffolds by physical adsorption, blend electrospinning, coaxial electrospinning as well as covalent immobilization after scaffolds fabrication. Although there has been a substantial number of studies dedicated to the methodology of preparing electrospun scaffolds to achieve biomolecules delivery, further studies are needed to improve the stability of incorporated protein, gene transfection efficiency as well as the accuracy of release kinetics control.

Until now, only a limited number of research efforts have focused on *in vivo* applications of electrospun scaffolds with protein or gene delivery. Consequently, more animal studies are needed to fully explore the potential of these bioactive scaffolds for clinical applications. Close cooperation between laboratory and clinics might eventually help to translate this promising technique from bench to bed, and it is likely that biomolecule delivery from electrospun scaffolds will provide therapeutic benefit in regenerative medicine in the near future.

6. References

1. Porter, J. R.; Ruckh, T. T.; Popat, K. C. *Biotechnol Prog* **2009**, *25*, 1539-1560.
2. Langer, R.; Vacanti, J. P. *Science* **1993**, *260*, 920-926.
3. Rosenberg, M. D. *Science* **1963**, *139*, 411-412.
4. Ma, Z.; Kotaki, M.; Inai, R.; Ramakrishna, S. *Tissue Eng* **2005**, *11*, 101-109.
5. Martins, A.; Duarte, A. R. C.; Faria, S.; Marques, A. P.; Reis, R. L.; Neves, N. M. *Biomaterials* **2010**, *31*, 5875-5885.
6. Wang, F.; Li, Z. Q.; Khan, M.; Tamama, K.; Kuppusamy, P.; Wagner, W. R.; Sen, C. K.; Guan, J. *Acta Biomater* **2010**, *6*, 1978-1991.
7. Murphy, W. L.; Peters, M. C.; Kohn, D. H.; Mooney, D. J. *Biomaterials* **2000**, *21*, 2521-2527.
8. Moioli, E. K.; Clark, P. A.; Xin, X.; Lal, S.; Mao, J. J. *Adv Drug Deliv Rev* **2007**, *59*, 308-324.
9. Tabata, Y. *Pharm Sci Technolo Today* **2000**, *3*, 80-89.
10. Varkey, M.; Gittens, S. A.; Uludag, H. *Expert Opin Drug Deliv* **2004**, *1*, 19-36.
11. Chen, F. M.; Zhang, M.; Wu, Z. F. *Biomaterials* **2010**, *31*, 6279-6308.
12. Lu, Z.; Zreiqat, H. *Tissue Eng Part A* **2010**, *16*, 3075-3084.
13. Roy, K.; Wang, D.; Hedley, M. L.; Barman, S. P. *Mol Ther* **2003**, *7*, 401-408.
14. Storrer, H.; Mooney, D. J. *Adv Drug Deliv Rev* **2006**, *58*, 500-514.
15. Babensee, J. E.; McIntire, L. V.; Mikos, A. G. *Pharm Res* **2000**, *17*, 497-504.
16. De Laporte, L.; Shea, L. D. *Adv Drug Deliv Rev* **2007**, *59*, 292-307.
17. Basmanav, F. B.; Kose, G. T.; Hasirci, V. *Biomaterials* **2008**, *29*, 4195-4204.
18. Censi, R.; Vermonden, T.; van Steenberghe, M. J.; Deschout, H.; Braeckmans, K.; De Smedt, S. C.; van Nostrum, C. F.; di Martino, P.; Hennink, W. E. *J Control Release* **2009**, *140*, 230-236.
19. Abbas, A. O.; Donovan, M. D.; Salem, A. K. *J Pharm Sci* **2008**, *97*, 2448-2461.
20. Sill, T. J.; von Recum, H. A. *Biomaterials* **2008**, *29*, 1989-2006.
21. Nie, H.; Soh, B. W.; Fu, Y. C.; Wang, C. H. *Biotechnol Bioeng* **2008**, *99*, 223-234.
22. Hoare, T. R.; Kohane, D. S. *Polymer* **2008**, *49*, 1993-2007.
23. Li, W. J.; Laurencin, C. T.; Caterson, E. J.; Tuan, R. S.; Ko, F. K. *J Biomed Mater Res* **2002**, *60*, 613-621.
24. Luu, Y. K.; Kim, K.; Hsiao, B. S.; Chu, B.; Hadjiargyrou, M. *J Control Release* **2003**, *89*, 341-353.
25. Pham, Q. P.; Sharma, U.; Mikos, A. G. *Tissue Eng* **2006**, *12*, 1197-1211.
26. Yang, F.; Both, S. K.; Yang, X.; Walboomers, X. F.; Jansen, J. A. *Acta Biomater* **2009**, *5*, 3295-3304.
27. Murugan, R.; Ramakrishna, S. *Tissue Eng* **2006**, *12*, 435-447.
28. Yarin, A. L.; Koombhongse, S.; Reneker, D. H. *J Appl Phys* **2001**, *89*, 3018-3026.
29. Venugopal, J.; Low, S.; Choon, A. T.; Ramakrishna, S. *J Biomed Mater Res B Appl Biomater* **2008**, *84*, 34-48.
30. Agarwal, S.; Wendorff, J. H.; Greiner, A. *AdvMater* **2009**, *21*, 3343-3351.
31. Zeugolis, D. I.; Khew, S. T.; Yew, E. S.; Ekaputra, A. K.; Tong, Y. W.; Yung, L. Y.; Huttmacher, D. W.; Sheppard, C.; Raghunath, M. *Biomaterials* **2008**, *29*, 2293-2305.

32. Dong, Y.; Liao, S.; Ngiam, M.; Chan, C. K.; Ramakrishna, S. *Tissue Eng Part B Rev* **2009**, *15*, 333-351.
33. Huang, X.; Brazel, C. S. *J Control Release* **2001**, *73*, 121-136.
34. Grassi, M.; Grassi, G. *Curr Drug Deliv* **2005**, *2*, 97-116.
35. Kootstra, N. A.; Verma, I. M. *Annu Rev Pharmacol Toxicol* **2003**, *43*, 413-439.
36. Nie, H.; Ho, M. L.; Wang, C. K.; Wang, C. H.; Fu, Y. C. *Biomaterials* **2009**, *30*, 892-901.
37. Nie, H.; Wang, C. H. *J Control Release* **2007**, *120*, 111-121.
38. Cleland, J. L. *Pharm Biotechnol* **1997**, *10*, 1-43.
39. Vasir, J. K.; Labhasetwar, V. *Adv Drug Deliv Rev* **2007**, *59*, 718-728.
40. Giteau, A.; Venier-Julienne, M. C.; Aubert-Pouessel, A.; Benoit, J. P. *Int J Pharm* **2008**, *350*, 14-26.
41. Shi, Y.; Huang, G. *Crit Rev Ther Drug Carrier Syst* **2009**, *26*, 29-84.
42. Yang, Y.; Li, X.; Qi, M.; Zhou, S.; Weng, J. *Eur J Pharm Biopharm* **2008**, *69*, 106-116.
43. Kowalczyk, T.; Nowicka, A.; Elbaum, D.; Kowalewski, T. A. *Biomacromolecules* **2008**, *9*, 2087-2090.
44. Zeng, J.; Aigner, A.; Czubyko, F.; Kissel, T.; Wendorff, J. H.; Greiner, A. *Biomacromolecules* **2005**, *6*, 1484-1488.
45. Yang, Y.; Li, X.; Cui, W.; Zhou, S.; Tan, R.; Wang, C. *J Biomed Mater Res A* **2008**, *86*, 374-385.
46. Li, Y.; Jiang, H.; Zhu, K. *J Mater Sci Mater Med* **2008**, *19*, 827-832.
47. Li, C.; Vepari, C.; Jin, H. J.; Kim, H. J.; Kaplan, D. L. *Biomaterials* **2006**, *27*, 3115-3124.
48. Schneider, A.; Wang, X. Y.; Kaplan, D. L.; Garlick, J. A.; Egles, C. *Acta Biomater* **2009**, *5*, 2570-2578.
49. Kim, B. S.; Oh, J. M.; Kim, K. S.; Seo, K. S.; Cho, J. S.; Khang, G.; Lee, H. B.; Park, K.; Kim, M. S. *Biomaterials* **2009**, *30*, 902-909.
50. Knoll, D.; Hermans, J. *J Biol Chem* **1983**, *258*, 5710-5715.
51. Michel, R.; Pasche, S.; Textor, M.; Castner, D. G. *Langmuir* **2005**, *21*, 12327-12332.
52. Wang, Y.; Annunziata, O. *J Phys Chem B* **2007**, *111*, 1222-1230.
53. Casper, C. L.; Yamaguchi, N.; Kiick, K. L.; Rabolt, J. F. *Biomacromolecules* **2005**, *6*, 1998-2007.
54. Fu, Y. C.; Nie, H.; Ho, M. L.; Wang, C. K.; Wang, C. H. *Biotechnol Bioeng* **2008**, *99*, 996-1006.
55. Chew, S. Y.; Wen, J.; Yim, E. K.; Leong, K. W. *Biomacromolecules* **2005**, *6*, 2017-2024.
56. Zhang, Y. Z.; Wang, X.; Feng, Y.; Li, J.; Lim, C. T.; Ramakrishna, S. *Biomacromolecules* **2006**, *7*, 1049-1057.
57. Liang, D.; Luu, Y. K.; Kim, K.; Hsiao, B. S.; Hadjiargyrou, M.; Chu, B. *Nucleic Acids Res* **2005**, *33*, e170. doi:10.1093/nar/gni171
58. Sun, Z. C.; Zussman, E.; Yarin, A. L.; Wendorff, J. H.; Greiner, A. *Adv Mater* **2003**, *15*, 1929-1932.
59. Chakraborty, S.; Liao, I. C.; Adler, A.; Leong, K. W. *Adv Drug Deliv Rev* **2009**, *61*, 1043-1054.
60. Doshi, J.; Reneker, D. H. *J Electrostat* **1995**, *35*, 151-160.
61. Jiang, H.; Hu, Y.; Zhao, P.; Li, Y.; Zhu, K. *J Biomed Mater Res B Appl Biomater* **2006**, *79*, 50-57.
62. Jiang, H.; Hu, Y.; Li, Y.; Zhao, P.; Zhu, K.; Chen, W. *J Control Release* **2005**, *108*, 237-243.

63. Li, X. Q.; Su, Y.; Chen, R.; He, C. L.; Wang, H. S.; Mo, X. M. *J Appl Polym Sci* **2009**, *111*, 1564-1570.
64. Liao, I. C.; Chew, S. Y.; Leong, K. W. *Nanomed* **2006**, *1*, 465-471.
65. Li, H.; Zhao, C. G.; Wang, Z. X.; Zhang, H.; Yuan, X. Y.; Kong, D. L. *J Biomat Sci-Polym Ed* **21**, 803-819.
66. Wang, J. G.; Liu, J. J.; Fan, C. Y.; Mo, X. M.; He, C. L.; Chen, F. *J Clinical Rehabilitative Tissue Eng Res* **2008**, *12*, 4440-4444.
67. Sahoo, S.; Ang, L. T.; Goh, J. C.; Toh, S. L. *J Biomed Mater Res A* **2009**, *93A*, 1539-1550.
68. Ji, W.; Yang, F.; van den Beucken, J. J.; Bian, Z.; Fan, M.; Chen, Z.; Jansen, J. A. *Acta Biomater* **2010**, *6*, 4199-4207.
69. Saraf, A.; Baggett, L. S.; Raphael, R. M.; Kasper, F. K.; Mikos, A. G. *J Control Release* **2010**, *143*, 95-103.
70. Liao, I. C.; Chen, S.; Liu, J. B.; Leong, K. W. *J Control Release* **2009**, *139*, 48-55.
71. Kim, H. S.; Yoo, H. S. *J Control Release* **2010**, *145*, 264-271.
72. Li, W.; Guo, Y.; Wang, H.; Shi, D.; Liang, C.; Ye, Z.; Qing, F.; Gong, J. *J Mater Sci Mater Med* **2008**, *19*, 847-854.
73. Choi, J. S.; Yoo, H. S. *J Bioact Compat Polym* **2007**, *22*, 508-524.
74. Choi, J. S.; Leong, K. W.; Yoo, H. S. *Biomaterials* **2008**, *29*, 587-96.
75. Ma, Z. W.; Kotaki, M.; Ramarkrishna, S. *J Membrane Sci* **2006**, *272*, 179-187.
76. Grafahrend, D.; Calvet, J. L.; Klinkhammer, K.; Salber, J.; Dalton, P. D.; Moller, M.; Klee, D. *Biotechnol Bioeng* **2008**, *101*, 609-621.
77. Sakai, S.; Yamada, Y.; Yamaguchi, T.; Ciach, T.; Kawakami, K. *J Biomed Mater Res A* **2009**, *88*, 281-287.
78. Park, Y.; Kang, E.; Kwon, O. J.; Hwang, T.; Park, H.; Lee, J. M.; Kim, J. H.; Yun, C. O. *J Control Release* **2010**, *148*, 75-82.
79. van der Walle, C. F.; Sharma, G.; Ravi Kumar, M. *Expert Opin Drug Deliv* **2009**, *6*, 177-186.
80. van de Weert, M.; Hennink, W. E.; Jiskoot, W. *Pharm Res* **2000**, *17*, 1159-1167.
81. Carpenter, J. F.; Pikal, M. J.; Chang, B. S.; Randolph, T. W. *Pharm Res* **1997**, *14*, 969-975.
82. Estey, T.; Kang, J.; Schwendeman, S. P.; Carpenter, J. F. *J Pharm Sci* **2006**, *95*, 1626-1639.
83. Houchin, M. L.; Topp, E. M. *J Pharm Sci* **2008**, *97*, 2395-2404.
84. Jiang, W.; Schwendeman, S. P. *Pharm Res* **2001**, *18*, 878-885.
85. Zhu, G.; Mallery, S. R.; Schwendeman, S. P. *Nat Biotechnol* **2000**, *18*, 52-57.
86. Mahr, J. A.; Gooding, L. R. *N Engl J Med* **2003**, *348*, 193-194.
88. Fernandez, C. A.; Rice, K. G. *Mol Pharm* **2009**, *6*, 1277-1289.
89. Yang, N. S.; Burkholder, J.; Roberts, B.; Martinell, B.; McCabe, D. *Proc Natl Acad Sci USA* **1990**, *87*, 9568-9572.
90. Lin, C.; Engbersen, J. F. *Expert Opin Drug Deliv* **2009**, *6*, 421-439.
91. Siepmann, J.; Siepmann, F. *Int J Pharm* **2008**, *364*, 328-343.

Appendix

ALP: alkaline phosphatase

BMP2: bone morphogenic protein 2 (protein form)

bmp2: bone morphogenic protein 2 (gene form)

BSA: bovine serum albumin

EGF: epidermal growth factor

FA: folic acid

HA: hyaluronic acid

HAp: hydroxylapatite

NGF: nerve growth factor

PCL: poly(ϵ -caprolactone)

PCL-b-PEG: poly(ϵ -caprolactone)-block-poly(ethylene glycol)

PDGF-bb: platelet-derived growth factor-bb

PDLLA: poly (_{D,L}-lactide)

PEG-b-PDLLA: poly (ethylene glycol)-block-poly(_{D,L}-lactide)

PLCL: poly(_L-lactide-co-epsilon-caprolactone)

PLGA: poly(lactide-co-glycolide)

PMMAAA: copolymer of methyl methacrylate (MMA) and acrylic acid (AA)

PSU: polysulphone

PVA: poly(vinyl alcohol)

pDNA: plasmid deoxyribonucleic acid

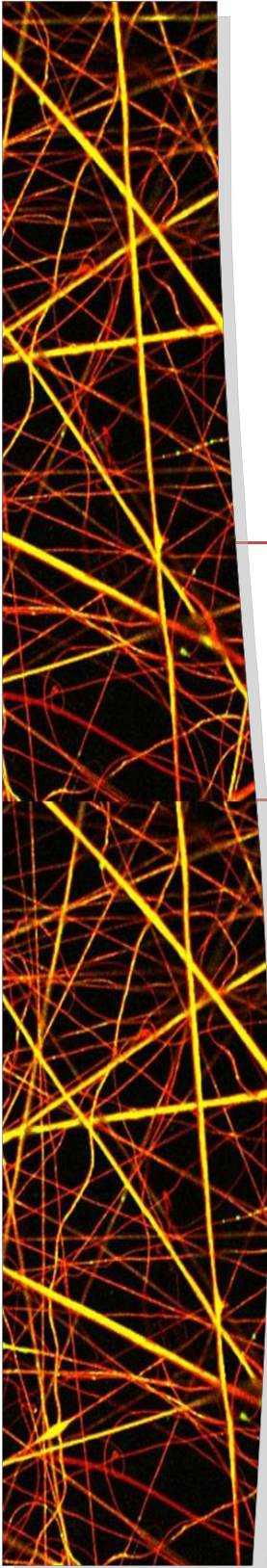
pGL3: plasmid DNA encoding luciferase

pBMP-2: plasmid DNA encoding bone morphogenic protein-2

pCMV β : plasmid DNA encoding β -galactosidase

pCMV-EGFP: plasmid DNA encoding enhanced green fluorescent protein with a cytomegalovirus promoter

pEGFP-N1: plasmid DNA encoding a red shifted variant of wild-type green fluorescent protein



**Incorporation of stromal cell-derived
factor-1 α in PCL/gelatin electrospun
membranes for guided bone regeneration**

Wei Ji, Fang Yang, Jinling Ma, Margaretha J. Bouma,
Otto C. Boerman, Zhi Chen, Jeroen J.J.P. van den Beucken,
John A. Jansen

Biomaterials. **2013**, 34, 735-745.

1. Introduction

Guided bone regeneration (GBR) is a frequently used strategy to treat bony defects in the craniomaxillofacial region. The principle of GBR is to create and maintain a secluded space by using a barrier membrane to prevent the invasion of fast growing epithelial and other soft tissues from migrating into the osseous defect, thereby allowing time for osteogenic cell populations originating from the parent bone to inhabit the osseous defect¹. Conventionally, GBR membranes require flexibility to adapt to and optimally cover a bone defect, to maintain the space for bone formation and to connect with the soft tissues², and biodegradability to eliminate the need for membrane removal surgery³. To date, most of the available biodegradable GBR membranes present the required competence as barrier membranes for space provision, yet the amount of regenerated bone is limited due to the relatively low regenerative capacity of bone tissue⁴. Consequently, the current research efforts focus on developing a bioactive GBR membrane that not only functions as a barrier membrane, but also exerts biological activity to stimulate *in situ* bone regeneration in the defect site.

In the past decades, many attempts have been made to enhance the biological activity of GBR membranes. One frequently used approach is to incorporate osteogenic (growth) factors into GBR membranes, hence to encourage the differentiation of osteogenic progenitor cell types in the secluded space under the membrane. Among the various choices of osteogenic factors, bone morphogenetic protein 2 (BMP-2) has been most frequently used to functionalize GBR membranes, withstanding its recently reported adverse effects (e.g. local inflammation and heterotopic ossification) related to uncontrolled release profiles⁵. Danesh-Meyer et al.⁶ previously reported that GBR membranes absorbed with BMP-2 promoted osseous repair compared to conventional GBR membranes, either with or without the use of various osseous grafting materials. In addition, Park et al.⁷ reported that BMP-2 conjugated chitosan membranes significantly increased osteoblastic cell attachment, proliferation as well as calcium deposition, indicating that BMP-2 conjugated membranes would be applicable for inducing bone formation in future GBR procedures.

Recently, an alternative approach has emerged as a promising strategy for *in situ* tissue regeneration, which focuses on cell recruitment. This cell recruitment approach maximizes the body's own regenerative capacity by recruiting endogenous stem/progenitor cells to the injury site to (i) exert local functional and reparative effects, and (ii) to synchronize the biological functions of other cell types via paracrine mechanisms^{8,9}. In view of the bone healing process, tissue regeneration in a bony defect is dependent on the recruitment of progenitor cells either derived from bone marrow or present at the defect site, for which these cells "sense" tissue injury, migrate to the injured sites, and undergo specific differentiation to form mature bone tissue¹⁰. Multiple types of progenitor cells re-

side within the bone marrow, and amongst them, the non-haemopoietic progenitor cells, which are commonly referred to as bone marrow stromal cells (BMSCs), are considered most potent during bone regeneration because these cells exhibit multi-lineage differentiation capacity¹¹. Additionally, the migratory capacity of BMSCs to sites of bone fracture has been reported previously¹⁰. In view of this, development of a bioactive membrane that can increase recruitment of BMSCs to the defect area in addition to simple space provision holds huge potential for an enhanced bone regeneration in clinical GBR applications.

To induce BMSCs recruitment, a commonly used strategy is to increase local concentrations of cytokines and/or chemokines at the target site¹², because cytokines and chemokines are important factors in regulating mobilization, trafficking and homing of stem/progenitor cells¹³. Among various cytokines or chemokines, stromal cell derived factor-1 α (SDF-1 α), also known as chemokine (C-X-C motif) ligand 12 (CXCL12), is particularly important in BMSCs homing and localization within the bone marrow¹⁴. Previous studies indicated that SDF-1 α activates cell recruitment mainly through its receptor CXCR4^{14,15}, suggesting that the SDF-1 α /CXCR4 axis plays an important role in stem cell/progenitor cell migration. Wynn et al.¹⁶ reported that SDF-1 α regulates the migration of human BMSCs in a dose-dependent manner by using a transwell migration assay. Recently, Kitaori et al.¹⁰ discovered that the SDF-1 α /CXCR4 axis plays a crucial role in the migration of BMSCs to a fracture site, and the recruited cells actively participated in endochondral bone repair observed in a segmental bone defect model.

On the basis of the aforementioned, a straightforward approach to generate bioactive GBR membranes with BMSCs recruitment capacity is to incorporate SDF-1 α into conventional barrier membranes. Nevertheless, limited research has been performed to explore the feasibility and performance of such a bioactive membrane with local delivery of SDF-1 α in GBR applications. Among the rare cases which investigated *in vivo* performance of locally delivered SDF-1 α , Thevenot et al.¹⁷ and Schantz et al.¹⁸ used mini-osmotic pumps and a customized apparatus comprising a reservoir and microneedle, respectively, to achieve sustained SDF-1 α delivery *in vivo*. However, these approaches are apparently not sufficiently sophisticated to be applied in clinical GBR procedures.

The current study aimed to (i) develop membranes absorbed with SDF-1 α as bioactive GBR membranes, and (ii) investigate their biological effects on BMSCs recruitment and bone regeneration using a rat cranial defect model. To this end, GBR membranes were prepared by blends of poly(ϵ -caprolactone) (PCL) and type B-gelatin using an electrospinning technique¹⁹, and the obtained membranes were further loaded with SDF-1 α via physical adsorption. PCL was chosen due to its good spinnability, flexibility, and biocompatibility²⁰, and the addition of type B-gelatin was to provide electrostatic affinity for loaded SDF-1 α ²¹ in order to improve SDF-1 α release kinetics. Our hypothesis was that the electrospun PCL/gelatin membrane loaded with SDF-1 α would stimulate BMSCs recruitment and enhance bone regeneration in the defect site.

2. Materials and Methods

2.1. Membrane preparation

GBR membranes were prepared using an electrospinning technique. To prepare the electrospinning solution, PCL (inherent viscosity 1.0–1.3 dl/g), gelatin powder from bovine skin (Type B, ~225 g Bloom), and organic solvent 2,2,2-trifluoroethanol (TFE) (purity \geq 99.8%) were obtained from Durect (Cupertino, USA), Sigma-Aldrich (St. Louis, USA) and Acros Organics (Geel, Belgium), respectively. PCL and type B-gelatin (w/w=1/1) were dissolved in 90% TFE in deionized H₂O at a concentration of 16% w/v. A commercially available electrospinning set-up (Advanced Surface Technology, Bleiswijk, The Netherlands) was used for the membrane preparation. The feeding rate for the solution was 2.0 ml/h, and the collection distance was 18 cm. A high voltage of 20 kV was applied to generate a stable polymer jet.

The membranes were collected on a rotating mandrel covered with aluminium foil and left in vacuum conditions overnight to eliminate solvent residues. The obtained membranes were cross-linked according to a previously described method²² using glutaraldehyde (Acros Organics, Geel, Belgium) vapour at room temperature for 24 h. After cross-linking, the membranes were washed with 100 mM glycine (Sigma-Aldrich, St. Louis, USA) solution followed by a rinse with distilled water. Thereafter, the membranes were punched into disc shape with 15 mm or 8 mm in diameter for *in vitro* and *in vivo* analysis, respectively. Samples were freeze dried for 72 h, and subsequently sterilized by ethylene oxide (Synergy Health, Venlo, Netherlands) before further use.

2.2. Membrane characterization

The morphology of the fabricated GBR membrane was observed by a high-resolution field emission scanning electron microscope (SEM; JEOL-SM3010, Tokyo, Japan), operated at an acceleration voltage of 3.0 kV. The fiber diameters were measured from the SEM micrographs obtained at random locations ($n \approx 100$) using Image J software (National Institutes of Health, Bethesda, USA).

Fourier transform infrared spectrometry (FTIR; Spectrum One, Perkin-Elmer, USA) was used to analyze the chemical structure of the membrane over a range of 650–4000 cm⁻¹ at a resolution of 4 cm⁻¹.

2.3. *In vitro* release experiment

Recombinant human SDF-1 α (R&D systems, Abingdon, UK) was labelled with ¹²⁵I as described previously²³ for *in vitro* release experiments. Briefly, in a 500 μ l eppendorf tube coated with 100 μ g iodogen, 10 μ l of 0.5 M phosphate buffer, pH 7.2 was added. SDF-1 α (2 μ g) and 10–15 MBq ¹²⁵I (Perkin-Elmer, Boston, USA) was added and the total volume was adjusted to 100 μ l with 0.05 M phosphate buffer. The reaction mixture was incubat-

ed at room temperature for 10 min and after which 100 μ l of saturated tyrosine solution in PBS was added. The labelling efficiency of the reaction was determined at 27% for SDF-1 α . To remove the non-incorporated 125 I, the reaction mixture was eluted on a pre-rinsed disposable NAP-5 column with 0.1% BSA in PBS (GE Healthcare, Diegem, Belgium). The specific activity of the 125 I-labeled SDF-1 α was 29 μ Ci/ μ g, and the radiochemical purity of the labelled protein was 98%, as determined by instant thin layer chromatography (ITLC).

Three groups with different loading amounts of SDF-1 α ($n=3$) were set up for the *in vitro* release experiment. In each group, a volume of 20 μ l 125 I-labeled/unlabelled mixture of SDF-1 α solution containing 50, 100, or 200 ng was adsorbed onto disc-shaped PCL/gelatin electrospun membranes (15 mm in diameter). Thereafter, the membranes ($n=3$) were placed separately in 10 ml glass vials and incubated in 3 ml sterile PBS at 37 °C on an orbital shaker at low rotational speed (60 rpm) for 35 days. At predetermined time intervals, the membranes were carefully transferred to new vials containing fresh PBS and the activity was measured in a shielded well-type gamma counter (Wizard, Pharmacia-LKB, Uppsala, Sweden). Standards were measured simultaneously to correct for radioactive decay. The remaining activity in the PCL/gelatin membranes was expressed as percentage of the initial dose.

2.4. Rat bone marrow stromal cells culture

Rat bone marrow stromal cells (BMSCs) were isolated from 7-week-old male Wistar rats (Charles River; Approval No.: RU-DEC 2011-142) and 12-week-old green fluorescent protein (GFP)-transgenic Sprague–Dawley rats (Approval No.: RU-DEC 2010-028), respectively, after the approval from Radboud University Nijmegen Animal Ethics Committee. Cell culture reagents including minimal essential medium (α -MEM), fetal bovine serum (FBS), gentamycin and fungizone were purchased from Gibco (Bleiswijk, Netherlands).

Briefly, two femora of each rat were extracted and washed three times in α -MEM supplemented with 0.5 mg/ml gentamycin and 3 μ g/ml fungizone. Epiphyses were cut off and diaphyses were flushed out with 15ml proliferation medium, consisting of α -MEM supplemented with 10% FBS and 50 μ g/ml gentamycin. The flush-out of bone marrow from different rats was pooled and cultured for 2 days in a humidified incubator (37 °C, 5% CO₂), after which the medium was refreshed to remove non-adherent cells. After primary culture for an additional 4 days, the cells were trypsinized and frozen in liquid nitrogen. Prior to the *in vitro* experiment, cells were thawed and expanded in proliferation medium up to passage 3-4 for further flowcytometry and migration analysis.

2.5. Characterization of CXCR4 expression on rat BMSCs

Prior to the cell migration assay, flowcytometry (both extracellular and intracellular staining) was performed to characterize the expression of CXCR4 in both wild type and

GFP-transgenic rat BMSCs (passage 3). Flowcytometry antibodies were all purchased from Abcam (Cambridge, UK).

For extracellular staining, cells were incubated on ice with primary rabbit polyclonal antibody to CXCR4 (20 µg/ml, 30 min), followed by incubation with secondary donkey F(ab')₂ polyclonal antibody to rabbit IgG conjugated with R-Phycoerythrin (10 µg/ml, 20 min). For intracellular staining, cells were incubated at 4°C for 45 min in Fixation/Permeabilization buffer, which was prepared by four times dilution of Fixation/Permeabilization concentrate (eBioscience, San Diego, USA) in Fixation/Permeabilization diluent (eBioscience, San Diego, USA). Cells were then stained with the aforementioned primary and secondary antibodies, which were diluted in Permeabilization buffer (eBioscience, San Diego, USA) using the same concentrations and time as described for extracellular staining. After staining, the cells were analysed using CyAn™ ADP 9 colour Analyser (Beckman Coulter, Inc., Miami, USA) with Summit Software 4.3.01.

2.6. *In vitro* rat BMSCs recruitment

A transwell migration model was used as previously described¹⁷ with slight modifications to examine rat BMSCs recruitment to the PCL/gelatin membrane with SDF-1α adsorption. In brief, wild type rat BMSCs (passage 4) were starved overnight in α-MEM supplemented with 0.2% bovine serum albumin (BSA; purity ≥ 98%; Sigma–Aldrich, St. Louis, USA) and 50 µg/ml gentamycin. Then, the cells were trypsinized and seeded onto ThinCert™ cell culture inserts (membrane pore 8µm, Greiner Bio-One) in a 24-well plate at cell density of 10,000 cells/insert.

The SDF-1α dose used for *in vitro* cell recruitment assay was consistent with the one described in section 2.3. In addition, membranes absorbed with 400 ng of SDF-1α were included to examine the high dose effect of SDF-1α on BMSCs recruitment. The group of bare membranes was set up as a negative control. In brief, 5 groups of PCL/gelatin membranes (15 mm in diameter; *n*=3) loaded with different amounts of SDF-1α (0-400 ng) were placed below the inserts, after which 200 µl and 600 µl of BMSCs proliferation medium was added in the upper and lower chambers, respectively. After 24h culture in a humidified incubator (37 °C, 5% CO₂), the inserts were removed and scraped on the upper side to remove adherent cells. Further, they were fixed in 10% formalin for 5 min, and crystal violet (0.05%) stained for 30 min to visualize the migrated cells. The inserts with stained cells were then photographed with Zeiss Imager Z1 together with AxioCam MRc5 camera using AxioVision 4.6.3 software (Carl Zeiss Microimaging GmbH, Göttingen, Germany). Quantification of migrated cells based on the obtained images was performed by two independent examiners (WJ and MB) using Image J software (National Institutes of Health, Bethesda, USA).

2.7. *Animal experiment design*

Eleven healthy 8-week old nude rats (CrI:NIH-Foxn1^{tmu}), weighing 250 g in average, were used as experimental animals. The protocol was approved by the Animal Ethical Committee of the Radboud University Nijmegen Medical Center (Approval No.: RU-DEC 2011-140) and national guidelines for the care and use of laboratory animals were observed. The animal experiment included two parts: (i) a short-term experiment used a single cranial defect (8 mm in diameter) in the center of rat skull, aiming to trace the engraftment of BMSCs; and (ii) a long-term experiment used bilateral cranial defects (5 mm in diameter), aiming to evaluate the biological performance of the obtained membranes. Sintered titanium fiber mesh (Bekaert N.v., Zwevegem, Belgium) was used in these studies as a filling material in the defects in order to avoid brain tissue dilation in cranial defect and to mimic clinical GBR strategy which usually involves filling of grafting materials in the defect. The fiber mesh, which has a volumetric porosity of 86%, density of 600 g/m² and fiber diameter of 45 μm, showed excellent bone biocompatibility previously²⁴. The titanium fiber mesh was punched into disc shape with the same diameter as the defect, and sterilized by autoclaving before implantation. The defect model and group information for the entire animal experiment are listed in Table 1.

Table 1. Animal experiment design

Purpose	Animal number	Animal Model	Groups ^a	Investigation period	Analysis method
^b In vivo cell tracking	2	Cranial defect (8 mm in diameter) + intravenous injection of GFP-transgenic rBMSCs (2×10 ⁶ cells)	(1) SDF- (2) SDF+ (n=1)	2 weeks	IVIS [®] Lumina Laser scanning confocal microscopy
^c In vivo biological evaluation	9	Bilateral cranial defect (5 mm in diameter)	(1) SDF- (2) SDF+ (3) EMP (n=6)	8 weeks	Micro CT Descriptive histology Histomorphometry

^a Groups in the animal experiment

SDF-: defect filled with titanium fiber mesh and covered with bare electrospun membrane

SDF+: defect filled with titanium fiber mesh and covered with SDF-1α loaded electrospun membrane

EMP: empty defect (to provide biological reference)

^b Disc shape membranes (10 mm diameter) with retention volume of 50 μl were used. In SDF+ group, 50 μl of SDF-1α solution (100 μg/ml) was absorbed by the electrospun membrane; whereas in SDF- group, the same volume of PBS was absorbed by the membrane.

^c Disc shape membranes (8 mm in diameter) were used. In SDF+ group, 20 μl of SDF-1α solution (100 μg/ml) was absorbed by the electrospun membrane; whereas in SDF- group, the same volume of PBS was absorbed by the membrane

2.8. Surgical procedure

Before surgery, the rats were anesthetized by isoflurane inhalation (Rhodia Organique Fine Limited, Avonmouth, Bristol, UK) via intubation. Then, the rats were immobilized on their abdomen and the skull was shaved and disinfected with chlorhexidine. A longitudinal incision was made from the nasal bone to the occipital protuberance. To minimize

pain, lidocaine HCl 1% (B. Braun, Melsungen, Germany) was dripped onto the periosteum before incision and exposure of the parietal bone.

2.8.1. *In vivo cell tracking*

Two rats were used to trace the recruitment of BMSCs. For this purpose, a cranial defect with 8 mm in diameter was created by marking the defect outline with a dental trephine drill (outside diameter 8 mm, ACE dental implant system, Brockton MA, USA). After that, a full-thickness bone defect was created by removing cortical bone with an ultrasonic device (Piezosurgery, Mectron, Carasco, Italy) in the middle of the skull with caution for the underlying dura mater and sagittal sinus and using constant cooling with sterile saline. Subsequently, the defect was filled with a disc-shaped titanium fiber mesh (8 mm in diameter) and then covered with an electrospun membrane with or without absorbing 50 μ l of SDF-1 α solution (100 μ g/ml) (SDF+ or SDF-). Finally, the skin and periosteal tissues were closed over the implants with Vicryl[®] 5-0 sutures. To minimize post-operative discomfort, Rimadyl (Pfizer Animal Health B.V, Capelle aan den IJssel, Netherlands) was administered subcutaneously (5 mg/kg) directly after the operation and for 2 days after surgery.

After 2 days of implantation, 2 ml PBS solution containing 2×10^6 GFP-transgenic rat BMSCs was injected into the tail vein of the rats. Thereafter, the recruitment of GFP-transgenic rat BMSCs at the defect site was monitored using *in vivo* bioluminescence imaging (IVIS[®] Lumina, Caliper Life Sciences, USA). Fluorescent intensity measurements were performed over the region of the cranial defect every two days, and imaging data were analysed using Living Image[®] 3.0 software (Caliper Life Sciences, USA). After 2 weeks, the rats were sacrificed using CO₂ suffocation, and the samples with surrounding tissue were retrieved for histological analysis.

2.8.2. *In vivo biological evaluation*

Nine animals were randomized into 3 groups (Table 1) for a long term study to evaluate biological responses in a cranial defect upon implantation of a PCL/gelatin membrane with or without absorbing 20 μ l of SDF-1 α solution (100 μ g/ml) (SDF+ or SDF-). Bilateral full-thickness bone defects (5 mm in diameter) were created by removing cortical bone with a dental trephine drill (outer diameter 5 mm, Hager & Meisinger GmbH, Neuss, Germany). For the implantation groups SDF- and SDF+, the defect was filled with a disc-shaped titanium fiber mesh (5 mm in diameter), and thereafter covered with an electrospun membrane (SDF- or SDF+). The empty group (EMP), in which the defect was left uncovered, was set up as a biological reference. After that, the skin and periosteal tissues were closed with Vicryl[®] 5-0 sutures, and the same post-surgery treatment as described in *section 2.8.1* was applied to the rats. After 8 weeks, the animals were sacrificed using CO₂ suffocation, and the implants with surrounding tissue were retrieved for

microcomputed tomography (micro-CT) imaging and histological analysis.

2.9. Micro-CT imaging

Three samples randomly selected from each group were used for micro-CT imaging to qualitatively visualize implant location and bone formation. The harvested cranial bone defects were imaged using a high resolution SkyScan-1072 micro-CT imaging system (SkyScan, Aartselaar, Belgium). For each sample, a total of 1023 micro-tomographic slices were gained using a slice increment of 20 μm in order to scan the whole defect (5 mm) and the surrounding bone. Then, using Nrecon V1.4 (SkyScan, Kontich, Belgium), a cone beam reconstruction was performed on the projected files. Finally, a 3D-reconstruction of the defect was obtained by using 3D creator software as previously described²⁵.

2.10. Histological preparations

The retrieved implants with surrounding tissue were fixed in 10% formalin, dehydrated in a graded series of ethanol and embedded in methylnmethacrylate. In the middle of the implants, perpendicular thin sections (10 μm) were prepared as previously described²⁶ using a microtome with a diamond blade (Leica Microsystems SP 1600, Nussloch, Germany).

For the samples retrieved from the cell tracking experiment, three sections of each implant were prepared and examined using laser scanning confocal microscopy (Olympus FV1000, Japan). The excitation wavelength for GFP was 488 nm, and images were captured with a 60 \times /1.35NA objective. For the samples retrieved from the biological evaluation experiment, three sections of each implant were prepared and stained with methylene blue and basic fuchsin for histological and histomorphometrical evaluation.

2.11. Histological and histomorphometrical evaluation

All histological sections ($n=3$ per implant) were photographed with the Zeiss Imager Z1 together with the AxioCam MRc5 camera using AxioVision 4.6.3 software (Carl Zeiss Microimaging GmbH, Göttingen, Germany). In each group, the probability of animals showing bone formation was determined. Furthermore, histomorphometrical evaluation was performed to quantify bone formation. In brief, the sections were scored using computer-based image analysis techniques (Leica[®] Qwin Pro-image analysis system, Wetzlar, Germany), which recognize bone tissue from implanted titanium fiber mesh based on different RGB values from highly magnified digitalized images. Manual corrections were also applied to ensure the precise selection of newly formed bone tissue within defect area. The bone formation area (μm^2) was determined as newly developed bone in two regions: (i) inside the titanium fiber mesh, and (ii) outside the titanium fiber mesh. The amount of newly formed bone was defined as:

Amount of bone formation = Total bone formation area (μm^2) / cross-sectional distance (μm) (Figure 1).

Three sections per specimen were measured and averaged.

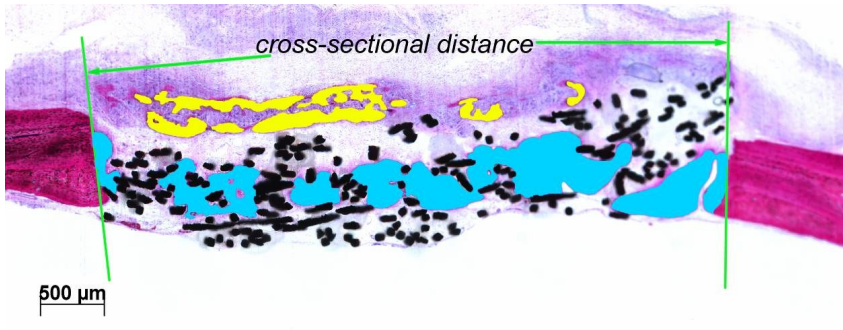


Figure 1. Schematic overview of histomorphometrical evaluation. The bone formation area (μm^2) was determined as newly developed bone in two regions: (i) inside the titanium fiber mesh (blue area) and (ii) outside titanium fiber mesh (yellow area). The amount of newly formed bone was defined as:

$$\text{Amount of bone formation} = \text{Total bone formation area } (\mu\text{m}^2) / \text{cross-sectional distance } (\mu\text{m})$$

2.12. Statistical analysis

Data was expressed as mean \pm standard deviation. For *in vitro* cell migration measurements, a one-way ANOVA with post Dunnett's multiple comparison was applied. The statistical analysis was performed using Graphpad InStat software (InStat[®] 3.05, Graphpad Software Inc., La Jolla, USA). For histological and histomorphometrical evaluation, statistical analysis was performed using SPSS 18.0 (SPSS, Chicago, USA). A Chi-square test was applied to compare the bone formation probability between the groups. Furthermore, an independent *t*-test was performed to compare the amount of newly formed bone between groups SDF- and SDF+.

3. Results

3.1. Characterization of PCL/gelatin electrospun membrane

The nanofibrous PCL/gelatin membranes were prepared by electrospinning, and their morphology was examined using SEM. SEM images (Figure 2a) showed a uniform fiber structure with average fiber diameters of 312 ± 146 nm.

FTIR spectra of prepared PCL/gelatin membrane are shown in Figure 2b. Infrared spectra for PCL related stretching modes were observed from the membrane, including 2940 cm^{-1} (asymmetric CH_2 stretching), 2869 cm^{-1} (symmetric CH_2 stretching), 1725 cm^{-1} (carbonyl stretching), and 1237 cm^{-1} (asymmetric COC stretching). Characteristic bands of protein appeared at approximately 1652 cm^{-1} (amide I) and 1542 cm^{-1} (amide II), respectively. The amide I band at 1652 cm^{-1} was attributed to both a random coil and α -helix conformation of gelatin²⁷.

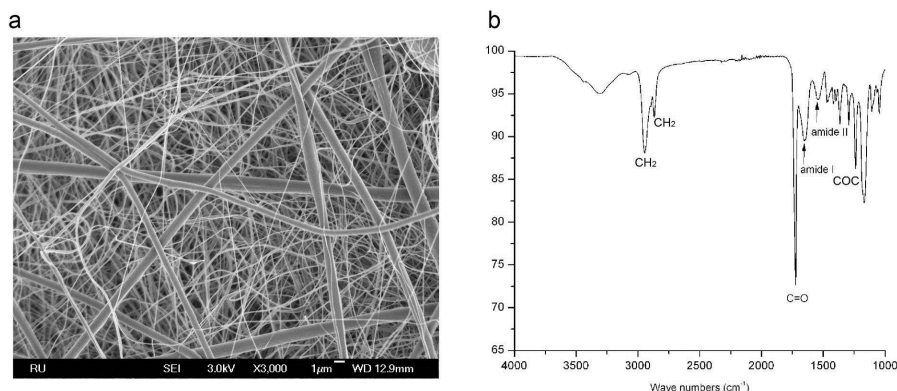


Figure 2. Characterization of prepared electrospun membrane.

3.2. *In vitro* SDF-1 α release

Figure 3 shows the cumulative protein release profiles of the electrospun membrane loaded with different amounts of SDF-1 α . For all three groups, a similar release pattern was observed, which included a burst release within 4 h, followed by a sustained release up to 35 days.

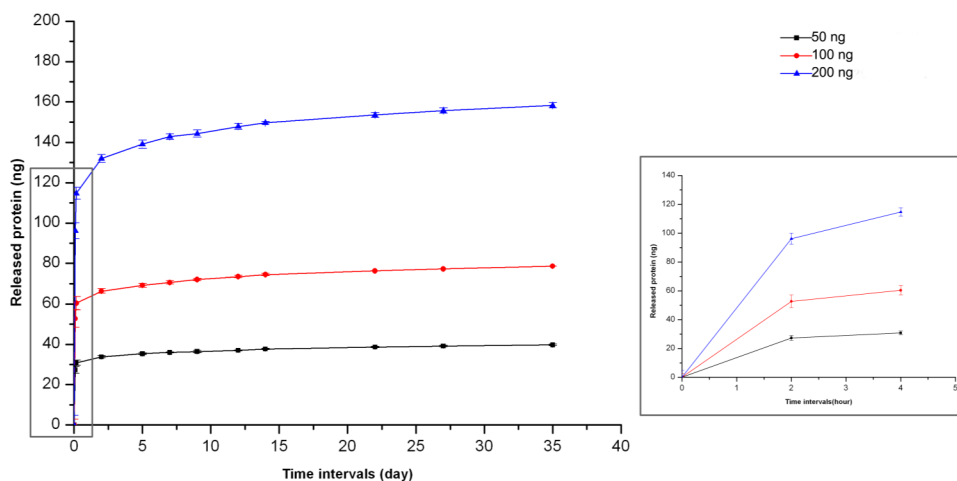


Figure 3. *In vitro* SDF-1 α release profiles

During burst release, 30.8 ± 1.3 ng, 60.4 ± 3.3 ng, and 114.7 ± 2.9 ng SDF-1 α was released from membranes loaded with 50, 100, and 200 ng SDF-1 α , respectively. The burst release percentage was similar ($p > 0.05$) for all three groups with around 60% burst release (Table 2). From day 2 onwards, the membranes loaded with different amounts of SDF-1 α exhibited similar sustained release profiles (approximately 0.35% release per day; $p > 0.05$), which resulted in $\sim 80\%$ cumulative release after 35 days (Table 2). For each group, the cumulative release curve was successfully fitted by an allometric power growth equation $y = kt^n$ (Table 2).

Table 2. Cumulative release (%) of membrane loaded with different amount of SDF-1 α (50–200ng) & allometric regression analysis ($y=kt^n$) of cumulative release

	50 ng (%)	100 ng (%)	200 ng (%)
Burst release (within 4h)	61.6 \pm 2.5	60.4 \pm 3.3	57.3 \pm 1.5
Total release (after 35 days)	79.4 \pm 0.4	78.6 \pm 0.3	79.1 \pm 0.5
<i>k</i>	64.27	63.01	62.59
<i>n</i>	0.059	0.062	0.067
Adjusted R ²	0.98	0.99	0.98

3.3. Expression of CXCR4 on rat BMSCs

Flowcytometry was performed to detect the expression of SDF-1 α receptor (CXCR4) on the rat BMSCs (passage 3) (Figure 4a&b). The results showed that CXCR4 could not be detected from extracellular staining (Figure 4a). In contrast, CXCR4 was highly detected from intracellular staining (Figure 4b). Similar CXCR4 expression patterns were observed for GFP-transgenic rat BMSCs (passage 3).

3.4. *In vitro* rat BMSCs recruitment

In vitro rat BMSCs recruitment was tested using a transwell system. Crystal violet staining showed that electrospun PCL/gelatin membranes with SDF-1 α release were able to induce rat BMSCs migration across the transwell membrane (Figure 4c). Compared to the bare PCL/gelatin membranes, SDF-1 α loaded membranes significantly enhanced rat BMSCs migration ($p < 0.05$). Membranes absorbed with different amounts of SDF-1 α (50, 100, 200, & 400 ng, respectively) resulted in 5.64 \pm 1.29, 6.14 \pm 2.92, 6.97 \pm 1.00, and 5.11 \pm 1.56 fold of migration, respectively, with no significant differences between different amounts ($p > 0.05$; Figure 4d).

3.5. Animal experiment

3.5.1. General observations

From the total of 11 animals available for surgery, one animal died during anaesthesia. The remaining 10 animals recovered uneventfully from the surgical procedure and remained in good health. No signs of wound complications were observed post-operatively and during the course of the experiment.

At the end of experiment, 2 and 16 samples were retrieved from *in vivo* cell tracking and biological evaluation experiments, respectively (Table 3). Macroscopic signs of inflammation or adverse tissue responses were absent for all the retrieved samples. For the biological evaluation experiment, two samples were lost (one from SDF- group and another from EMP group) due to animal death during anaesthesia. In addition, one sample from

SDF+ group was excluded from evaluation due to an inappropriate histological preparation (Table 3).

Table 3. Summary of samples retrieved from animal experiment

Purpose	Groups	Number of im- planted samples	Number of re- trieved samples	Number of samples for evaluation
<i>In vivo</i> cell tracking	SDF-	1	1	1
	SDF+	1	1	1
<i>In vivo</i> biological evaluation	SDF-	5 ^a	5	5
	SDF+	6	6	5 ^b
	EMP	5 ^a	5	5

^a Both SDF- and EMP group lost one sample due to animal death caused by anaesthesia during surgery.

^b One sample from SDF+ group was excluded from evaluation due to the inappropriate histological preparation.

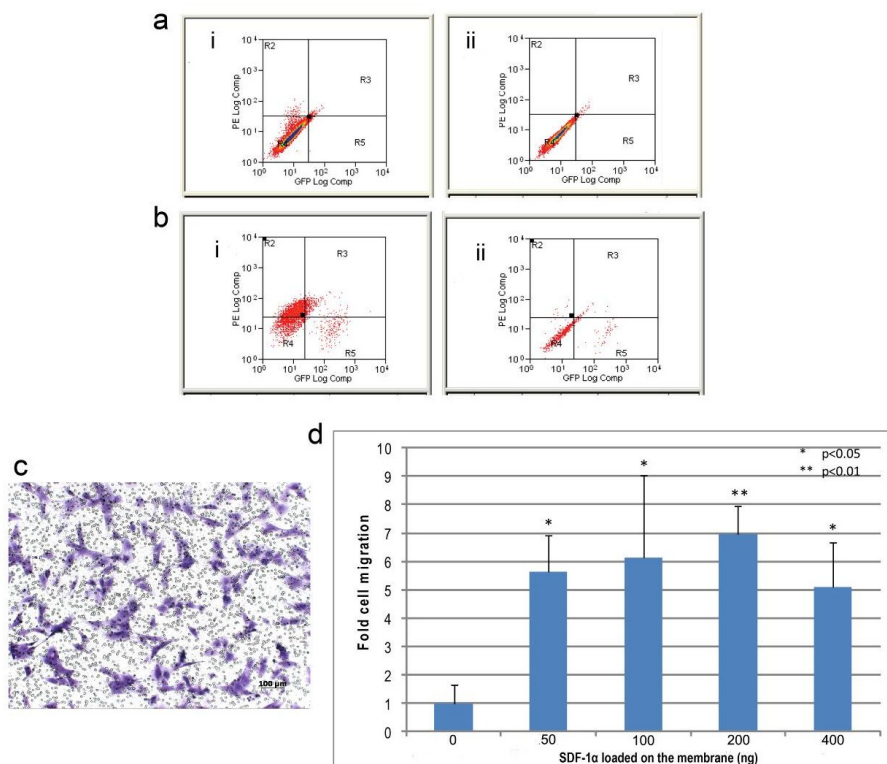
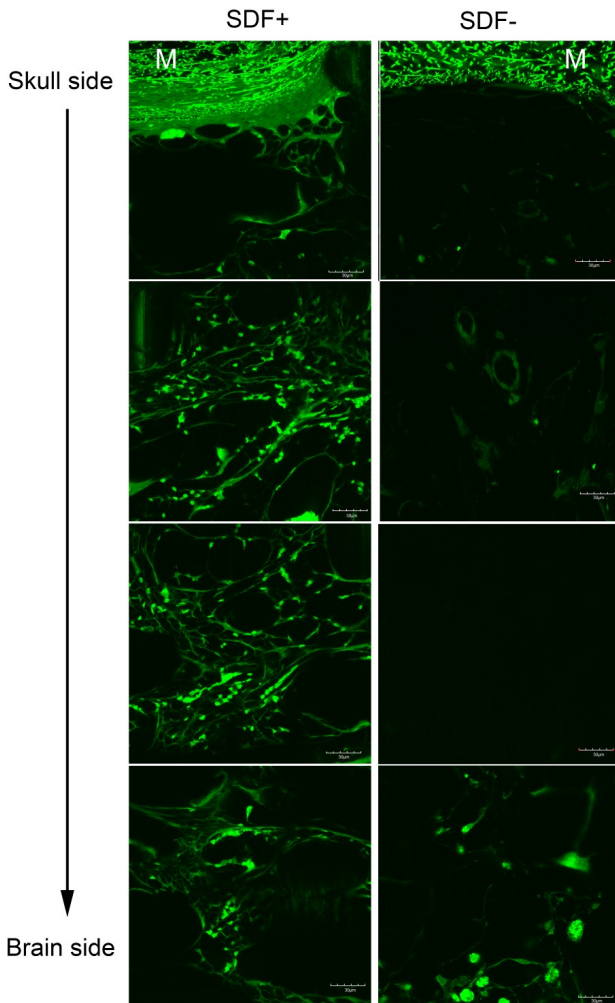


Figure 4. CXCR4 expression on rat BMSCs and *in vitro* rat BMSCs migration upon to SDF-1 α loaded membrane. The expression of SDF-1 α receptor (CXCR4) on rat BMSCs was detected using flowcytometry. (a) A representative example of extracellular expression of CXCR4 in rat BMSCs by antibody staining (i) and isotype control (ii). No obvious cell population was observed in PE positive region (R2), indicating negative extracellular expression of CXCR4. (b) A representative example of intracellular expression of CXCR4 in rat BMSCs by antibody staining (i) and isotype control (ii). Obvious cell population was observed in PE positive region (R2), indicating the

positive intracellular expression of CXCR4. (c) rat BMSCs migration across transwell membranes (pore 8 μm) was quantified after 24 h by removing cells from the seeded side and crystal violet staining on cells on the underside. (Representative image from the membrane loaded with 100 ng SDF-1 α , scale bar = 100 μm). (d) Five different amount of SDF-1 α (0–400 ng) was loaded on the electrospun membrane and tested *in vitro* chemotactic effect on rat BMSCs using transwell migration system. Compared to the bare membrane, the addition of SDF-1 α significantly induced the rat BMSCs migration ($p < 0.05$), and there was no dose-dependent effect on rat BMSCs migration.

3.5.2. *In vivo* cell tracking

In vivo tracking of GFP-BMSCs using luminescence appeared to be not possible, as no fluorescent signal was observed from *in vivo* bioluminescence imaging. As an alternative method, the infiltration of GFP-BMSCs within the cranial defect was assessed by laser



scanning confocal microscopy using (non-stained) histological sections (Figure 5). Autofluorescence of polymeric membrane and newly formed blood vessel structures was observed in the cranial defect region. Compared to the bare membrane, apparently more GFP-signal was observed for SDF-1 α loaded PCL/gelatin membrane throughout the whole thickness of defect the area. However, the exact contribution of GFP-rat BMSCs to the GFP-signal could not be ascertained due to the relatively high autofluorescence of endogenous tissue.

Figure 5. Laser scanning confocal microscope images of the samples retrieved from the rats with GFP-transgenic rat BMSCs injection. Autofluorescence of polymeric membrane (indicated as “M”) and newly formed blood vessel structures was observed in the cranial defect region. Compared to the bare membrane, apparently more GFP-signals were observed for

SDF-1 α loaded PCL/gelatin membrane throughout the whole thickness of defect area. However, exact contribution of GFP-rat BMSCs to the GFP-signal could not be ascertained due to the relatively high autofluorescence of endogenous tissue. Scale bar = 30 μm .

3.5.3. Biological evaluation

3.5.3.1. Micro-CT imaging

The implant location and bone formation in the skull defects ($n=3$, randomly selected) was imaged with micro-CT. The micro-CT images (Figure 6) showed no bone formation for control group (empty defect, EMP) after 8 weeks of implantation. Due to scattering of the titanium fiber mesh, reliable quantification of bone formation within the cranial defect area was not possible.

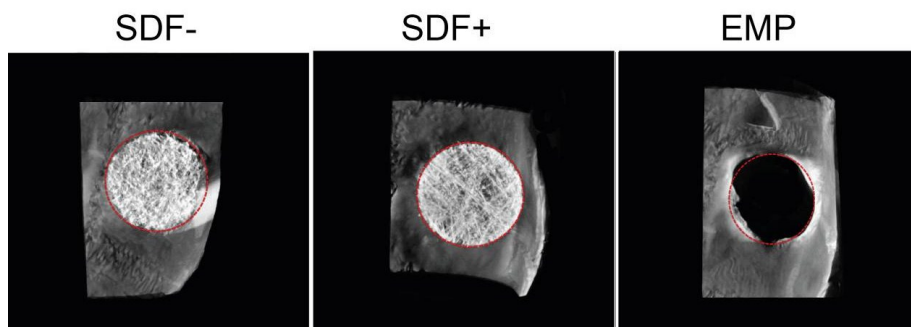


Figure 6. Representative micro-CT images of the cranial defects after 8 weeks of implantation. Original defect area (5 mm in diameter) was indicated by dash red circle. After 8 weeks of implantation, no bone formation was observed in control group (EMP, empty defect). Due to scattering of the titanium fiber mesh, reliable quantification of bone formation within the cranial defect area from implantation group (SDF- and SDF+) was not possible.

3.5.3.2. Bone formation probability

Regarding bone formation, animal variation was observed among animals from the same group regarding the bone formation (Table 4). Overall, 3 and 2 out of 5 animals from implantation groups SDF- & SDF+, respectively, showed bone ingrowth in the defect area. In contrast, only 1 animal from control group (EMP) showed spontaneous bone formation in the defect site. Chi-square analysis was performed to compare the bone formation probability caused by animal variation among three groups. Statistical analysis showed that there was no statistical difference ($p>0.05$) among groups (Table 4).

Table 4. Summary of animals showing bone formation after 8-week implantation

Group	Probability of animals showing bone formation ^a
SDF-	3/5
SDF+	2/5
EMP	1/5

^a Chi-square analysis indicated no statistical differences ($p>0.05$) among 3 groups regarding the probability of animals showing bone formation.

3.5.3.3. Descriptive histology

Figure 7 presents an overview of histological sections of different groups after 8-week implantation. In the control group (EMP), original defect edges were observed, and the existing gap was mainly occupied by soft tissues. Furthermore, dura mater was extruding from defect area and adherent to the soft tissue originating from skin side. Alternately, in both implantation groups (SDF- & SDF+), titanium fiber mesh remained inside the defect and covered with PCL/gelatin membrane. Mild fibrous encapsulation and fibroblast infiltration was observed surrounding the implanted membrane in both implantation groups (SDF- & SDF+) (Figure 7).

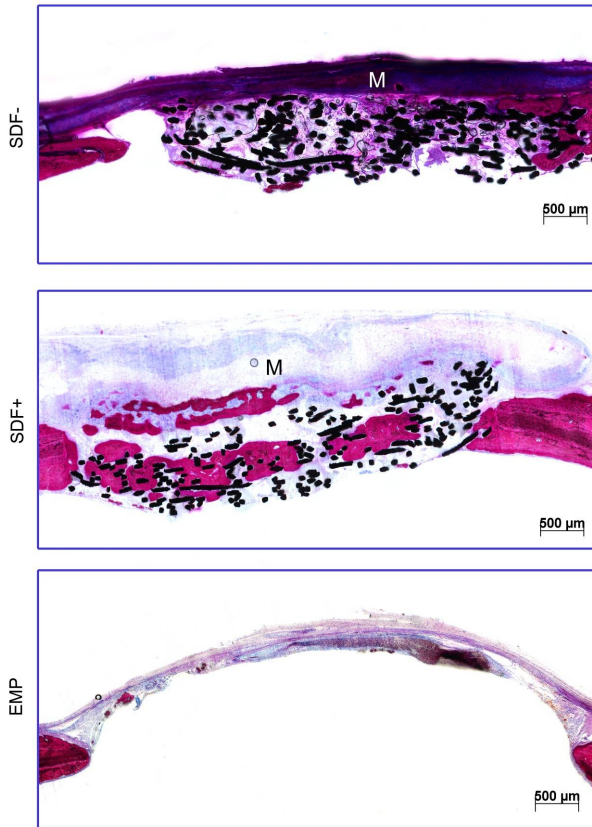
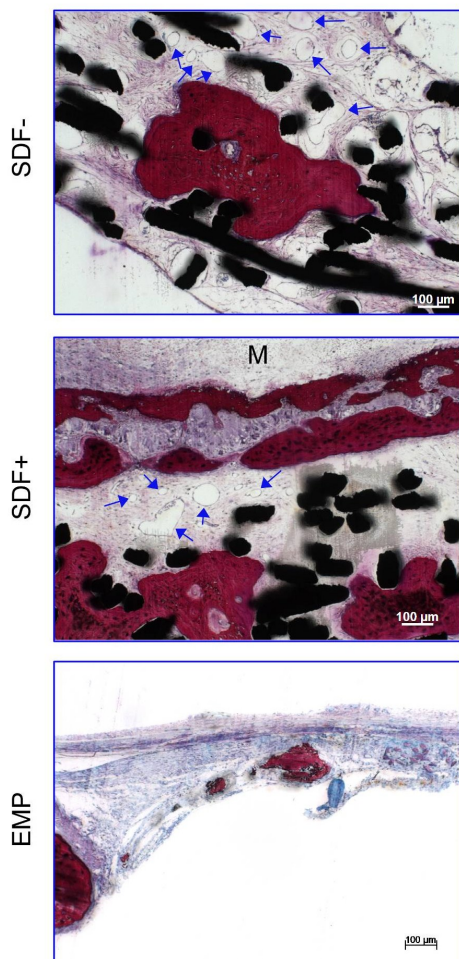


Figure 7. Representative histological images (general view) of cranial defects after 8 weeks of implantation. Methylene blue and basic fuchsin staining on the sections, in which bone appears red while cells appear blue and the titanium fibers appear black. Scale bar = 500 μ m

For the specimens showing bone formation, bone ingrowth within the porous titanium fiber mesh was observed in both SDF- and SDF+ group, accompanied by newly formed vascular structures (Figure 8). In particular, specimens from SDF+ group also showed new bone formation outside the titanium fiber mesh in the area beneath the SDF-1 α loaded membrane, with intensive cell assembling between the newly formed bone fragments (Figure 8).

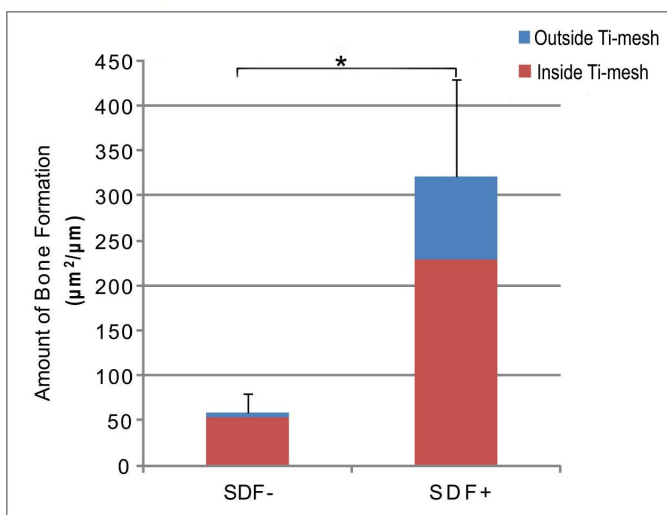


3.5.3.4. Histomorphometrical evaluation

Figure 9 shows the results of histomorphometrical evaluation between two implantation groups. The total amount of bone formation in SDF- and SDF+ group was $58 \pm 22 \mu\text{m}^2/\mu\text{m}$ and $321 \pm 108 \mu\text{m}^2/\mu\text{m}$, respectively ($p=0.02$). For SDF- group, $93 \pm 7\%$ of total amount of bone formation was formed inside the titanium fiber mesh, with approximate 7% of new bone formed outside the titanium mesh. In contrast, $71 \pm 1\%$ of new bone formation amount in SDF+ group was formed inside the titanium fiber mesh, whereas $29 \pm 1\%$ of the newly formed bone was observed outside the titanium fiber mesh.

Figure 8. Magnified histological sections of three groups. Both SDF- and SDF+ group showed bone formation inside titanium fiber mesh, in accompany with newly formed vascular structures (indicated by arrows). In particular, SDF+ group showed bone formation closely beneath the implanted membrane (indicated as "M"), with intensive cell infiltrations between the newly formed bone fragments. In contrast, limited bone formation was observed from control group (EMP). Scale bar = 100 μm .

Figure 9. Results of histomorphometrical evaluation. The total amount of bone formation in SDF- and SDF+ group were $57.83 \pm 21.99 \mu\text{m}^2/\mu\text{m}$ and $321.74 \pm 108.35 \mu\text{m}^2/\mu\text{m}$, respectively, which was significantly different between groups ($p=0.02$).



4. Discussion

The aim of current study was to generate electrospun membranes with SDF-1 α release as bioactive GBR membranes and to evaluate the effects on BMSCs recruitment and bone regeneration. We hypothesized that an electrospun membrane loaded with SDF-1 α would induce BMSCs recruitment, and hence enhance bone regeneration in the defect site. For this purpose, different amounts of SDF-1 α were loaded on PCL/gelatin electrospun membranes via physical adsorption and the obtained membranes were used in an *in vitro* SDF-1 α release experiment, BMSCs recruitment assay, and subsequently implanted in rat cranial defects. Our main findings showed that PCL/gelatin electrospun membranes acted as an effective SDF-1 α carrier, providing a diffusion-controlled SDF-1 α release profile. Furthermore, the SDF-1 α loaded membranes significantly induced *in vitro* BMSCs recruitment, although no dose-dependent effect of SDF-1 α was observed on BMSCs recruitment. Despite animal individual variation, SDF-1 α loaded membranes significantly increased bone formation in rat cranial defects after 8-week implantation. Animals implanted with SDF-1 α loaded membranes showed 6 fold higher amount of total bone formation compared to the ones implanted with bare membranes, albeit the contribution of *in vivo* BMSCs recruitment to the bone formation could not be ascertained.

Physical adsorption was found as an efficient approach to functionalize PCL/gelatin membrane with SDF-1 α release. The membrane loaded with different amounts of SDF-1 α showed a universal release profile, including an approximately 60% release of loaded protein within 4 h, followed by sustained release up to 35 days. Such a release profile is predominantly controlled by a diffusion mechanism, as evidenced by the release component (n) close to 0.5 calculated based on Ritger and Peppas equation ($y = kt^n$), which indicates a diffusion controlled release from a thin film system²⁸. A large initial burst release (~60%) was observed in the current study, which was similar to a previous report, where SDF-1 α was loaded in a hydrogel²⁹. A large burst release is often regarded as a negative consequence for certain long term controlled release devices, as it might shorten the release profile of loaded biomolecule, which requires more frequent dosing³⁰. However, in our case for SDF-1 α delivery, we assume the high initial burst release is favorable for clinical setting up, because it is likely to enable local SDF-1 α up to effective threshold within a short time period, hence triggering stem/progenitor cell recruitment as well as orchestrating subsequent tissue regeneration processes.

The SDF-1 α loaded PCL/gelatin electrospun membrane showed a strong cell recruiting capacity *in vitro*, which is evidenced by significantly enhanced rat BMSCs migration in response to the SDF-1 α loaded PCL/gelatin membrane. This can be attributed to the released gradients of exogenous SDF-1 α leading to BMSCs mobilization^{16,17}. Controversial results existed in previous research regarding the SDF-1 α threshold to induce BMSCs mobilization. Otsuru et al³¹ previously reported that 1000ng/ml SDF-1 α supplemented in

the medium induced maximum migration of mouse bone marrow-derived osteoblast progenitor cells. In contrast, Schantz et al¹⁸ reported that human MSCs migrated toward an SDF-1 stimulus with maximal chemotaxis at a concentration of 100 ng/ml. In the current study, there was no significant difference in BMSCs migration when SDF-1 α loading amount exceeded 50 ng in the membrane. Based on our protein release profile (approximate 70% release within 24 h), we assume that threshold SDF-1 α concentration to induce maximum rat BMSCs chemotaxis is ~35 ng/ml. Such findings indicate the potential usage of SDF-1 α loaded PCL/gelatin membrane to achieve a more cost-effective stem/progenitor cell recruiting capacity, which might be beneficial for further clinical application.

The molecular mechanism regulating BMSCs migrating towards SDF-1 α stimuli has been extensively investigated. It is generally accepted that CXCR4, a chemokine CXC-motif receptor, is the functional receptor corresponding to SDF-1 α in regulating stem/progenitor cell migration^{12, 14, 15, 32}. When the cells were treated with anti-CXCR4 antibody, inhibited migration of marrow stromal cells was shown in response to exogenous SDF-1 α ^{16, 18}. However, controversial findings exist regarding the CXCR4 expression on the progenitor cells isolated from bone marrow. Honczarenko et al¹⁴ previously reported that 45% of human BMSCs showed surface expression of CXCR4. In contrast, our results demonstrated CXCR4 expression in BMSCs was predominantly intracellular, which corroborates several other reports^{16, 18, 33}. It seems that the intracellular CXCR4 can be functionally expressed on the cell membrane to mediate SDF-1 α dependent cell migration³⁴. However, future studies are needed to clarify the mechanism responsible for such dynamic CXCR4 expression in regulating progenitor cells mobility for a comprehensive understanding the role of SDF-1 α /CXCR4 axis in stem cell/progenitor cell homing strategy. A rat cranial defect was used as a defect model to mimic the clinical situation for GBR application because it provides a suitable non-load bearing bone healing model with relative biological resemblance to the atrophic mandibular bone in humans³⁵. In two implantation groups (SDF- and SDF+), a titanium fiber mesh was placed to avoid the dilation of brain tissue beneath the defect in the defect^{36, 37}. In addition, the non-degradable titanium fiber mesh also provided a defined defect area for further quantification of bone formation. In current study, bilateral cranial defects with 5 mm in diameter were created in nude rats. After 8 weeks, limited spontaneous healing was observed from animals with empty defects ($n=5$). Such findings were different from previous report, which conventionally claims that a rat cranial defect with diameter less than 8mm shows spontaneous healing capacity through 8-week investigation period³⁸.

PCL/gelatin membrane loaded with 2 mg of SDF-1 α enhanced bone formation in rat cranial defects (5 mm in diameter) after 8-week implantation, which is evidenced by the histological and histomorphometrical results. Animals implanted with bare membranes

showed majority of bone formation and vascularization structures inside the titanium fiber mesh, and bare new bone formation was observed outside the titanium fiber mesh. In contrast, animals implanted with SDF-1 α loaded membranes showed approximate 30% of newly formed bone outside the titanium fiber mesh and closely beneath the membrane. Furthermore, intensive cell infiltrations were observed within the new bone fragments in such area in accompany with vascularization structures nearby. Such observations indicate that membranes with SDF-1 α delivery played important roles in new bone formation. There are two plausible mechanisms contributing to the enhanced new bone formation in response to local SDF-1 α stimuli. First, the bone marrow-derived osteoblast progenitor cells existed in the circulating blood^{31, 39, 40}, might be recruited to the defect site in response to local release of SDF-1 α via aforementioned SDF-1 α /CXCR4 axis. Those recruited cells contribute to the bone healing process by not only exerting their osteogenic capacity in the defect site, but also secreting a number of cytokines and growth factors to promote tissue regeneration⁴¹. Second, the local release of SDF-1 α might also generate proangiogenic environment in the defect site by mobilizing other progenitor cells resident in bone marrow, such as hematopoietic stem cell (HSC) and endothelial progenitor cell (EPC), to the defect site through SDF-1 α /CXCR4 axis^{17, 42, 43}. Those cells could enhance angiogenesis in the defect area, hence indirectly enhancing bone formation. Although it is still unclear which mechanism plays the dominant role in bone regeneration processes, our results indicate a great potential of locally delivered SDF-1 α from PCL/gelatin membrane to achieve cell recruitment strategy by using SDF-1 α loaded membrane to promote bone formation in GBR application.

Although a few recent studies reported the *in vivo* BMSCs recruitment by using subcutaneous implantation model^{42, 44}, no available studies investigated the *in vivo* BMSCs recruitment in bony defects as well as the contribution of BMSCs recruitment to the bone regeneration. Therefore, in the current study, we also set up an experiment aiming to trace the *in vivo* cell mobilization by intravenous injection of GFP-transgenic rat BMSCs into experimental animals. Such method was previously reported as an effective approach to trace BMSCs migration in rat brain tissue⁴⁵. However, due to the strong autofluorescence of host tissues, we were unable to determine GFP-fluorescent signals from live animals by using bioluminescence imaging or from histological sections by using fluorescent microscopy. Such observations suggest that the GFP-fluorescent signal might not be an optimal markers for *in vivo* cell tracing in bony tissue due to its short wavelength as well as close fluorescent spectrum with the natural tissue⁴⁶. It is necessary to conduct further experiments using cells with more sensitive labelling marker, such as luciferase⁴⁷, to elucidate *in vivo* BMSCs mobilization and corresponding biological function to bone regeneration.

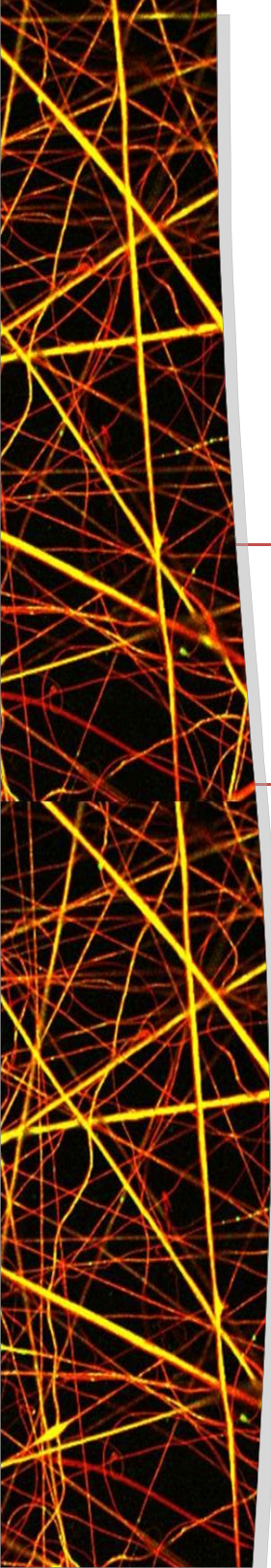
5. Conclusions

The results of current study show that the PCL/gelatin electrospun membranes with SDF-1 α adsorption provide a diffusion-controlled SDF-1 α release profile. The local release of SDF-1 α significantly induced *in vitro* rat BMSCs recruitment, although no dose-dependent of SDF-1 α was observed. Regarding bone formation, SDF-1 α loaded membranes significantly increased bone formation in rat cranial defects after 8-week implantation, as evidenced by a 6-fold increase in the amount of bone formation compared to the bare membranes. However, the current study could not ascertain the contribution of *in vivo* BMSCs recruitment to the bone formation in cranial defects due to the strong auto-fluorescence caused by host tissues.

6. References

1. Gentile, P.; Chiono, V.; Tonda-Turo, C.; Ferreira, A. M.; Ciardelli, G. *Biotechnol J* **2011**, *6*, 1187-1197.
2. Obata, A.; Hotta, T.; Wakita, T.; Ota, Y.; Kasuga, T. *Acta Biomater* **2010**, *6*, 1248-1257.
3. Retzepi, M.; Donos, N. *Clin Oral Implants Res* **2010**, *21*, 567-576.
4. Sculean, A.; Nikolidakis, D.; Schwarz, F. *J Clin Periodontol* **2008**, *35*, 106-116.
5. Haidar, Z. S.; Hamdy, R. C.; Tabrizian, M. *Biotechnol Lett* **2009**, *31*, 1817-1824.
6. Danesh-Meyer, M. J. *Ann R Australas Coll Dent Surg* **2000**, *15*, 144-149.
7. Park, Y. J.; Kim, K. H.; Lee, J. Y.; Ku, Y.; Lee, S. J.; Min, B. M.; Chung, C. P. *Biotechnol Appl Biochem* **2006**, *43*, 17-24.
8. Mao, J. J.; Stosich, M. S.; Moiola, E. K.; Lee, C. H.; Fu, S. Y.; Bastian, B.; Eisig, S. B.; Zemnick, C.; Ascherman, J.; Wu, J.; Rohde, C.; Ahn, J. *Tissue Eng Part B Rev* **2010**, *16*, 257-262.
9. Chen, F. M.; Wu, L. A.; Zhang, M.; Zhang, R.; Sun, H. H. *Biomaterials* **2011**, *32*, 3189-3209.
10. Kitaori, T.; Ito, H.; Schwarz, E. M.; Tsutsumi, R.; Yoshitomi, H.; Oishi, S.; Nakano, M.; Fujii, N.; Nagasawa, T.; Nakamura, T. *Arthritis Rheum* **2009**, *60*, 813-823.
11. Fong, E. L.; Chan, C. K.; Goodman, S. B. *Biomaterials* **2011**, *32*, 395-409.
12. Chavakis, E.; Urbich, C.; Dimmeler, S. *J Mol Cell Cardiol* **2008**, *45*, 514-522.
13. Liu, Z. J.; Zhuge, Y.; Velazquez, O. C. *J Cell Biochem* **2009**, *106*, 984-991.
14. Honczarenko, M.; Le, Y.; Swierkowski, M.; Ghiran, I.; Glodek, A. M.; Silberstein, L. E. *Stem Cells* **2006**, *24*, 1030-1041.
15. Peled, A.; Petit, I.; Kollet, O.; Magid, M.; Ponomaryov, T.; Byk, T.; Nagler, A.; Ben-Hur, H.; Many, A.; Shultz, L.; Lider, O.; Alon, R.; Zipori, D.; Lapidot, T. *Science* **1999**, *283*, 845-848.
16. Wynn, R. F.; Hart, C. A.; Corradi-Perini, C.; O'Neill, L.; Evans, C. A.; Wraith, J. E.; Fairbairn, L. J.; Bellantuono, I. *Blood* **2004**, *104*, 2643-2645.
17. Thevenot, P. T.; Nair, A. M.; Shen, J.; Lotfi, P.; Ko, C. Y.; Tang, L. *Biomaterials* **2010**, *31*, 3997-4008.
18. Schantz, J. T.; Chim, H.; Whiteman, M. *Tissue Eng* **2007**, *13*, 2615-2624.
19. Yang, F.; Both, S. K.; Yang, X.; Walboomers, X. F.; Jansen, J. A. *Acta Biomater* **2009**, *5*, 3295-3304.
20. Lee, E. J.; Teng, S. H.; Jang, T. S.; Wang, P.; Yook, S. W.; Kim, H. E.; Koh, Y. H. *Acta Biomater* **2010**, *6*, 3557-3565.
21. Ikada, Y.; Tabata, Y. *Adv Drug Deliv Rev* **1998**, *31*, 287-301.
22. Zhang, Y.; Venugopal, J.; Huang, Z.-M.; Lim, C. T.; Ramakrishna, S. *Polymer* **2006**, *47*, 2911-2917.
23. Fraker, P. J.; Speck, J. C., Jr. *Biochem Biophys Res Commun* **1978**, *80*, 849-857.
24. van den Dolder, J.; Farber, E.; Spauwen, P. H.; Jansen, J. A. *Biomaterials* **2003**, *24*, 1745-1750.
25. Schouten, C.; Meijer, G. J.; van den Beucken, J. J.; Spauwen, P. H.; Jansen, J. A. *Biomaterials* **2009**, *30*, 4539-4549.
26. van der Lubbe, H. B.; Klein, C. P.; de Groot, K. *Stain Technol* **1988**, *63*, 171-176.
27. Ghasemi-Mobarakeh, L.; Prabhakaran, M. P.; Morshed, M.; Nasr-Esfahani, M. H.; Ramakrishna, S. *Biomaterials* **2008**, *29*, 4532-4539.

28. Grassi, M.; Grassi, G. *Curr Drug Deliv* **2005**, *2*, 97-116.
29. Kimura, Y.; Tabata, Y. *J Biomat Sci-Polym Ed* **2010**, *21*, 37-51.
30. Huang, X.; Brazel, C. S. *J Control Release* **2001**, *73*, 121-36.
31. Otsuru, S.; Tamai, K.; Yamazaki, T.; Yoshikawa, H.; Kaneda, Y. *Stem Cells* **2008**, *26*, 223-34.
32. Gebura, K.; Bogunia-Kubik, K. *Postepy Hig Med Dosw (Online)* **2012**, *66*, 252-66.
33. Wang, J.; Guan, E.; Roderiquez, G.; Calvert, V.; Alvarez, R.; Norcross, M. A. *J Biol Chem* **2001**, *276*, 49236-49243.
34. Kollet, O.; Petit, I.; Kahn, J.; Samira, S.; Dar, A.; Peled, A.; Deutsch, V.; Gunetti, M.; Piacibello, W.; Nagler, A.; Lapidot, T. *Blood* **2002**, *100*, 2778-2786.
35. Oortgiesen, D. A. W.; Meijer, G. J.; de Vries, R. B. M.; Walboomers, X. F.; Jansen, J. A., Animal models for the evaluation of tissue engineering constructs. In *Tissue Engineering; from lab to clinic*, Pallua, N.; Suschek, C. V., Eds. Springer-Verlag: Berlin, 2011; pp 131-154.
36. Vehof, J. W.; Spauwen, P. H.; Jansen, J. A. *Biomaterials* **2000**, *21*, 2003-2009.
37. Ji, W.; Wang, H.; van den Beucken, J. J.; Yang, F.; Walboomers, X. F.; Leeuwenburgh, S.; Jansen, J. A. *Adv Drug Deliv Rev* **2012**, *64*, 1152-1164
38. Cooper, G. M.; Mooney, M. P.; Gosain, A. K.; Campbell, P. G.; Losee, J. E.; Huard, J. *Plast Reconstr Surg* **2010**, *125*, 1685-1692.
39. Wan, C.; He, Q.; Li, G. *J Orthop Res* **2006**, *24*, 610-618.
40. Eghbali-Fatourechi, G. Z.; Lamsam, J.; Fraser, D.; Nagel, D.; Riggs, B. L.; Khosla, S. *N Engl J Med* **2005**, *352*, 1959-1966.
41. Bryan, D.; Walker, K. B.; Ferguson, M.; Thorpe, R. *Cytokine* **2005**, *31*, 429-438.
42. Thevenot, P.; Nair, A.; Dey, J.; Yang, J.; Tang, L. *Tissue Eng Part C Methods* **2008**, *14*, 319-331.
43. Hattori, K.; Heissig, B.; Rafii, S. *Leuk Lymphoma* **2003**, *44*, 575-582.
44. Ratanavaraporn, J.; Furuya, H.; Kohara, H.; Tabata, Y. *Biomaterials* **2011**, *32*, 2797-2811.
45. Wang, Y.; Deng, Y.; Zhou, G. Q. *Brain Res* **2008**, *1195*, 104-112.
46. Georgakoudi, I.; Jacobson, B. C.; Muller, M. G.; Sheets, E. E.; Badizadegan, K.; Carr-Locke, D. L.; Crum, C. P.; Boone, C. W.; Dasari, R. R.; Van Dam, J.; Feld, M. S. *Cancer Res* **2002**, *62*, 682-687.
47. Granero-Molto, F.; Weis, J. A.; Miga, M. I.; Landis, B.; Myers, T. J.; O'Rear, L.; Longobardi, L.; Jansen, E. D.; Mortlock, D. P.; Spagnoli, A. *Stem Cells* **2009**, *27*, 1887-1898.



**Fibrous scaffolds loaded with protein
prepared by blend and coaxial
Electrospinning**

Wei Ji, Fang Yang, Jeroen J.J.P. van den Beucken,
Zhuan Bian, Mingwen Fan, Zhi Chen, John A. Jansen

Acta Biomaterialia. **2010**, 6, 4199-4207.

1. Introduction

The structural and functional properties of the natural extracellular matrix (ECM) are crucial for the proliferation, differentiation and migration of cells. As a consequence, there is an increasing tendency to design scaffold materials, as applied in tissue regeneration approaches, according to the characteristics of ECM. Natural ECM is composed of nano-scaled collagen fibers in which biomolecules (e.g. cytokines and growth factors) are incorporated. As early as the 1960s, it was claimed that the nanoscaled architecture of ECM influences the adhesion and orientation of cells¹, while the release of biomolecules from the ECM regulates cellular proliferation and differentiation². In view of this, it seems logical to assume that scaffolds, as used for tissue regeneration, should provide more than only physical support for cells. An appropriate architecture has to be combined with the release of biomolecules in the design process of scaffolds in order to modulate an optimal cellular behavior. Tissue engineering scaffolds have been prepared using a multitude of different techniques, such as gas foaming, emulsion freeze drying and rapid prototyping³. Recently, a new technique named electrospinning has attracted a lot of attention due to its relative simplicity regarding the generation of fibrous scaffolds with nanoscale dimensions. Electrospinning utilizes electrostatic forces to spin polymer solutions or melts into whipped jets, revealing continuous fibers with diameters from a few nanometers to micrometers after solvent evaporation in the spinning process^{4,5}. In addition to the nanoscale properties, electrospun scaffolds have been considered as an effective delivery system due to the stereological porous structure and high specific surface area⁶⁻⁸.

Enhancement of the biological functionality of electrospun scaffolds by incorporating biomolecules during the electrospinning process can be generally achieved by two different approaches: blend electrospinning and coaxial electrospinning. Blend electrospinning involves mixing of the proteinaceous biomolecules with the polymer solution. Some researchers also named this method as "emulsion electrospinning"⁹ because the aqueous protein solution was first emulsified by ultra-sonication, then the protein emulsion was mixed with polymer solution for electrospinning. Considering its same principle, we assume that it still belongs to blend electrospinning approach. Different from blend electrospinning, in the coaxial electrospinning, two solutions (e.g. polymer solution and biological solution) are coaxially and simultaneously electrospun through different feeding capillary channels in one nozzle to generate composite nano-fibers with core-shell structures. A previous study indicated that the aqueous biological solution is unspinnable due to its low viscosity¹⁰. Therefore, in both approaches, hydrophilic polymers (e.g. poly(ethylene glycol), poly(ethylene oxide), poly(ethylene imine), and dextran) are usually added in the aqueous biological solution to improve its fiber-forming property^{6,8,11-15}. The addition of these hydrophilic polymers can also be helpful to modulate the release

profiles of the biomolecules^{7,8,11}, as their addition enhances the water uptake of the electrospun scaffolds¹¹.

Compared to coaxial electrospinning, blend electrospinning is assumed to be relatively easy to perform, but the biomolecules may lose their bioactivity due to conformational changes in the organic solution environment. As coaxial electrospinning utilizes two separate channels for different solutions (i.e. organic polymer solution and aqueous biological solution), it is hypothesized to be beneficial for maintaining the functional activity of the biomolecules. On the other hand, it may be not easy to set the parameters for stable coaxial electrospinning in order to form uniform fibrous structure due to the difference in conductivity and viscosity of the two solutions. Up to now, considerable efforts have been conducted on the exploration of the methodology of preparing protein loaded electrospun scaffolds using these two techniques. Although previous studies provided different protein release profiles from blend^{6,9,11,16} and coaxial fibers^{7,8,12}, little attention has been paid to compare these two techniques to determine which method provides a more controllable release system for biomolecules from the electrospun scaffolds. Furthermore, there is limited information about the effect of electrospinning conditions on activity of the biomolecules. Based on our literature survey, only a few recent studies investigated the stability of lysozyme loaded in blend electrospun scaffolds^{9, 16}. However, compared to other therapeutic proteins, lysozyme is a small molecular protein (14 kDa) with a relative simple structure¹⁷. It is still necessary to further investigate the effect of different electrospinning process on those functional protein with complicated structure.

In view of the aforementioned, the aim of the present study was to generate polycaprolactone-based scaffolds with incorporation of biomolecules via either blend or coaxial electrospinning techniques. These types of electrospinning techniques were compared in terms of the processing set up, scaffold characterization as well as the release kinetics and biological activity of the loaded protein. Bovine serum albumin (BSA) was used as a model protein to determine the release profiles, and alkaline phosphatase (ALP) was used to determine the activity of the biomolecule after electrospinning.

2. Materials and Methods

2.1. Materials

Granular poly(ϵ -caprolactone) (PCL; *Mn* 80kDa), poly(ethylene glycol) (PEG; *Mn* 35kDa), bovine albumin serum (BSA; purity $\geq 98\%$), alkaline phosphates (ALP; from bovine intestinal mucosa; P7640, ≥ 10 DEA units/mg solid, specific activity: 42500U/mg), fluorescein isothiocyanate-conjugated bovine serum albumin (fitcBSA, *Mw* 67kDa), Rhodamine B (purity $\geq 80\%$) and formic acid solution (50% *w/v*) were purchased from Sigma–Aldrich, Inc. (St Louise, MO, USA). Organic solvents 2,2,2-trifluoroethanol (TFE) (purity $\geq 99.8\%$) and acetonitril (purity $\geq 99.0\%$) were obtained from Acros (Geel, Belgium) and Lab-scan

(Meppel, The Netherlands), respectively.

2.2. Electrospinning processing parameters

Four different types of scaffolds were prepared by either blend or coaxial electrospinning, of which the processing parameters and analytical methods are presented in Table 1. The coaxial electrospinning was conducted using a compound nozzle, and the solution for fiber core and shell is delivered to the co-axial inner and outer needle, respectively. The exit orifice diameters of the inner and outer capillaries are 0.5 and 0.8 mm, respectively. Electrospun fibers were collected on a grounded rotating plate covered by aluminum foil, unless it has been specified otherwise. Subsequently, they were freeze dried for 3 days before further characterization.

2.3. Morphological characterization of electrospun scaffolds

2.3.1. Scanning Electron Microscopy (SEM)

Electrospun nanofibrous scaffolds, mounted on metal stubs using conductive double-sided tape, were sputter-coated with gold using a JEOL JFC-1200 equipment. Scaffold morphology was examined using scanning electron microscopy (JEOL JSM-6310) at an accelerating voltage of 10 kV. Fiber diameters of the scaffolds were analysed with image visualization software (ImageJ 1.42q; Wayne Rasband, National Institutes of Health, USA (<http://rsb.info.nih.gov/ij>)). Approximate 130~150 counts for each scaffold were used to calculate the fiber diameter.

2.3.2. Transmission Electron Microscopy (TEM)

The fiber structure of the blend and coaxial scaffolds with BSA incorporated was examined using a JEOL 1010 Transmission Electron microscope, equipped with a Kodak mega-plus 4 CCD camera, operated at 60 kV. The samples for TEM were prepared by direct deposition of the electrospun fibers onto copper grids.

2.3.3. Laser Scanning Confocal Microscopy (LSCM)

To visualize the presences and distributions of the protein in the electrospun scaffolds, samples for confocal microscope were prepared using Rhodamin B (50 µg/ml) and fitcBSA to stain the polymer and protein, respectively. A thin layer of electrospun fibers were collected on glass slides, and then observed by laser scanning confocal microscopy (Olympus FV1000, Japan). The excitation wavelengths for Rhodamin B and fitc BSA were 559 nm and 488 nm, respectively, and multi-track images were captured with a 60×/1.35NA objective.

2.4. Determination of protein loading efficiency

The total protein content was determined according to the method of Sah¹⁸ with modify-

cations. Briefly, freeze dried scaffolds ($n=3$) were incubated in 2 ml dimethylsulfoxide (DMSO) for 1 hour, then 4 ml 0.2 M-NaOH solution containing 0.5% SDS was added for another 1-h incubation. The protein concentration in this solution was measured by a Micro BCA™ assay (Pierce, Rockford, USA). Results are presented as “loading efficiency” values, which indicate the percentage of protein loaded in the scaffolds with respect to the total amount of protein used in the process.

2.5. Release study *in vitro*

The electrospun scaffolds with incorporated BSA (**b**-BSA/PEG, **c**-BSA/PEG and **c**-BSA) (Table 1) were cut into small squares (2cm×2cm) before protein release *in vitro*. The release study was performed in MilliQ water and samples were incubated in a shaking water bath (37°C; 70rpm). Initially, 1.5 ml of MilliQ water was added to immerse the fiber meshes, A sample volume of 200 μ l was taken at $t = 0.5, 1.0, 2.0, 4.0$ and 24 h. Thereafter, the release medium was refilled to 1.5 ml and a sample volume of 500 μ l was taken at $t = 2, 3, 7$ days, and similarly every week until 42 days, with replenishment of the release medium to 1.5ml each time when a sample was taken out.

For each group, the assay samples were taken in triplicate ($n=3$) at each time interval. The BSA concentration in the collecting supernatant was analysed by high performance liquid chromatography (HPLC) using a reversed-phase (RP)-HPLC column (Atlantis®, Waters corp., Milford, MA, USA) connected to a L2130 HPLC pump and a L-2400 UV detector set at 280 nm (Hitachi corp., Tokyo, Japan). Before each analysis, samples were filtered using Acrodisk® filters (Waters corp., Milford, MA, USA). A 40/60 mixture of acetonitril/water containing 0.1% (w/v) formic acid was used as mobile phase with a flowing rate of 0.4 ml/min. The results for the release test are presented as cumulative release as a function of time:

$$\text{Cumulative amount of release (\%)} = 100 \times M_t / M_\infty$$

where M_t is the amount of BSA released at time t , and M_∞ is the total amount of BSA loaded in the membranes corrected using the measured protein loading efficiency.

At the end of release study, the release kinetics from the three groups were calculated to regression analysis according to the Ritger and Peppas equation¹⁹: $M_t/M_\infty = kt^n$

in which k is a constant related to the structure and geometric characteristics of the system, and n is the release exponent indicating the mechanism of the protein release²⁰.

Furthermore, the morphology of the post-release samples was assessed on a high-resolution field emission scanning electron microscope (FESEM, JEOL, SM3010, Tokyo, Japan), operated at an acceleration voltage of 3.0 kV.

2.6. Biological activity of the incorporated protein in electrospun scaffolds

2.6.1. Sample preparation

To evaluate the effect of the electrospinning process on protein activity, ALP was added as the protein component (Table 1). Because the conventional chloroform extraction^{7,9} to obtain the protein from the electrospun scaffolds was shown to severely decrease the protein activity (data not shown), the samples for protein functional assay were prepared without PCL polymer in the electrospinning solution under the same electrospinning parameters (Table 1). The collected droplets, not fibers ($n=5$) were dissolved in MilliQ water and evaluated for biological functionality using an ALP activity assay and for secondary structure analysis using circular dichroism (CD) spectroscopy. Freshly dissolved ALP served as a control.

2.6.2. ALP activity assay

ALP activity measurements were performed according to a previously described method²¹. In brief, 20 μl of 0.5 M 2-amino-2-methyl-1-propanol (AMP) buffer (Sigma) was added to 80 μl of the samples or standards. Then, 100 μl of substrate solution prepared from p-(nitrophenyl phosphate) was added and the mixtures were incubated at 37 °C for 1 h. ALP activity was measured at 405 nm using an ELISA micro-plate reader (Bio-Tek Instruments Inc., Winooski, VT, USA).

2.6.3. Circular Dichroism (CD) analysis

CD spectra were recorded in the range of 190 to 250 nm at a scan of 2 seconds per 0.5 nm with a Jasco J-810 spectropolarimeter (Oklahoma, USA). A quartz cell of 0.1 cm thickness was used. Values of the CD spectra were expressed as mean residue ellipticities (in $\text{deg. cm}^2 \text{dmol}^{-1}$). Results were further conducted a non-linear regression analysis to illustrate the constitution of secondary structure using the Gauss–Newton algorithm method.

2.7. Statistical analysis

Data are represented as mean \pm standard deviation. Statistical analysis were conducted using one way ANOVA with a post-hoc Tukey test calculated by Graphpad InStat software (InStat[®] 3.05, Graphpad Software Inc., San Diego, CA, USA). Statistical significance was set at $p < 0.05$.

Table 1. Experimental groups and sample preparations

Sample code	Preparation method	Prepare solution	Flow rate (ml/h)	Collecting distance (cm)	Voltage (kV)	Analysis
b -BSA/PEG	Blend electrospinning	12% PCL/TFE+ (0.2% BSA/MillliQ +10% PEG/MillliQ) (v:v=3:1)	1.8	15	26	Characterization(SEM & TEM) &Protein release
b -BSA	Blend electrospinning	12% PCL/TFE+0.2% BSA/MillliQ (v:v=3:1)	1.8	15	--	Un-electrospinnable and excluded for further characterization
c -BSA/PEG	Coaxial electrospinning	Shell: 12% PCL/TFE Core: (0.2% BSA/MillliQ +10% PEG/MillliQ)	Shell: 1.8 Core: 0.6	15	16	Characterization (SEM & TEM) &Protein release
c -BSA	Coaxial electrospinning	Shell: 12% PCL/TFE Core: 0.2% BSA/MillliQ	Shell: 1.8 Core: 0.6	15	12	Characterization (SEM & TEM) &Protein release
c -PEG	Coaxial electrospinning	Shell: 12% PCL/TFE Core: 10% PEG/MillliQ	shell 1.8 core 0.6	15	14	Characterization (SEM & TEM)
b -fitcBSA/PEG*	Blend electrospinning	12% PCL/ rhodamin B/ TFE + (0.2% fitcBSA/MillliQ +10% PEG/MillliQ) (v:v=3:1)	1.8	15	24	Protein distribution (Laser confocal)
c -fitcBSA/PEG*	Coaxial electrospinning	Shell: 12% PCL/ rhodamin B/ TFE Core: (0.2% fitcBSA/MillliQ +10% PEG/MillliQ)	Shell: 1.8 Core: 0.6	15	16	Protein distribution (Laser confocal)
c -fitcBSA*	Coaxial electrospinning	Shell: 12% PCL/ rhodamin B/ TFE Core: 0.2% fitcBSA/MillliQ	Shell: 1.8 Core: 0.6	15	16	Protein distribution (Laser confocal)
b -ALP/PEG**	Blend electrospinning	TFE+(0.2%ALP/MillliQ+10%PEG/MillliQ) (v:v=3:1)	1.8	15	26	Protein activity & CD analysis
c -ALP/PEG**	Coaxial electrospinning	Shell: TFE Core:(0.2%ALP/MillliQ+10%PEG/MillliQ)	Shell: 1.8 Core: 0.6	15	17	Protein activity & CD analysis
c -ALP**	Coaxial electrospinning	Shell: TFE Core:0.2% ALP/MillliQ	Shell: 1.8 Core: 0.6	15	14	Protein activity & CD analysis

*Rhodamine B was used (50µg/ml) to stain the PCL/TFE solution.

**labelled samples was collected as droplets without fiber structure due to the absence of polymers

3. Results

3.1. Characterization of electrospun scaffolds

During scaffold preparation, it was found that **b**-BSA solution could not be electrospun into fibers because a stable processing condition could not be achieved. For the rest of the groups, SEM images showed irregular fiber morphology for the blend electrospun scaffold (**b**-BSA/PEG) with obvious beaded structure, whereas the coaxially electrospun scaffolds (**c**-BSA/PEG, **c**-BSA and **c**-PEG) revealed a relatively uniform fiber morphology (Figure 1). The average fiber diameter was significantly different for each group ($p < 0.05$), i.e. 460, 420, 340 and 660 nm for **b**-BSA/PEG, **c**-BSA/PEG, **c**-BSA and **c**-PEG, respectively.

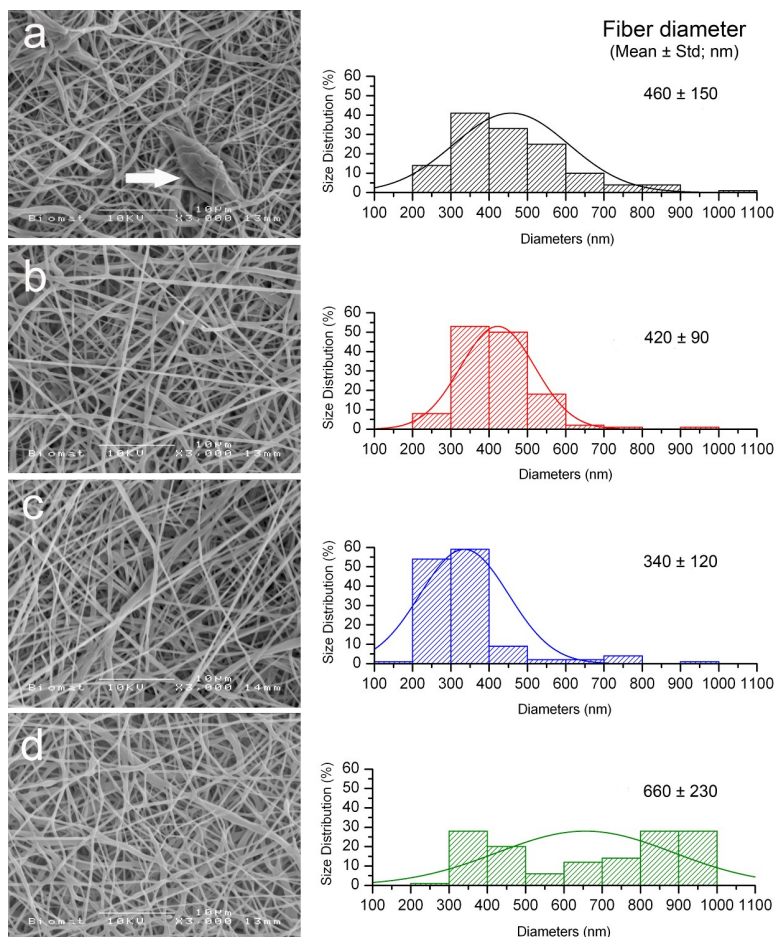


Figure 1. SEM images of virgin fibrous scaffolds prepared by blend or coaxial electrospinning techniques and their fiber diameter distributions. (a) blend scaffold **b**-BSA/PEG; (b) coaxial scaffold **c**-BSA/PEG; (c) coaxial scaffold **c**-BSA; (d) coaxial scaffold **c**-PEG. Arrow indicates the beads-formation in the blend electrospinning process. Fiber diameters in the different scaffolds are significantly different at $p < 0.05$ level (one way ANOVA, Tukey's test).

TEM demonstrated that the coaxially electrospun scaffolds exhibited an obvious core-shell structure (Figure 2), indicated by the difference in electron density between the inner core and outer shell of the fibers. This different electron density was not observed for blend electrospun fibers.

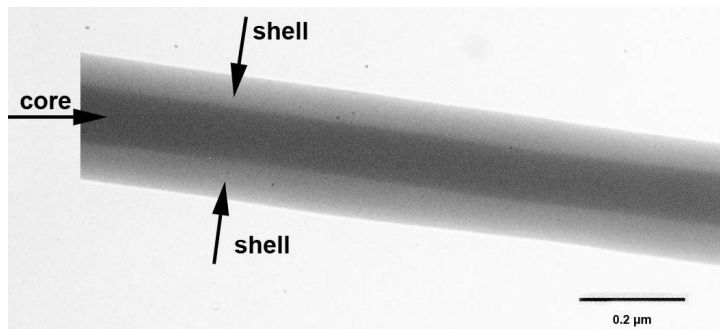


Figure 2. TEM image of coaxial fiber *c*-BSA/PEG. Core-shell structure can be observed from coaxial scaffold *c*-BSA/PEG. Arrows indicate the core and shell parts within the fiber. Scale bar = 200 nm

LSCM was used to visualize protein distribution within the electrospun fibers prepared by the two techniques. The red stain can be attributed to Rhodamin B, as present in the polymer shell solution, whereas the green stain was from the FITC-label linked to BSA in the core solution. The coaxially electrospun fibers *c*-fitcBSA/PEG exhibited a relatively homogenous protein distribution (Figure 3a). In contrast, the blend sample *b*-fitcBSA/PEG showed a bead-like appearance, in which the beads contained stronger green (fitcBSA) signal than the fiber strings (Figure 3b).

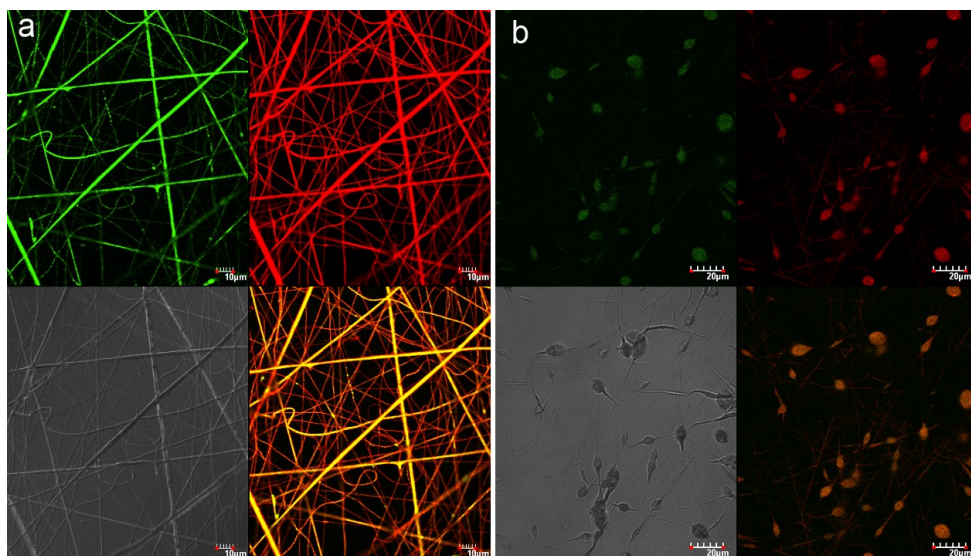


Figure 3. Laser scanning confocal microscopy images of blend and coaxial electrospun scaffolds. Laser scanning confocal microscopy images visualize protein distribution in blend and coaxial electrospun scaffolds. (a) coaxial scaffold *c*-BSA/PEG; (b) blend scaffold *b*-BSA/PEG. The panels in each image are: upper left: fitc (green); upper right: rhodamin B (red); bottom left: natural light; bottom right: the merger of fitc and rhodamin B.

3.2. Protein loading efficiency and *in vitro* release

The protein loading efficiency could only be measured for the coaxial scaffold *c*-BSA, due to the interference of PEG with the micro-BCA assay, and the average loading efficiency was $92.1 \pm 1.7\%$. Considering the similarities in protein/polymer ratios, 92.1% was used as the protein loading efficiency to calculate the loaded protein for all types of scaffolds.

Figure 4 shows the cumulative protein release curves for the protein incorporated scaffolds (*b*-BSA/PEG, *c*-BSA/PEG and *c*-BSA). For all three groups, a burst release was observed within 4 hours, which was $16.20 \pm 1.17\%$, $15.12 \pm 1.90\%$ and $13.39 \pm 1.46\%$ for *b*-BSA/PEG, *c*-BSA/PEG and *c*-BSA scaffolds, respectively, and these values were insignificantly different ($p > 0.05$) from each other. From day 10 on-ward, the three types of scaffolds exhibited a similar sustained release profiles, proximal 0.7% of cumulative release per day till the end of the release study. After 5 weeks, the three types of scaffolds showed a total cumulative release ranging from $\sim 45\%$ to $\sim 70\%$. For each of these scaffolds, the cumulative release curve was successfully fitted by an allometric power growth equation $y = kt^n$ (Table 2).

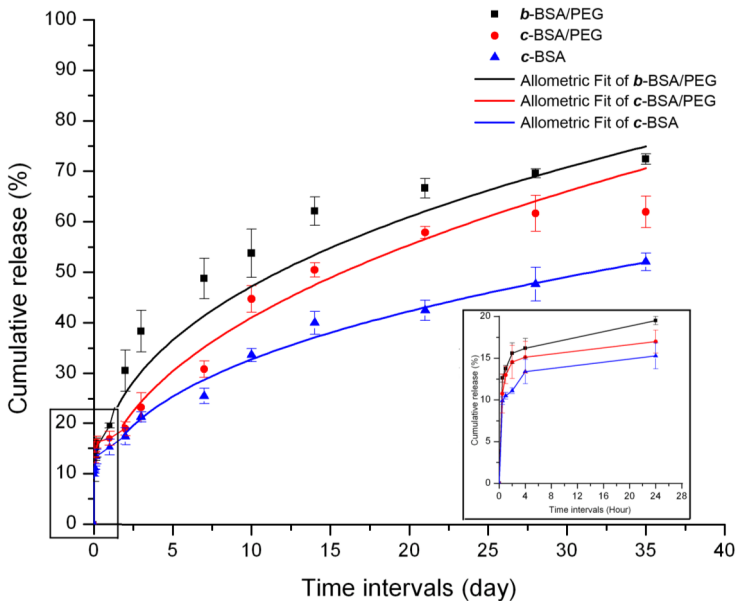


Figure 4. Protein release profiles from electrospun scaffolds. Protein release profiles of blend and coaxial electrospun scaffolds loaded with 0.2% BSA.

Table 2 Allometric regression analysis ($y = kt^n$) of protein release for each protein loaded scaffold

	<i>b</i> -BSA/PEG	<i>c</i> -BSA/PEG	<i>c</i> -BSA
<i>k</i>	20.2	15.1	14.0
<i>n</i>	0.37	0.43	0.37
Adj.R-Square	0.99	0.97	0.98

The post-release SEM images (Figure 5) illustrate morphological changes of electrospun fibers after the 35-day release study. The fibers in the blend electrospun scaffolds **b**-BSA/PEG showed rough and eroded-like fiber surfaces with very obvious pits and cavities presented, whereas the fibers in the coaxial scaffolds **c**-BSA/PEG and **c**-BSA became compressed and collapsed compared to their previous smoothly cylindrical shape.

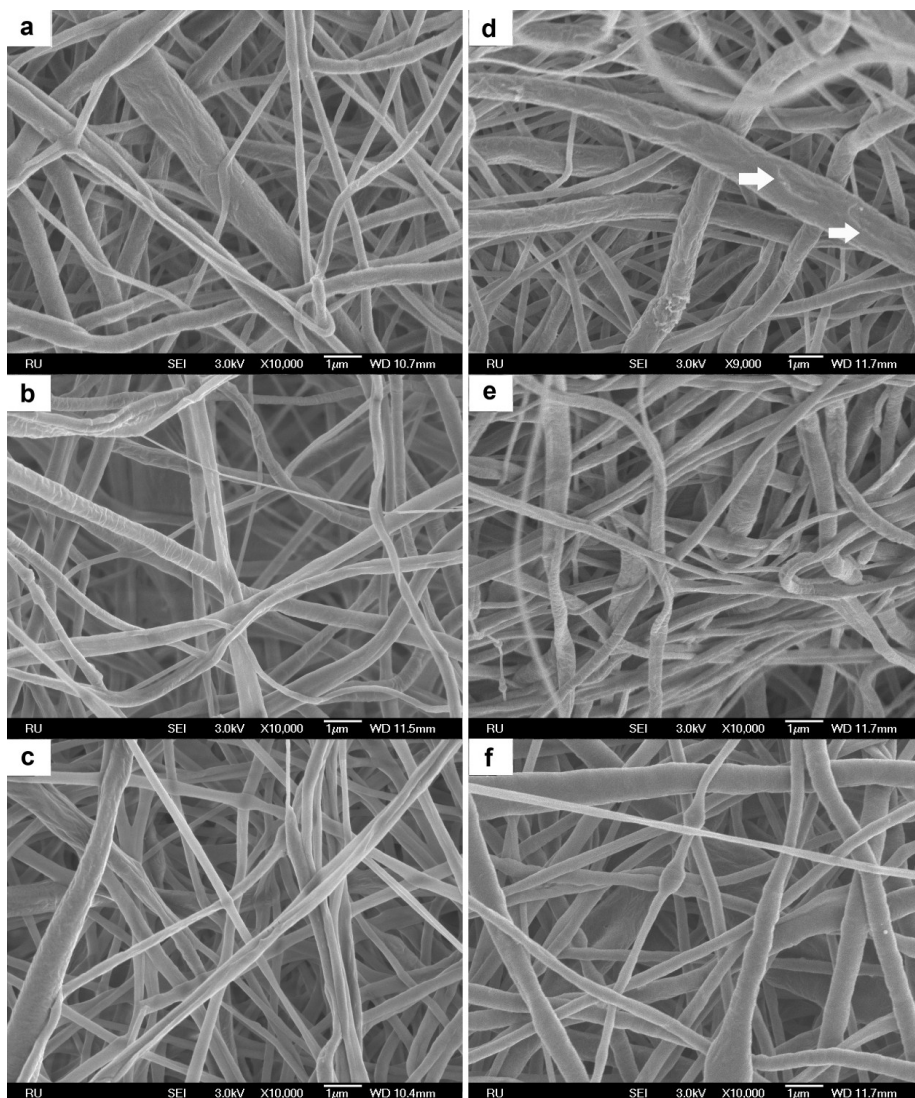


Figure 5. FESEM images of electrospun scaffolds with BSA incorporation before and after release study. (a),(b)&(c) are virgin scaffolds; (d),(e)&(f) are scaffolds after 35 days *in vitro* release. (a)&(d) blend scaffolds **b**-BSA/PEG; (b)&(e) coaxial scaffolds **c**-BSA/PEG; (c)&(f) coaxial scaffolds **c**-BSA. Arrows indicate cavity-like damaged fiber surface after 35-day release in blend scaffold **b**-BSA/PEG.

3.3. Protein activity and secondary structure

Compared to freshly dissolved one, the ALP samples after electrospinning had a significant decrease in enzyme activity ($p < 0.001$) (Figure 6). Among them, the ALP through coaxial electrospinning with PEG loaded (*c*-ALP/PEG) maintained $76.2 \pm 8.4\%$ of enzyme activity, which was significantly higher ($p < 0.05$) than *b*-ALP/PEG ($49.3 \pm 4.5\%$) and *c*-ALP ($13.4 \pm 1.7\%$).

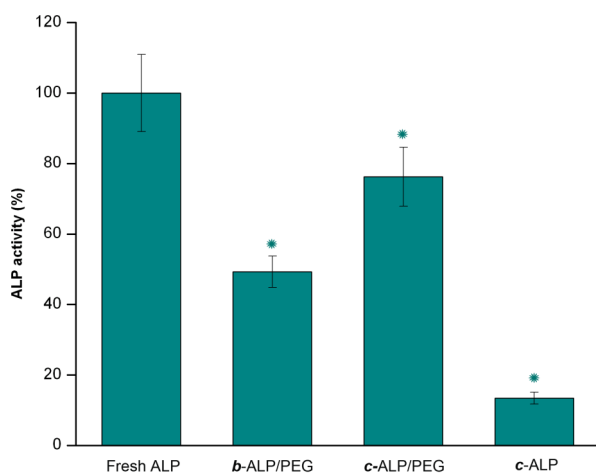
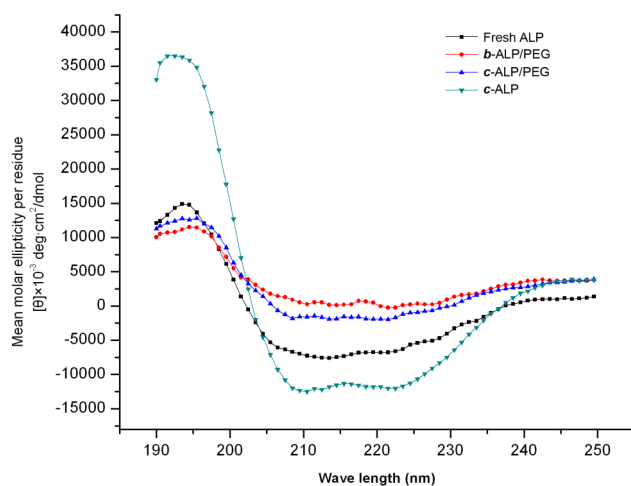


Figure 6. Protein activity preservation after the electrospinning process. ALP was used as model protein to determine the protein activity preservation. Enzyme activity was determined after electrospinning. Data are related to the activity of freshly dissolved ALP solution. *statistically significant difference ($p < 0.05$) compared to freshly dissolved ALP.

The far-ultraviolet circular dichroism (CD) spectrum (Figure 7) illustrates the conformational change of ALP after electrospinning process. Compared to freshly dissolved ALP, noticeable changes in molar CD values were observed at 190~200 nm and 208~222 nm after electrospinning process. The secondary structure analysis further quantified the conformational change of the electrospun ALP (Table 3). After electrospinning process, protein *b*-ALP/PEG and *c*-ALP/PEG revealed a significant decrease of α -helix and increase



of β -sheet, as well as a slight decrease of random coil structure, whereas *c*-ALP showed a noticeable increase (4 fold) of random coil structure.

Figure 7. Protein conformational change after electrospinning. Far ultraviolet circular dichroism spectrum of the freshly dissolved and electrospun ALP. The protein concentration was $50 \mu\text{g/ml}$ in a 0.1 cm path-length cell.

Table 3 Secondary structure analysis of the freshly dissolved and electrospun ALP

	α -helix (%)	β -sheet (%)	random coil (%)
<i>Fresh ALP</i>	42.2	53.1	4.7
<i>b-ALP/PEG</i>	20.2	78.0	1.8
<i>c-ALP/PEG</i>	28.2	70.5	1.3
<i>c-ALP</i>	55.6	28.4	16.0

The analysis was conducted based on the CD spectrum using the Gauss–Newton algorithm method

4. Discussion

Electrospinning has evolved as a powerful method to generate scaffolds which consist of (nano)fibrous networks with morphological similarities to the native extracellular matrix (ECM). In order to further mimic ECM composition, the present study focused on the incorporation of proteinaceous biomolecules into the electrospun fibers by using a blend and coaxial electrospinning approach. The obtained scaffolds were evaluated for their (i) morphology, (ii) biomolecular loading, distribution and release, and (iii) biological activity of the loaded biomolecules. The main findings were that both electrospinning techniques can be used for the preparation of nano-scaled electrospun scaffolds with incorporated biomolecules, and coaxial electrospinning was superior to the blend electrospinning as it provided uniform scaffold morphology, sustained release profiles as well as high conversion of protein activity. Morphologically, coaxial electrospinning generated a uniform fiber structure with homogeneous protein distribution throughout the fibers in a core/shell fashion, whereas blend electrospinning resulted in a bead-like fibrous structure with heterogeneous protein distribution. The *in vitro* release experiment showed an instantaneous burst release for all electrospun scaffolds, after which a more sustained release profile was observed with a total cumulative release ranging from ~45% to ~70% after five weeks. Although both electrospinning techniques depressed the biological activity of the loaded protein, the addition of PEG demonstrated to be able to preserve protein activity in coaxial electrospinning for up to 75%.

In our study, coaxial electrospinning demonstrated a superior feasibility compared to blend electrospinning for the incorporation of protein within the scaffolds. As aqueous protein solutions are reported to be un-electrospinnable due to their high fluidity²², PEG is usually added to the aqueous protein solutions to improve its viscosity and to stabilize the processing parameters^{7,8,12}. Our attempts for blend electrospinning confirmed that it is difficult to achieve stable electrospinning when the aqueous protein solution without PEG is mixed with the polymer solution. However, we were able to successfully set the parameters for coaxial electrospinning using an aqueous protein solution without PEG as supporting polymer. The optimal coaxial electrospinning process might be partially explained by the good electrospinnability of the shell polymer solution (12% PCL/TFE), which

was assumed to play a major role in the coaxial electrospinning process⁷. Furthermore, it was favored by the selection of optimal feeding rate ratios between core and shell solutions. It has been reported that at flow rate ratio (core: shell) between 1:3 and 1:6 allows the formation of stable core/shell Taylor cones and yield consistent electrospun core-shell fibers²³. TEM confirmed the successful achievement of core-shell structure fibers by using coaxial electrospinning. Previously, Saraf *et al.*²⁴ also showed the core/shell structure using LSCM. However, the two structure components of our coaxial fibers could not be separately detected in the LSCM images due to the thin fiber diameter as well as the limited resolution of confocal microscopy.

Scaffold characterization demonstrated that blend and coaxial electrospinning techniques resulted in different fiber morphology. Consistent with a previous report, SEM showed that the coaxial electrospun scaffolds exhibited a relatively uniform fibrous structure⁷, whereas blend electrospun scaffolds presented a bead-like structure^{14, 25}. An explanation for this morphological difference is that the mixture of aqueous protein and organic polymer components in the blend system behaves as an emulsion. Consequently, during electrospinning, the dispersed aqueous phase tends to accumulate centrally in the polymer jets, thereby forming beads in the fibers²⁵.

Due to its moderate molecular weight (60kDa) and relatively low cost, BSA was used as a model protein loaded in the scaffolds for the release study, and the loading efficiency for coaxial scaffold *c*-BSA was 92.1%. This value can be representative for the other protein loaded scaffolds because the protein loading during electrospinning is related to the process set up, i.e. the feeding rate and collecting method²⁶. In addition, it is logical to assume similar loading efficiency among the three types of BSA-loaded scaffolds prepared in this study, as standardized processing parameters we used for all of them.

The release experiment revealed different protein release profiles from the three types of BSA loaded electrospun scaffolds incorporated BSA. A similar burst release occurred within 4 hours for the three types of BSA loaded electrospun scaffolds. This burst effect may be related to the migration of BSA during drying and storage steps, which made certain amount of BSA molecules locating near the fiber surface²⁷, and its high solubility and partition coefficients can lead to a rapid release through short diffusion pathways due to thermodynamic imbalances²⁸. After burst release stage, compared to the blend scaffolds (*b*-BSA/PEG), coaxial electrospun scaffold (*c*-BSA/PEG and *c*-BSA) showed a more sustained protein release profile, and PEG accelerated protein release from coaxial electrospun scaffolds. The different release profiles can be related to the different fiber structure and protein distribution within scaffolds. The heterogeneously distributed protein in the blend fibers dispersed randomly upon activation in the release medium²⁰. The cavity-like fiber structure in the post-release blend scaffold suggests the dissolution of protein or protein/PEG mixture on the fibers, which corroborates with a previous re-

port⁷. In contrast, the core-shell-structured coaxial fibers provide a protein reservoir system, with a barrier membrane that controls the protein diffusion rate²⁰. Our results showed that the addition of PEG in the core part of coaxial fibers can accelerate the protein diffusion. It has been shown that in high mass polymer crowded solution (i.e. PEG, dextran, etc), molecules diffused much faster than expected, in spite of the increased viscosity of the solution^{29, 30}. This phenomenon was attributed to the fact that diffusing molecules were affected by the “microviscosity” of the local environment rather than the “macroviscosity” of the solution as a whole. And high mass polymers behave as a porous medium, in which proteins can associate relatively freely²⁹.

Empirical mathematical models might only be realistic in certain, extreme cases, but they give an indication for the underlying drug release mechanism under very specific conditions and thus can be useful for a comparison of different drug release profiles²⁰. In our case, due to the slow biodegradability and good biomolecular permeability of PCL, diffusion was the predominant release mechanism, which can be calculated by the Ritger & Peppas equation ($y=kt^n$)^{31, 32}. In this equation, k is a constant related to the structure and geometric characteristics of the release system, while n is the release exponent indicating the release mechanism. In the ideal case, the release is totally controlled by diffusion when $n=0.45$ ¹⁹, and a zero-order kinetics ($n=0$) can be correspond to a surface eroding polymer matrices³³. Release exponents that are in between these extreme values indicate so-called “anomalous” transport, thus, an overlapping of different types of phenomena²⁰. The coaxial scaffold ϵ -BSA/PEG showed a release exponent (n) close to 0.45, suggesting that the protein release kinetics better followed the mechanism of diffusion. On the contrary, the blend electrospun scaffold showed a lower release exponent ($n=0.37$), indicating that the release process was relatively irregular protein transportation.

Further, we compared the influence of different electrospinning process on the protein activity by using ALP as a model protein. ALP exists as a dimer of identical subunits each containing 429 amino acids³⁴, which relatively closely resembles the complexity of other therapeutic proteins. So far, there has been rare report on the activity and conformational change of ALP after blend or coaxial electrospinning process. The results indicated that both electrospinning techniques depressed the biological activity of the incorporated ALP, suggesting that high voltage and contact with organic solvents are harmful to the loaded biomolecules. Although the coaxial electrospinning greatly minimizes the interaction of protein with organic solvents before electrospinning, the measured low activity of ϵ -ALP provided the evidence that this method alone is not enough to preserve protein activity as assumed before. However, the addition of PEG in coaxial electrospinning was shown to be beneficial for protein activity preservation, most likely because PEG is proposed to eliminate protein adsorption to the organic polymer phase during

electrospinning³⁵⁻³⁷. Due to the limitation of the protein extraction method, PCL was not added to the sample preparation for the protein activity test. As PCL was very stable in ambient conditions³⁸, it is unlikely to affect the activity of the loaded protein.

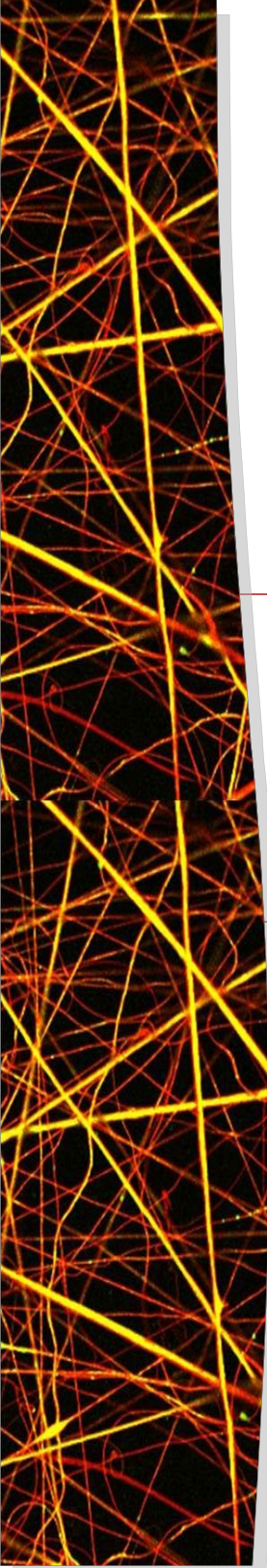
5. Conclusion

In this study, protein-loaded nano-scaled electrospun scaffolds with protein were prepared using blend and coaxial electrospinning techniques. Morphologically, the coaxial scaffolds showed uniform fiber morphology with core-shell structure, whereas the blend scaffolds exhibited a bead-like fiber structure. Protein distribution was homogeneous in the coaxial fibers, but heterogeneous in blend fibers. The different fiber structure and protein distribution affected protein release from the two types of scaffolds. The coaxial scaffolds revealed more sustained release profiles than the comparable blend scaffold, while the addition of PEG favored protein release. Both electrospinning techniques decreased the biological activity of the incorporated protein. However, the coaxial electrospinning method, where PEG was used as an additive, provided a superior conservation of protein activity preservation up to approximately 75%. Consequently, coaxial electrospinning represents a promising method for protein incorporation with minimal or no effects on fiber morphology and preservation of biological activity of the loaded protein in the scaffolds.

6. References

1. Rosenberg, M. D. *Science* **1963**, 139, 411-412.
2. Ma, Z.; Kotaki, M.; Inai, R.; Ramakrishna, S. *Tissue Eng* **2005**, 11, 101-109.
3. Weigel, T.; Schinkel, G.; Lendlein, A. *Expert Rev Med Devices* **2006**, 3, 835-851.
4. Pham, Q. P.; Sharma, U.; Mikos, A. G. *Tissue Eng* **2006**, 12, 1197-1211.
5. Yang, F.; Both, S. K.; Yang, X.; Walboomers, X. F.; Jansen, J. A. *Acta Biomater* **2009**, 5, 3295-3304.
6. Li, C.; Vepari, C.; Jin, H. J.; Kim, H. J.; Kaplan, D. L. *Biomaterials* **2006**, 27, 3115-3124.
7. Zhang, Y. Z.; Wang, X.; Feng, Y.; Li, J.; Lim, C. T.; Ramakrishna, S. *Biomacromolecules* **2006**, 7, 1049-1057.
8. Jiang, H.; Hu, Y.; Zhao, P.; Li, Y.; Zhu, K. *J Biomed Mater Res B Appl Biomater* **2006**, 79, 50-57.
9. Yang, Y.; Li, X.; Qi, M.; Zhou, S.; Weng, J. *Eur J Pharm Biopharm* **2008**, 69, 106-116.
10. Kowalczyk, T.; Nowicka, A.; Elbaum, D.; Kowalewski, T. A. *Biomacromolecules* **2008**, 9, 2087-2090.
11. Li, Y.; Jiang, H.; Zhu, K. *J Mater Sci Mater Med* **2008**, 19, 827-832.
12. Liao, I. C.; Chew, S. Y.; Leong, K. W. *Nanomed* **2006**, 1, 465-471.
13. Casper, C. L.; Yamaguchi, N.; Kiick, K. L.; Rabolt, J. F. *Biomacromolecules* **2005**, 6, 1998-2007.
14. Maretschek, S.; Greiner, A.; Kissel, T. *J Control Release* **2008**, 127, 180-187.
15. Schneider, A.; Wang, X. Y.; Kaplan, D. L.; Garlick, J. A.; Egles, C. *Acta Biomater* **2009**, 5, 2570-2578.
16. Kim, T. G.; Lee, D. S.; Park, T. G. *Int J Pharm* **2007**, 338, 276-283.
17. Merlini, G.; Bellotti, V. *Clin Chim Acta* **2005**, 357, 168-172.
18. Sah, H. *J Pharm Sci* **1997**, 86, 1315-1318.
19. Grassi, M.; Grassi, G., Mathematical modelling and controlled drug delivery: matrix systems. *Curr Drug Deliv* **2005**, 2, (1), 97-116.
20. Siepmann, J.; Siepmann, F. *Int J Pharm* **2008**, 364, 328-343.
21. Yang, F.; Both, S. K.; Yang, X.; Walboomers, X. F.; Jansen, J. A., *Acta Biomater* **2009**, 5, 3295-3304.
22. Dror, Y.; Ziv, T.; Makarov, V.; Wolf, H.; Admon, A.; Zussman, E. *Biomacromolecules* **2008**, 9, 2749-2754.
23. Chakraborty, S.; Liao, I. C.; Adler, A.; Leong, K. W. *Adv Drug Deliv Rev* **2009**, 61, 1043-1054.
24. Saraf, A.; Lozier, G.; Haesslein, A.; Kasper, F. K.; Raphael, R. M.; Baggett, L. S.; Mikos, A. G. *Tissue Eng Part C Methods* **2009**, 15, 333-344.
25. Qi, H. X.; Hu, P.; Xu, J.; Wang, A. J. *Biomacromolecules* **2006**, 7, 2327-2330.
26. Sill, T. J.; von Recum, H. A. *Biomaterials* **2008**, 29, 1989-2006.
27. Allison, S. D. *Expert Opin Drug Deliv* **2008**, 5, 615-628.
28. Huang, X.; Brazel, C. S. *J Control Release* **2001**, 73, 121-136.
29. Kozer, N.; Schreiber, G. *J Mol Biol* **2004**, 336, 763-774.
30. Vergara, A.; L, P.; R, S. *Macromolecules* **2002**, 35, 1389-1398.

31. Luong-Van, E.; Grondahl, L.; Chua, K. N.; Leong, K. W.; Nurcombe, V.; Cool, S. M. *Biomaterials* **2006**, *27*, 2042-2050.
32. Dong, Y.; Liao, S.; Ngiam, M.; Chan, C. K.; Ramakrishna, S. *Tissue Eng Part B Rev* **2009**, *15*, 333-351.
33. Siepmann, J.; Gopferich, A. *Adv Drug Deliv Rev* **2001**, *48*, 229-247.
34. Coleman, J. E. *Annu Rev Biophys Biomol Struct* **1992**, *21*, 441-83.
35. Knoll, D.; Hermans, J. *J Biol Chem* **1983**, *258*, 5710-5715.
36. Michel, R.; Pasche, S.; Textor, M.; Castner, D. G. *Langmuir* **2005**, *21*, 12327-12332.
37. Wang, Y.; Annunziata, O. *J Phys Chem B* **2007**, *111*, 1222-1230.
38. Hutmacher, D. *Biomaterials* **2000**, *21*, 2529-2543.



Coaxially electrospun scaffolds based on hydroxyl-Functionalized poly(ϵ -caprolactone) and loaded with VEGF for tissue engineering applications

Hajar Seyednejad*, Wei Ji*, Fang Yang, Cornelus F. van Nostrum, Tina Vermonden, Jeroen J.J.P. van den Beucken, Wouter J.A. Dhert, Wim E. Hennink, John A. Jansen

** Equal contributions as first author*

Biomacromolecules. **2012**, 13, 3650-3660.

1. Introduction

Suitable scaffolds for tissue engineering (TE) applications are structures based on biodegradable and biocompatible materials, which can support cell attachment and proliferation, deliver biochemical factors (i.e. growth factors), and enable diffusion of vital cell nutrients/metabolic products into/out of the scaffold, respectively¹. In fact, the success of TE approaches depends on the integration of all these factors in an implantable device. Therefore, development of biocompatible scaffolds, which are capable to deliver active biomolecules (e.g. growth factors) at the desired site with a sufficient local dose for a specific time frame and that support cell adhesion and preserve cell function is of great importance². There are two methods of incorporating biomolecules in polymeric matrices: (1) chemical bonding of the biomolecules of interest to the polymer matrix and (2) physical encapsulation of the biomolecules inside the polymer matrix^{3,4}. One of the methods that can be used for the physical incorporation of biomolecules to obtain bioactive scaffolds is electrospinning⁵, which is a versatile and simple method to produce ultrafine fibrous structures from polymer solutions mimicking the fibrous structure of the extracellular matrix (ECM)^{6,7}. The diameters of the fibers obtained using this technique range from several nanometers to a few microns⁸. Several researchers have developed electrospun nanofibers based on both natural polymers such as chitosan⁹, alginate¹⁰, gelatin¹¹, and synthetic polymers including poly(ϵ -caprolactone) (PCL)¹², poly(lactic-co-glycolic acid)¹³⁻¹⁷, and poly(L-lactide-co-caprolactone)¹⁸⁻²¹.

Coaxial electrospinning is an advanced technique comprising of two concentric needles rendering the possibility to make fiber mesh scaffolds with core/sheath morphology prepared from an immiscible organic polymer solution and an aqueous biomolecule solution²². As a result, the obtained scaffolds are loaded with biomolecules that after release promote cell adhesion and growth. The most frequently used polymer for coaxial electrospinning is PCL²³⁻²⁷ due to its ease of processing into fibers. However, PCL is a slowly degrading polyester that is eliminated from the body only after 2 to 4 years²⁸, is intrinsically hydrophobic and lacks functional groups to promote cell adhesion^{29,30}.

We have recently developed a novel polyester, poly(hydroxymethylglycolide-co- ϵ -caprolactone) (pHMGCCL)³¹, which is based on PCL and features a tunable degradation rate³² and has hydroxyl groups for further biofunctionalization³³. Previously, we have shown that the scaffolds made of this polymer exhibit superior human mesenchymal stem cells adhesion, proliferation, and differentiation properties as compared to PCL matrices, both in 2D³⁴ and 3D³⁵ forms. In the present study, we aimed to improve the properties of coaxially electrospun PCL scaffolds with respect to hydrophilicity, degradation rate, biomolecule release rate, and cell adhesion/proliferation by incorporating pHMGCL into these structures. Therefore, we prepared scaffolds using pHMGCL/PCL solutions to prepare the fiber shell. An aqueous solution of bovine serum albumin (BSA), as

a model protein and protein stabilizer, as well as vascular endothelial growth factor (VEGF), as a potent angiogenic factor³⁶ were selected as representative biomolecules and formed the core of the fibers. The release of protein from different scaffolds was investigated and to demonstrate that the bioactivity of released VEGF was preserved, the effect of released VEGF on attachment and proliferation of endothelial cells seeded on these scaffolds was demonstrated.

2. Materials and Methods

2.1. Materials

All chemicals used in this study were purchased from Sigma-Aldrich and used as received, unless stated otherwise. All solvents were purchased from Biosolve (Valkenswaard, The Netherlands). Toluene was distilled from P₂O₅ and stored over 3 Å molecular sieves under argon. Tetrahydrofuran (THF) was distilled from sodium/benzophenone. 3S-Benzyloxymethyl-1,4-dioxane-2,5-dione (benzyl-protected hydroxymethyl glycolide, BMG) was synthesized as described by Leemhuis et al.^{37, 38}. ε-Caprolactone (CL) and silica gel (0.035-0.070 mm, 60 Å) were obtained from Acros (Geel, Belgium), and benzyl alcohol (BnOH) was provided by Merck (Darmstadt, Germany), Pd/C (palladium, 10 wt % (dry basis) on activated carbon, wet (50% water w/w), Degussa type E101 NE/W) were obtained from Aldrich (Zwijndrecht, The Netherlands). Recombinant human VEGF 165 was purchased from R&D Systems (Netherlands).

For cell culture study, human umbilical vein endothelial cells (HUVECs) were purchased from BD (Franklin Lakes, USA). The endothelial medium (EM, containing basal medium 200, low serum growth supplements (LSGS) kit containing 2% fetal bovine serum (FBS), 10 ng/ml epidermal growth factor, 3 ng/ml basic fibroblast growth factor (bFGF), 10 mg/ml heparin, 0.2 mg/ml bovine serum albumin (BSA), 1 mg/ml hydrocortisone, and 0.2% gentamicin/amphotericin B) was purchased from Cascade Biologics (Oregon, USA) and assay medium (AM, containing minimal essential medium (α-MEM), 10% FBS, 50 µg/ml gentamycin) was purchased from Gibco-BRL.

2.2. Synthesis of PCL

PCL was synthesized via ring opening polymerization of ε-caprolactone (CL) using BnOH and SnOct₂ as initiator and catalyst, respectively, according to a previously described method³⁴. The molar ratio of CL/BnOH was 1000/1 in the feed. The obtained PCL was characterized by ¹H NMR, GPC and DSC.

2.3. Synthesis of Poly(hydroxymethylglycolide-co-ε-caprolactone), (pHMGCL)

A random copolymer of benzyl protected hydroxymethylglycolide (BMG) and ε-caprolactone (p(BMGCL)) was synthesized, using monomer-to-initiator molar ratio of

300/1, by ring opening polymerization method as described before³⁵. Briefly, ϵ -CL (2.29 ml, 0.02 mol), BMG (1.6 g, 0.007 mol), BnOH (9.94 mg, 0.09 mmol), and SnOct₂ (18.61 mg, 0.04 mmol) were loaded into a dry schlenk tube, equipped with a magnetic stirrer, under a dry nitrogen atmosphere. Following 2 hours of evacuation, the tube was subsequently closed and immersed in an oil bath pre-heated at 130 °C. The polymerization was performed overnight and the formed polymer was precipitated in methanol, filtrated, and dried in vacuum overnight. The protective benzyl groups of pBMGCL were removed in a hydrogenation reaction using Pd/C catalyst essentially as described by Leemhuis et al.³⁷. In short, pBMGCL (4.0 g, 8.5 mmol) was dissolved in dry THF (400 ml) and subsequently the Pd/C catalyst (3.0 g, 7.4 mmol) was added. The flask was filled with hydrogen in three consecutive steps of evacuation, refilling with H₂ and the reaction was done at room temperature under an H₂ pressure overnight. The catalyst was removed afterwards using a glass filter and THF by evaporation. pBMGCL and pHMGCL were characterized by ¹H NMR, DSC and GPC.

2.4. Fabrication of Coaxial Electrospun Scaffolds

Different types of scaffolds were prepared by coaxial electrospinning. The processing parameters used to obtain these scaffold are presented in Table 1. In general, coaxial electrospinning was performed using a nozzle, which delivered the core and shell solutions to the inner and outer needles, respectively, as previously described³⁹. The diameters of the inner and outer needles were 0.5 and 0.8 mm, respectively. The electrospun fibers were collected on a stationary plate covered with an aluminum foil and the scaffolds were freeze-dried for three days before further characterization.

2.5. Scanning Electron Microscopy (SEM)

The morphology of the prepared fibrous scaffolds was studied by SEM. Scaffolds were mounted on metal stubs using conductive double-sided tapes and subsequently sputter-coated with platinum. The morphology of the fibers was examined by SEM (JEOL JSM-3010) at an accelerating voltage of 3.0kV. Fiber diameters were measured by ImageJ software and more than 100 counts were used for each scaffold.

2.6. Transmission Electron Microscopy (TEM)

The core-shell structure of fibers was examined using a JEOL 1010 transmission electron microscope equipped with a Kodak megaplug 4 CCD camera, operated at 60 kV. The samples for TEM were prepared by direct deposition of the electrospun fibers onto copper grids.

2.7. Fluorescence Microscopy (FM)

In order to visualize the presence and distribution of BSA inside the coaxial fibers, sam-

ples for fluorescent microscopy were prepared using FITC-labeled protein, which was dissolved in the core solution (Table 1, Groups 5-7). A thin layer of electrospun fibers was collected on a glass slide and observed using an automated fluorescence microscope (Axio Imager Microscope Z1; Carl Zeiss Micro imaging GmbH, Gottingen, Germany). The excitation and emission wavelengths for FITC-BSA were 488 and 525 nm, respectively, and images were captured with a 40X/ 0.75 objective.

2.8. Nuclear Magnetic Resonance (NMR)

NMR measurements of the polymers were performed using a Gemini 300 MHz spectrometer (Varian Associates Inc., NMR Instruments, Palo Alto, CA). Chemical shifts were recorded in ppm with reference to the solvent peak ($\delta = 7.26$ ppm for CDCl_3 in ^1H NMR).

Table 1. Experimental groups of coaxial electrospun scaffolds used in this study.

Sample code	Solutions	Voltage (kV)	Analysis
Group 1	20% PCL/TFE + 0.2% BSA/MilliQ	10	Characterization (SEM, DSC, loading efficiency) & protein release
Group 2	20% PCL/pHMGCL(1:1)/TFE + 0.2% BSA/MilliQ	11	Characterization (SEM, DSC, loading efficiency) & protein release
Group 3	20% PCL/pHMGCL(1:2)/TFE + 0.2% BSA/MilliQ	13	Characterization (SEM, DSC, loading efficiency), protein release, endothelial cell proliferation
Group 4	20% PCL/pHMGCL(1:2)/TFE + 0.2% BSA + 5 μg VEGF /MilliQ	12	Endothelial cell proliferation
Group 5	20% PCL/TFE + 0.2% FITC-BSA/MilliQ	10	FM
Group 6	20% PCL/pHMGCL(1:1)/TFE + 0.2% FITC-BSA/MilliQ	11	FM
Group 7	20% PCL/pHMGCL(1:2)/TFE + 0.2% FITC-BSA/MilliQ	13	FM

The flow rate of core and shell solutions was 1.8 and 0.6 mL hr^{-1} , respectively, and the collection distance (18 cm) was constant for all the groups.

2.9. Differential Scanning Calorimetry (DSC)

The thermal properties of polymers and scaffolds were evaluated by differential scanning calorimetry (DSC). For the polymers, scans were taken from -80 $^{\circ}\text{C}$ to 100 $^{\circ}\text{C}$ with a heating rate of 10 $^{\circ}\text{C}/\text{min}$ and a cooling rate of 0.5 $^{\circ}\text{C}/\text{min}$ under a nitrogen flow of 50 ml/min . The glass transition temperature (T_g) was recorded as the midpoint of heat ca-

capacity change in the second heating run. Melting temperature (T_m) and heat of fusion (ΔH_f) were determined from the onset of endothermic peak position and integration of endothermic area in the second heating run, respectively. For scaffolds, the samples were equilibrated at $-90\text{ }^\circ\text{C}$ and then heated to $100\text{ }^\circ\text{C}$ with a heating rate of $10\text{ }^\circ\text{C}/\text{min}$. The thermal transitions of the scaffolds were reported for the first and second heating runs.

2.10. Gel Permeation Chromatography (GPC)

The molecular weights of the polymers were measured by means of GPC using a 2695 Waters Alliance system and a Waters 2414 refractive index detector. Two PL-gel $5\text{ }\mu\text{m}$ mixed-D columns fitted with a guard column (Polymer Labs, M_w range 0.2- 400 KDa) were used. The columns were calibrated with polystyrene standards of known molecular weights using AR grade THF, eluting at $1\text{ ml}/\text{min}$ flow rate at $30\text{ }^\circ\text{C}$. The concentration of the polymers was approximately $5\text{ mg}/\text{ml}$ and the injection volume was $50\text{ }\mu\text{l}$.

2.11. Water Contact Angle Measurements (CA)

The wettability of polymer films was evaluated by measuring advancing and receding water contact angles using sessile drop technique (Data Physics, OSC50). Uniform polymeric films were prepared by means of spin coating method (Specialty Coating Systems, Inc., model P6708D) using polymer solutions in chloroform ($0.2\text{ g}/\text{ml}$) and spin coated for 120 s at a speed of $1800\text{-}2000\text{ rpm}$ on round glass cover slips (Fisher Scientific, The Netherlands). Subsequently, the films were put in a vacuum oven at room temperature for 48 h to evaporate the solvent.

For advancing contact angle (Adv-CA), a water droplet ($10\text{ }\mu\text{l}$) was placed onto the surface of a polymeric film and the contact angle between water and surface was measured immediately by taking pictures of the droplet using an optical microscope and averaging the right and left angles using surface contact angle software (SCA20, Data Physics). For the receding contact angle (Rec-CA), the water droplet was withdrawn slowly and the contact angle was measured after different time points. The reported values are mean values of at least four measurements.

2.12. Protein Loading Efficiency (LE)

The protein loading efficiency of the scaffolds was determined according to the method described by Ji et al.⁴⁰ To get accurate weight of scaffolds, scaffolds were freeze-dried prior to assessing to eliminate the moisture and solvent remnant which will interfere with the scaffold weight. Briefly, round pieces (diameter of 1 cm , weighing approximately 20 mg) of freeze-dried scaffolds ($n=3$) were incubated in 2 ml of dimethylsulfoxide for 1 h to dissolve the polymer. Subsequently, 4 ml of 0.2 M NaOH aqueous solution containing 0.5% sodium dodecyl sulfate was added and the obtained solution was incubated for

1 hour at room temperature. Next, the protein concentration in this solution was measured by Micro-BCA™ assay (Pierce, Rockford, IL). Results are presented as the “loading efficiency” of scaffolds, which is defined as the percentage of protein loaded in the scaffolds with respect to the total amount of protein used in the process.

2.13. *In-vitro* Release Study

The release of BSA from the different fibrous scaffolds was investigated as described by Ji et al.⁴¹. In short, round BSA-loaded scaffolds punched out of the electrospun mat (diameter of 1cm, thickness of approximately 2 mm, weighing approximately 20 mg) were introduced in MilliQ water (1.5 mL) at 37 °C. Initially, 1.5 ml of MilliQ water was added to immerse the fiber meshes, and a sample volume of 200 µl was taken at t = 0.5, 1.0, 2.0, 4.0 and 24 h. Thereafter, the release medium was refilled to 1.5 ml and a sample volume of 500 µl was taken at different time intervals up to 35 days, with replenishment of the release medium to 1.5 ml each time a sample was taken out. Release experiments were performed in triplicate under a dynamic situation (100rpm). The BSA concentration in the samples was determined by high performance liquid chromatography (HPLC) using a HPLC column (Hypersil Gold, Thermo Scientific, USA) connected to a L2130 HPLC pump and a L-2400 UV detector set at 280 nm (Hitachi Corp., Tokyo, Japan). A 40/60 mixture of acetonitrile/water containing 0.1% (w/v) formic acid was used as the mobile phase with a flow rate of 0.4 ml min⁻¹. The results are presented as cumulative release as a function of time according to the following equation:

$$\text{Cumulative release (\%)} = 100 \times \frac{M_t}{M_\infty}$$

where M_t is the amount of protein released at time t and M_∞ is the amount of protein loaded in the scaffold. BSA standards (1.8 - 180 µg/ml) were used for calibration.

2.14. VEGF Bioactivity Assay

An *in vitro* cell-based assay was used to investigate the biological activity of VEGF released from the scaffolds. A scaffold based on PCL/pHMGCL 1:2 (Group 4, Table 2) with VEGF loading was selected for this assay because of its attractive BSA release properties. Scaffolds with or without VEGF incorporation were punched into circular shape (15 mm in diameter) for cell culture substrates. They were freeze dried for 2 days, followed by ethylene oxide sterilization (Synergy Health, Ede, The Netherlands) before cell culture experiment. The total amount of VEGF in the single substrate of S-VEGF was calculated according to the weight ratio of VEGF in the entire scaffolds. The average total amount of VEGF in each S+VEGF substrate was (1.6±0.4) µg.

HUVECs were expanded in endothelial medium (EM) at 37 °C in a humid atmosphere with 5% CO₂ according to the guidelines provided by BD. The medium was changed twice

a week, and cells from passage 8 were used. Afterwards, cells were seeded at a density of 40×10^3 cells/cm², and cultured in assay medium (AM) to exclude potential effects of factors supplemented in EM. Five groups were set up in cell culture experiment:

1. (S): Naïve scaffolds in AM
2. (S+VEGF): Scaffolds loaded with VEGF in AM
3. (S+T_{VEGF}): Naïve scaffolds in AM supplemented with total amount of VEGF (1.6 µg)
4. (S+S_{VEGF}): Naïve scaffolds in AM supplemented with 12.5 ng/ml VEGF (after each medium refreshment)
5. (TCP+S_{VEGF}): Tissue culture plates in AM supplemented with 12.5 ng/ml VEGF (after each medium refreshment)

Prior to the cell seeding, all the scaffolds were placed in 24-well plates and incubated assay medium for 1 hour at 37 °C to increase cell attachment. The medium was refreshed at 1 day after cell seeding, and thereafter 2 times per week. For S+T_{VEGF} group, no VEGF was further supplemented after refreshing medium at day 1. For S+S_{VEGF} and TCP+S_{VEGF} group, an amount of VEGF (12.5 ng/ml) was supplemented every time after medium refreshment.

HUVECs growth, as measured by total cellular DNA content, was assessed by Quant-iT™ Picogreen® dsDNA assay kit (Molecular Probes, Eugene, USA) according to the instructions of the manufacturer. At selected time points (1, 4, and 7 days post-seeding), samples (n=3) were prepared by washing the cell layers twice with PBS and adding 1ml of MilliQ to each well, after which repetitive freezing (-80 °C) and thawing (room temperature) cycles were performed followed by 10 minutes of sonication.

For the standard curve, serial dilutions of dsDNA stock were prepared (concentrations ranging from 0–2000 ng/ml). Next, 100 µL of either sample or dsDNA was added to the wells, followed by 100 µL of working solution. After 2-5 minutes of incubation in the dark, DNA was measured on a fluorescence cuvette reader (microplate fluorescence reader, Bio-Tek, Winooski, USA) with a 485 nm excitation filter and a 530 nm emission filter. Data were normalized to S+S_{VEGF} group and expressed as fold of DNA content.

The morphology of HUVECs cultured on the scaffolds was also examined. Two samples of each group at each time point were seeded with HUVECs at a density of 40×10^3 cells/cm² and incubated in AM for 4 and 7 days.

After these culture periods, cell layers were rinsed twice with PBS, fixed with 2% glutaraldehyde in cacodylate buffer [Na(CH₃)₂AsO₂·3H₂O] for 5 min and dehydrated in a graded series of ethanol. Finally, cell layers were dried using tetramethylsilane (TMS), sputter coated with gold/platinum composite, and the cells were examined morphologically using a scanning electron microscope (JEOL, SEM 6340F).

In addition, cytoskeletal structure of HUVEC was observed using confocal laser scan mi-

crosscopy (CLSM, Olympus FV1000) for samples cultured for 4 days. Fixation of the cell-scaffold samples was carried out for 20 minutes in freshly prepared 2% (v/v) paraformaldehyde. Then the samples were washed in PBS for three times, permeabilized in PBS containing a 10% (v/v) FBS plus 0.5% (v/v) Triton-X 100 (Sigma Aldrich, St. Louis, MO, USA) for 20 minutes, and incubated in PBS containing a 10% (v/v) FBS for 30 minutes. Thereafter, samples were stained with Alexa-fluor 568 conjugated phalloidin for filamentous actin fluorescence (1:200) and DAPI staining for nuclei UV-visualization (1:2000) for 1.5 hours. Antibodies were purchased from Invitrogen (Molecular probes®, Carlsbad, CA, USA). Subsequently, specimens were thoroughly washed with PBS, and rinsed with deionised water for 2 minutes, then mounted in VECTASHIELD® Mounting Medium (Vector Laboratories, Inc., Burlingame, CA, USA) on glass slides. Finally specimens were examined using Olympus FV1000 confocal laser scanning microscope (Olympus, Tokyo, Japan) and multi-track images were captured with a 60×/1.35NA objective.

2.15. Statistical Analysis

Statistical analysis of the data was done using a one-way analysis of variance (ANOVA) with a post hoc Bonferroni multiple comparison test⁴¹ for cell growth at individual time points using GraphPad InStat software (version 3.05; San Diego, CA). A p-value < 0.05 was considered statistically significant.

3. Results and Discussion

3.1. Polymer Synthesis and Characterization

PCL and pHMGCL were synthesized via ring opening polymerization (ROP) at 130 °C for 16 hours using BnOH and SnOct₂ as initiator and catalyst, respectively, as described before^{34, 35}. The BMG/CL monomer molar ratio in the feed was 25/75 and the obtained pBMGCL was subsequently deprotected by removal of the benzyl groups to yield pHMGCL. ¹H NMR analysis showed that the HMG/CL monomer molar ratio in the polymer was very close to that of the feed (Table 2). DSC analysis showed that the melting temperature of PCL and pHMGCL was 54 and 37 °C, respectively. The crystallinity of pHMGCL was substantially lower than PCL as indicated by the heat of fusion (ΔH) which was 65 and 31 J/g for PCL and pHMGCL, respectively. GPC analysis showed that the molecular weights (M_n) of PCL and pHMGCL were 71.1 and 17.3 kDa, respectively. The polydispersities were around 2 and in agreement with values generally obtained for polymers synthesized using ROP⁴².

3.2. Scaffolds Preparation and Characterization

BSA-loaded PCL scaffolds were prepared by coaxially electrospinning a PCL solution in TFE (20 w/v %) and a BSA solution in MilliQ water (0.2 w/v %), as shell and core solutions,

respectively (Group 1, Table 1). Scaffolds with a uniform fibrous structure and with a fiber diameter of $0.7 \pm 0.1 \mu\text{m}$ were formed (Figure 1A). However, preparation of scaffolds of acceptable quality composed of only pHMGCL as shell forming polymer was not possible likely due to the low molecular weight of this polymer as compared to PCL (M_w of 35 versus 128 kDa) and hence low viscosity of the 20 w/v% polymer solution. The viscosity of pHMGCL solution was raised by increasing the concentration from 20 w/v % up to 40 w/v %. However, the resulting solution was sticky and not electrospinnable due to blockage of the nozzle. An attempt to increase the molecular weight of pHMGCL by increasing M/I ratio did not yield significantly longer polymer chains likely because of traces of impurities present in the synthesized monomer.³⁴

Table 2. Characteristics of the polymers used in this study.

Polymer	Monomer/Initiator molar ratio	BMG/CL molar ratio in feed	HMG/CL molar ratio in polymer (¹ H NMR)	Yield (%)	DSC			GPC	
					T _g (°C) ^a	T _m (°C) ^a	ΔH (J/g) ^a	M _w (kDa) ^b	PDI ^b
PCL	1000	0 / 100	-	98	-60.8	53.7	65.4	128	1.8
pHMGCL	300	25 / 75	22 / 77	93	-53.1	37.1	31.6	35	2.0

Measured by ^a) DSC and ^b) GPC.

To increase the hydrophilicity of the scaffolds, pHMGCL was blended with PCL in different weight ratios (Group 2 and 3 scaffolds, Table 1). SEM analysis of these scaffolds showed absence of beads and a uniform structure (Figure 1, B and C) composed of fibers with the same diameters as the fibers of the PCL scaffold. In our approach, using solutions of pHMGCL and PCL resulted in good electrospinning conditions (e.g. stable Taylor cone and continuous jet ejecting during process). According to other reports^{24, 43} the formation of uniform fibers is affected by the feed rate ratio between the core and the shell solutions. A flow rate ratio (core: shell) between 1:3 and 1:6 allows the formation of stable core/shell Taylor cones that subsequently after evaporation of the solvents yields uniform core/shell fibers. Therefore, an inner/outer solution flow rate of 1:3 was chosen.

TEM analysis showed that the obtained coaxially electrospun scaffolds were composed of core-sheath structure (Figure 2), indicated by the difference in electron density between the inner core and outer shell of the fibers. The sharp boundaries between core and shell layers can be observed clearly in Figure 2 and is attributed to the immiscibility of core/ shell solutions.

The successful loading of FITC-BSA inside the nanofibers was shown by means of fluorescence microscopy (FM) and Figure 2 demonstrates a uniform distribution of protein (indicated by green stain) in the fibers. The fibrous bead-free morphology observed in these images is also consistent with SEM images shown in Figure 3.

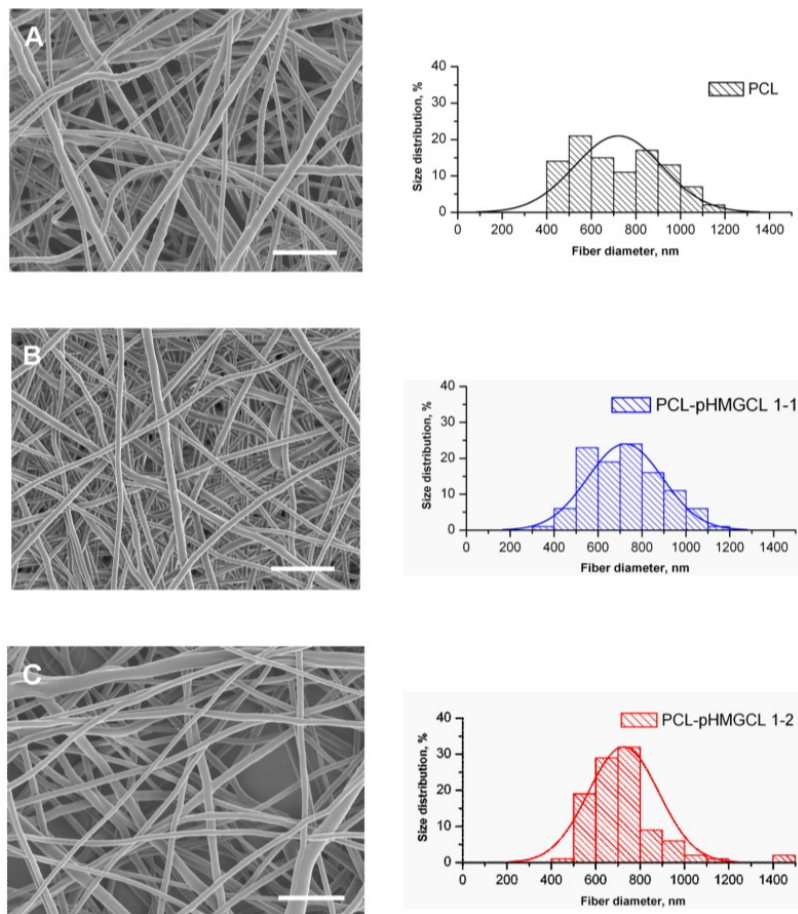


Figure 1. Left: Scanning electron microscopy images of fibrous scaffolds (A) PCL, (B) PCL/pHMGCCL 1:1, and (C) PCL/pHMGCCL 1:2 (scale bar is 5 μm). Right: Fiber size distribution of electrospun coaxial scaffolds obtained using ImageJ software and considering more than 100 counts per scaffold.

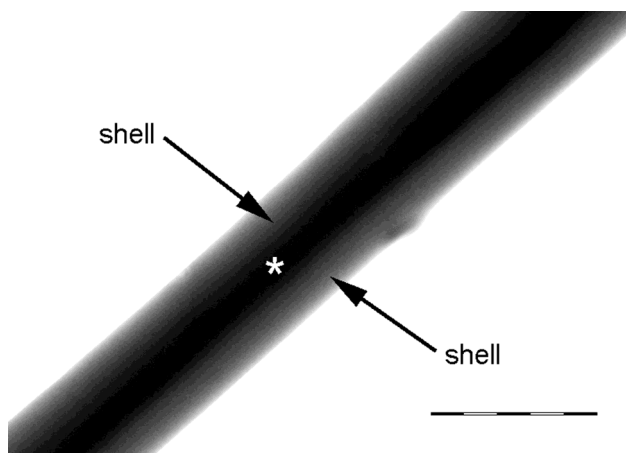


Figure 2. TEM image of PCL coaxial fibers. Core and shell part were indicated by asterisk and arrows, respectively. (scale bar is 500 nm).

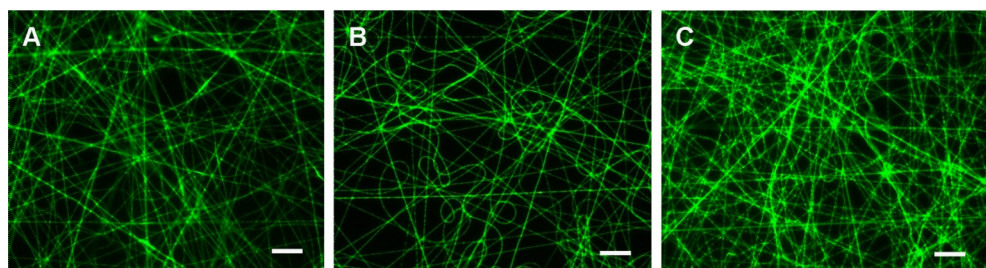


Figure 3. Fluorescent microscopy images of FITC-BSA loaded in coaxial fibrous scaffolds (A) PCL, (B) PCL/pHMGCL 1:1, and (C) PCL/pHMGCL 1:2. Scale bar is 20 μm .

Contact angle (CA) measurements on spun-coated films of the same composition as the electrospun scaffolds were performed to study the blend composition-dependent surface hydrophilicity. Figure 4 shows that the advancing contact angle (Adv-CA) for a PCL film was $77.7 \pm 4.5^\circ$. For the PCL/pHMGCL blends of 1:1 and 1:2 weight ratios, the Adv-CA's were $76.8 \pm 3.4^\circ$ and $75.8 \pm 1.4^\circ$ (Figure 4A), respectively. The receding CA's (Rec-CA) were measured in time and Figure 3 shows that they slightly decreased for PCL films from $74.7 \pm 4.1^\circ$ to $68.7 \pm 6.5^\circ$ within 20 minutes. Interestingly, for films prepared of PCL/pHMGCL 1:1 blend, the Rec-CA decreased from $70.4 \pm 2.1^\circ$ to $55.1 \pm 3.3^\circ$ within 10 minutes whereas for films of PCL/pHMGCL 1:2 blend, the Rec-CA decreased even more from $68.4 \pm 1.9^\circ$ to $47.7 \pm 1.2^\circ$ in 10 minutes. It was not possible to measure the Rec-CA further due to an almost full spreading of the water droplets on the surface (Figure 4B). The considerable decrease in Rec-CA in time can be attributed to the reorientation of the polar hydroxyl groups of pHMGCL on the surface of the polymeric film upon exposure to water. This is in agreement with our previous findings³⁴ where we showed that receding contact angles on polymeric films of pHMGCL decrease substantially with increasing the percentage of hydrophilic units in this copolymer and also decrease in time. However, the full water-spreading as we observed for the blends was not observed on the film containing only pHMGCL with maximum 10 molar% of HMG units³⁴.

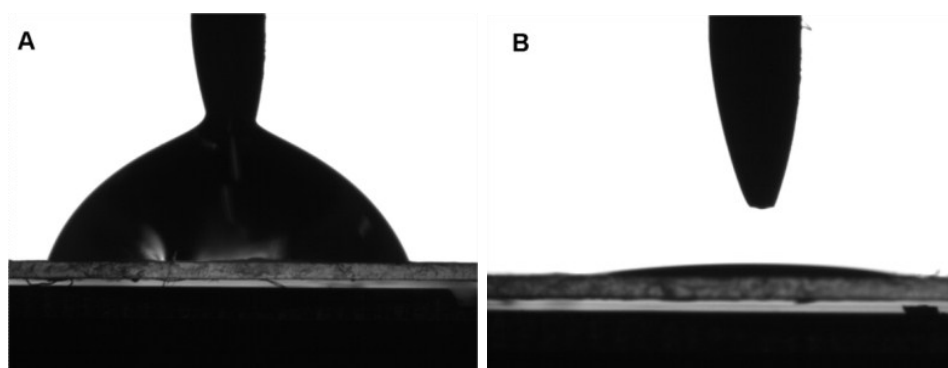


Figure 4. : (A) Advancing contact angle and (B) receding contact angle after 20 minutes water exposure on film of PCL/pHMGCL 1:2. (to be continued)

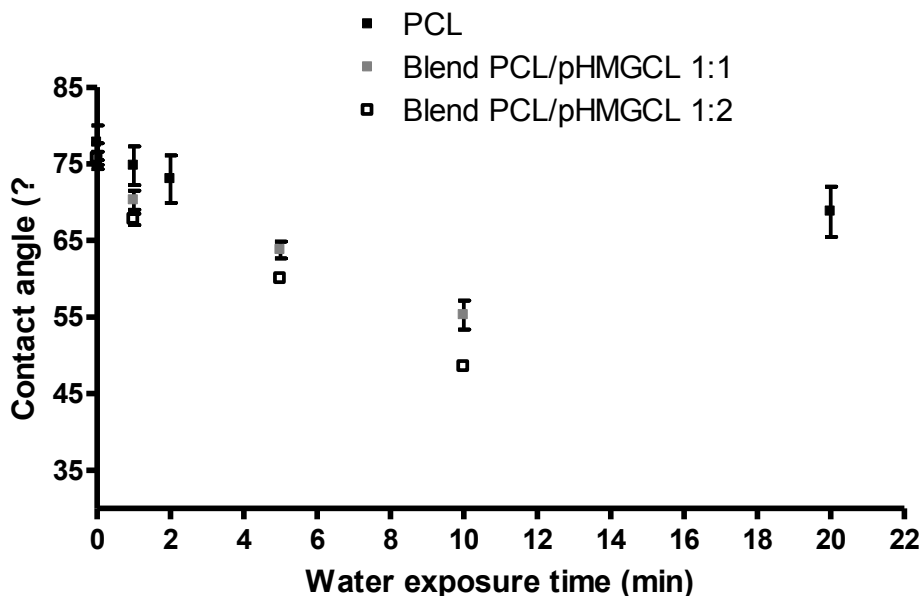


Figure 4. (continued with previous page) Advancing and the time-dependent receding contact angles on polymeric films of different compositions ($n=3 \pm \text{SD}$).

The thermal properties of the scaffolds were analyzed using DSC. As shown in Table 3, a single melting peak was observed for scaffolds with PCL/pHMGCL blends as the shell (Table 1, Groups 2 and 3). The heat of fusion of these scaffolds (in the first heating run) decreased from 73 to 54 J/g with increasing pHMGCL content in the blend from 0 % pHMGCL in PCL scaffolds to 67 % in PCL/pHMGCL 1:2 scaffolds. However, ΔH values measured at the second heating run were slightly lower than those obtained in the first heating cycles most probably due to the thermal history of the samples. Further, ΔH values (second heating run) were in good agreement with the calculated ΔH values (Table 3). The glass transition temperatures (T_g) of the scaffolds were -58.6 °C, -55.2 °C, and -47.4 °C for PCL, PCL/pHMGCL 1:1, and PCL/pHMGCL 1:2, respectively. Table 3 shows that the experimental T_g 's are in good agreement with those calculated by the Fox equation⁴⁴:

$$\frac{1}{T_g} = \frac{W_1}{T_{g,1}} + \frac{W_2}{T_{g,2}}$$

in which W_1 and W_2 are the weight fractions and $T_{g,1}$ and $T_{g,2}$ are the glass transition temperatures of the components in a blend. Based on these results, it can be concluded that electrospun scaffolds of pHMGCL and PCL consist of a miscible blend of the two polymers.

Table 3. Thermal properties of coaxial electrospun scaffolds before and after release.

Scaffold	Calculated Values		Before release				After release			
	T_g (°C)*	ΔH (J/g)**	First heating run			Second heating run		Second heating run		
			T_g (°C)	T_m (°C)	ΔH (J/g)	T_m (°C)	ΔH (J/g)	T_m (°C)	ΔH (J/g)	
PCL	N.A.	N.A.	-58.6	55.9	73.2	55.1	63.6	55.2	61.2	
PCL/pHMGCL 1:1	-57.5	48.5	-55.2	54.6	63.6	55.5	50.6	49.0	72.3	
PCL/pHMGCL 1:2	-55.8	42.7	-47.4	53.6	54.3	55.8	40.7	48.6	78.2	

* based on Fox equation, ** based on weight percentage of caprolactone in the blends.

3.3. BSA Loading Efficiency and in-vitro Release

BSA was chosen as a model protein for VEGF in this study due to similarities in their molecular weight ($M_{w,BSA} = 67$ kDa, $M_{w,VEGF} = 45$ kDa)⁴⁵⁻⁴⁷ and hydrodynamic radius ($R_{h,BSA} = 3.5$ nm⁴⁸, $R_{h,VEGF} = 3$ nm⁴⁹). The measured protein loading was $93.1 \pm 1.2\%$, $93.3 \pm 0.5\%$, and $93.1 \pm 1.5\%$ for PCL, PCL/pHMGCL 1:1, and PCL/pHMGCL 1:2, respectively. The BSA release profiles of the different scaffolds are shown in Figure 5.

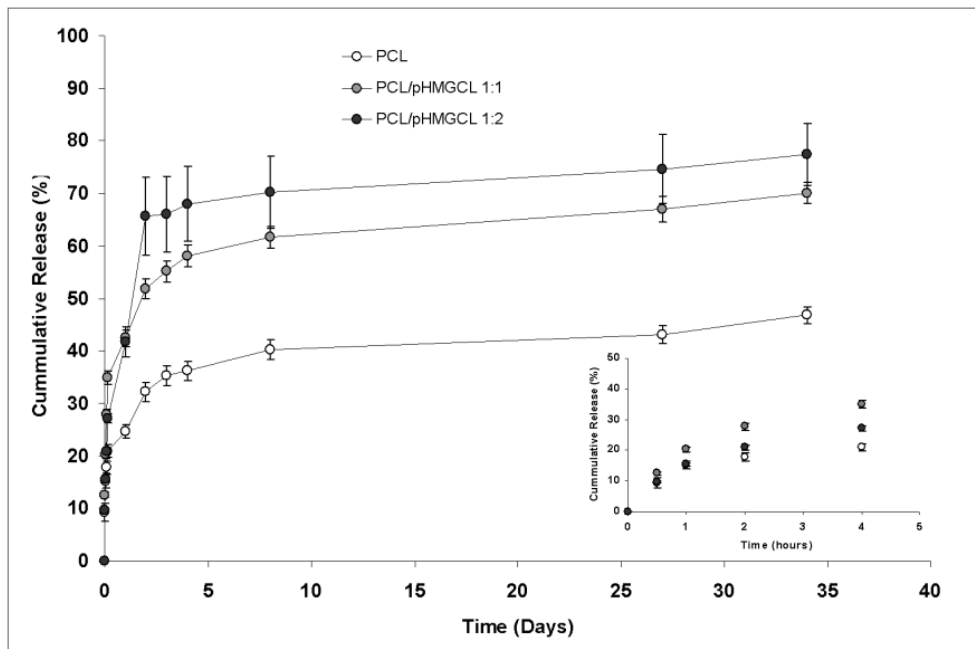


Figure 5. BSA release profiles of coaxial electrospun scaffolds (Group 1, 2 and 3) loaded with 0.2% BSA (n=3). Results are shown as mean \pm SD. The cumulative release is reported based on the amount of protein loaded in each scaffold. The insert shows the burst release of BSA up to 4 hours.

This figure shows that three stages can be distinguished in the release profiles; up to 4 hours an initial release ('burst' phase) followed by a gradual sustained release up to 10 days (phase 1) and a slow release up to 35 days (phase 2) (Table 4). The protein release from PCL scaffolds was predominantly controlled by a diffusion mechanism corresponding to our previous studies⁵⁰, whereas the protein release from PCL/pHMGCL 1:1, and

PCL/pHMGCL 1:2 scaffolds were controlled by both diffusion and degradation mechanisms. The burst release was $21.0 \pm 1.2\%$, $34.9 \pm 1.3\%$, and $27.2 \pm 0.8\%$ for PCL, PCL/pHMGCL 1:1, and PCL/pHMGCL 1:2 scaffolds, respectively. This burst release of protein is most likely due to either the presence of some non-uniformities (such as cracks, open ends, etc.) in the fibers structure and/or partial mixing of core and shell solutions during electrospinning, which might lead to presence of protein on the surface of fibers instead of in the core. In current study, the largest burst release was observed for the PCL/pHMGCL 1:1 group, which might be related to the exposure of protein on the fiber surface as a result of the electrospinning processing for this polymer combination. After this burst release, the protein was released in a sustained manner reaching $40.2 \pm 1.8\%$, $61.7 \pm 2.1\%$, and $70.1 \pm 6.8\%$ for PCL, PCL/pHMGCL 1:1, and PCL/pHMGCL 1:2 scaffolds after 10 days. After this phase, a very small amount of BSA was released in the next phase for all scaffolds up to 35 days and reached 46.8 ± 2.1 , 70.1 ± 2.3 , and 77.5 ± 5.1 for PCL, PCL/pHMGCL 1:1, and PCL/pHMGCL 1:2 scaffolds, respectively.

Table 4. Percentage of BSA released from coaxial scaffolds as burst (0-4 hrs), phase 1 (4 hrs-10 days), and phase 2 (10-35 days). Data are presented as means \pm standard deviations ($n=3$ samples from the same scaffold).

	Burst Release (0-4 hrs)	Phase 1 (4hrs- 10 days)	Phase 2 (10- 35 days)
Group 1	21.0 ± 1.2	19.2 ± 1.8	2.1 ± 2.1
Group 2	34.9 ± 1.3	26.8 ± 2.1	8.4 ± 2.3
Group 3	27.2 ± 0.8	42.9 ± 6.8	7.4 ± 5.1

It has been reported that several parameters among which shell thickness, surface area, defects, permeability, and solubility of the drug in the polymer shell control the rate of drug release from coaxial fibrous scaffolds⁵¹. For the coaxial fibers of the present study, it is most likely that the protein release is due to diffusion across nanopores in the polymeric shell, degradation of polymeric shell, and/ or a combination of these factors⁵². Degradation does not likely play a role in the mechanism of BSA release from PCL scaffolds because this polymer undergoes a very slow hydrolytic degradation, which takes more than 2 years^{32, 53, 54}. However, in our previous degradation study of pHMGCL with 10% HMG content³², we showed that this polymer degrades much faster than PCL and undergoes more than 10% weight loss within 35 days while the M_n drops from 30 kDa to less than 8 kDa. Based on these results it can be assumed that the pHMGCL used in the present study (containing > 20 molar % of hydrophilic HMG units) degrades even faster, as we also observed for related copolymers of HMG with lactide (pLHMGA)⁵⁵. Indeed, measuring the dry weight of post-release scaffolds and comparing that with the initial weight of scaffolds, showed that PCL, PCL/pHMGCL (1:1), and PCL/pHMGCL (1:2)

scaffolds lost 0.3 ± 0.4 , 17.5 ± 4.5 , and 26.0 ± 4.0 percent of their initial weight in 35 days. Since the weight of incorporated protein (BSA) is negligible compared to the weight of scaffolds, this mass loss cannot be related to the protein release and is therefore indicative of polymer degradation. SEM images of post-release scaffolds confirmed that PCL fibers were intact after 35 days (Figure 6, A and B), while fibers of scaffolds containing pHMGCL in the shell showed signs of degradation as observed by fibers fragmentation (Figure 6, C-F). Investigating the thermal properties of scaffolds after 35 days of protein release showed that crystallinity of scaffolds composed of pHMGCL/PCL (as reflected by ΔH) was notably increased while the crystallinity of PCL scaffolds was unchanged (Table 3). This increase in ΔH can be attributed to the preferential hydrolytic degradation of amorphous regions in the pHMGCL structure, resulting in crystallization of CL segments of the pHMGCL/PCL blend that were initially present in amorphous regions of the material.

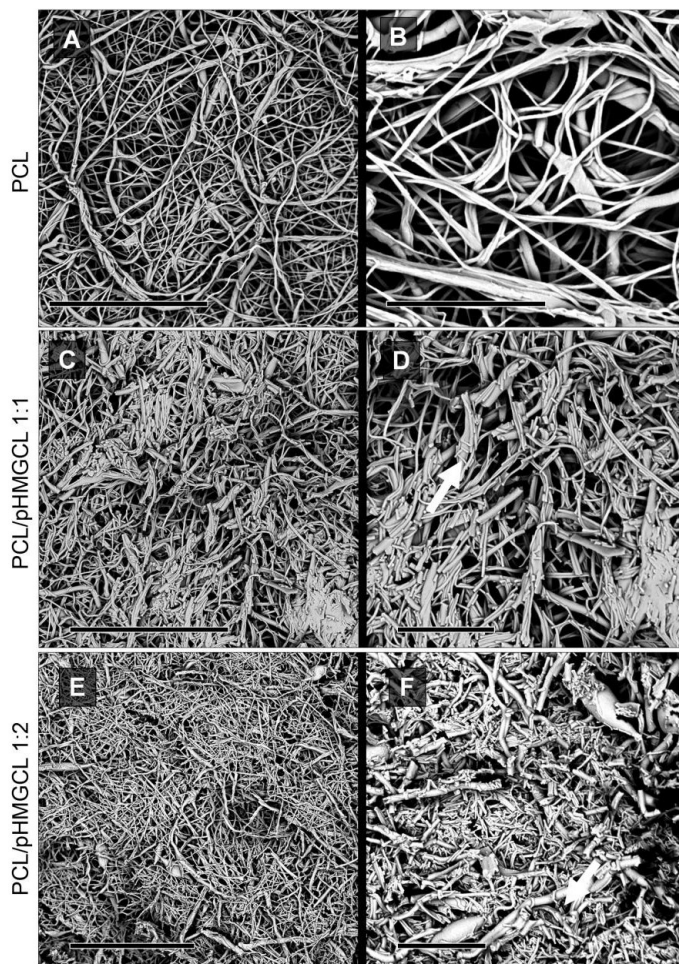


Figure 6. SEM images of BSA-loaded nanofibrous scaffolds after 35 days incubation in MilliQ-water at 37 °C. Scale bar is 30 μm (left) and 10 μm (right). White arrows show degraded fibers.

Increasing the weight fraction of hydrophilic pHMGCL in the fibers shell from 0% in PCL scaffold to 50 and 67% in PCL/pHMGCL scaffolds (1:1 and 1:2, respectively) resulted in a significant increase in amount of released protein after 10 days (PCL vs. 1:1 and 1:2 blend: $p < 0.05$ and $p < 0.001$, respectively) and after 35 days (PCL vs. 1:1 and 1:2 blend: $p < 0.05$ and $p < 0.01$, respectively). In addition, increasing the pHMGCL weight fraction in the blend from 50% in 1:1 scaffold to 67% in 1:2 scaffold, resulted in a significantly increased release of protein after 10 days ($p < 0.05$), however, the cumulative release after 35 days was not significantly different ($p > 0.05$).

Overall, it can be concluded that the protein release from PCL scaffolds is likely governed by diffusion via nanopores in the fibers shell, which have a size (slightly) bigger than the hydrodynamic diameter of BSA (less than 5 nm)⁴⁸, while the protein release from pHMGCL/PCL scaffolds is likely controlled by a combination of diffusion and shell degradation.

3.4. VEGF Bioactivity

As the biological half-life of VEGF is very short (30 min)⁵⁶, administration of this growth factor intravenously requires high doses and/ or multiple injections^{56, 57}. However, administration of large amounts of VEGF should be avoided as it results in catastrophic pathological vessel formation at non-targeted sites⁵⁶. Therefore, it is important to develop a polymeric matrix which is capable of slow releasing this protein at the defect site for TE application (e.g. bone regeneration). Previous research revealed different approaches to prepare fibrous scaffolds with VEGF release, including physical adsorption⁵⁸, blending protein with polymer solution for scaffolds preparation⁵⁹, as well as coaxial electrospinning with VEGF encoding plasmid in the core part⁶⁰. Amongst different approaches, we are particularly interested in coaxial electrospinning because this approach has great potential in preserving proteins during the electrospinning process due to different feeding capillary channels into one nozzle to generate composite nanofibers with a core-shell structure⁵⁰. In addition, it provides homogeneous protein distribution throughout the fibers, and proteins can be delivered in a controlled manner due to the shell barrier⁶¹. In this study, we prepared VEGF loaded nanofibrous scaffolds from PCL/pHMGCL 1:2 solution using BSA in the core as protein stabilizer⁶². This type of scaffold was chosen based on the *in vitro* release results which showed faster and higher overall release of the protein (Figure 5). Although the data are obtained from BSA as a model protein, one can assume that the loading efficiency and release profile of VEGF are comparable to the ones of BSA due to their similarity in size⁴⁶.

The bioactivity of released VEGF was analyzed by observing the growth of HUVECs cultured on the scaffolds loaded with VEGF (S+VEGF) in the assay medium, which contains no essential growth component for HUVEC growth. The scaffold without VEGF (S) was used as control. Furthermore, as a previous study indicated that HUVEC could proliferate

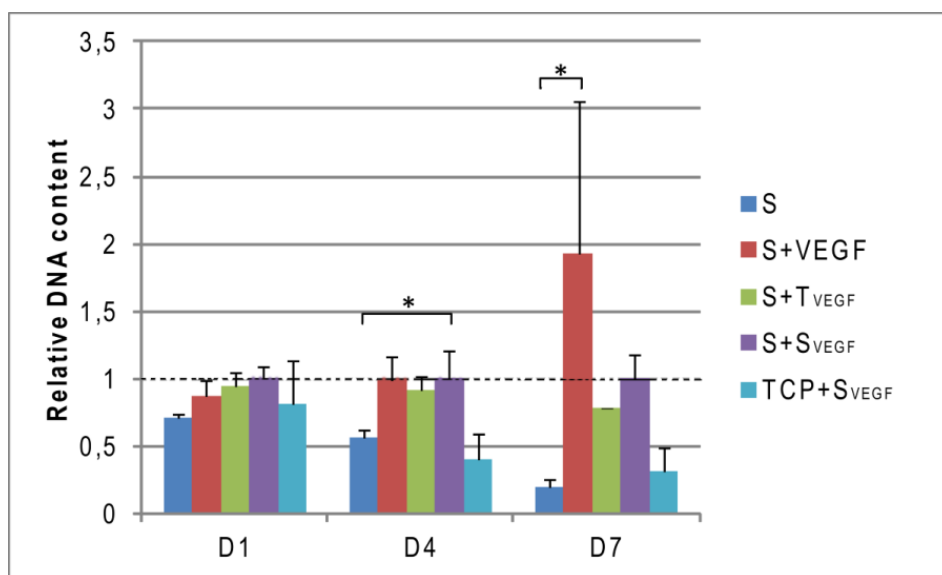


Figure 7. Relative DNA content of human umbilical vein endothelial cells (HUVECs) on scaffolds ($n=3$) on day 1, 4 and 7 post-seeding. Five groups in the experiment are: (S): Naïve scaffolds in AM; (S+VEGF): Scaffolds loading with VEGF in AM; (S+T_{VEGF}): Naïve scaffolds in AM supplemented with total amount of VEGF (1.6 μg); (S+S_{VEGF}): Naïve scaffolds in AM supplemented with 12.5 ng/ml VEGF; (TCP+S_{VEGF}): Tissue culture plates in AM supplemented with 12.5 ng/ml VEGF. Relative DNA amount as compared to (S+S_{VEGF}) and expressed as fold of DNA content (Mean \pm SD).

in the AM with sustained supplementation of VEGF (12.5 ng/ml)⁶³, we set up the group S+S_{VEGF} as reference for HUVECs growth on the scaffolds. In addition, S+T_{VEGF} was set up to distinguish the burst release effect on the cell growth. The DNA content of each group at different time intervals was related to the control group S+S_{VEGF}, and the relative DNA content of HUVECs on post-seeding day 1, 4 and 7 is presented in Figure 7. This figure shows that all groups displayed similar DNA content at day 1, indicating similar cell attachment and growth after cell seeding. After 4 days, HUVECs cultured on S showed significantly lower DNA content compared to S+S_{VEGF} ($p<0.05$), whereas no statistical difference was observed among other three groups. After 7 days, the relative DNA content from S+VEGF group was 4 fold higher than S group, which was significantly different ($p<0.05$). Since the DNA content is positively correlated with the number of viable cells, it can be concluded that the VEGF-releasing scaffolds supported more viable HUVECs growth and proliferation compared to bare scaffolds up to 7 days, which most likely is attributed to the bioactive VEGF released from coaxial scaffolds. In addition, no statistical differences were observed from HUVECs cultured on VEGF releasing scaffolds (S+VEGF) and VEGF supplemented medium, suggesting that the released VEGF had similar bioactivity compared to those having VEGF freshly added in the medium. Similar results were recently reported by Jia et al.⁶⁴, in which VEGF was loaded with dextran as the core component of poly(lactide-co-glycolide) (PLGA) coaxial electrospun scaffolds and it was

shown that the released VEGF preserved its bioactivity and supported HUVECs growth up to 5 days.

Furthermore, the cell proliferation was also confirmed by SEM. As demonstrated in Figure 8a, spreading of HUVECs was observed on VEGF-releasing scaffolds (S+VEGF) on day 4, whereas the cells grown on the naïve scaffolds (S) were clustered. Moreover, on day 7, obviously more cell confluence was observed on VEGF-releasing scaffolds (S+VEGF) than

the other groups, which confirmed the trend of aforementioned DNA content results presented in Figure 7. It is also worthwhile to mention that on day 4, the HUVECs in S+VEGF group showed a good attachment on scaffolds, as evidenced by confocal microscopic images (Figure 8b). Moreover, it showed similar confluence as S+T_{VEGF}. However, on day 7, S+VEGF group showed apparently more confluence than other groups, albeit that the cells were patchy on the scaffolds, which is probably due to the large surface volume of electrospun scaffolds as well as the limited number of the cells. These results suggest that the cell growth was supported by the sustained release of bioactive VEGF from coaxial scaffolds up to day 7.

Taken together, the current study demonstrates that the released pro-angiogenic factor VEGF remained biologically active up to 7 days, suggesting coaxial electrospinning is favorable for growth factor release with well maintenance of bioactivity. Although *in vitro* data suggested promising potential of using growth factor loaded core/shell fibers for TE

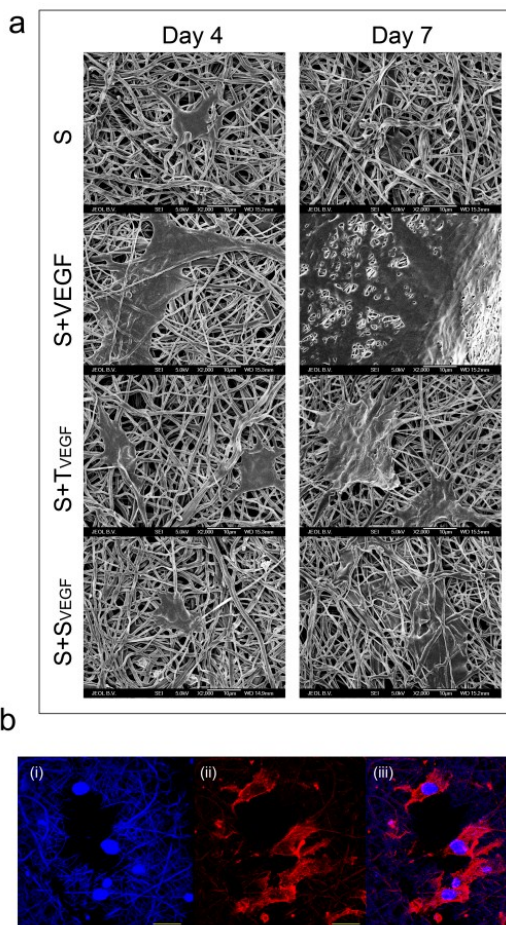


Figure 8. Morphology of human umbilical vein endothelial cells (HUVECs) cultured on scaffolds. (a) SEM pictures of HUVECs cultured on different groups after 4 and 7 days. Scale bar is 10 μ m. (b) Representative confocal images of HUVECs cultured on scaffolds loading with VEGF in AM (S+VEGF) after 4 days. (i) DAPI staining for nuclei UV-visualization (Blue); (ii) Alexa-fluor 568 conjugated phalloidin for actin (Red); (iii) the merger of DAPI and actin staining. Autofluorescence caused by polymeric fibrous scaffolds was observed at different track. (Scale bar is 20 μ m)

ments are necessary to fully understand the relationship between the dosage and release profile of loaded growth factor and corresponding biological responses.

4. Conclusions

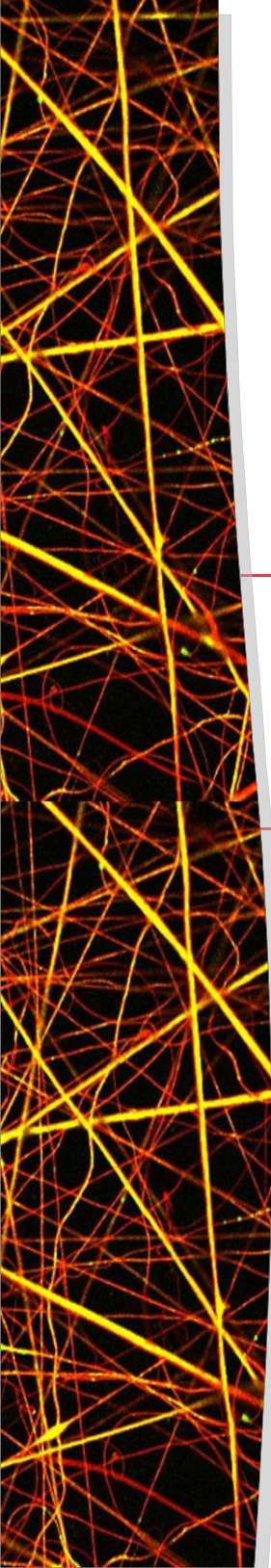
The current study describes the preparation and characterization of VEGF-loaded nanofibrous electrospun scaffolds based on blends of a hydroxyl-functionalized polyester (pHMGCL) and PCL by means of coaxial electrospinning. DSC analysis showed that these two polymers are miscible at a molecular level. It was shown by contact angle measurements that scaffolds containing pHMGCL exhibited significantly higher surface hydrophilicity compared to those based on PCL only. BSA as a model protein was loaded into these fibers and it was shown that the *in vitro* release of this protein is likely governed by combination of diffusion and degradation. Scaffolds composed of pHMGCL showed an enhanced protein release as compared to PCL scaffolds, likely due to enhanced hydrolysis rate of pHMGCL/PCL blend while PCL scaffolds did not degrade in the time frame investigated. It has shown previously that the increased hydrophilicity of pHMGCL scaffolds results in a considerable increase in adhesion of human mesenchymal stem cells seeded onto these scaffolds comparing to their counterpart PCL scaffolds. In the present study, it was demonstrated that loaded VEGF in pHMGCL containing scaffolds preserved its bioactivity to support HUVECs growth up to 7 days. Therefore, these bioactive electrospun scaffolds based on blends of pHMGCL and PCL are capable of releasing VEGF in a sustained manner and can be considered as attractive candidates for TE applications.

5. References

1. Dvir, T.; Timko, B. P.; Kohane, D. S.; Langer, R. *Nat. Nanotechnol.* **2011**, *6*, 13-22.
2. Mourino, V.; Boccaccini, A. R. *J. R. S. Interface* **2010**, *7*, 209-227.
3. Chen, R. R.; Mooney, D. J. *Pharm. Res.* **2003**, *20*, 1103-1112.
4. Richardson, T. P.; Peters, M. C.; Ennett, A. B.; Mooney, D. J. *Nat. Biotechnol.* **2001**, *19*, 1029-1034.
5. Levenberg, S.; Langer, R. In *Current Topics in Developmental Biology*, **2004**, *61*, 113-134.
6. Gan, Z.; Yu, D.; Zhong, Z.; Liang, Q.; Jing, X. *Polymer* **1999**, *40*, 2859-2862.
7. Sill, T. J.; von Recum, H. A. *Biomaterials* **2008**, *29*, 1989-2006.
8. Huang, Z. M.; Zhang, Y. Z.; Kotaki, M.; Ramakrishna, S. *Compos. Sci. Technol.* **2003**, *63*, 2223-2253.
9. Sasmazel, H. T. *Int. J. Biol. Macromol.* **2011**, *49*, 838-846.
10. Jeong, S. I.; Krebs, M. D.; Bonino, C. A.; Samorezov, J. E.; Khan, S. A.; Alsberg, E. *Tissue Eng.* **2011**, *17A*, 59-70.
11. Gluck, J. M.; Rahgozar, P.; Ingle, N. P.; Rofail, F.; Petrosian, A.; Cline, M. G.; Jordan, M. C.; Roos, K. P.; MacLellan, W. R.; Shemin, R. J.; Heydarkhan-Hagvall, S. *J. Biomed. Mater. Res.* **2011**, *99 B*, 180-190.
12. Cipitria, A.; Skelton, A.; Dargaville, T. R.; Dalton, P. D.; Huttmacher, D. W. *J. Mater. Chem.* **2011**, *21*, 9419-9453.
13. Meng, Z. X.; Xu, X. X.; Zheng, W.; Zhou, H. M.; Li, L.; Zheng, Y. F.; Lou, X. *Colloids Surf.* **2011**, *84B*, 97-102.
14. Meng, Z. X.; Zheng, W.; Li, L.; Zheng, Y. F. *Mater. Chem. Phys.* **2011**, *125*, 606-611.
15. Han, J.; Lazarovici, P.; Pomerantz, C.; Chen, X.; Wei, Y.; Lelkes, P. I. *Biomacromolecules* **2011**, *12*, 399-408.
16. Sahoo, S.; Toh, S. L.; Goh, J. C. H. *Biomaterials* **2010**, *31*, 2990-2998.
17. Lee, J. Y.; Bashur, C. A.; Goldstein, A. S.; Schmidt, C. E. *Biomaterials* **2009**, *30*, 4325-4335.
18. Yan, S.; Xiaoqiang, L.; Lianjiang, T.; Chen, H.; Xiumei, M. *Polymer* **2009**, *50*, 4212-4219.
19. Kim, S.; Kim, S. S.; Lee, S. H.; Eun Ahn, S.; Gwak, S. J.; Song, J. H.; Kim, B. S.; Chung, H. M. *Biomaterials* **2008**, *29*, 1043-1053.
20. Zhu, Y.; Leong, M. F.; Ong, W. F.; Chan-Park, M. B.; Chian, K. S. *Biomaterials* **2007**, *28*, 861-868.
21. Inoguchi, H.; Kwon, I. K.; Inoue, E.; Takamizawa, K.; Maehara, Y.; Matsuda, T. *Biomaterials* **2006**, *27*, 1470-1478.
22. Ji, W.; Sun, Y.; Yang, F.; Van Den Beucken, J. J. J. P.; Fan, M.; Chen, Z.; Jansen, J. A. *Pharm. Res.* **2011**, *28*, 1259-1272.
23. Drexler, J. W.; Powell, H. M. *Acta Biomaterialia* **2011**, *7*, 1133-1139.
24. Ji, W.; Yang, F.; Seyednejad, H.; Chen, Z.; Hennink, W. E.; Anderson, J. M.; van den Beucken, J. J.; Jansen, J. A. *Biomaterials* **2012**, *33*, 6604-6614.
25. Saraf, A.; Baggett, L. S.; Raphael, R. M.; Kasper, F. K.; Mikos, A. G. *J. Controlled Release* **2010**, *143*, 95-103.
26. Liao, I. C.; Chen, S.; Liu, J. B.; Leong, K. W. *J. Controlled Release* **2009**, *139*, 48-55.

27. Park, H. J.; Zhang, Y.; Georgescu, S. P.; Johnson, K. L.; Kong, D.; Galper, J. B. *Stem Cell Rev.* **2006**, *2*, 93-102.
28. Li, S.; Liu, L.; Garreau, H.; Vert, M. *Biomacromolecules* **2003**, *4*, 372-377.
29. Zeng, J.; Chen, X.; Liang, Q.; Xu, X.; Jing, X. *Macromol. Biosci.* **2004**, *4*, 1118-1125.
30. Yildirim, E. D.; Ayan, H.; Vasilets, V. N.; Fridman, A.; Gucer, S.; Sun, W. *Plasma Processes Polym.* **2008**, *5*, 58-66.
31. Loontjens, C. A. M.; Vermonden, T.; Leemhuis, M.; Van Steenberg, M. J.; Van Nostrum, C. F.; Hennink, W. E. *Macromolecules* **2007**, *40*, 7208-7216.
32. Seyednejad, H.; Ji, W.; Schuurman, W.; Dhert, W. J. A.; Malda, J.; Yang, F.; Jansen, J. A.; van Nostrum, C.; Vermonden, T.; Hennink, W. E. *Macromol. Biosci.* **2011**, *11*, 1684-1692.
33. Seyednejad, H.; Ghassemi, A. H.; Van Nostrum, C. F.; Vermonden, T.; Hennink, W. E. *J. Controlled Release* **2011**, *152*, 168-176.
34. Seyednejad, H.; Vermonden, T.; Fedorovich, N. E.; Van Eijk, R.; Van Steenberg, M. J.; Dhert, W. J. A.; Van Nostrum, C. F.; Hennink, W. E. *Biomacromolecules* **2009**, *10*, 3048-3054.
35. Seyednejad, H.; Gawlitta, D.; Dhert, W. J. A.; Van Nostrum, C. F.; Vermonden, T.; Hennink, W. E. *Acta Biomater.* **2011**, *7*, 1999-2006.
36. Patel, Z. S.; Young, S.; Tabata, Y.; Jansen, J. A.; Wong, M. E. K.; Mikos, A. G. *Bone* **2008**, *43*, 931-940.
37. Leemhuis, M.; Van Nostrum, C. F.; Kruijtzter, J. A. W.; Zhong, Z. Y.; Ten Breteler, M. R.; Dijkstra, P. J.; Feijen, J.; Hennink, W. E. *Macromolecules* **2006**, *39*, 3500-3508.
38. Leemhuis, M.; van Steenis, J. H.; van Uxem, M. J.; van Nostrum, C. F.; Hennink, W. E. *Eur. J. Org. Chem.* **2003**, *17*, 3344-3349.
39. Zhang, Y. Z.; Wang, X.; Feng, Y.; Li, J.; Lim, C. T.; Ramakrishna, S. *Biomacromolecules* **2006**, *7*, 1049-57.
40. Kitaori, T.; Ito, H.; Schwarz, E. M.; Tsutsumi, R.; Yoshitomi, H.; Oishi, S.; Nakano, M.; Fujii, N.; Nagasawa, T.; Nakamura, T. *Arthritis Rheum* **2009**, *60*, 813-823.
41. Ji, W.; Wang, H.; van den Beucken, J. J.; Yang, F.; Walboomers, X. F.; Leeuwenburgh, S.; Jansen, J. A. *Adv. Drug Deliv. Rev.* **2012**, *64*, 1152-1164.
42. Philippe Dubois, O. C. In *Handbook of ring-opening polymerization*. **2009**, 21-23.
43. Chakraborty, S.; Liao, I. C.; Adler, A.; Leong, K. W. *Adv. Drug Deliv. Rev.* **2009**, *61*, 1043-1054.
44. Parashar, P.; Ramakrishna, K.; Ramaprasad, A. T. *J. Applied Polym. Sci.* **2011**, *120*, 1729-1735.
45. Censi, R.; Vermonden, T.; van Steenberg, M. J.; Deschout, H.; Braeckmans, K.; De Smedt, S. C.; van Nostrum, C. F.; di Martino, P.; Hennink, W. E. *J. Controlled Release* **2009**, *140*, 230-236.
46. Oredein-Mccoy, O.; Krogman, N. R.; Weikel, A. L.; Hindenlang, M. D.; Allcock, H. R.; Laurencin, C. T. *J. Microencapsulation* **2009**, *26*, 544-555.
47. Stefanini, M. O.; Wu, F. T. H.; Mac Gabhann, F.; Popel, A. S. *BMC Sys. Biol.* **2008**, *2*, 77.
48. Hulse, W.; Forbes, R. *Int. J. Pharm.* **2011**, *416*, 394-397.
49. Kisko, K.; Brozzo, M. S.; Missimer, J.; Schleier, T.; Menzel, A.; Leppanen, V. M.; Alitalo, K.; Walzthoeni, T.; Aebersold, R.; Ballmer-Hofer, K. *FASEB J.* **2011**, *25*, 2980-2986.
50. Ji, W.; Yang, F.; van den Beucken, J. J.; Bian, Z.; Fan, M.; Chen, Z.; Jansen, J. A. *Acta Biomater.* **2010**, *6*, 4199-4207.

51. Zhang, Y. Z.; Wang, X.; Feng, Y.; Li, J.; Lim, C. T.; Ramakrishna, S. *Biomacromolecules* **2006**, *7*, 1049-1057.
52. Sahoo, S.; Ang, L. T.; Goh, J. C. H.; Toh, S. L. *J. Biomed. Mater. Res.* **2010**, *93A*, 1539-1550.
53. Sun, H.; Mei, L.; Song, C.; Cui, X.; Wang, P. *Biomaterials* **2006**, *27*, 1735-1740.
54. Woodruff, M. A.; Hutmacher, D. W. *Prog. Polym. Sci.* **2010**, *35*, 1217-1256.
55. Leemhuis, M.; Kruijtzter, J. A. W.; van Nostrum, C. F.; Hennick, W. E. *Biomacromolecules* **2007**, *8*, 2943-2949.
56. Lee, K.; Silva, E. A.; Mooney, D. J. *J. R. S. Interface* **2011**, *8*, 153-170.
57. Fischbach, C.; Mooney, D.; Werner, C., Polymeric Systems for Bioinspired Delivery of Angiogenic Molecules Polymers for Regenerative Medicine. In Springer Berlin / Heidelberg, **2006**, 203, 191-221.
58. Singh, S.; Wu, B. M.; Dunn, J. C. *J. Biomed. Mater. Res. A* **2012**, *100*, 720-727.
59. Kaigler, D.; Wang, Z.; Horger, K.; Mooney, D. J.; Krebsbach, P. H. *J. Bone Miner. Res.* **2006**, *21*, 735-44.
60. He, S.; Xia, T.; Wang, H.; Wei, L.; Luo, X.; Li, X. *Acta Biomater.* **2012**, *8*, 2659-69.
61. Ji, W.; Sun, Y.; Yang, F.; van den Beucken, J.; Fan, M. W.; Chen, Z.; Jansen, J. A. *Pharm. Res.* **2011**, *28*, 1259-1272.
62. Valmikinathan, C. M.; Defroda, S.; Yu, X. *Biomacromolecules* **2009**, *10*, 1084-1089.
63. Geutjes, P. J.; Nillesen, S. T.; Lammers, G.; Daamen, W. F.; van Kuppevelt, T. H. *Protein Expr. Purif.* **2010**, *69*, 76-82.
64. Jia, X.; Zhao, C.; Li, P.; Zhang, H.; Huang, Y.; Li, H.; Fan, J.; Feng, W.; Yuan, X.; Fan, Y. *J. Biomater. Sci. Polym. Ed.* **2011**, *22*, 1811-1827.
65. Li, H.; Zhao, C. G.; Wang, Z. X.; Zhang, H.; Yuan, X. Y.; Kong, D. L. *J. Biomater. Sci. Polym. Ed.* **2010**, *21*, 803-819.
66. Liao, I. C.; Chew, S. Y.; Leong, K. W. *Nanomed.* **2006**, *1*, 465-471.



Biocompatibility and degradation characteristics of poly(lactide-co-glycolide)-based electrospun nanofibrous scaffolds with nanoapatite incorporation

Wei Ji, Fang Yang, Hajar Seyednejad, Zhi Chen,
Wim E. Hennink, James M. Anderson,
Jeroen J.J.P. van den Beucken, John A. Jansen

Biomaterials. **2012**, 33, 6604-6614.

1. Introduction

In view of the biomedical application of biomaterials, nanofibrous scaffolds composed of biodegradable polymers gain increasing popularity, due to their morphological similarities to the native extracellular matrix¹. Among the multiple techniques used for nanofiber fabrication, e.g. phase separation and self-assembly, electrospinning is the most popular and cost-effective method to produce ultrathin polymeric fibers, which can be easily employed in the laboratory and scaled up to industrial levels². Regarding polymers used for electrospinning, poly(lactide-co-glycolide) (PLGA) is one of the most preferred ones and already approved by Food and Drug Administration (FDA) as a constituent of many biomaterial-based devices owing to its adjustable biodegradability and biocompatibility.

Although PLGA-based nanofibrous scaffolds are expected to have a promising application future in wound healing³, cardiac tissue regeneration⁴, as well as guided bone regeneration (GBR) membranes⁵, emerging concern exists regarding biocompatibility issues related to PLGA degradation products after implantation. It has been shown that during PLGA degradation, the accumulation of acidic degradation products (i.e. lactic and glycolic acid) decreases the pH in the surrounding tissue, which can trigger inflammatory and foreign body reactions *in vivo*^{6,7}. Upon clinical application, these reactions resulted in obvious symptoms, such as suddenly emerging pain, swollen tissues, and even persistent fistula⁸. Furthermore, recent research indicated that the high surface-to-volume ratio of nanofibrous scaffolds can even alter the tissue reaction to implanted PLGA-based materials toward an inferior level level^{9,10}. Consequently, it is necessary to comprehensively investigate the biocompatibility characteristics related to PLGA-based nanofibrous scaffolds for biomedical application.

Biocompatibility is defined as “the ability of a biomaterial to perform its desired function with respect to a medical therapy, without eliciting any undesirable local or systemic effects in the recipient or beneficiary of that therapy, but generating the most appropriate beneficial cellular or tissue response in that specific situation, and optimizing the clinically relevant performance of that therapy”¹¹. In general, the host tissue reacts to an implant by initiating an inflammatory response that consists of blood clot formation and the recruitment of macrophages, neutrophils, and lymphocytes to the site of implantation via several steps^{12,13}. First, macrophages recognize proteins adsorbed to the biomaterial surface and may adhere to the surface via specific cell surface receptors interacting with those adsorbed proteins; then, the secretion of active cytokines and growth factors, especially by macrophages, further orchestrates the cellular response to the biomaterial; in case of a persistent inflammatory response, activated macrophages may fuse to form foreign body giant cells (FBGCs) at the tissue/biomaterial interface¹³. In view of these steps, it is clear that (i) the cellular reaction to the materials, and (ii) cytokine lev-

els/balance are two important factors that determine the outcome of biocompatibility⁹. In other words, macrophages and foreign body giant cells (FBGCs) are considered as key determinants for the biocompatibility of implanted materials at a cellular level, while cytokines are involved at a molecular level by orchestrating cell recruitment and behavior⁹.

In view of the biological aspects of the host tissue response, it is accepted that a comprehensive understanding of biocompatibility issues related to implanted materials should be based on a sound evaluation of both cellular reactions and cytokine expression after implantation. However, a quite obvious limitation exists in current research regarding to biocompatibility issues of PLGA-based nanofibrous scaffolds based on our literature survey. In previous attempts to improve the biocompatibility of PLGA, titania nanoparticles¹⁴, tripolyphosphate (TPP) nanoparticles¹⁵, and demineralized bone particles (DBPs)⁶ were incorporated into PLGA scaffolds, all of which have shown *in vitro* effects by neutralizing the acidic degradation products of PLGA scaffolds to some extent. However, few studies presented direct evidence indicating that this neutralization indeed improved the host tissue response *in vivo*. Among these few cases, Yoon et al.⁶ reported that DBP/PLGA composite scaffolds evoked significantly less inflammation and fibrous capsule formation compared to pure PLGA scaffolds upon subcutaneous implantation in rats. Unfortunately, the authors only evaluated the biological response for a period of up to 5 days after implantation, which is too short to observe effects of PLGA degradation on biocompatibility issues. Furthermore, a very small number of studies focused on *in vivo* cytokine expression in response to implanted materials. Previous work of Brodbeck et al. revealed that *in vivo* gene expression of interleukin-1 β (IL-1 β), tumor necrosis factor- α (TNF- α), transforming growth factor- β (TGF- β), and interleukin-10 (IL-10) played an important role in directing the process between wound-healing and inflammation¹⁶. Nevertheless, to our knowledge, almost no information is available so far about the expression profile of cytokines in protein level related to the biocompatibility of biodegradable polymers.

In view of this, the current study aimed to evaluate i) the biocompatibility of PLGA electrospun nanofibrous scaffolds in both virgin and pre-degraded state, and ii) the effect of incorporated nano-apatitic particles (nAp) on degradation and biocompatibility of such scaffolds. To that end, PLGA was blended with poly(ϵ -caprolactone) (PCL) to prepare electrospun scaffolds to warrant the integrity of the electrospun scaffolds, as pure PLGA electrospun scaffolds are known to shrink substantially at 37°C^{17,18}. Nano-apatitic particles (nAp) were chosen as a neutralizing additive due to their alkaline properties and similarities to the mineral component in bone. Our hypothesis was that nAp incorporation in PLGA improved the tissue response by neutralizing the acidic degradation products.

2. Materials and methods

2.1. Materials

PLGA 5050 (Purasorb® PDLG 5010) was purchased from Purac Biomaterials BV (Gorinchem, the Netherlands). Granular PCL (Mn 80 kDa) and docusate sodium salt (AOT) (purity ≥ 99.0%) were purchased from Sigma–Aldrich (St. Louis, USA). Nano apatitic powder (Budenheim, Tri-Cafos P/C53-80; A80308A, MV 500 (T-C-P)) was kindly provided by Prof. Dr. Marc Bohner (RMS Foundation, Bettlach, Switzerland). Organic solvents 2,2,2-trifluoroethanol (TFE) (purity ≥ 99.8%) and 1,1,1,3,3,3-hexafluoroisopropanol (HFIP) (purity ≥ 99.0%) were obtained from Acros (Geel, Belgium) and Sigma–Aldrich, respectively.

2.2. Scaffold preparation

Four groups of electrospun scaffolds were prepared (see Table 1) and named as nX based on the theoretical weight percentage of nAp in the prepared scaffolds. For the electrospinning solution for bare scaffolds (n0), polymers (PLGA/PCL=3/1(w/w)) were dissolved at a concentration of 16% w/v in 90% TFE in deionized H₂O mixed with HFIP (v/v=1/1). For the electrospinning solutions containing nAp, a previously described method with modifications was used¹⁹. In brief, the amount of nAp was defined according to the weight ratio of nAp and polymers, and nAp powder was suspended in the solvent by ultrasonic and vigorous stirring before adding the polymers. AOT salt (0.05% w/v) was used as a surfactant and dissolved in the solvent to obtain stable particle suspension in the polymer solution as previously described¹⁹.

Table 1. The composition of 10 ml electrospinning solution and obtained nAp loading efficiency for different groups

	SCAFFOLDS			
	n0	n10	n20 ^b	n30 ^b
PLGA (g)	1.2	1.2	1.5	1.5
PCL (g)	0.4	0.4	0.5	0.5
nAp (g)	--	0.18	0.5	0.86
AOT (mg)	--	5.0	5.0	5.0
Solvent	HFIP/90%TFE (1:1)	HFIP/90%TFE (1:1)	HFIP/90%TFE (1:1)	HFIP/90%TFE (1:1)
Total volume (ml)	10	10	10	10
Theoretical nAp %	--	10.0	20	30.0
Actual nAp % ^a	--	10.9	22.1	31.2
nAp loading efficiency (Actual%/Theoretical%)	--	1.09	1.10	1.04

^a Actual nAp (%) was obtained from TGA results.

^b In order to achieve similar fiber diameter in four groups, n20 & n30 were prepared with PLGA/PCL=3/1(w/w) at a concentration of 20% w/v.

2.3. Scaffold characterization

The morphology of the fabricated scaffolds was observed by a high-resolution field emission scanning electron microscope (FESEM; JEOL, SM3010, Tokyo, Japan), operated at an acceleration voltage of 3.0 kV. The fiber diameters were measured from the SEM micrographs obtained at random locations ($n = 100$) using Image J software (National Institutes of Health, Bethesda, USA) based on SEM micrographs.

Transmission electron microscopy (TEM, JEOL 1010, Tokyo, Japan) was used to visualize nanoapatite incorporation. The TEM samples were prepared by directly depositing the electrospun fibers onto the Formvar-coated copper grids.

Fourier transform infrared spectrometry (FTIR; Spectrum One, Perkin–Elmer, USA) was used to analyze the chemical structure of the scaffolds with nAp incorporation over a range of 520–4000 cm^{-1} at a resolution of 4 cm^{-1} . X-ray diffraction (XRD) was used to observe the crystallographic structure of the scaffolds (PW3710, Philips, The Netherlands) with Cu $K\alpha$ radiation (45 kV, 40 mA). The scanning range was from 20 to 40° with a step size of 0.02°. The nAp powder used for scaffold preparation was also examined by FTIR and XRD to provide reference.

To verify the actual content of nAp in the composite membrane, thermogravimetric analysis (TGA) was carried out from room temperature to 600 °C using a TGA instrument Q50 (New Castle, DE, USA) at a heating rate of 10 °C/min in air.

2.4. *In vitro* degradation

Prior to initiation of the degradation experiment, the scaffolds containing 15 mg PLGA each were treated with argon plasma cleaner (PDC-001, Harrick Scientific Corp., USA) for 4 min with the radio frequency power set at 30W under vacuum condition to improve hydrophilicity. After that, they were incubated in 2 ml phosphate buffer saline (PBS; pH 7.4) at 37°C under shaking condition (60 rpm). The PBS solution was not changed throughout the 56-day *in vitro* degradation experiment. The pH of the solution with or without scaffolds was measured at selective time intervals using a pH meter ($n=3$).

At the end of the degradation experiment, the molecular weight (M_w) of degraded polymers from one out of three samples in each group was determined by means of gel permeation chromatography (GPC) using a 2695 Waters Alliance system and a Waters 2414 refractive index detector. Two PL-gel 5 μm mixed-D columns fitted with a guard column (Polymer Labs, M_w range of 0.2–400 kDa) were used. The columns were calibrated with polystyrene standards of known molecular weights using Analytical Grade (AR) tetrahydrofuran (THF). The flow rate was 1 ml/min at 30°C. The concentration of samples was approximately 5 mg/ml and the injection volume was 50 μl . As the scaffolds in the current study were prepared by the blends of PLGA and PCL, the original molecular weight for each polymer was also examined by GPC as reference.

2.5. Design of the *in vivo* evaluation

Fifteen healthy 8-week-old male Wistar rats (~250 g) were used as experimental animals. The protocol was approved by the Animal Ethical Committee of the Radboud University Nijmegen Medical Center (Approval no: RU-DEC 2011-038) and national guidelines for the care and use of laboratory animals were applied.

Based on the *in vitro* degradation data, n0 and n30 were enrolled for a 4-week *in vivo* evaluation. In order to evaluate the effect during the entire PLGA degradation period (~7 weeks), pre-degraded n0 and n30 (i.e. incubated in sterile PBS (pH 7.4) for 3 weeks without changing medium) were included in the animal experiment. Prior to initiation of the animal experiment, all scaffolds (1.5×1.5 cm²) were sterilized by γ -irradiation (Isotron, Ede, Netherlands) and then used for both direct implantation (D-system) and cage implantation (C-system) to obtain histological and exudates samples, respectively. The cages were prepared as described previously¹⁶ and sterilized by autoclaving. Empty cages were implanted as controls. Table 2 shows an overview of the experimental groups for *in vivo* evaluation.

Table 2. Experimental groups of scaffolds and numbers of samples (n) for *in vivo* evaluation

Sample code	Cage implantation (C-system) (anterior pockets)	Direct implantation (D-system) (posterior pockets)
n0	n=6	n=6
n30	n=6	n=6
p-n0 (3-week pre-degraded n0)	n=6	n=6
p-n30 (3-week predegraded n30)	n=6	n=6
Negative control	Empty cage	-

2.6. Animal surgery

The animals were anesthetized with isoflurane, and their backs were shaved and sterilized with alcohol and iodine scrub. Four paravertebral incisions (2 cm each) per rat were made approximately 1 cm lateral to the vertebral column to expose the dorsal subcutis. Subcutaneous pockets were created by blunt dissection. The anterior pockets were used for implantation of scaffolds following C-system, whereas the posterior pockets were used for corresponding scaffolds following D-system (Figure 1). After insertion of an implant, the skin was closed using skin staples (Agraves®, InstruVet C.V., Cuijk, the Netherlands). A total of 48 scaffolds (n=6 for each experimental group/implantation system) plus 6 empty cages were distributed over 15 rats according to a randomization scheme.

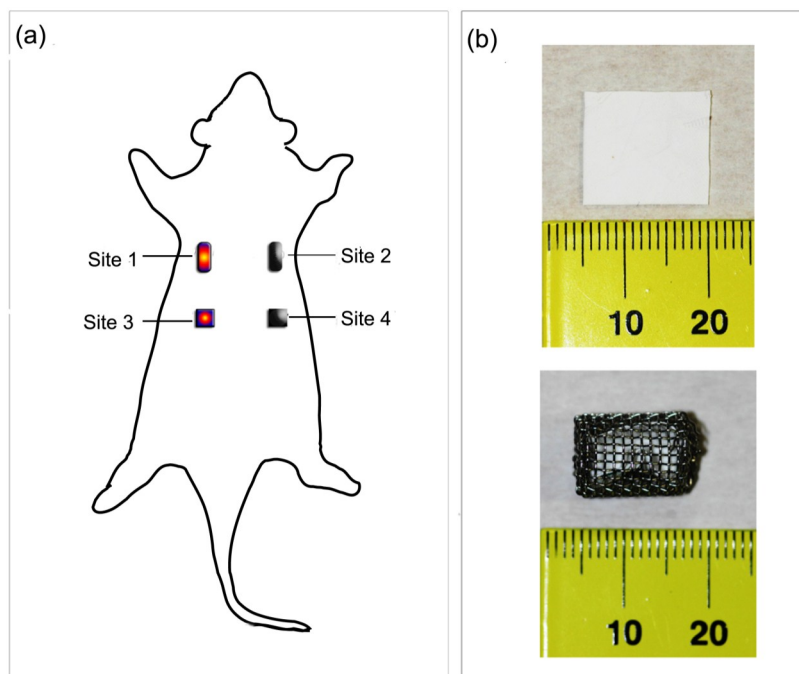


Figure 1. Implantation scheme for *in vivo* evaluation (a), and (b)scaffolds in cage and direct implantation system. (a) Four subcutaneous pockets were made per rat, as shown as sites 1-4. The anterior pockets (sites 1&2) were used for samples in cage system (C-system). The posterior pockets (sites 3&4) were used for corresponding samples in direct implantation system (D-system). Scaffolds from the different groups were indicated as different colors in the scheme, and different groups were randomized in 15 rats. If an empty cage was implanted in anterior pocket, no scaffold was implanted in the corresponding posterior pocket. (b) Scaffolds were cut into small squares ($1.5 \times 1.5 \text{ cm}^2$) for both direct and cage implantation system. The cages were prepared by surgical-grade stainless steel wire mesh cages (1.5 cm in length, 0.8 cm in diameter, 0.25-mm wire diameter and 0.8-mm opening width with 58% open area), as previously described¹⁶

2.7. Sample retrieval and histological processing

At week 1 and 4 post-surgery, exudate samples were collected from the cage implant systems using 25 gauge needles. The collected exudates were further centrifuged at 1000 rpm at 4°C to isolate supernatants, which were kept at -80°C till further analysis. Immediately after exudate collection at week 4 post-surgery, the animals were euthanized using CO₂ suffocation, and the tissue-covered specimens were retrieved. The samples from C-system implantation were lysed in 1 ml TRIzol[®] reagent (Invitrogen, USA) after PBS rinsing. The samples from D-system implantation were fixed in 10% formalin, dehydrated in a graded series of ethanol and embedded in paraffin, after which 6 μm sections were cut in a transversal direction using a standard microtome (RM 2165; Leica, Germany). The sections were cut from at least three arbitrary regions perpendicular to the long axis of the tissue capsule. Paraffin sections were stained with hematoxylin/eosin (HE).

2.8. Immunohistochemistry

For the identification of macrophages and FBGCs in the paraffin sections, CD68 immunohistochemical staining and tartrate-resistant acid phosphatase (TRAP) staining were performed. For CD68 staining, the sections were treated with 10% H₂O₂ in methanol to inactivate endogenous peroxidase, and post-fixed with 10% formaldehyde in PBS. After three times washing with 0.075% glycine in PBS, the sections were heated in citrate buffer (pH 6.0) for 10 min at 70 °C. After rinsing with PBS, the sections were pre-incubated with 10% normal donkey serum (NDS, Chemicon, USA) followed by the overnight incubation of mouse anti-rat CD68, (1:200; Serotec, DPC, the Netherlands) at 4 °C. Subsequently, the sections were rinsed with PBS, incubated with biotinylated secondary antibody donkey-anti-mouse IgG (1:500; Jackson Labs, USA) for 1 h, rinsed with PBS, and treated with 3,3'-diaminobenzidine (DAB). For TRAP staining, the sections were pre-incubated 0.2M Tris-MgCl₂ buffer (pH 9.0) for 2 h at 37 °C. After rinsing with distilled water, the sections were incubated in acidic phosphate medium (pH 5.0) consisting of hexazotized pararosaniline (4 ml), Naphthol AS-BI Phosphate (25 mg), N,N-Dimethylformamide (2.5 ml), veronal buffer (12.5 ml) and MgCl₂ (0.5g) for 1 h at 37 °C. After staining, the sections were counterstained with hematoxyline for 10 s, rinsed in water, dehydrated and mounted with DPX (BDH Laboratory Supplies, England).

2.9. Histological evaluation

All sections were photographed with the Zeiss Imager Z1 together with the AxioCam MRc5 camera using the AxioVision 4.6.3 software (Carl Zeiss Microimaging GmbH, Germany). Histological evaluation on all sections was performed by two independent examiners (W.J and J.J.B) based on the obtained images. For the analyses of HE stained sections, a refined histomorphometric grading scale was used (Table 3)²⁰. The performed quantitative evaluation of the fibrous capsule in each section was based on four different areas (image size: 678×510 μm²) of entire fibrous capsules surrounding the scaffolds as previously described²¹.

2.10. Measurement of cytokines in exudates

The exudates extracted from cages were assayed for cytokines with a bioplex bead array (Bio-Rad: Hemel Hempstead, UK) using rat inflammation cytokine 10-plex magnetic bead assay kit (Milliplex®, Cat# RCYTOMAG-80K-10, Millipore, USA) according to the manufacturer's instructions. Ten different cytokines were detected, including the chemokine growth-regulated oncogene-KC (GRO-KC, CXCL1), monocyte chemotactic protein-1 (MCP-1), granulocyte-macrophage colony-stimulating factor (GM-CSF), and vascular endothelial growth factor (VEGF), as well as cytokines TNF-α, IL-1β, IL-4, IL-6, IL-10 and IL-13. Cytokine concentrations (pg/ml) were determined from fluorescence intensities (FI)

Table 3. Histological grading scale for tissue response

	Score
<u><i>Histological grading scale for capsule quality</i></u>	
Capsule tissue is fibrous, not dense, resembling connective or fat tissue in the non-injured regions	4
Capsule tissue is fibrous but immature, showing fibroblasts and little collagen	3
Capsule tissue is granulous and dense, containing both fibroblasts and many inflammatory cells	2
Capsule tissue consists of masses of inflammatory cells with little or no signs of connective tissue organization	1
Cannot be evaluated because of infection or other factors not necessarily related to the material	0
<u><i>Histological grading scale for capsule thickness</i></u>	
1-4 fibroblasts	4
5-9 fibroblasts	3
10-30 fibroblasts	2
>30 fibroblasts	1
Not applicable	0
<u><i>Histological grading for cell infiltration</i></u>	
Only fibroblasts contact the surface	4
Scattered macrophages and leucocytes are present	3
One layer of macrophages and leucocytes are present	2
Multiple layers of macrophages and leucocytes present	1
Cannot be evaluated	0

compared to a linear standard curve generated from standards of known concentration provided by the manufacturer.

2.11. Real-time polymerase chain reaction (PCR)

The total RNA of the infiltrated cells was isolated from the scaffolds in C-system using TRIzol[®] reagent according to manufacturer's instructions. In brief, samples were mixed vigorously to lyse the cells followed by centrifugation at 10,000 g for 10 min at 4 °C. The supernatants were transferred to a new tube and 200µL chloroform was added, mixed, incubated for 3 min and centrifuged at 10,000 g for 15 min. The resulting aqueous layer was collected, mixed with 500µl isopropanol and RNA was pelleted by centrifugation at 10,000 g for 15 min. The pellet was washed with 70% ethanol and RNA was finally dissolved in 27µl deionized water. The total RNA concentration was measured using a Nanodrop (Nanodrop Technologies, USA). The reverse transcriptase (RT) reaction was performed to obtain cDNA by using Superscript[™] III First-strand Synthesis System (Invitrogen, USA) according to manufacturer's protocol as previously described²².

Gene expression was evaluated for interleukin-1β (IL-1β), tumor necrosis factor-α (TNF-α), transforming growth factor-β (TGF-β), and interleukin-10 (IL-10). The expression levels were analyzed versus the housekeeping gene beta-actin (β-Act) as previously described²³. The forward and reverse primer sequences for each gene are listed in Table 4. Relative mRNA expression was quantified using the comparative Ct (ΔCt) method and

Table 4. Forward and reverse primer sequences

Primers	Forward (5'→3')	Reverse (5'→3')
IL-1 β	CTGTGACTCGTGGGATGATG	GGGATTTTGTGCTTGCTTGT
TNF- α	ACTCCCAGAAAAGCAAGCAA	CGAGCAGGAATGAGAAGAGG
TGF- β	ATACGCCTGAGTGGCTGTCT	TGGGACTGATCCCATTGATT
IL-10	AATAACTGCACCCACTTCCC	CAACCCAAGTAACCCCTAAAGTC
β -Act	TTC AACACCCCAGCCATGT	TGTGGTACGACCAGGGCATACT

2.12. Statistical analysis

Data were expressed as mean \pm standard deviation. For fiber diameter and pH measurements, statistical analysis was performed with a one-way ANOVA and post-hoc Tukey Multiple Comparisons test. For histological evaluation, a non-parametric ANOVA (Kruskal–Wallis) with post Dunn's multiple comparison test was applied. The statistic analysis was performed using Graphpad InStat software (InStat[®] 3.05, Graphpad Software Inc., USA). For cytokine concentrations measured in exudates, a paired t-test was performed to detect the difference of each cytokine concentration related to time intervals. To compare the difference in cytokine concentrations between groups at the same time interval, a non-parametric ANOVA (Kruskal–Wallis) with post-hoc multiple comparison test was applied using SPSS 18.0 (SPSS, Chicago, Illinois) and statistical package R (<http://www.R-project.org>)²⁴.

3. Results

3.1. Scaffold characterization

The nanofibrous scaffolds with different amounts of nAp were prepared by electrospinning, and their morphologies were examined using SEM and TEM. SEM images (Figure 2a) showed a uniform fiber structure for electrospun fibers of each composition with similar average fiber diameters ranging from 731 to 780 nm ($p > 0.05$). TEM (Figure 2b) demonstrated that most nAp particles were embedded within the fibers and only some were exposed at the fiber surface.

The FTIR spectra of the different scaffolds are shown in Figure 2c. Typical bands attributed to PO₄³⁻ can be observed from the spectrum of reference nAp powder. The bands at 1089 and 1027 cm⁻¹ can be assigned to the triple degenerated γ 3 anti-symmetric stretching of P–O band, and the bands at 601, and 563 cm⁻¹ can be attributed to the triple degenerated γ 4 vibration of O–P–O bond²⁵. The bands at 628 cm⁻¹ can be assigned to the libration mode of OH⁻ group²⁶. Identical bands for O–P–O bonds and OH⁻ group can only be observed from the scaffolds with nAp incorporation (n10, n20, and n30).

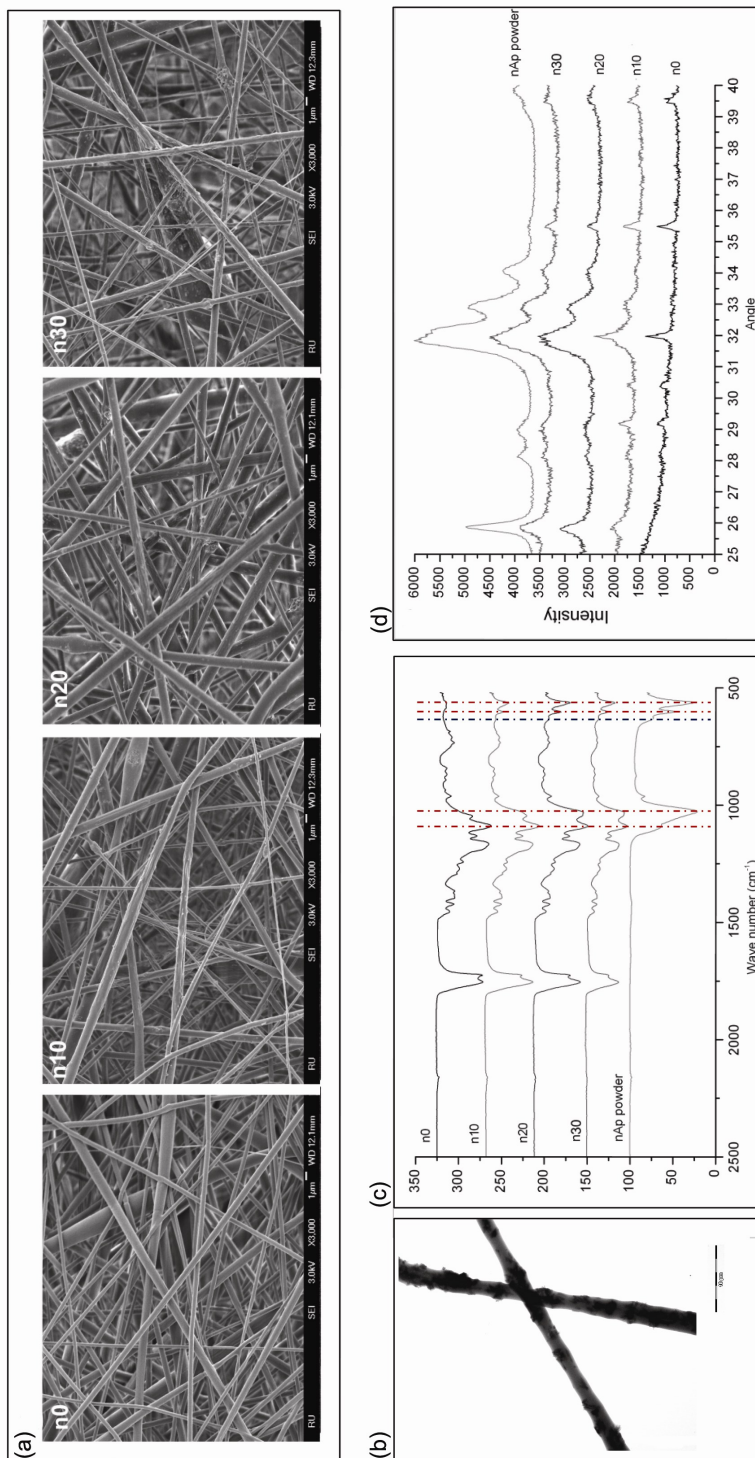


Figure 2. Characterization of virgin nanofibrous scaffolds prepared by blend electrospinning. (a) SEM images of scaffolds with different amount of nAp incorporation. Scale bar = 1 μ m (b) Representative TEM image of scaffolds with nAp incorporation (n20). Scale bar = 10 μ m (c) FTIR and (d) XRD spectra of nAp powder and electrospun scaffolds. Dash line in red and blue indicated the characteristic FTIR peak for phosphate and hydroxyl group, respectively

The corresponding XRD patterns of different scaffolds are depicted in Figure 2d. As a reference, the pattern of nAp powder indicated the Bragg peaks at 25.9° , 31.8° , 32.9° and 34.1° 2θ , which respectively correspond to the characteristic reflections of 002, 211, 300 and 202 of an apatitic structure¹⁹. The characteristic peaks of nAp at 25.9° and 34.1° were observed in the XRD patterns of scaffolds with nAp incorporation, while both other characteristic peaks were masked by peaks contributed by the polymer, as can be determined from the XRD pattern of the bare polymer scaffolds.

The actual content of nAp incorporated in the scaffolds was evaluated by TGA, and the nAp loading efficiency was between 1.04 and 1.10 (Table 1).

3.2. *In vitro* degradation of scaffolds

The *in vitro* degradation of polymeric scaffolds incubated in PBS at 37°C under dynamic (60 rpm) conditions was monitored by the pH change of PBS during a 56-day degradation period and GPC measurements for the scaffolds after that period.

As shown in Figure 3a, a fast pH decrease from pH 7.4 to around pH 5 (day 0-day 4) was observed for all types of scaffolds upon immersion in PBS, followed by a phase with relatively stable pH until week 3. Thereafter, pH-levels slowly continued decreasing until the end of the degradation study (week 8). For n0, the final pH-value of the solution decreased to 2.58 ± 0.03 . Compared to n0, the composite scaffolds showed an nAp amount-dependent effect on final pH-levels: final pH values for n10, n20, and n30 were significantly higher than n0 ($p < 0.05$; 3.59 ± 0.01 , 4.03 ± 0.01 , and 4.28 ± 0.05 , respectively), and they were significantly different from each other ($p < 0.01$).

GPC was performed to examine the molecular weight (M_w) of polymers in the scaffolds after an 8-week degradation study. GPC results showed that the M_w of PLGA in the bare scaffolds (n0) could not be detected, and the M_w of PCL decreased from 105.6 to 26.9 kD. Compared to the n0, scaffolds with nAp incorporation showed an nAp amount-dependent higher post-degradation M_w of PLGA and PCL (Figure 3b).

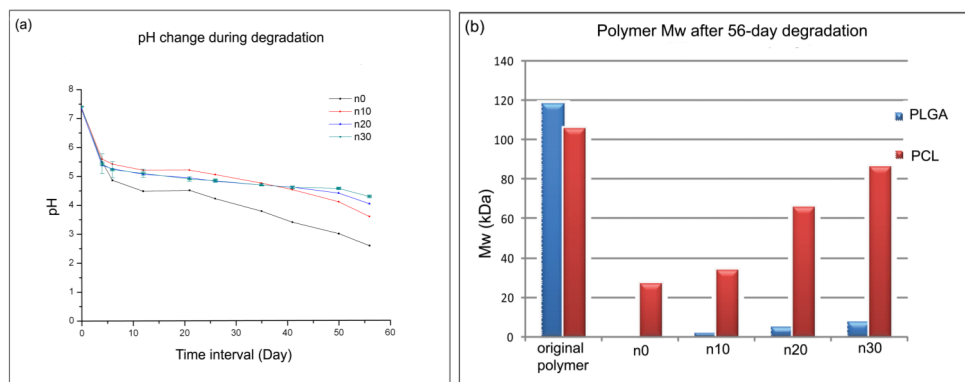


Figure 3. *In vitro* degradation behavior of scaffolds.

3.3. Descriptive histology of host tissue response

The host tissue response to bare and composite scaffolds in virgin (n0 & n30) and pre-degraded state (p-n0 & p-n30) was evaluated after a 4-week subcutaneous implantation period. Representative sections (HE-staining) of different scaffolds implanted in the D-system are presented in Figure 4.

Histological observation showed that fibrous encapsulation occurred for all types of scaffolds, and endogenous cells which mainly include fibroblasts and leucocytes infiltrated at the interface between the scaffold and the fibrous capsule.

The presence of multinuclear cells was observed in the sections of n0 (Figure 4), whereas these were not observed in the histological sections of the other types of scaffolds.

Histological grading results (Figure 5) based on the HE-stained sections showed that incorporation of nAp significantly ($p < 0.001$) decreased cell infiltration between the fibrous capsule walls and the scaffolds remnants for both virgin and pre-

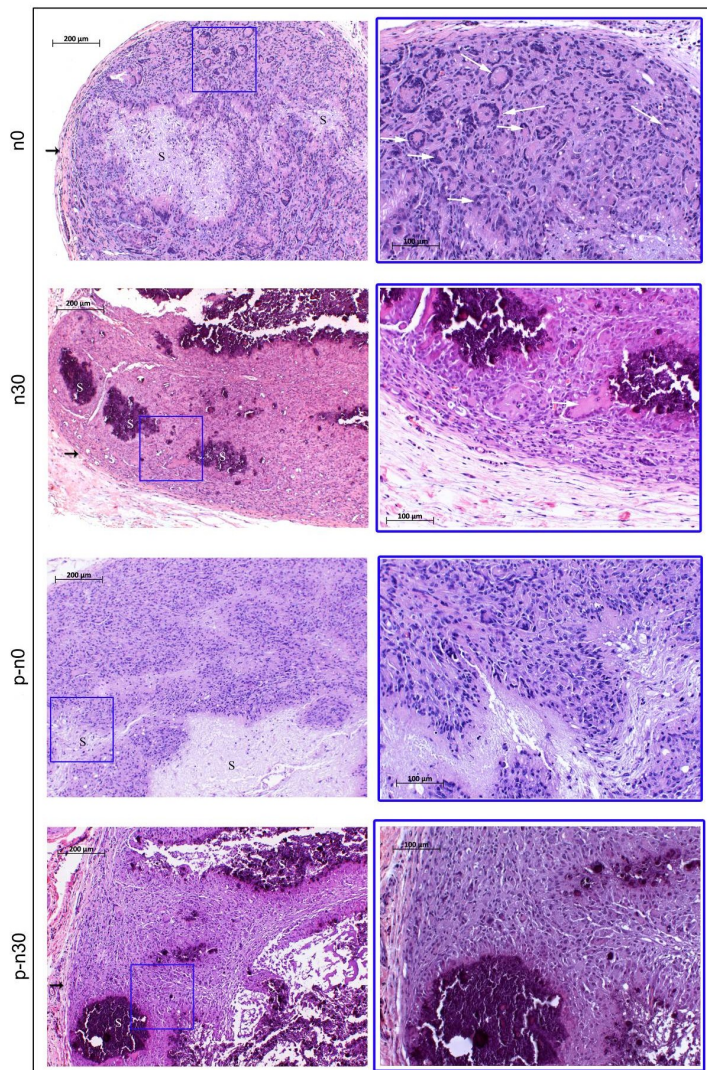


Figure 4. HE staining of different groups of scaffolds after 4-week subcutaneous implantation. The left column showed HE stained sections from 4-week subcutaneously implanted scaffolds. The fibrous capsule wall was indicated by black arrow (à), and the scaffold remnant was indicated as "S". Magnified images in the blue squared area were displayed in the right column, where multiple multinuclear cells (indicated by white arrows) can be observed between the fibrous capsule layers and scaffold interface in HE stained section of n0.

degraded scaffolds. In contrast, similar capsule quality and thickness were observed for all types of scaffolds, which mainly consisted of multiple layers (5–9 layers) of fibroblasts with little collagen structure.

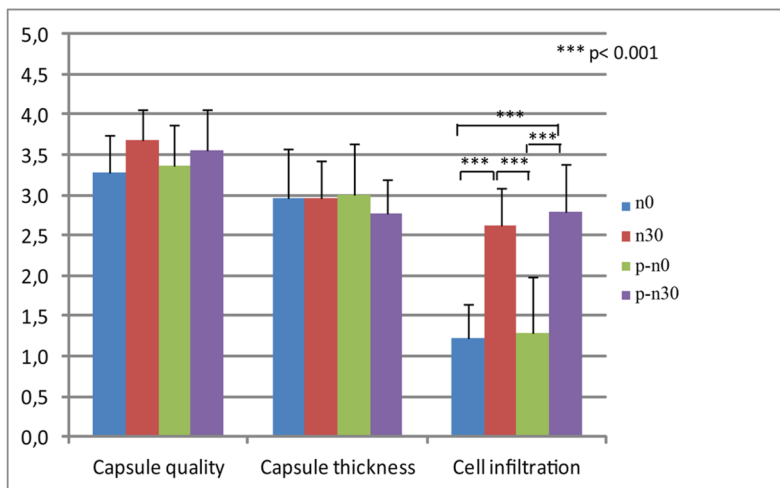


Figure 5. Histological grading of different groups of scaffolds after 4-week subcutaneous implantation. Histological grading analysis indicated that the incorporation of nAp significantly ($p < 0.001$) reduce macrophages infiltration between the fibrous capsule walls and the interface of degrading scaffolds in both virgin and pre-degraded status.

Figure 6 shows CD68- and TRAP-staining, performed to confirm macrophage infiltration and FBGCs formation. An apparently increased CD68(+) staining was observed for n0 (Figure 6a) and p-n0 (Figure 6c), whereas the scaffolds with nAp incorporation in both virgin (n30; Figure 6b) and pre-degraded (p-n30; Figure 6d) status showed less CD68(+) cell infiltration. Furthermore, n0 showed evidently most TRAP(+) cells in the vicinity of the scaffold (Figure 6e), while only limited TRAP(+) cells were observed for p-n0 and n30 (Figure 6f&g). Hardly any TRAP(+) cells were observed for p-n30 (Figure 6h).

3.4. Expression of inflammatory cytokines

At protein level, cytokine expression was examined from the exudates samples extracted from the implants in the C-system after 1 week and 4 weeks of implantation. From the ten different cytokines that were analyzed, concentrations of GM-CSF, IL-4, IL-6, IL-10 and IL-13 were below the detection limit (8 pg/ml). Irrespective of marginal significant differences as indicated in Figure 7, the cytokine expression of GRO-KC, MCP-1 and VEGF was relatively high for all groups after 1 week and a significant decrease ($p < 0.05$) after 4 weeks. In contrast, the expression of TNF- α and IL-1 β was relatively low for all groups after 1 week and increased after 4 weeks.

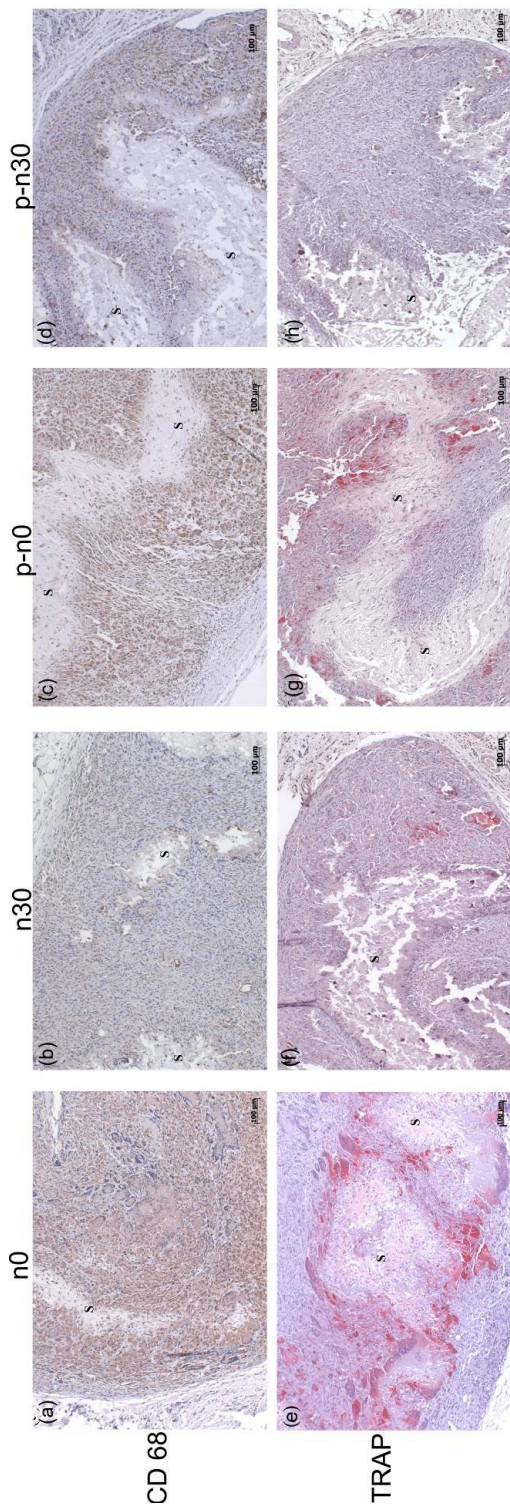


Figure 6. (Immuno)histochemical staining of scaffolds after 4-week subcutaneous implantation. CD68 (a-d) & TRAP (e-h) staining of different groups of scaffolds after 4-week subcutaneous implantation. The scaffold remnant was indicated as "s". Apparently more positive staining of CD 68 (c & e) and TRAP (e & g) can also be observed in the sections of bare scaffolds in both virgin and pre-degraded status compared to the scaffolds with nAp incorporation.

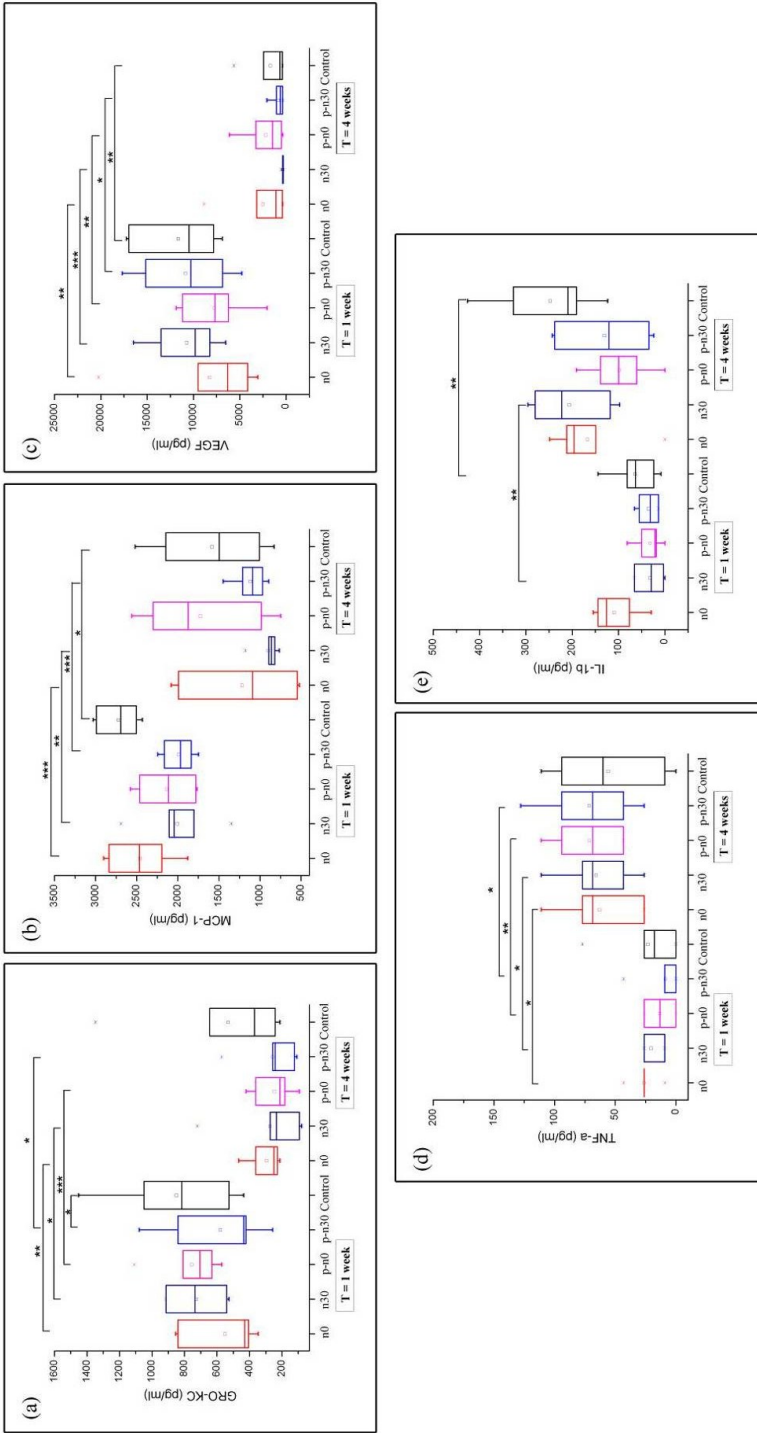


Figure 7. The concentrations of detected cytokines in the exudates after 1 week and 4 weeks from different groups. GRO-KC, MCP-1, VEGF, TNF- α , and IL- β were detected from exudates after 1 week and 4 weeks of subcutaneous implantation of four types of scaffolds in C- system. Empty cage was used as negative control. Statistical difference was indicated as * $p < 0.05$, ** $p < 0.01$, and *** $p < 0.001$, respectively

At gene level, the relative gene expression of IL-1 β , TNF- α , TGF- β , and IL-10 from the infiltrated cells that attached to the materials in the C-system after 4 weeks of implantation were analyzed using qPCR. As the empty cage does not contain the material, therefore, no gene values were obtained from this group. As shown in Figure 8, IL-1 β and IL-10 expression was similar for all groups. However, compared to n0, gene expression of TNF- α was significantly decreased in p-n0 ($p < 0.05$), and gene expression of TGF- β was significantly increased in n30 ($p < 0.05$).

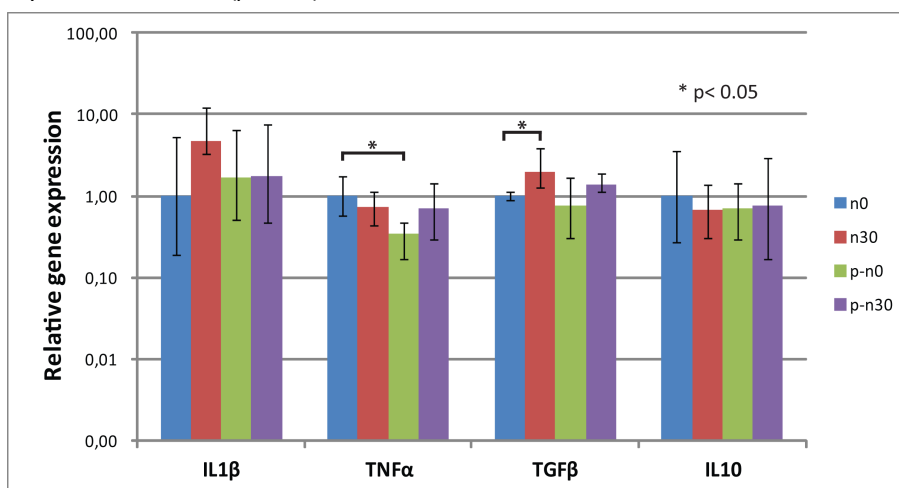


Figure 8. Relative gene expression of IL-1 β , TNF- α , TGF- β , and IL-10 from the cells infiltrated in the scaffolds after 4 weeks of implantation. Data was expressed as $2^{-\Delta\Delta C_t}$ and 95% confidence interval relative to the n0 group ($n=6$). Values were normalized with β -Act.

4. Discussion

The aim of this study was to evaluate the effect of nAp incorporation into PLGA-based nanofibrous scaffolds on degradation and biocompatibility characteristics. Our hypothesis was that nAp incorporation into the nanofibrous scaffolds would neutralize acidic degradation products, and hence could slow down scaffold degradation and improve the tissue response. For this purpose, four groups of PLGA/PCL blended (w/w=3/1) polymeric electrospun scaffolds were prepared with 0–30 wt% nAp incorporation (n0–n30). The generated scaffolds were characterized, and enrolled in an *in vitro* degradation study. Subsequently, n0 and n30, in a virgin and pre-degraded state, were subcutaneously implanted for 4 weeks using both direct and cage implantation to evaluate the *in vivo* tissue response. Our main findings showed that the incorporation of nAp evokes an nAp amount-dependent buffering effect during degradation. Further, nAp incorporation decreased polymer degradation, as shown by a higher post-degradation polymer Mw. Regarding biocompatibility, the current study indicated that nAp incorporation significantly improved the tissue response during 4-week of subcutaneous implantation, as evidenced

by less infiltration of inflammatory cells as well as less FBGCs formation surrounding the scaffolds. However, only marginal differences in cytokine expression were observed between all groups.

The current study confirmed the buffering effect of nAp on pH decline during the degradation of PLGA-based scaffolds. In principle, the pH decline during *in vitro* degradation can be attributed to the release of acidic PLGA degradation products (i.e. lactic acid and glycolic acid), as PCL degradation results in non-acidic free caprolactone and its cyclic dimer and trimer²⁷. In this study, a fast pH decrease occurred within the first few days for all groups, followed by a phase with relatively stable pH till week 3, and thereafter another obvious pH drop. This result corroborates earlier findings about the degradation behavior of electrospun PLGA nanofibers²⁸. Furthermore, the pH change during PLGA degradation is positively related to the amount of acidic degradation products released during different stages of PLGA degradation²⁸. Our results also revealed that the embedded nAp particles reduced polymer degradation in an nAp amount-dependent manner, which resulted in higher polymer *Mw* after 56-day *in vitro*. Similar findings were previously reported when a strong alkaline salt (i.e. sodium tripolyphosphate) was used instead of nAp¹⁵. However, it is more interesting to notice from the current study that the acidic degradation products derived from PLGA-based scaffolds can also be neutralized by nAp particles, which represent weak alkaline components that are well known for their similarity to the inorganic phase in bone matrix, and capability to support osteoblast-like cell proliferation and differentiation¹⁹.

It has been confirmed in this study that the nAp incorporation improves the host tissue response to PLGA-based nanofibrous scaffolds in both virgin and pre-degrade state, by showing significantly less infiltration of macrophages as well as apparent less FBGCs formation after 4 weeks of subcutaneous implantation. We attributed this observation to the lower amount of soluble degradation products and their distribution throughout the implant vicinity. Such findings are consistent with previous research, which indicated that the determining factor for the foreign body reaction of degradable implantable materials is the physical presence of particulate degradation products or the transient chemical characteristics of the degrading milieu with the capacity to stimulate inflammatory cells, especially macrophages and giant cells¹¹. In contrast to previous research, which evaluated *in vivo* responses of PLGA up to 5 days after subcutaneous implantation⁶, the current study involved 3-week pre-degraded scaffolds (p-n0 and p-n30) in subcutaneous implantation (4 weeks) to cover the entire degradation period of PLGA-based nanofibers, which is up to 7 weeks (leading to 20% of mass loss) as previously reported²⁸. Those pre-degraded scaffolds (p-n0 and p-n30) showed similar histological response, compared to their corresponding virgin state scaffolds (n0 and n30, respectively), indicating that the inflammatory reaction caused by the degradation products existed during the entire material degradation period.

The current study further analyzed the effect of nAp incorporation on *in vivo* cytokine expression profiles in order to explore the molecular mechanism related to the histological results. Despite differences in the histological observations, similar cytokine expression (gene and protein level) was observed for all four experimental groups, albeit that marginal differences were observed at gene level for TNF- α and TGF- β , and for GRO-KC at protein level after 1 week of implantation. The probable reason for this observation is that the 'normal' foreign body reaction resulting from the empty cage already induces a basal level of inflammation, which concealed partial effect of the samples in the cages to the surrounding tissues in terms of cytokine expression²⁹. Nevertheless, the histological observations from direct implantation system, which avoid masking effects of responses to the cages, demonstrate the resultant effect of nAp incorporation on improved tissue responses.

In this study, we have shown that by incorporating nAp into the PLGA-based scaffolds, polymer degradation can be slowed down, and that the inflammatory reaction initiated by the acidic degradation products could also be effectively reduced *in vivo*. PLGA has long been widely used to develop different types of medical devices (e.g. scaffolds, drug carriers, wound healing materials, etc.). To avoid future adverse inflammatory reactions upon biomedical application of PLGA-based devices, of the incorporation of a weak alkaline salt such as nAp, instead of previously reported strong alkaline salt¹⁵, appears sufficiently effective to diminish potential *in vivo* adverse tissue reaction to PLGA and its degradation products. Furthermore, different from alternative bulk hydroxyapatite, which shows slow *in vivo* degradation³⁰, the nAp particles undergo a relative fast dissolution because of the nanoscale particle size and increased interfacial surface area³¹. The dissolution of nAp does not generate any toxic chemicals apart from Ca²⁺ and PO₄³⁻, which are naturally found in hard tissues as well as in blood³¹. In consequence, the usage of nAp particles presents one of the most viable options to improve the tissue response of PLGA-based devices from the safety issue point of view.

5. Conclusions

The results of the current study show that the incorporation of nAp can slow down the degradation of PLGA-based materials in an nAp amount-dependent manner. In view of biocompatibility of PLGA-based materials, the current study showed that nAp incorporation significantly improves the tissue response during 4-week of subcutaneous implantation, by showing less infiltration of inflammatory cells as well as less FBGCs formation surrounding the scaffolds. However, no effects of nAp-incorporation on cytokine expression were observed.

6. References

1. Ji, W.; Sun, Y.; Yang, F.; van den Beucken, J.; Fan, M. W.; Chen, Z.; Jansen, J. A. *Pharm Res* **2011**, *28*, 1259-1272.
2. Jayaraman, K.; Kotaki, M.; Zhang, Y.; Mo, X.; Ramakrishna, S. *J Nanosci Nanotechnol* **2004**, *4*, 52-65.
3. Chen, D. W.; Liao, J. Y.; Liu, S. J.; Chan, E. C. *Int J Nanomedicine* **2012**, *7*, 763-771.
4. Prabhakaran, M. P.; Kai, D.; Ghasemi-Mobarakeh, L.; Ramakrishna, S. *Biomed Mater* **2011**, *6*, 055001.
5. Gentile, P.; Chiono, V.; Tonda-Turo, C.; Ferreira, A. M.; Ciardelli, G. *Biotechnol J* **2011**, *6*, 1187-1197.
6. Yoon, S. J.; Kim, S. H.; Ha, H. J.; Ko, Y. K.; So, J. W.; Kim, M. S.; Yang, Y. I.; Khang, G.; Rhee, J. M.; Lee, H. B. *Tissue Eng Part A* **2008**, *14*, 539-547.
7. Lendlein, A.; Langer, R. *Science* **2002**, *296*, 1673-1676.
8. Bostman, O.; Pihlajamaki, H. *Biomaterials* **2000**, *21*, 2615-2621.
9. Anderson, J. M.; McNally, A. K. *Semin Immunopathol* **2011**, *33*, 221-233.
10. Anderson, J. M.; Rodriguez, A.; Chang, D. T. *Semin Immunol* **2008**, *20*, 86-100.
11. Williams, D. F. *Biomaterials* **2008**, *29*, 2941-2953.
12. Anderson, J. M. *Annual Review of Materials Research* **2001**, *31*, 81-110.
13. Kao, W. J. *Biomaterials* **1999**, *20*, 2213-2221.
14. Liu, H.; Slamovich, E. B.; Webster, T. J. *Int J Nanomedicine* **2006**, *1*, 541-545.
15. Xie, S.; Zhu, Q.; Wang, B.; Gu, H.; Liu, W.; Cui, L.; Cen, L.; Cao, Y. *Biomaterials* **2010**, *31*, 5100-5109.
16. Brodbeck, W. G.; Voskerician, G.; Ziats, N. P.; Nakayama, Y.; Matsuda, T.; Anderson, J. M. *J Biomed Mater Res A* **2003**, *64*, 320-329.
17. Li, X.; Su, Y.; Chen, R.; He, C.; Wang, H.; Mo, X. *J Appl Polym Sci* **2009**, *111*, 1564-1570.
18. Zong, X.; Ran, S.; Kim, K. S.; Fang, D.; Hsiao, B. S.; Chu, B. *Biomacromolecules* **2003**, *4*, 416-423.
19. Yang, F.; Both, S. K.; Yang, X.; Walboomers, X. F.; Jansen, J. A. *Acta Biomater* **2009**, *5*, 3295-3304.
20. van den Beucken, J. J.; Walboomers, X. F.; Vos, M. R.; Sommerdijk, N. A.; Nolte, R. J.; Jansen, J. A. *J Biomed Mater Res A* **2006**, *77*, 202-211.
21. Link, D. P.; van den Dolder, J.; van den Beucken, J. J.; Cuijpers, V. M.; Wolke, J. G.; Mikos, A. G.; Jansen, J. A. *J Biomed Mater Res A* **2008**, *87*, 760-769.
22. Lamers, E.; Walboomers, X. F.; Domanski, M.; te Riet, J.; van Delft, F. C.; Luttge, R.; Winnubst, L. A.; Gardeniers, H. J.; Jansen, J. A. *Biomaterials* **2010**, *31*, 3307-3316.
23. Prodanov, L.; te Riet, J.; Lamers, E.; Domanski, M.; Luttge, R.; van Loon, J. J.; Jansen, J. A.; Walboomers, X. F. *Biomaterials* **2010**, *31*, 7758-7765.
24. Development Core Team, R.; R: A language and environment for statistical computing. . In R Foundation for Statistical Computing: Vienna, Austria., 2011.
25. Yang, P.; Quan, Z.; Li, C.; Kang, X.; Lian, H.; Lin, J. *Biomaterials* **2008**, *29*, 4341-4347.
26. Ślósarczyka, A.; Paszkiewicz, Z.; Paluszkiwicz, C. *J Mol Struct* **2005**, *744*, 657-661.

27. Hakkarainen, M., Aliphatic Polyesters: Abiotic and Biotic Degradation and Degradation Products. In *Advances in Polymer Science*, Springer-Verlag: Berlin Heidelberg, 2000; Vol. 157, pp 113-138.
28. Dong, Y.; Liao, S.; Ngiam, M.; Chan, C. K.; Ramakrishna, S. *Tissue Eng Part B Rev* **2009**, 15, 333-351.
29. Schutte, R. J.; Xie, L.; Klitzman, B.; Reichert, W. M. *Biomaterials* **2009**, 30, 160-168.
30. Habraken, W. J.; Liao, H. B.; Zhang, Z.; Wolke, J. G.; Grijpma, D. W.; Mikos, A. G.; Feijen, J.; Jansen, J. A. *Acta Biomater* **2010**, 6, 2200-2211.
31. Uskokovic, V.; Uskokovic, D. P. *J Biomed Mater Res B Appl Biomater* **2011**, 96, 152-191.



**Summary, closing remarks and
future perspectives**

**Samenvatting, slotwoord en
toekomstperspectieven**

结语及展望

Summary and address to the aims

Bone tissue engineering presents a potential alternative strategy to repair large bony defects, particularly large bone gaps and composite defects in the craniomaxillofacial region. Conventional bone tissue engineering approaches involve pre-culture of osteoprogenitor cells on a scaffold, followed by implantation of the cell/scaffolds complex into defect site. In this cell-based approach, exogenously delivered osteoprogenitor cells, relying on growth factors secreted by donor tissue, contribute to the bone tissue regeneration process, whereas the scaffolds simply provide physical support for the cells to allow tissue ingrowth. Although so far cell-based approaches represent the ultimate challenge for tissue engineering approaches¹, it is still far from feasible to translate this approach from laboratory to clinical application in the near future from a regulatory and ethical point of view. In consequence, there is an increasing demand to generate bioactive scaffolds that can provide not only physical support for cells, but also a local release of biomolecules (e.g. growth factors, cytokines, etc) to stimulate endogenous tissue regeneration without using exogenously delivered cells.

Recently, electrospinning has emerged as a popular technique to prepare tissue engineering scaffolds due to its relative simplicity regarding the generation of fibrous scaffolds with nano- or submicron-scale dimensions that morphologically resemble the natural extracellular matrix. In addition, electrospinning generates ultrathin fibers with a large specific surface area, which enables an effective incorporation and delivery of biomolecules. These characteristics render electrospinning with superiority in preparation of bioactive scaffolds over other scaffold preparation techniques.

The aim of this thesis was to fabricate bioactive electrospun scaffolds with biomolecule incorporation to achieve optimal bone regeneration. **Chapter 1** gives a general introduction on bone tissue engineering, electrospinning technique, as well as a description of the aims of this thesis. Each following chapter discusses a separated study. This summary addresses the aims as described in the first chapter in successive order.

1. What is the current state of the art in local delivery of biomolecules for bone regeneration?

Chapter 2 highlights recent advances in local delivery of biomolecules from synthetic biomaterials to repair bony defects in craniomaxillofacial (CMF) region in both normal and compromised healing conditions.

There are two major types of biomolecules which are frequently used to the clinical treatment of CMF bone defects based on a molecular weight threshold (5kDa): (i) large biomolecules and (ii) small biomolecules. Large biomolecules include inflammatory cytokines- and chemokines, morphogenetic and angiogenic factors. For instance, stromal cell derived factor-1 alpha (SDF-1 α) is a powerful chemokine involved in cell recruitment in a

variety of tissues; bone morphogenetic proteins (BMP-2,4,7) play important roles in osteogenic differentiations of skeletal cells; vascular endothelial growth factor (VEGF) isoforms are involved in the regulation of the interaction between angiogenesis and osteogenesis. On the other hand, small molecules, including antibiotics, AMPs, antitumor drug, siRNA and shRNA, as well as anti-osteoporotics, are rapidly emerging in recent years as an interesting adjunct for upgrading the clinical treatment of CMF bone regeneration under compromised healing conditions.

Furthermore, **Chapter 2** provides a perspective on the efficacy of biomolecule delivery in CMF bone regeneration by reviewing presently available reports of pre-clinical studies using various animal models, in which calvarial defects, mandibular and alveolar bony defects and sinus elevation are included. Most of the preclinical studies have so far been focused on the morphogenetic molecules and angiogenic molecules delivery, and quite limited research efforts involved delivery of small molecules.

2. What are current available methods to functionalize electrospun scaffolds with biomolecules, and what are pros and cons for different methods?

Within the past five years, electrospun scaffolds have gained an exponentially increasing popularity in tissue regeneration area because of their ultrathin fiber diameter and large surface-volume ratio, which is favorable for biomolecule delivery. **Chapter 3** reviews current techniques that can be used to prepare bioactive electrospun scaffolds, including physical adsorption, blend electrospinning, coaxial electrospinning, and covalent immobilization. In addition, **Chapter 3** analyses the existing challenges (i.e. protein instability, low gene transfection efficiency, and difficulties in accurate kinetics prediction) to achieve biomolecule release from electrospun scaffolds, which necessitate further research to fully exploit the biomedical applications of these bioactive scaffolds.

3. Can electrospun scaffolds be functionalized with SDF-1 α by physical adsorption to achieve cell recruitment?

As described earlier, physical adsorption is the easiest method to functionalize electrospun scaffolds with biomolecules. In **Chapter 4**, we prepared electrospun scaffolds using polymer blends of poly(ϵ -caprolactone) (PCL) and type B-gelatin. Furthermore, we functionalized scaffolds with stromal cell derived factor-1 α (SDF-1 α) via physical adsorption in order to obtain cell recruitment capacity for guided bone regeneration (GBR) applications. The results of **Chapter 4** showed that PCL/gelatin electrospun scaffolds with SDF-1 α adsorption provided a diffusion-controlled SDF-1 α release profile. Furthermore, the scaffolds loaded with different amounts of SDF-1 α (50–400 ng) significantly induced chemotactic migration of BMSCs *in vitro* without dose-dependent effects. Eight weeks after implantation in rat cranial defects, SDF-1 α loaded scaffolds yielded a 6-fold increase in the amount of bone formation compared to the bare membranes, albeit that contribu-

tion of *in vivo* BMSCs recruitment to the bone regeneration could not be ascertained. In conclusion, the results of **Chapter 4** indicate the potential for using SDF-1 α loaded PCL/gelatin electrospun scaffolds as a bioactive GBR membrane, which is beneficial for optimizing clinical application of GBR strategies.

4. What is the superior method to generate bioactive electrospun scaffolds with sustained release of biomolecules, in respect of spinnability, release profiles, and bioactivity preservation?

Although physical adsorption is the easiest method to load biomolecules, this approach provides a large burst release, which might be a disadvantage for those biomolecules demanding a long-term biological effect. In view of this, it was necessary to figure out an optimal method to fabricate electrospun scaffolds with sustained release of biomolecules. So far, blend electrospinning and coaxial electrospinning represent two main alternatives to fabricate electrospun scaffolds with a sustained release profile. The aim of **Chapter 5** was to compare both techniques with respect to processing set-up, scaffold characteristics, release kinetics, and biological activity of the loaded protein. Bovine serum albumin was used as a model protein to determine release profiles, while alkaline phosphatase was used to determine protein activity after the electrospinning process. Coaxial electrospinning resulted in uniform fiber morphology with a core-shell structure, and a homogeneous protein distribution throughout the core of the fibers. In contrast, blend electrospinning formed bead-like fibers with a heterogeneous protein distribution in the fibers. The coaxial scaffold exhibited more sustained release profiles than the comparative blend scaffold, and the additive poly (ethylene glycol) (PEG) in the coaxial scaffold accelerated protein release. Both electrospinning processes decreased the biological activity of the incorporated protein, but coaxial electrospinning with PEG as an additive showed up to 75% preservation of the initial biological activity. Consequently, **Chapter 5** concluded that coaxial electrospinning was superior compared to blend electrospinning for the preparation of nanofibrous scaffolds with a uniform fibrous structure, protein distribution and sustained protein release kinetics as well as high preservation of the protein activity.

5. What is the application potential for coaxial electrospun nanofibrous scaffolds with growth factor release?

In **Chapter 6**, we fabricated nanofibrous scaffolds based on blends of a hydroxyl functionalized polyester poly(hydroxymethylglycolide-co- ϵ -caprolactone) (pHMGCL) and poly(ϵ -caprolactone) (PCL), loaded with bovine serum albumin (BSA) as a protein stabilizer and vascular endothelial growth factor (VEGF) as a potent angiogenic factor by means of a coaxial electrospinning technique. The scaffolds were characterized by scanning electron microscopy (SEM), fluorescence microscopy (FM), and differential scanning calorimetry

(DSC). The scaffolds displayed a uniform fibrous structure with a fiber diameter around 700 nm. The release of BSA from the core of the fibers was studied by high performance liquid chromatography (HPLC) and it was shown that the coaxial scaffolds composed of blends of pHMGCCL and PCL exhibited faster release than the comparative PCL scaffolds. VEGF was incorporated in the core of the scaffolds and the effect of the released protein on the attachment and proliferation of endothelial cells was investigated. It was shown that the incorporated protein preserved its biological activity and resulted in initial higher numbers of adhered cells. Thus, **Chapter 6** indicated that coaxially electrospun scaffolds based on blends of pHMGCCL/PCL loaded with VEGF can be considered as a promising candidate for tissue engineering applications.

6. What are biocompatibility and degradation characteristics of PLGA-based nanofibrous electrospun scaffolds?

Regarding polymers used for electrospinning, poly(lactide-co-glycolide) (PLGA) is one of the most preferred ones and already approved by the Food and Drug Administration (FDA) as a constituent of many biomaterial-based devices owing to its adjustable biodegradability and biocompatibility. However, increasing concerns exist regarding biocompatibility issues related to PLGA degradation products after implantation. The aim of **Chapter 7** was to evaluate the effect of nano-apatitic particles (nAp) incorporation on the degradation characteristics and biocompatibility of PLGA-based nanofibrous scaffolds. Composite PLGA/PCL blended (w/w=3/1) polymeric electrospun scaffolds with 0–30 wt% of nAp incorporation (n0–30) were prepared. The obtained scaffolds were firstly evaluated by morphological, physical and chemical characterization, followed by an *in vitro* degradation study. Further, n0 and n30 in both virgin and 3-week pre-degraded status were subcutaneously implanted in rats, either directly or in stainless steel mesh cages, to evaluate *in vivo* tissue response. The results showed that the incorporation of nAp yields a nAp amount-dependent buffering effect on pH-levels during degradation and delayed polymer degradation based on molecular weight analysis. Regarding biocompatibility, nAp incorporation significantly improved the tissue response during a 4-week subcutaneous implantation period, showing both less infiltration of inflammatory cells (monocyte/macrophages) and less foreign body giant cells (FBGCs) formation surrounding the scaffolds. Similar cytokine expression (gene and protein level) was observed for all groups of implanted scaffolds, although marginal differences were found for TNF- α and TGF- β at gene level as well as GRO-KC at protein level after 1 week of implantation. In conclusion, the results of **Chapter 7** indicated that hybridization of the weak alkaline salt nAp in PLGA-based electrospun scaffolds is effective to decrease the *in vivo* adverse tissue response to PLGA materials, which is beneficial for optimizing final clinical application of different PLGA-based biomedical devices.

Closing remarks and future perspectives

Since the first patent on electrospinning process was filed in 1934², electrospinning has been fully developed and widely used in filtration and texture manufacturing industry. However, outside those types of industry, there was little interest in electrospinning or electrospun nanofiber until the mid-1990s³. In recent years, electrospinning has emerged as a cost-effective technique to generate porous scaffolds with a biomimetic characteristic due to the fibers that have similarity in geometry to fibrous components in the extracellular matrix (ECM). Currently, most of the research still stays within laboratory level and quite far away from large-scale application. The current naïve situation of translating bioactive electrospun scaffolds into clinical application might be mainly attributed by challenges arising from two aspects: (1) *in vitro* release kinetics detection, and (2) *in vivo* dosing prediction.

In previous studies, the *in vitro* release kinetics was investigated based on different methods, including radioiodination, HPLC and enzyme-linked immunosorbent assay (ELISA). In this thesis, we explored two methods to detect *in vitro* biomolecules release profile based on different loading approach. In **Chapter 4**, we used ¹²⁵I radioiodination method to detect the release of SDF-1 α which was physically adsorbed on the electrospun scaffolds. In contrast, in **Chapter 5&6**, since the protein was incorporated inside the core-shell structure fibers and it is not applicable to involve radioiodinated protein during electrospinning due to local safety regulatory issues, HPLC was applied to detect *in vitro* release kinetics of BSA, which was used as a model protein to generally predict release profile for other loaded growth factors⁴⁻⁸. In addition to radioiodination and HPLC, ELISA is another frequently used method to detect *in vitro* release of therapeutic proteins, such as fibroblast growth factor (FGF)⁹ and bone morphogenetic protein-2 (BMP-2)¹⁰.

Among the different detection methods, radioiodination and ELISA are most frequently used to detect the release kinetics of therapeutic proteinaceous molecules. However, there is emerging concern about the reliability of ELISA to detect growth factor release. Piskounova et al reported that after 4 weeks of measurement, roughly 80% of BMP-2 was released based on radioiodination¹¹, whereas less than 12% of BMP-2 was measured from the same samples using ELISA method¹². Such obvious deviation might be attributed to the weak points of ELISA-based methods. In principle, ELISA only recognizes the “sound protein” with specific epitope to which antibodies can bind, and such epitope is apparently fragile to physical and chemical environments of delivery system¹³. In addition, protein loss during sampling and dilution, as well as low affinity towards protein aggregates may also contribute to the under estimation of total release. In consequence, the accurate detection of growth factor release is a big challenge for current biomolecules delivery, and there is great necessity to optimize the current physical/chemical

detection methods to comprehensively understand the release behavior of loaded growth factors.

As aforementioned, radioiodination is the most reliable method to detect the release profile of proteinaceous molecules, because it recognizes the radionuclides of iodine that are directly conjugated with target molecule, and the radioactivity is positively related to the total mass of the loaded biomolecules. However, some inherent practical concerns hinder the general use of this method. Firstly, since tyrosines are the sites of radioiodination¹⁴, it would be rather challenging to label the proteins and peptides containing few or no tyrosines as sites for iodination. Secondly, some molecules are inactivated when their tyrosines are iodinated. For instance, iodination of tyrosine residue A19 or B16 leads to the inactivation of insulin¹⁵. In view of this, there is a great necessity to improve the design of labelling technique structure-reactivity relationships, and such improvement will be beneficial for the comprehensive understanding and wide application of radioiodination method.

Another important issue for clinical application of biomolecules loaded electrospun scaffolds is to predict an optimal dosing for *in vivo* application, which is not only of scientific interest, but a pre-requisite for an efficient improvement of the safety of the pharmaceutical and therapeutic treatments. The prediction of *in vivo* optimal dosing is strongly dependent on quantification of (1) the *in vivo* release kinetics and (2) the biological activity of loaded protein. Unfortunately, limited information is available so far regarding the *in vivo* release. Several previous studies investigated the *in vivo* growth factor release profile by using carrier free protein for radioiodination in order to achieve a specific radiolabeling^{16,17}. However, most of commercially available growth factors for clinical application are mixed with multiple kinds of additives to improve the stability and shelf-life, which yield an open question to determine whether these additives which potentially affect the delivery system (e.g. osmotic pressure, pH, etc.) will alter the *in vivo* release profile. On the other hand, biomolecules, particularly the therapeutic proteins, have a complex conformational structure and are fragile to the surrounding physical/chemical environment (e.g., pH, humidity, etc) during sample preparation, processing and storage processes. Therefore, the biological activity of proteinaceous biomolecules can be affected by any conformation changes and aggregations, which will influence the effective dosing when they are applied *in vivo*. Consequently, further *in vivo* studies are needed to investigate the influence of protein conformational changes and aggregation on the biological activity.

In summary, bioactive electrospun scaffolds with biomolecules incorporation present a promising acellular approach for tissue regeneration. On one hand, the flexibility of obtained electrospun scaffolds render them feasible for many applications which includes GBR membranes as addressed in this thesis, as well as potential scaffolds for interface

tissue regeneration such as periosteum, ligament, and joint tissue. On the other hand, the high surface-volume ratio owing to the ultrathin fiber diameter enables electrospun scaffolds as an effective carrier to load various kinds of biomolecules via different methods to synchronize tissue regeneration process. In order to translate such a promising approach from bench to bed, extensive research efforts are needed to achieve (1) a controlled release kinetics and (2) optimal *in vivo* dosing.

References

1. Robey, P. G. *Tissue Eng Part B Rev* **2011**, *17*, 423-430.
2. Dzenis, Y. *Science* **2004**, *304*, 1917-1919.
3. Reneker, D.; Chun, I. *Nanotechnology* **1996**, *7*, 216-223.
4. Jiang, H. L.; Hu, Y. Q.; Zhao, P. C.; Li, Y.; Zhu, K. J. *J Biomed Mater Res B Appl Biomater* **2006**, *79*, 50-57.
5. Liao, I. C.; Chew, S. Y.; Leong, K. W. *Nanomedicine* **2006**, *1*, 465-471.
6. Yang, Y.; Li, X.; Cui, W.; Zhou, S.; Tan, R.; Wang, C. *J Biomed Mater Res A* **2008**, *86*, 374-385.
7. Zeng, J.; Aigner, A.; Czubayko, F.; Kissel, T.; Wendorff, J. H.; Greiner, A. *Biomacromolecules* **2005**, *6*, 1484-1488.
8. Kowalczyk, T.; Nowicka, A.; Elbaum, D.; Kowalewski, T. A. *Biomacromolecules* **2008**, *9*, 2087-2090.
9. Sahoo, S.; Ang, L. T.; Goh, J. C. H.; Toh, S. L. *J Biomed Mater Res A* **2010**, *93*, 1539-1550.
10. Srouji, S.; Ben-David, D.; Lotan, R.; Livne, E.; Avrahami, R.; Zussman, E. *Tissue Eng Part A* **2011**, *17*, 269-277.
11. Piskounova, S.; Gedda, L.; Hulsart-Billstrom, G.; Hilborn, J.; Bowden, T. *J Tissue Eng Regen Med* **2012**. doi: 10.1002/term.1584.
12. Bergman, K.; Engstrand, T.; Hilborn, J.; Ossipov, D.; Piskounova, S.; Bowden, T. *J Biomed Mater Res A* **2009**, *91*, 1111-1118.
13. Luca, L.; Capelle, M. A.; Machaidze, G.; Arvinte, T.; Jordan, O.; Gurny, R. *Int J Pharm* **391**, 48-54.
14. Coene, H.; Mertens, J.; Mazière, B., In *Radioiodination reactions for pharmaceutical: compendium for effective sythesis strategies*, Springer: Dordrecht, 2006.
15. Garratt, C. J.; Harrison, D. M.; Wicks, M. *Biochem J* **1972**, *126*, 123-131.
16. van der Zande, M.; Walboomers, X. F.; Olalde, B.; Jurado, M. J.; Alava, J. I.; Boerman, O. C.; Jansen, J. A. *J Tissue Eng Regen Med* **2011**, *5*, 476-482.
17. Bodde, E. W.; Boerman, O. C.; Russel, F. G.; Mikos, A. G.; Spauwen, P. H.; Jansen, J. A. *J Biomed Mater Res A* **2008**, *87*, 780-791.

**Samenvatting, slotopmerkingen en
toekomstperspectieven**

Samenvatting en evaluatie van de doelstellingen

Bot tissue engineering is een potentieel alternatieve strategie om grote botdefecten, met name grote bot lacunes en composiet gebreken, in de craniomaxillofacial regio te herstellen. De conventionele bot tissue engineering aanpak omvat *in vitro* kweek van osteoprogenitorcellen op een dragermateriaal, gevolgd door implantatie van een cel/scaffold construct in een defect. Deze cel-gebaseerde benadering met exogeen aangeleverde osteoprogenitorcellen gaat uit van effecten van groeifactoren, gesecreteerd door donorweefsel, welke bijdragen aan het botregeneratieproces, waarbij de dragermaterialen eenvoudige fysieke dragers zijn voor de cellen om weefselingroei mogelijk te maken. Hoewel tot nu toe cel-gebaseerde benaderingen de ultieme uitdaging voor tissue engineering vertegenwoordigen¹, is het nog verre van haalbaar, vooral vanuit een regelgevend en ethisch oogpunt, om deze aanpak te vertalen van laboratorium naar klinische toepassing in de nabije toekomst. Bijgevolg is er een toenemende vraag naar biologisch actieve dragermaterialen, die niet alleen als fysieke drager voor cellen kunnen fungeren, maar ook een lokale afgifte van biomoleculen (bijvoorbeeld groeifactoren, cytokines, enz.) bewerkstelligen om endogene weefselregeneratie te stimuleren zonder exogeen aangeleverde cellen.

Onlangs heeft electrospinning zich ontpopt als een populaire techniek om tissue engineering scaffolds te maken vanwege de relatieve eenvoud met betrekking tot de generatie van vezelige materialen met nano-of submicron-schaal dimensies, die morfologisch lijken op de natuurlijke extracellulaire matrix. Bovendien genereert electrospinning ultradunne vezels met een groot specifiek oppervlak, dat een effectieve opname en afgifte van biomoleculen mogelijk maakt. Deze kenmerken zorgen ervoor dat electrospinning superioriteit heeft voor het maken van bioactieve scaffolds ten opzichte van andere scaffold preparatie-technieken.

Het doel van dit proefschrift was om bioactieve elektrogeweven scaffolds te fabriceren met biomoleculen incorporatie om een optimale botregeneratie te bereiken. **Hoofdstuk 1** geeft een algemene inleiding op bot tissue engineering, electrospinning, alsmede een beschrijving van de doelstellingen van dit proefschrift. Elke volgende hoofdstuk bespreekt een aparte studie, waarvan hieronder de doelstellingen en resultaten samengevat zijn.

1. Wat is de huidige stand van de techniek voor de lokale afgifte van biomoleculen voor botregeneratie?

Hoofdstuk 2 belicht recente ontwikkelingen in de lokale afgifte van biomoleculen van synthetische biomaterialen om botdefecten in het craniomaxillofaciale (CMF) gebied in zowel normale en gecompromitteerde omstandigheden te herstellen.

Er zijn twee belangrijke klassen van biomoleculen die vaak worden gebruikt voor de

klinische behandeling van CMF botdefecten, gebaseerd op molecuulgewicht (drempelwaarde 5 kDa): (i) grote biomoleculen en (ii) kleine biomoleculen. Grote biomoleculen omvatten inflammatoire cyto- en chemokines, morfogenetische en angiogene factoren. Zo is stromal-derived factor-1 alpha (SDF-1 α) een krachtig chemokine betrokken bij cel rekrutering in verschillende weefsels, spelen botmorfogenetische eiwitten (BMP-2, 4, 7) een belangrijke rol in de osteogene differentiatie van skeletcellen en zijn vasculaire endotheliale groeifactor (VEGF) isovormen betrokken bij de regulering van de interactie tussen angiogenese en osteogenesis. Anderzijds worden kleine moleculen, zoals antibiotica, AMPs, antitumor drug, siRNA en shRNA, evenals anti-osteoporotics, de laatste jaren meer en meer gezien als een snel groeiend hulpmiddel voor het verbeteren van de klinische behandeling van CMF botregeneratie onder gecompromitteerde genezingsomstandigheden.

Bovendien geeft **Hoofdstuk 2** een kijk op de werkzaamheid van afgegeven biomoleculen in CMF botregeneratie door de herziening van op dit moment beschikbare literatuur van pre-klinische studies met behulp van verschillende diermodellen, waarbij calvariale, mandibulaire en alveolaire botdefecten en sinushoogte werden inbegrepen. De meeste pre-klinisch onderzoeken tot nu toe waren gericht op de afgifte van morfogenetische moleculen en angiogene moleculen en een slechts beperkte hoeveelheid onderzoeksinstellingen richtte zich op afgifte van kleine moleculen.

2. Wat zijn de huidige beschikbare methoden om elektrospun scaffolds te functionaliseren met biomoleculen, en wat zijn voor- en nadelen voor de verschillende methoden?

In de afgelopen vijf jaar hebben electrospun scaffolds een exponentieel toenemende populariteit gekregen in het gebied van weefselregeneratie vanwege hun ultradunne vezeldiameter en grote oppervlakte/volume verhouding, hetgeen gunstig is voor biomoleculair afgifte. **Hoofdstuk 3** bespreekt huidige technieken, die kunnen worden gebruikt om bioactieve electrospun scaffolds te verkrijgen, waaronder fysische adsorptie, blend electrospinning, coaxiale electrospinning en covalente immobilisatie. Daarnaast worden in **Hoofdstuk 3** de bestaande uitdagingen (d.w.z. eiwit instabiliteit, lage-gen transfectie-efficiëntie, en moeilijkheden in nauwkeurige kinetiek voorspelling) geanalyseerd om biomoleculair afgifte te bereiken van elektrospun scaffolds, waarvoor verder onderzoek noodzakelijk is om biomedische toepassingen van deze bioactieve steigers volledig te kunnen benutten.

3. Kunnen elektrospun scaffolds worden gefunctionaliseerd met SDF-1 α door fysieke adsorptie en celrekrutering bewerkstelligen?

Zoals eerder beschreven, is fysische adsorptie de meest eenvoudige manier om elektrospun scaffolds te functionaliseren met biomoleculen. In **hoofdstuk 4** hebben we elektrospun scaffolds gemaakt met behulp van mengsels van polymeren van poly(ϵ -caprolacton)

(PCL) en type B-gelatine. Verder hebben we gefunctionaliseerde scaffolds gemaakt met SDF-1 α via fysische adsorptie om celrecruterende capaciteit voor guided bone regeneration (GBR) toepassingen te verkrijgen. De resultaten van **hoofdstuk 4** tonen dat PCL/gelatine electrospun scaffolds met SDF-1 α adsorptie een diffusie-gecontroleerd SDF-1 α afgifteprofiel hebben. Bovendien werden verschillende hoeveelheden SDF-1 α (50-400 ng) gebruikt, welke allen aanzienlijke chemotactische migratie van BMSCs *in vitro* induceerden zonder dosisafhankelijke effecten. Acht weken na implantatie in craniale defecten in ratten, lieten SDF-1 α loaded scaffolds een 6-voudige toename zien in de hoeveelheid botvorming ten opzichte van de kale scaffolds, zij het dat bijdrage van *in vivo* gerekruteerde BMSCs aan botregeneratie niet kon worden vastgesteld. Kortom, de resultaten van **Hoofdstuk 4** tonen duidelijk het potentieel van SDF-1 α geladen PCL/gelatine electrospun scaffolds als bioactieve GBR membraan, hetgeen gunstig is voor het optimaliseren van klinische toepassingen van GBR strategieën.

4. Wat is de beste methode om bioactieve electrospun scaffolds te genereren met gereguleerde afgifte van biomoleculen t.a.v. spinbaarheid, afgifteprofielen en behoud van bioactiviteit?

Hoewel fysieke adsorptie de meest eenvoudige manier is om biomoleculen te laden, biedt deze aanpak een grote burst release, hetgeen een nadeel kan zijn voor deze biomoleculen, welke een lange-termijn biologisch effect dienen te realiseren. Daarom was het noodzakelijk om een optimale methode te zoeken voor het maken van electrospun scaffolds met gereguleerde afgifte van biomoleculen. Tot nu toe vertegenwoordigen mix electrospinning en coaxiale electrospinning twee belangrijke alternatieven voor het maken van electrospun scaffolds met een vertraagd afgifte profiel. In **Hoofdstuk 5** had als doel om beide technieken te vergelijken met betrekking tot verwerking, afgiftekinetiek en biologische activiteit van het biomolecuul. Albumine werd gebruikt als een model-eiwit om afgifteprofielen te bepalen, terwijl alkalische fosfatase werd gebruikt om eiwit activiteit te bepalen na het elektrospinproces. Coaxiale electrospinning resulteerde in een uniforme vezelmorfologie met een kern-mantel structuur en een homogene eiwitverdeling in de kern van de vezels. Anderzijds werden via mix electrospinning 'druppelvormige' vezels gevormd met een heterogene eiwitverdeling in de vezels. De coaxiale scaffolds vertoonden een meer constant afgifteprofiel dan de mix scaffolds en het additief poly(ethyleenglycol) (PEG) in de coaxiale scaffolds versnelde de eiwit afgifte. Beide electrospinningprocessen verlaagden de biologische activiteit van het opgenomen eiwit, maar coaxiale electrospinning met PEG als additief resulteerde in 75% behoud van de oorspronkelijke biologische activiteit. Bijgevolg werd uit **hoofdstuk 5** geconcludeerd dat coaxiale electrospinning superieur is aan mix electrospinning t.a.v. de bereiding van nanofiber scaffolds met een uniforme vezelstructuur, homogene eiwitverdeling, constante eiwit afgiftekinetiek en hoog behoud van de eiwitactiviteit.

5. Wat zijn de toepassingsmogelijkheden voor coaxiale elektrospun nanofiber scaffolds met groeifactor release?

In **hoofdstuk 6** werden nanofibrous scaffolds vervaardigd gebaseerd op mengsels van een hydroxyl gefunctionaliseerde polyester poly(hydroxymethylglycolide-co- ϵ -caprolacton) (pHMGCL) en poly(ϵ -caprolacton) (PCL), geladen met bovine serum albumine (BSA) als proteïnestabilisator en vascular endothelial groeifactor (VEGF) als een krachtige angiogene factor door middel van coaxiale electrospinning. De scaffolds werden gekarakteriseerd middels scanning elektronenmicroscopie (SEM), fluorescentiemicroscopie (FM) en differentiële scanning calorimetrie (DSC). De scaffolds vertoonden een uniforme vezelstructuur met een vezeldiameter van ~ 700 nm. De afgifte van BSA uit de kern van de vezels werd bestudeerd via high-performance vloeistofchromatografie (HPLC) en er werd aangetoond dat de coaxiale scaffolds bestaande uit mengsels van PCL en pHMGCL snellere afgifte realiseerden dan vergelijkbare PCL scaffolds. VEGF was opgenomen in de kern van de scaffolds en het effect van het vrijgekomen eiwit op de hechting en proliferatie van endotheelcellen werd onderzocht. Er werd aangetoond dat het opgenomen eiwit zijn biologische activiteit behoudt en dat afgifte resulteert in grotere aantallen hechtende cellen en meer celgroei. Aldus gaf **hoofdstuk 6** aan dat coaxiale elektrospun scaffolds gebaseerd op mengsels van pHMGCL/PCL en geladen met VEGF kunnen worden gezien als een veelbelovende kandidaat voor tissue engineering toepassingen.

6. Wat zijn biocompatibiliteit en degradatie karakteristieken van PLGA-gebaseerde nanofiber elektrospun scaffolds?

Binnen de polymeren die voor electrospinning gebruikt worden, is poly(lactide-co-glycolide acid) (PLGA) een van de meest geprefereerde, te meer vanwege reeds door de Food and Drug Administration (FDA) goedgekeurde devices met PLGA als bestanddeel en door de variabele biologische afbreekbaarheid en biocompatibiliteit. Echter, een toenemende bezorgdheid bestaat omtrent biocompatibiliteit kwesties in verband met PLGA afbraakproducten na implantatie. Het doel van **hoofdstuk 7** was om het effect van apatiet nano-deeltjes (nAP) incorporatie te evalueren op de degradatie en biocompatibiliteit van PLGA-gebaseerde nanofiber scaffolds. Composiet PLGA/PCL (w/w = 3/1) elektrospun scaffolds met 0-30 % nAP (n0-30) werden bereid. De verkregen scaffolds werden eerst beoordeeld via morfologische, fysische en chemische karakterisering, gevolgd door een *in vitro* degradatiestudie. Verder werden n0 en n30 in zowel nieuwe als 3-week pre-aangetaste toestand subcutaan geïmplantieerd in ratten, hetzij rechtstreeks, hetzij in roestvrijstalen gaas kooien, om de *in vivo* weefselreactie te evalueren. De resultaten toonden dat de opname van nAP een hoeveelheid-afhankelijk bufferend effect op zowel de pH-niveaus tijdens degradatie als een vertraagde polymeerafbraak gebaseerd op moleculaire gewicht bewerkstelligde. Met betrekking tot de biocompatibiliteit, verbeterde

nAP incorporatie aanzienlijk de weefselreactie tijdens een 4-weekse subcutane implantatie periode, met minder infiltratie van inflammatoire cellen (monocyten/macrofagen) en minder vreemd lichaam reuzencellen (FBGC's) formatie rond de scaffolds. Een vergelijkbare cytokine expressie (gen en eiwitniveau) werd waargenomen voor alle groepen geïmplanteerde scaffolds, hoewel marginale verschillen werden gevonden voor TNF- α en TGF- β op genniveau en GRO-KC op eiwitniveau na 1 week implantatie. Concluderend werd gesteld dat de resultaten van **hoofdstuk 7** aangegeven dat hybridisatie van het alkalische zout nAP in PLGA-gebaseerde electrospun scaffolds effectief is om de *in vivo* nadelige weefselreactie op PLGA materialen te verminderen, wat gunstig is voor het optimaliseren van klinische toepassingen voor verschillende PLGA-gebaseerde biomedische devices.

Slotopmerkingen en toekomstperspectief

Sinds het eerste patent op het elektrospinningproces werd ingediend in 1934², is electrospinning volledig ontwikkeld en op grote schaal gebruikt in de filtratie en textuur industrie. Echter, afgezien van die soorten van industrie, was er weinig belangstelling voor electrospinning of electrospun nanovezels tot het midden van de 90-er jaren³. In de afgelopen jaren is gebleken dat electrospinning een kosteneffectieve techniek is om poreuze scaffolds te genereren met biomimetische kenmerken veroorzaakt door de vezels die overeenstemmen qua geometrie met vezelige componenten in de extracellulaire matrix (ECM) van weefsel. Momenteel bevindt het onderzoek zich nog steeds grotendeels op laboratorium niveau en derhalve vrij ver van grootschalige toepassing. De huidige situatie t.a.v. het vertalen van bioactieve electrospun scaffolds naar klinische toepassingen kan vooral worden toegeschreven aan de uitdagingen die voortvloeien uit twee aspecten: (1) *in vitro* vrijgavekinetiek detectie, en (2) *in vivo* dosering voorspellingen.

In voorgaande studies werd de *in vitro* afgiftekinetiek onderzocht op basis van verschillende methoden, zoals radioiodinatie, HPLC en enzyme-linked immunosorbent assays (ELISA). In dit proefschrift onderzochten we twee methodes om *in vitro* een biomoleculen afgifteprofiel te bestuderen op basis van een verschillende aanpak. In **hoofdstuk 4** hebben we gebruik gemaakt ¹²⁵I radioiodinatie om de release van fysisch-geadsorbeerde SDF-1 α aan de electrospun scaffolds te bestuderen. Daarentegen werd in **hoofdstukken 5 en 6**, omdat het eiwit is opgenomen in de kern-mantelstructuur van de vezels en deze opzet niet geschikt is voor radioactief geïodeerde eiwitten wegens lokale veiligheid regelgevingskwesaties, HPLC toegepast voor detectie van *in vitro* afgiftekinetiek van BSA, welk werd gebruikt als model eiwit⁴⁻⁸. Naast radioiodinatie en HPLC, is ELISA een veelgebruikte methode voor het bestuderen van *in vitro* afgifte van eiwitten, zoals fibroblast groeifactor (FGF)⁹ en bot morfogenetische proteïne-2 (BMP-2)¹⁰.

Binnen de verschillende detectiemethoden worden radioiodinatie en ELISA het meest gebruikt om de afgiftekinetiek van therapeutische eiwitachtige moleculen te detecteren.

Er is echter bezorgdheid ontstaan over de betrouwbaarheid van ELISA voor de detectie van groeifactor afgifte. Piskounova et al. melden dat na 4 weken gemeten, ongeveer 80% van BMP-2 werd afgegeven op basis radioiodinatie¹¹, terwijl minder dan 12% BMP-2 afgifte werd gemeten van dezelfde monsters met ELISA¹². Zulke duidelijke afwijkingen kunnen worden toegeschreven aan de zwakke punten van ELISA-gebaseerde methoden. In principe herkent ELISA alleen het specifieke epitoom van een eiwit waaraan antilichamen kunnen binden en dergelijke epitopen zijn blijkbaar kwetsbaar in fysische en chemische omgevingen¹³. Bovendien kan eiwitverlies tijdens bemonstering en verdunning, evenals lage affiniteit voor proteïneaggregaten, ook bijdragen aan de onderschatting van de totale release. Bijgevolg is de nauwkeurige detectie van groeifactor release een grote uitdaging voor de huidige biomoleculen release, en bestaat er een grote noodzaak om de huidige fysieke/chemische detectiemethoden te optimaliseren om volledig het release gedrag van geladen groeifactoren volledig te begrijpen.

Zoals vermeld is radioiodinatie de meest betrouwbare methode om het afgifteprofiel van eiwitachtige moleculen te detecteren, omdat het gebaseerd is op detectie van radionucliden die direct geconjugeerd zijn aan het doelmolecule en de radioactiviteit positief gerelateerd is aan de totale hoeveelheid van de geladen biomoleculen. Sommige inherent-praktische overwegingen belemmeren het algemene gebruik van deze methode. Enerzijds zijn tyrosinen de sites van radioiodinatie¹⁴ en is het derhalve niet mogelijk om eiwitten en peptiden met weinig of geen tyrosines te conjugereren met een radiolabel. Daarnaast worden sommige moleculen geïnactiveerd wanneer hun tyrosines worden geconjugeerd. Een voorbeeld is de jodering van tyrosine residuen A19 of B16, hetgeen leidt tot de inactivering van insuline¹⁵. Hierdoor is er een grote noodzaak om het design van labeling techniek te relateren aan structuur-activiteit en daarmee een verbetering teweeg te brengen voor een diepgaand begrip en brede toepassing van radioiodinatie methodes.

Een ander belangrijk punt voor klinische toepassing van biomolecuul-geladen electrospun scaffolds is te voorspellen wat de optimale dosering is voor *in vivo* toepassingen, hetgeen niet alleen van wetenschappelijk belang, maar ook voorwaarde is voor een efficiënte verbetering van de veiligheid van farmaceutische en therapeutische behandelingen. De voorspelling van *in vivo* optimale dosering is sterk afhankelijk van kwantificering van (1) de *in vivo* afgiftekinetiek en (2) de biologische activiteit van geladen eiwitten. Helaas is slechts beperkte informatie beschikbaar tot nu toe met betrekking tot de *in vivo* afgifte. Verschillende eerdere studies onderzochten *in vivo* groeifactor afgifteprofielen met dragervrij proteïnes voor radioiodinatie om een specifieke radiolabeling te bereiken^{16,17}. Echter, de meeste in de handel verkrijgbare groeifactoren voor klinische toepassing zijn gemengd met verschillende soorten additieven om de stabiliteit en houdbaarheid te waarborgen, waarbij onduidelijkheid bestaat of deze additieven invloed hebben op het afgiftesysteem (bijvoorbeeld osmotische druk, pH, enz.) en dus het *in vivo*

afgifteprofiel. Anderzijds hebben biomoleculen, in het bijzonder de therapeutische eiwitten, een complexe structuur en conformationele kwetsbaarheid t.a.v. de omringende fysisch-chemische omgeving (bijv. pH, vochtigheid, enz.) tijdens de voorbehandeling, verwerking en opslag. Daarom kan de biologische activiteit van eiwitachtige biomoleculen worden aangetast door conformatie-veranderingen en aggregaties, die de effectieve dosering beïnvloeden wanneer ze worden toegepast *in vivo*. Derhalve is het voor verder *in vivo* onderzoek nodig om de invloed van eiwit conformatie-veranderingen en -aggregatie op de biologische activiteit te onderzoeken.

Kortom, bioactieve elektrospun scaffolds met biomolecuul incorporatie representeren een veelbelovende a-cellulaire aanpak voor weefselregeneratie. Aan de ene kant is de flexibiliteit van de verkregen elektrospun scaffolds interessant en aanwendbaar voor vele toepassingen die GBR membranen omvat, zoals beschreven in dit proefschrift, alsook voor toepassingen op het gebied van interface weefselregeneratie, zoals periost en ligament weefsel. Anderzijds is het door de hoge oppervlakte-volumeverhouding vanwege de ultradunne vezeldiameter mogelijk elektrospun scaffolds een effectieve drager te laten zijn om verschillende soorten biomoleculen te laden via verschillende methoden om het weefselregeneratie proces te sturen. Om zo'n veelbelovende benadering van laboratorium naar bed te vertalen is uitgebreid onderzoek nodig om (1) een gecontroleerde afgiftekinetiek en (2) een *in vivo* optimale dosering te bereiken.

References

1. Robey, P. G. *Tissue Eng Part B Rev* **2011**, 17, 423-430.
2. Dzenis, Y. *Science* **2004**, 304, 1917-1919.
3. Reneker, D.; Chun, I. *Nanotechnology* **1996**, 7, 216-223.
4. Jiang, H. L.; Hu, Y. Q.; Zhao, P. C.; Li, Y.; Zhu, K. J. *J Biomed Mater Res B Appl Biomater* **2006**, 79, 50-57.
5. Liao, I. C.; Chew, S. Y.; Leong, K. W. *Nanomedicine* **2006**, 1, 465-471.
6. Yang, Y.; Li, X.; Cui, W.; Zhou, S.; Tan, R.; Wang, C. *J Biomed Mater Res A* **2008**, 86, 374-385.
7. Zeng, J.; Aigner, A.; Czubyko, F.; Kissel, T.; Wendorff, J. H.; Greiner, A. *Biomacromolecules* **2005**, 6, 1484-1488.
8. Kowalczyk, T.; Nowicka, A.; Elbaum, D.; Kowalewski, T. A. *Biomacromolecules* **2008**, 9, 2087-2090.
9. Sahoo, S.; Ang, L. T.; Goh, J. C. H.; Toh, S. L. *J Biomed Mater Res A* **2010**, 93, 1539-1550.
10. Srouji, S.; Ben-David, D.; Lotan, R.; Livne, E.; Avrahami, R.; Zussman, E. *Tissue Eng Part A* **2011**, 17, 269-277.
11. Piskounova, S.; Gedda, L.; Hulsart-Billstrom, G.; Hilborn, J.; Bowden, T. *J Tissue Eng Regen Med* **2012**. doi: 10.1002/term.1584.
12. Bergman, K.; Engstrand, T.; Hilborn, J.; Ossipov, D.; Piskounova, S.; Bowden, T. *J Biomed Mater Res A* **2009**, 91, 1111-1118.
13. Luca, L.; Capelle, M. A.; Machaidze, G.; Arvinte, T.; Jordan, O.; Gurny, R. *Int J Pharm* 391, 48-54.
14. Coene, H.; Mertens, J.; Mazière, B., In *Radioiodination reactions for pharmaceutical: compendium for effective sythesis strategies*, Springer: Dordrecht, 2006.
15. Garratt, C. J.; Harrison, D. M.; Wicks, M. *Biochem J* **1972**, 126, 123-131.
16. van der Zande, M.; Walboomers, X. F.; Olalde, B.; Jurado, M. J.; Alava, J. I.; Boerman, O. C.; Jansen, J. A. *J Tissue Eng Regen Med* **2011**, 5, 476-482.
17. Bodde, E. W.; Boerman, O. C.; Russel, F. G.; Mikos, A. G.; Spauwen, P. H.; Jansen, J. A. *J Biomed Mater Res A* **2008**, 87, 780-791.

结语及展望

骨组织工程技术成为临床修复大面积骨缺损,尤其是颅颌面复杂性骨缺损一种新兴途径。论文**第一章**介绍了骨组织工程的概念和研究现状。传统的骨组织工程技术包括以下几个步骤,从宿主体内分离具有成骨潜力的前体细胞,并将其接种到组织工程支架上进行预培养;将培养成熟的细胞/支架复合体移植进入缺损部位,实现组织修复。在这一过程中,外援性的前体细胞在修复过程中起着主要作用,而组织工程支架则主要对接种的细胞和缺损部位的修复提供物理支撑作用。近年来,越来越多的临床和实验表明,理想的组织工程支架不应该仅仅起着物理支架作用,同时还应该起到局部释放生物活性分子的作用,以刺激宿主内源性组织积极参与修复过程。

论文**第二章**概述了局部控释生物活性分子修复颅颌面骨缺损的相关研究进展。根据分子量大小(5kDa),生物活性分子可以广义的分为生物大分子和生物小分子。生物大分子主要包括炎症趋化因子,形态决定因子和成血管因子。它们在调控成骨细胞趋化(例如SDF-1 α),分化(例如BMP-2,4,7),以及骨组织血管形成(例如VEGF)过程中发挥重要作用。生物小分子则包括生长因子小分子多肽,抗炎因子,抗肿瘤因子以及抗组织疏松因子。它们在调控病理性骨修复过程中发挥重要作用。

目前,利用生物材料制备生物活性分子的控释系统在体内主要应用于以下三类缺损,分别是:颅骨缺损,下颌骨及牙槽骨缺损,以及上颌窦提升。绝大多数体内应用目前尚属于动物实验阶段。其真正的其临床应用,需要在载药载体的设计,保存所加载因子的生物学功能的保存,以及体内的释放曲线调控等方面做更多更系统的研究。

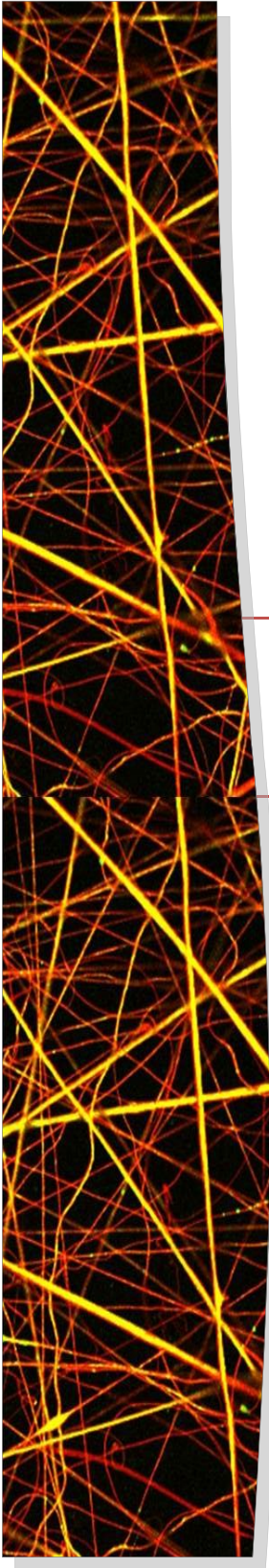
制备组织工程支架的方法有很多,其中静电纺丝技术因为可以生成与天然的细胞外基质物理结构高度相似的纳米/微米纤维,于近年来受到越来越多科研人员的关注。同时,电纺丝纤维极其细小的纤维直径(纳米/微米级别)增大了整个支架的表面积,使其成为了生物活性分子的有效载体。目前主要有四种方法可以制备复合生物活性分子的电纺纤维支架:物理吸附,混合电纺,同轴电纺,以及化学改性。论文第三章分析比较了这四种方法在复合生物活性分子领域中的应用以及各自的优缺点和面临的挑战。此外,论文**四至七章**分别应用了物理吸附,混合电纺,以及同轴电纺制备出复合了不同生物活性分子的电纺纤维支架,并分别评价了支架的理化性能,药物释放曲线和体内外生物学表现。

应当指出的是,尽管静电纺丝技术创始于1934年,并且已经充分发展并应用于工业,但是在生物活性分子释放领域中的应用还依旧停留于实验室评价阶段。造成这一现象的主要原因可能来源于以下两方面的研究瓶颈:体外释放曲线的检测,以及体内剂量的预测。前者主要面临的挑战来自于现有试验技术手段的局限性。以往的研究结果现实,为了检测生物活性分子的体外释放曲线,最常用的技术手段包括酶联免疫技术和放射性同位素标记技术。然而近年来越来越多的研究结果质疑利用酶联免疫技术来检测蛋白释放曲线的可靠性,因为蛋白的抗原抗体结合位点有可能在支架制备过程中,或者蛋白释放过程,以及样本的存储检测过程中被破坏,因

而无法被检测到。

相比之下，放射性同位素直接标记目标蛋白的酪氨酸，因而在检测目标蛋白的释放曲线方面能提供更可靠的结果。但这一方法的局限性在于如果目标蛋白不含有或含有极少量的酪氨酸，那么同位素标记便有可能不成功。此外，有些蛋白分子的生物活性靶点包含酪氨酸，同位素标记则有可能导致其生物活性的丧失。另外一个重要挑战来自于预测生物活性分子的体内优化剂量。体内剂量的准确预测依赖于准确估计生物活性分子的体内释放曲线和体内生物学活性。然而体内复杂的理化环境，以及生物活性分子复杂多变的理化特性都能影响其在体内的生物学行为，因此给准确预测体内生物活性分子的优化剂量带来了挑战。

总而言之，复合生物活性分子的电纺纤维支架代表了一种新兴的组织修复手段。一方面，电纺纤维支架良好的柔韧性以及可塑性使其在引导型组织修复，以及交界组织修复（例如牙周膜，韧带，关节等）中具有良好的应用前景。另一方面，超细纤维直径所带来的巨大表面积使得电纺纤维支架能够有效加载并释放多种生物活性分子，以促进组织修复。为了更好的将这一技术从实验室转化向临床，未来需要更多的研究以阐明生物活性分子的控释以及体内剂量的优化。



“If I have seen further than others,
it is by standing upon the shoulders of giants.”

Isaac Newton

1632-1727

Acknowledgement

I can still vividly recall that sunny September afternoon in the year of 2001 when I took Hippocrates Oath as a fresh medical student in Wuhan University. The sentences from the Oath greatly thrilled my dream of being a Doctor, although at that time, the word “Doctor” to me just merely means some vague images from TV serials Grey’s Anatomy. Today, when I complete my doctoral thesis in Nijmegen, the word “Doctor” contains much more profound meaning than before. It reminds me of an arduous and inspiring journey to search and re-search somewhere for something important to be known, not only in science, but also in life.

Without any doubts, the past four years in Nijmegen is the most remarkable and memorable period in my journey of life. I am very pleased to see how much I have learned and grew in the past four years. This journey would never have been so vivid and impressive without so many people who have kindly helped me in innumerable ways. This thesis would never have been completed without these supports either. Although it is not possible to mention everyone by name, I would like to specifically to acknowledge following people.

First and foremost, I would like to express my deepest gratitude to my supervisor Prof. Dr. John Jansen. Dear John, you actually enlightened and guided me to unravel the world of regenerative medicine, and you taught me to do research in a broad and perspective view. Your expertise not only as a dentist, but also a scientist convinced me that it is possible and necessary to combine clinics and research to enrich the meaning of being a doctor. I learned so much from you in the past years, not only from your profound knowledge in bone tissue engineering, but also from your way of critical thinking, and highly efficient working attitude. My research experience in your lab, together with implicit and explicit influence from you, will constitute a profoundly valuable asset in my future career.

It is also a great pleasure to acknowledge my co-supervisors, Dr. Fang Yang, who gave me solid supports from engineering and material sciences aspects. Dear Fang, you leaded me into the field of electrospinning from the very beginning of installing the electrospinning machine, and manipulating the receipts for different polymer solutions. You also helped me to develop my own ideas and to do the research that I am interested. I could not count how many times that I went to you when I was deeply in stress and frustration in the past four years. You always encouraged and inspired me, using your optimistic and easy-going attitude towards work and life. You are more than a supervisor, but also a friend to me. Thank you for your accompany in the past four years, scientifically and personally.

I would like to also express my great appreciation to my other supervisor. Dr. Jeroen van den Beucken. Dear Jeoren, I have learned a lot from your expertise in biological sciences,

your working enthusiasm, as well as your critical and sometimes “out of box” way of thinking. More importantly, you taught me how to solve the problem in a straight forward way, not only in science, but also in life. I highly appreciate that you always encouraged me, and sometimes had even more confidence in me than I had in myself. Without your guidance, help and support, this thesis would never have been accomplished. Your expertise and detailed attention to every word and every concept contributed greatly to improve the quality of this thesis. Thank you for your inspiring optimism and laughter in the past four years!

I am also deeply grateful to my Chinese supervisor Prof. Dr. Zhi Chen. Dear Prof. Chen, I admire your dedication to research, meticulous scholarship, and modest personality. Thank you for guiding me into the clinical field of tooth aesthetic restoration; thank you for providing me a broad platform to do my interested research; thank you for enriching my dreams to pursue a challenging and comprehensive life abroad; thank you for kind support and advice when I am confused facing the crossroad of life. No matter where I will end up with, I will always appreciate the days that being your student.

Furthermore, I would like to thank all the collaborators in this thesis for their excellent help and contributions to the project. Some people I would like to address in particular. Prof. Dr. Wim Hennink, I highly value your opinion and knowledge in field of pharmaceutical sciences. Thank you very much for your excellent contributions to my research, especially on the studies I performed together with Hajar.

Dr. Hajar Seyednejad, dear Hajar, I really enjoyed working together with you. It was really inspiring for me to explore electrospinning using a new scaffolding material, which was generated by you. Thank you for sharing your extensive knowledge in material sciences, and your effort to explain GPC-related technicalities to me, thank you for your highly efficient working spirit to translate our work into publications, and thank you for your experiences and suggestions in my career choices! Although you are currently in the States, I hope we can have opportunities to collaborate in future!

Prof. Dr. Otto Boerman, thank you for the pleasant cooperation and for your very expert advice. I am pleased that our effort led to a joint publication in a good journal. I would also like to thank Gerben Franssen for his effort in labeling growth factors.

I acknowledge prof. Dr. Marc Bohner from RMS foundation for generously providing me with nanoapatite, Dr. Dennis Lowik from department of Organic Chemistry, for assisting me in Circular Dichroism analysis, Mr. Richard Huijbens from department of Rheumatology for his kind assistance in Luminex analysis, Mr. Huib Croes from Microscopic Imaging Center (MIC) for his patience in instructing me using confocal microscopy, and Dr. Ewald Bronkhorst from faculty of Dentistry for his expertise and advice in statistical analysis.

I would like to acknowledge all the people from the Animal Facility (CDL) Radboud University Nijmegen, who helped me with my experiments. My special thanks go to Bianca, Linda and Daphne. without them, I wouldn't have been able to carry out my animal studies.

I am indebted to all my colleagues from Department of Biomaterials, who accompany me through such impressive journey of life with their vivid characteristics of each person. Every conversation and joke that we had during coffee break, every minute that we worked together in the cell culture/chemical lab, every question and discussion that we had in the routine research seminar are my precious memories which I will miss a lot in my future life. My special appreciations go to Eva and Natasja. Dear girls, thank you so much for always standing beside me to go through those happy and sad moments in my work and life. The rejoice that I had with you to search wedding gowns in city center, and the tears that I cried on your shoulders when facing the family loss have been deeply engraved in my mind.

I would also like to mention Jinling, Huanan, Ljupcho, Matilde (Mati) and Arnold. Guys, we started our PhD more or less the same time, and we shared so many funny moments in the past four years: the night lost in mid-town of Houston searching for the pub area; the remarkable NBTE meeting in Lunteren with Arnold as the most excellent Chairman and Ljupcho as the most enthusiastic speaker ever; the impressive trip to Chengdu for World Biomaterials Congress; and the most excitingly, your presence in my wedding day in Beijing! Dear Mati, I am so glad that you caught my bouquet on that day, and I wish all your dreams coming true! Dear Ljupcho and Arnold, you looked awesome on that day and your speech in Chinese was FANTASTIC! Although we may apart from each other in different continents (Asia, Europe and North America), I would never forget the days we worked together, the countless coffee break and hanging out together in Biomaterials. I hope we can always keep in touch and encourage each other in our new period of life.

It would not be a complete memory for the days in Biomaterials, if I missed the names of "nerdy group": Alexey, Daniel, and Ruggero. Thanks a lot for your active sociability to build up an entertaining atmosphere inside and outside the office. Thanks a lot for all the (normal or nerdy) discussions that we had (work related or not) to cheer up myself from the stressed moments in the final period of Ph.D. I do appreciate the cheerful moments that I spent together with you guys. May the force be with you!

There are some other names that I could not forget. Dear Edwin, Meike, Wanxun, Rosa, and Kemal, thanks a lot for giving me kind help in qPCR, image design, cell culture, HPLC, and calcium phosphate processing, respectively. Thanks a lot for being my (ex)office mates. From the time that I spent with you, I have learned the attitude of being punctuate, open-minded, easy-going, and optimistic to life and people around you. Dear

Frank, Joop, Sander, Adelina and Sanne, thank you for your constructive suggestions and comments during my study. Dear Vincent, Martijn and Monique, thank you for your great technique supports in the past four years. Indeed, you are the “super heros” and give me strong back up during my study.

The journey in Nijmegen would not be so colorful if I had not met my Chinese friends, both inside and outside the department of Biomaterials. I am grateful to have your accompany in the past four years, to share our growing pains and happiness as overseas students. The time we spent together to encourage each other and to enjoy life together was priceless memories to me. Thank you Xiao, Jiabo, Xuehui, Meng, Minqin, Na, and Xiangzhen in particular!

Last but not least, I would like to express my deepest gratitude to my families, especially to my husband Justin, and my parents. Without their unconditional love, support and understanding through all these years, this thesis would never have been possible to be finished.

亲爱的爸爸妈妈，感谢你们赋予我生命，并且教会我独立思考，独立选择人生道路的能力。感谢你们这么多年来对我无私的关怀和支持，让我能全力以赴去追寻自己的梦想。爸爸妈妈，我爱你们！

亲爱的思佳，感谢你在我失落的时候支持我，在我脆弱的时候鼓励我，在我焦虑的时候安慰包容我。我们已经分享了彼此人生中最重要的一年，我希望我们也会像妈妈说的那样“永远平静而自信，快乐地面对生活”，分享彼此将来更加丰富精彩的人生旅程！





List of Publications & Awards

Peer-reviewed Journals

1. **W. Ji**, F. Yang, J. Ma, M.J. Bouma, O.C. Boerman, Z. Chen, J.J. van den Beucken, J.A. Jansen, Incorporation of stromal cell-derived factor-1alpha in PCL/gelatin electrospun membranes for guided bone regeneration, *Biomaterials*, 34 (2013) 735-745.
2. **W. Ji**, F. Yang, H. Seyednejad, Z. Chen, W.E. Hennink, J.M. Anderson, J.J. van den Beucken, J.A. Jansen, Biocompatibility and degradation characteristics of PLGA-based electrospun nanofibrous scaffolds with nanoapatite incorporation, *Biomaterials*, 33 (2012) 6604-6614.
3. **W. Ji**, H. Wang, J.J. van den Beucken, F. Yang, X.F. Walboomers, S. Leeuwenburgh, J.A. Jansen, Local delivery of small and large biomolecules in craniomaxillofacial bone, *Advanced Drug Delivery Reviews*, 64 (2012) 1152-1164.
4. H. Seyednejad*, **W. Ji***, F. Yang, C.F. van Nostrum, T. Vermonden, J.J. van den Beucken, W.J. Dhert, W.E. Hennink, J.A. Jansen, Coaxially Electrospun Scaffolds Based on Hydroxyl-Functionalized Poly(epsilon-caprolactone) and Loaded with VEGF for Tissue Engineering Applications, *Biomacromolecules*, 13 (2012) 3650-3660. * Equal contributions as first author
5. **W. Ji**, F. Yang, J.J. van den Beucken, Z. Bian, M. Fan, Z. Chen, J.A. Jansen, Fibrous scaffolds loaded with protein prepared by blend or coaxial electrospinning, *Acta Biomaterialia*, 6 (2010) 4199-4207.
6. **W. Ji**, Y. Sun, F. Yang, J.J. van den Beucken, M. Fan, Z. Chen, J.A. Jansen, Bioactive electrospun scaffolds delivering growth factors and genes for tissue engineering applications, *Pharmaceutical Research*, 28 (2011) 1259-1272.
7. H. Seyednejad, **W. Ji**, W. Schuurman, W.J. Dhert, J. Malda, F. Yang, J.A. Jansen, C. van Nostrum, T. Vermonden, W.E. Hennink, An electrospun degradable scaffold based on a novel hydrophilic polyester for tissue-engineering applications, *Macromolecular Bioscience*, 11 (2011) 1684-1692.
8. J. Ma, S.K. Both, **W. Ji**, F. Yang, H.K. Prins, M.N. Helder, J. Pan, FZ. Cui, J.A. Jansen, J.J. van den Beucken, Adipose tissue-derived MSCs as monocultures or cocultures with human umbilical vein endothelial cells: performance in vitro and in rat cranial defects, *Regenerative Medicine*, Submitted
9. **W. Ji**, Z. Chen, J.E. Frencken, Strength of tunnel-restored teeth with different materials and marginal ridge height, *Dental materials*, 25 (2009) 1363-1370.

Awards

1. Belgian Symposium on Tissue Engineering, Leuven, Belgium (2012, September 17-18). Oral presentation: “Electrospun PCL/gelatin nanofibrous membrane with SDF1 α release for guided bone regeneration” – *European Science Foundation (ESF) Travel Award*.
2. The 4th International Conference of Tissue Engineering, Crete, Greece (2011, June 01-05). Oral presentation: “Effect of nanoapatite on degradation behavior and tissue response of PLGA-based electrospun nanofibrous scaffold” – *Best Lecture Award* in rapid-fire session
3. Ph.D retreat in Nijmegen Center of Molecular & Life Sciences (NCMLS), Wageningen, the Netherlands (2012, April 26-27). Oral presentation: “Nanofibrous membrane with stromal cell derived-1 α incorporation for guided bone regeneration” – *Nominations for Best Lecture Award*.

Curriculum Vitae



Wei Ji (纪伟) was born on May 02, 1983 and grew up in Wuhan, China. In 2001, she was enrolled in School of Dentistry, Wuhan University in a continuous 7-year Dental Medicine program, from which she received basic medicine education, resident training for general dentist and postgraduate training for Endodontist. During her study, she became interested in life science closely related to the medical problems. Therefore, since 2003, she spent her weekends to attend a dual-major of Biological Sciences in College of Life Sciences at Wuhan University. In 2008, she fulfilled the requirements to obtain a Dual-Bachelor degree of Biological Sciences. In the same year, she also received her Master degree in Dental Medicine, and passed Chinese Medical Licensing Examination as an Endodontist.

In 2007, she attended a Dental Student Exchange Program between Wuhan University and Radboud University Nijmegen. She spent two months in Department of Global Oral Health. During this period, she followed both clinical and laboratorial training under supervision of Dr. J.E. Frencken. Such experience enriched her understanding to be a dentist, and gave her strong interest to do clinical related research.

In November of 2008, she started working as a PhD student at the Department of Biomaterials of the Radboud University Nijmegen Medical Center. She participated in a KNAW-PSA supported research project entitled "Nanomaterials for Bone Regeneration". In this project, she explored the fabrication and material properties of nanoscaled fibrous scaffolds prepared by electrospinning technique using different synthetic polymers. She also investigated the incorporation and release of different biomolecules from the obtained scaffolds, and the corresponding biological performance both *in vitro* and *in vivo*. These studies were in collaboration with Department of Nuclear Medicine at the Radboud University Nijmegen and Department of Pharmaceutical Sciences at Utrecht University. This PhD research came to a successful end in October of 2012. The results of the performed studies are described in this thesis.

Since December of 2012, she has started working as a postdoctoral research associate in Prometheus, the division of Skeletal Tissue Engineering of Katholieke Universiteit Leuven (KU Leuven) in Belgium. She is involved in an ERC-advanced research project: Manufacturing of a Biological Tissue: Regeneration of the Joint by Developmental Engineering. Her current research interest is to investigate molecular mechanism to regulate bone morphogenetic proteins (BMPs) technology in cellular strategy for bone regeneration.

“There are no such things as limits to growth,
because there are no limits to the human capacity for
intelligence, imagination, and wonder”

Ronald Reagan

1911-2004